INL/EXT-21-64546

Light Water Reactor Sustainability Program

Risk-Informed Analysis for Enhanced Resilient Nuclear Power Plant with Initiatives including ATF, FLEX, and Advanced Battery Technology

September 2021

U.S. Department of Energy

Office of Nuclear Energy

INL/EXT-21-64546

Risk-Informed Analysis for Enhanced Resilient Nuclear Power Plant with Initiatives including ATF, FLEX, and Advanced Battery Technology

Sai Zhang, Hongbin Zhang, Jooyoung Park, Tao Liu, Thomas A. Ulrich, Ronald L. Boring, Zhegang Ma (Idaho National Laboratory)

Hongbing Jiang (Tennessee Valley Authority)

September 2021

Prepared for the
U.S. Department of Energy
Office of Nuclear Energy

Page intentionally left blank

EXECUTIVE SUMMARY

This report documents the activities performed by the Idaho National Laboratory (INL) during fiscal year (FY) 2021 for the U.S. Department of Energy (DOE) Light Water Reactor Sustainability (LWRS) Program, Risk-Informed Systems Analysis (RISA) Pathway as part of Enhanced Resilient Plant (ERP) Systems project. The purpose of the RISA Pathway research and development is to support plant owner-operator decisions with the aim to improve the economics, reliability, and maintain the high levels of safety of current nuclear power plants over periods of extended plant operations. The concept of ERP refers to a nuclear power plant (NPP) that is enhanced with various industry initiatives such as accident-tolerant fuel (ATF), optimal use of diverse and flexible coping strategy (FLEX), enhancements to plant components and systems, the incorporation of augmented or new passive cooling systems, and advanced battery technology with extended capacity. The objective of the ERP research effort is to use the RISA methods and toolkit in industry applications, including methods development and early demonstration of technologies, in order to enhance existing reactors' safety features and to substantially reduce operating costs through risk-informed approaches to plant design modifications and their characterization.

The ERP research and development (R&D) efforts in FY 2021 are focused on three industry initiatives, including ATF, FLEX, and advanced battery technology with extended capacity. One focus area of the ATF efforts is to extend the FY 2020 analyses on a generic boiling water reactor (BWR). The same analysis process and tools as in the FY 2020 work were used with two near-term ATF cladding (i.e., Iron-Chromium-Aluminum [FeCrAl] cladding and Chromium [Cr]-coated cladding) designs under four types of postulated scenarios, including general transient (TRANS), loss of main feedwater (LOMFW), small loss-of-coolant accident (SLOCA), and inadvertent open relief valve (IORV). Another focus area of ATF efforts is to conduct a benchmark study between two probabilistic risk assessment (PRA) models—one is the generic pressurized water reactor (PWR) Systems Analysis Programs for Hands-on Integrated Reliability Evaluations (SAPHIRE) model used in the FYs 2018 and 2019 ATF analyses under the ERP project, and the other is the plant-specific PRA model of a reference PWR plant in U.S.. An agreement was reached between the ERP team and the reference plant to conduct a benchmark study between the generic SAPHIRE model and the plant-specific PRA model. A third-party consulting company, Jensen Hughes, was subcontracted to conduct the benchmark study. The FLEX efforts are focused on continued development of a dynamic approach for FLEX human reliability analysis (HRA) using Event Modeling Risk Assessment using Linked Diagrams (EMRALD) computer software. The efforts on the advanced battery technology include a risk impact analysis and an economic impact analysis of deploying batteries with extended capacity at a generic BWR plant. Besides the above three industry-initiative-focused analyses, the work of optimizing mitigating system performance index (MSPI) through advanced artificial intelligence (AI) and machine learning (ML) techniques is also planned under the ERP project and some preliminary work is done in the FY 2021.

In the BWR ATF general transient analysis, 14 scenarios were developed and analyzed using Reactor Excursion and Leak Analysis Program 5-3D (RELAP5-3D) for thermal hydraulic (TH) analysis with traditional fuel design and near-term ATF designs. Ten scenarios are general transients with reactor scram, and the other four scenarios are anticipated transients without scram (ATWS). The RELAP5-3D simulation results, including the time to core damage (CD) and the production of hydrogen for traditional fuel design (Zircaloy or Zry) and two near-term ATF designs (FeCrAl and Cr-coated), are presented from Table ES-1 to Table ES-4. For the scenarios with reactor scram, the results show the gain of coping time, or the delay of time to CD, is less than or equal to 30 minutes for most scenarios. For FeCrAl, a gain of coping time ranges from 10 to 35 minutes; for Cr-coated cladding, a gain of coping time ranges from 5 to 19 minutes. For the ATWS scenarios, the results show the gain of coping time is less than 12 minutes for all scenarios. For FeCrAl, a gain of coping time ranges from 5 to 12 minutes; for Cr-coated cladding, a gain of coping time ranges from 2 to 7 minutes.

With only a marginal increase of the time to CD with FeCrAl and Cr-coated against the conventional Zry-cladding design based on the RELAP5-3D simulation results, the risk-benefit on behalf of the core damage frequency (CDF) as the risk metrics would be very small and it is not quantified. However, the RELAP5-3D simulation results show the clear benefit in adopting ATF due to much less hydrogen produced at the time of CD. For the scenarios with reactor scram, the results show the hydrogen production can be a few times lower for the Cr-coated cladding and up to two orders of magnitude lower for FeCrAl cladding than with Zircaloy cladding cases. For the ATWS scenarios, the results show the hydrogen production can be a few times lower for the Cr-coated cladding and up to two orders of magnitude lower for FeCrAl cladding than with Zircaloy cladding cases.

Table ES-1. Comparison of Time to CD with ATF Designs for General Transients with Reactor Scram.[1]

Scenario	Scenario Description[a]	Time to CD t_{CD} (hh:mm)					
		Zry	Cr-coated	Δt	Zry	FeCrAl	Δt
TRANS-1	Reactor trip, no HPI, no DEP	1:07	1:12	0:05	1:07	1:17	0:10
TRANS-2	Reactor trip, AC, HPI, DEP, Control Rod Drive Injection, no Containment HR	10:02	10:13	0:11	10:02	10:27	0:25
TRANS-3	Reactor trip, AC, HPI, no DEP	8:01	8:14	0:13	8:01	8:28	0:27
TRANS-4	Reactor trip, AC, HPI, DEP, no LPI	7:10	7:15	0:05	7:10	7:25	0:15
TRANS-SORV-1	Reactor trip, AC, 1 SRV Open, no HPI, no DEP	0:57	1:02	0:05	0:57	1:06	0:09
TRANS-SORV-2	Reactor trip, AC, 1 SRV Open, DEP, CS, no Containment HR	13:46	14:05	0:19	13:46	14:21	0:35
TRANS-SORV-3	Reactor trip, AC, 1 SRV Open, no DEP, no LPCI	8:14	8:19	0:05	8:14	8:28	0:14
TRANS-SORV-4	Reactor trip, AC, 1 SRV Open, DEP, LPCI, no Containment HR	13:18	13:30	0:12	13:18	13:46	0:28
TRANS-SORV-5	Reactor trip, AC, 2 SRVs Open, DEP, CS, no Containment HR	13:42	13:53	0:11	13:42	14:13	0:31
TRANS-LOOP-1	Reactor trip, LOOP, AC, HPI, DEP, LPCI, no Containment HR	18:44	19:02	0:18	18:44	19:14	0:30

a. Note: The scenario descriptions provide the status or success/failure operations of systems and components, e.g., “Reactor trip” indicates the reactor is successfully tripped, “HPI” means the high-pressure injection is successful, “no LPI” means the low-pressure injection is failed.

[1] Acronyms used in this table and the remaining tables in the executive summary that are not defined yet: AC (alternating current), ADS (automatic depressurization system), CS (core spray), DEP (depressurization), HFE (human failure event), HPI (high-pressure injection, which can be achieved using high-pressure core injection [HPCI] or reactor core isolation cooling [RCIC]), HR (heat removal), IE (initiating event), LOOP (loss of offsite power), LPI (low-pressure injection, which can be achieved using low-pressure core injection [LPCI] or core spray), SLCS (standby liquid control system), SORV (stuck-opened relief valve), SRV (safety relief valve).

Table ES-2. Comparison of H_2 Productions with ATF Designs for General Transients with Reactor Scram.

Scenario	Scenario Description	Total H_2 (kg)			H_2 %	
		Zry	Cr-coated	FeCrAl	Cr-coated	FeCrAl
TRANS-1	Reactor trip, no HPI, no DEP	21.2	5.6	0.4	26.6	1.9
TRANS-2	Reactor trip, AC, HPI, DEP, Control Rod Drive Injection, no Containment HR	13.6	2.6	0.2	18.8	1.2
TRANS-3	Reactor trip, AC, HPI, no DEP	31.2	6.0	0.6	19.4	1.9
TRANS-4	Reactor trip, AC, HPI, DEP, no LPI	9.0	1.5	0.1	16.2	1.1
TRANS-SORV-1	Reactor trip, AC, 1 SRV Open, no HPI, no DEP	51.1	5.4	0.5	10.5	1.0
TRANS-SORV-2	Reactor trip, AC, 1 SRV Open, DEP, CS, no Containment HR	20.4	5.2	0.3	25.3	1.7
TRANS-SORV-3	Reactor trip, AC, 1 SRV Open, no DEP, no LPCI	12.2	3.3	0.2	27.3	1.5
TRANS-SORV-4	Reactor trip, AC, 1 SRV Open, DEP, LPCI, no Containment HR	18.4	5.0	0.3	26.9	1.8
TRANS-SORV-5	Reactor trip, AC, 2 SRVs Open, DEP, CS, no Containment HR	18.2	11.2	0.3	61.6	1.8
TRANS-LOOP-1	Reactor trip, LOOP, AC, HPI, DEP, LPCI, no Containment HR	21.2	5.6	0.4	26.6	1.9

Table ES-3. Time to CD Comparison for ATWS Scenarios with ATF Designs.

Scenario	Scenario Description	Time to CD t_{CD} (hh:mm)					
		Zry	Cr-coated	Δt	Zry	FeCrAl	Δt
TRANS-ATWS-1	No trip, AC, SRVs Open, Recirc Pump Trip, No SLCS, No ADS, No DEP, No LPI	0:27	0:29	0:03	0:27	0:33	0:06
TRANS-ATWS-2	No trip, AC, SRVs Open, No Recirc Pump Trip, No SLCS, No ADS, No DEP, No LPI	0:26	0:29	0:03	0:26	0:32	0:06
TRANS-ATWS-3	No trip, AC, SRVs Open, Recirc Pump Trip, SLCS, No ADS, No DEP, No LPI	1:12	1:19	0:07	1:12	1:24	0:12
TRANS-ATWS-4	No trip, AC, SRVs Open, Recirc Pump Trip, SLCS, ADS, DEP, No LPI	0:48	0:50	0:02	0:48	0:53	0:05

Table ES-4. Comparison of H_2 Productions for ATWS Scenarios with ATF Designs.

Scenario	Scenario Description	Total H_2 (kg)			H_2 %	
		Zry	Cr-coated	FeCrAl	Cr-coated	FeCrAl
TRANS-ATWS-1	No trip, AC, SRVs Open, Recirc Pump Trip, No SLCS, No ADS, No DEP, No LPI	20.8	3.0	0.2	14.4	1.0
TRANS-ATWS-2	No trip, AC, SRVs Open, No Recirc Pump Trip, No SLCS, No ADS, No DEP, No LPI	19.2	2.9	0.2	15.1	1.0
TRANS-ATWS-3	No trip, AC, SRVs Open, Recirc Pump Trip, SLCS, No ADS, No DEP, No LPI	26.8	4.8	0.3	18.0	1.3
TRANS-ATWS-4	No trip, AC, SRVs Open, Recirc Pump Trip, SLCS, ADS, DEP, No LPI	19.7	7.4	0.1	37.3	0.7

In the BWR ATF LOMFW analysis, 12 scenarios were developed and analyzed using RELAP5-3D for TH analysis with traditional fuel design and near-term ATF designs. Nine scenarios are LOMFW scenarios with reactor scram, and the other three scenarios are LOMFW-initiated ATWS. The RELAP5-3D simulation results, including the time to CD and the production of hydrogen for traditional fuel design (Zircaloy, or Zry) and two near-term ATF designs (FeCrAl and Cr-coated), are presented from Table ES-5 to Table ES-8. For the scenarios with reactor scram, the results show the gain of coping time, or the delay of time to CD, is less than or equal to 30 minutes for most scenarios. For FeCrAl, a gain of coping time ranges from 9 to 35 minutes; for Cr-coated cladding, a gain of coping time ranges from 5 to 22 minutes. For the LOMFW-initiated ATWS scenarios, the results show the gain of coping time is less than 10 minutes for all the scenarios. For FeCrAl, a gain of coping time is about 10 minutes for LOMFW-ATWS-1, 7 minutes for LOMFW-ATWS-2 and no gain for LOMFW-ATWS-3; for Cr-coated cladding, a gain of coping time is about 5 minutes for LOMFW-ATWS-1, 3 minutes for LOMFW-ATWS-2, and no gain for LOMFW-ATWS-3.

With only a marginal increase of the time to CD with FeCrAl and Cr-coated against the conventional Zry-cladding design based on the RELAP5-3D simulation results, the risk-benefit on behalf of CDF as the risk metric would be very small and it is not quantified. However, the RELAP5-3D simulation results show the clear benefit in adopting ATF due to much less hydrogen produced at the time of CD. For the scenarios with reactor scram, the results show the hydrogen production can be a few times lower for the Cr-coated cladding, and up to two orders of magnitude lower for FeCrAl cladding than with Zircaloy cladding cases. For the LOMFW-initiated ATWS scenarios, the results show the hydrogen production can be a few times lower for the Cr-coated cladding and up to two orders of magnitude lower for FeCrAl cladding than with Zircaloy cladding cases.

Table ES-5. Comparison of Time to CD with ATF Designs for LOMFW with Reactor Scram.

Scenario	Scenario Description	Time to CD t_{CD} (hh:mm)					
		Zry	Cr-coated	Δt	Zry	FeCrAl	Δt
LOMFW-1	LOMFW IE, Reactor scram, no HPI, no DEP	1:07	1:12	0:05	1:07	1:17	0:10
LOMFW-2	LOMFW IE, Reactor scram, AC, HPI, DEP, Control Rod Drive Injection, no Containment HR	10:02	10:13	0:11	10:02	10:27	0:25
LOMFW-3	Reactor trip, AC, HPI, no DEP	8:01	8:14	0:13	8:01	8:28	0:27
LOMFW-4	LOMFW IE, Reactor scram, AC, no HPI, DEP, CS, no Containment HR	16:08	16:30	0:22	16:08	16:32	0:24

Scenario	Scenario Description	Time to CD t_{CD} (hh:mm)					
		Zry	Cr-coated	Δt	Zry	FeCrAl	Δt
LOMFW-SORV-1	LOMFW IE, Reactor scram, AC, 1 SRV Open, no HPI, no DEP	0:57	1:02	0:05	0:57	1:06	0:09
LOMFW-SORV-2	LOMFW IE, Reactor scram, 1 SRV Open, DEP, CS, no Containment HR	13:46	14:05	0:19	13:46	14:21	0:35
LOMFW-SORV-3	LOMFW IE, Reactor scram, 1 SRV Open, no DEP, no LPCI	8:14	8:19	0:05	8:14	8:28	0:14
LOMFW-SORV-4	LOMFW IE, Reactor scram, AC, 2 SRVs Open, DEP, CS, no Containment HR	13:42	13:53	0:11	13:42	14:13	0:31
LOMFW-LOOP-1	LOMFW IE, Reactor scram, LOOP, AC, HPI, DEP, LPCI, no Containment HR	18:44	19:02	0:18	18:44	19:14	0:30

Table ES-6. Comparison of H_2 Productions with ATF Designs for LOMFW with Reactor Scram.

Scenario	Scenario Description	Total H_2 (kg)			H_2 %	
		Zry	Cr-coated	FeCrAl	Cr-coated	FeCrAl
LOMFW-1	LOMFW IE, Reactor scram, no HPI, no DEP	21.2	5.6	0.4	26.6	1.9
LOMFW-2	LOMFW IE, Reactor scram, AC, HPI, DEP, Control Rod Drive Injection, no Containment HR	13.6	2.6	0.2	18.8	1.2
LOMFW-3	Reactor trip, AC, HPI, no DEP	31.2	6.0	0.6	19.4	1.9
LOMFW-4	LOMFW IE, Reactor scram, AC, no HPI, DEP, CS, no Containment HR	20.6	5.3	0.4	25.8	1.8
LOMFW-SORV-1	LOMFW IE, Reactor scram, AC, 1 SRV Open, no HPI, no DEP	51.1	5.4	0.5	10.5	1.0
LOMFW-SORV-2	LOMFW IE, Reactor scram, 1 SRV Open, DEP, CS, no Containment HR	20.4	5.2	0.3	25.3	1.7
LOMFW-SORV-3	LOMFW IE, Reactor scram, 1 SRV Open, no DEP, no LPCI	12.2	3.3	0.2	27.3	1.5
LOMFW-SORV-4	LOMFW IE, Reactor scram, AC, 2 SRVs Open, DEP, CS, no Containment HR	18.2	11.2	0.3	61.6	1.8
LOMFW-LOOP-1	LOMFW IE, Reactor scram, LOOP, AC, HPI, DEP, LPCI, no Containment HR	21.2	5.6	0.4	26.6	1.9

Table ES-7. Time to CD Comparison for LOMFW-ATWS Scenarios with ATF Designs.

Scenario	Scenario Description	Time to CD t_{CD} (hh:mm)					
		Zry	Cr-coated	Δt	Zry	FeCrAl	Δt
LOMFW-ATWS-1	No trip, AC, SRVs Open, Recirc Pump Tripped, SLCS, No ADS, No DEP, No LPI	0:53	0:58	0:05	0:53	1:03	0:10
LOMFW-ATWS-2	No trip, AC, SRVs Open, Recirc Pump Tripped, No SLCS, No ADS, No DEP, No LPI	0:30	0:33	0:03	0:30	0:37	0:07
LOMFW-ATWS-3	No trip, AC, SRVs Open, Recirc Pump Tripped, SLCS, ADS, DEP, LPI	0:16	0:16	0:00	0:16	0:16	0:00

Table ES-8. Comparing H_2 Productions for LOMFW-ATWS Scenarios with ATF Designs.

Scenario	Scenario Description	Total H_2 (kg)			H_2 %	
		Zry	Cr-coated	FeCrAl	Cr-coated	FeCrAl
LOMFW-ATWS-1	No trip, AC, SRVs Open, Recirc Pump Tripped, SLCS, No ADS, No DEP, No LPI	22.4	3.8	0.3	16.9	1.2
LOMFW-ATWS-2	No trip, AC, SRVs Open, Recirc Pump Tripped, No SLCS, No ADS, No DEP, No LPI	18.5	2.7	0.2	14.7	1.0
LOMFW-ATWS-3[a]	No trip, AC, SRVs Open, Recirc Pump Tripped, SLCS, ADS, DEP, LPI	1.0E-02	2.9E-07	2.3E-08	0.0	0.0

a. Due to convergence issues, simulations stopped when peak clad temperature (PCT) reaches 1275 K for LOMFW-ATWS-3. Additionally, the PCT reaches the limit almost instantaneously due to the power spike and the short time duration results in very small hydrogen production.

In the BWR ATF SLOCA analysis, three scenarios were developed and analyzed using RELAP5-3D for TH analysis with traditional fuel design and near-term ATF designs. The RELAP5-3D simulation results, including the time to CD and the production of hydrogen for traditional fuel design (Zircaloy or Zry) and two near-term ATF designs (FeCrAl and Cr-coated), are presented in Tables ES-9 and ES-10. The results show the gain of coping time, or the delay of time to CD, is less than 24 minutes for all scenarios. For FeCrAl, a gain of coping time of 12 minutes and 24 minutes for SLOCA-1 and SLOCA-2, respectively. For Cr-coated cladding, a gain of coping time of 4 minutes and 13 minutes for SLOCA-1 and SLOCA-2, respectively.

With only a marginal increase of the time to CD with FeCrAl and Cr-coated against the conventional Zry-cladding design based on the RELAP5-3D simulation results, the risk-benefit on behalf of CDF as the risk metric would be very small and it is not quantified. However, the RELAP5-3D simulation results show the clear benefit in adopting ATF due to much less hydrogen produced at the time of CD. The results show the hydrogen production can be a few times lower for the Cr-coated cladding and up to two orders of magnitude lower for FeCrAl cladding than with Zircaloy cladding cases.

Table ES-9. Time to CD Comparison for SLOCA Scenarios with ATF Designs.

Scenario	Scenario Description	Time to CD t_{CD} (hh:mm)					
		Zry	Cr-coated	Δt	Zry	FeCrAl	Δt
SLOCA-1	SLOCA IE, Reactor scram, no HPI, no DEP	0:49	0:53	0:04	0:49	1:01	0:12
SLOCA-2	SLOCA IE, Reactor scram, AC, HPI, no DEP, no LPI, no Containment HR	11:32	11:45	0:13	11:32	11:56	0:24

Table ES-10. Comparison of H_2 Productions for SLOCA Scenarios with ATF Designs.

Scenario	Scenario Description	Total H_2 (kg)			H_2 %	
		Zry	Cr-coated	FeCrAl	Cr-coated	FeCrAl
SLOCA-1	SLOCA IE, Reactor scram, no HPI, no DEP	29.5	6.9	0.6	23.4	2.1
SLOCA-2	SLOCA IE, Reactor scram, AC, HPI, no DEP, no LPI, no Containment HR	43.5	6.0	0.8	13.8	1.8

In the BWR ATF IORV analysis, four scenarios were developed and analyzed using RELAP5-3D for TH analysis with traditional fuel design and near-term ATF designs. The RELAP5-3D simulation results, including the time to CD and the production of hydrogen for traditional fuel design (Zircaloy or Zry) and two near-term ATF designs (FeCrAl and Cr-coated), are presented in Tables ES-11 and ES-12. The results show the gain of coping time, or the delay of time to CD ranges from 5 to 35 minutes for FeCrAl cladding, and 2 to 19 minutes for Cr-coated cladding.

With only a marginal increase of the time to CD with FeCrAl and Cr-coated against the conventional Zry-cladding design based on the RELAP5-3D simulation results, the risk-benefit on behalf of CDF as the risk metric would be very small and it is not quantified. However, the RELAP5-3D simulation results show the clear benefit in adopting ATF due to much less hydrogen produced at the time of CD. The results show the hydrogen production can be a few times lower for the Cr-coated cladding and up to two orders of magnitude lower for FeCrAl cladding than with Zircaloy cladding cases.

Table ES-11. Comparison of Time to CD with ATF Designs for IORV Accident.

Scenario	Scenario Description	Time to CD t_{CD} (hh:mm)					
		Zry	Cr-coated	Δt	Zry	FeCrAl	Δt
IORV-1	IORV, Reactor trip, AC, no HPI, no DEP	0:57	1:02	0:05	0:57	1:06	0:09
IORV-2	IORV, Reactor trip, AC, HPI, no DEP, no LPI	8:14	8:19	0:05	8:14	8:28	0:14
IORV-3	IORV, Reactor trip, AC, HPI, DEP, CS, no Containment HR	13:46	14:05	0:19	13:46	14:21	0:35
IORV-4	IORV, Reactor trip, AC, no HPI, DEP, no LPI	0:50	0:52	0:02	0:50	0:55	0:05

Table ES-12. Comparison of H_2 Productions with ATF Designs for IORV Accident.

Scenario	Scenario Description	Total H_2 (kg)			H_2 %	
		Zry	Cr-coated	FeCrAl	Cr-coated	FeCrAl
IORV-1	IORV, Reactor trip, AC, no HPI, no DEP	51.1	5.4	0.5	10.5	1.0
IORV-2	IORV, Reactor trip, AC, HPI, no DEP, no LPI	12.2	3.3	0.2	27.3	1.5
IORV-3	IORV, Reactor trip, AC, HPI, DEP, CS, no Containment HR	20.4	5.2	0.3	25.3	1.7
IORV-4	IORV, Reactor trip, AC, no HPI, DEP, no LPI	22.8	2.8	0.15	12.3	0.66

In the benchmark study between the generic PWR SAPHIRE model and the representative plant-specific PRA model, some minor differences have been identified when comparing the accident sequences from the reference plant event trees (ETs) to the generic PWR ETs. Some potential adjustments to the generic PWR model have been suggested based on these identified differences. However, as the generic PWR SAPHIRE model stands, it adequately portrays ATF risk insights and utilities could use these insights to support ATF license amendment request submittals.

The FLEX study developed an enhanced approach to FLEX dynamic HRA using the EMRALD dynamic risk analysis software. In FY 2021, EMRALD was upgraded by correcting some limitations of the previous methods such as the procedure-based modeling and the PRA/HRA-based modeling. This FLEX study assumed an extended loss of AC power scenario and included human stress modeling based on observations in stress test experience. As a result, this study observed the human error probabilities from the EMRALD model are similar or slightly higher in comparison with those from the Integrated Human Event Analysis System for Event and Condition Assessment (IDHEAS-ECA) method (Xing, J., Y. Chang, and J. DeJesus, 2020). A new type of human error that has not been specifically considered in existing HRA, i.e., overtime failure, is also obtained from the EMRALD model for each human failure event. Lastly, this study estimated failure probabilities of recovery actions by application of a unique methodology not available in any other HRA methods.

The battery study conducted a preliminary evaluation of the potential costs and benefits of deploying increased-capacity batteries at a generic BWR plant. Nine alternatives for extending battery capacity are developed, including eight alternatives for providing additional DC power and one alternative for providing additional AC power. Potential benefits of reducing plant risk are quantified through incorporation of the alternatives into LOOP scenarios of the generic BWR SAPHIRE model. Potential costs of implementing the alternatives are qualitatively discussed and ranked. The alternatives are compared based on their impacts on plant risk and economics. The developed alternatives will be presented to industry partners to evaluate the feasibility of listed alternatives and potentially propose additional alternatives. In the future work, a multi-criterion benefit evaluation methodology will be utilized for a more comprehensive evaluation.

In the MSPI study, an MSPI estimation tool has been developed with the incorporation of the plant operation data, plant PRA data, and industry baseline values to automate the calculation process of MSPI and the generation of the report. This tool has been verified with the example data sets from an NPP. The case study demonstrates the feasibility of the proposed calculation tool. This is the first stage in an effort to optimize the MSPI through advanced artificial intelligence and machine learning techniques to improve NPP safety and efficiency. Future research efforts will be dedicated to the development of an MSPI optimization process, by applying artificial intelligence and machine learning techniques to optimize the performance index with the data-based reasoning to address the off-normal equipment conditions, to

utilize the ranking of the root causes and potential resolutions to find the best option of economically reducing MSPI value, and to facilitate and simplify the risk-informed and reliability-related decision-making for continuous improvement.

CONTENTS

FIGURES

TABLES

ACRONYMS

AC	alternating current
ADS	automatic depressurization system
AFW	auxiliary feedwater
AI	artificial intelligence
ATF	accident-tolerant fuel
ATWS	anticipated transients without scram
BC	boundary condition
BCR	benefit-to-cost ratio
BDBEE	beyond design basis external event
BOC	beginning of the cycle
BWR	boiling water reactor
CBA	cost-benefit analysis
CCDP	conditional core damage probability
CCF	common-cause failure
CD	core damage
CDF	core damage frequency
CFR	Code of Federal Regulations
CLD	causal-loop diagram
CPT	cumulative prospect theory
Cr	Chromium
CRDHS	control rod drives hydraulic system
CS	core spray
CSS	containment spray system
CST	condensate storage tank
CT	completion time
CVS	containment venting system
DBA	design-basis accident
DC	direct current
DEP	depressurization
DG	diesel generator
DID	defense in depth
DM	decision maker
DOE	Department of Energy

DW	drywell
EAC	emergency AC
ECCS	emergency core cooling system
EDG	emergency diesel generator
EIA	economic impact analysis
ELAP	extended loss-of-AC-power
EOC	end of the cycle
EPRI	Electric Power Research Institute
EPS	emergency power system
ERP	enhanced resilient plant
ESD	event sequence diagram
ET	event tree
FeCrAl	Iron-Chromium-Aluminum
FLEX	diverse and flexible coping strategy
FT	fault tree
FTLR	fail-to-load-and-run
FTR	fail to run
FTS	fail to start
FV	Fussell-Vesely
FY	fiscal year
GE	General Electric
GNF	Global Nuclear Fuel
GOMS	goals, operators, methods, and selection
GUI	graphical user interface
HEP	human error probabilities
HFE	human failure event
HPCI	high-pressure core injection
HPI	high-pressure injection
HR	heat removal
HRA	human reliability analysis
HX	heat exchanger
ICCDP	incremental conditional core damage probability
ICLERP	incremental conditional large early release probability
IDHEAS-ECA	Integrated Human Event Analysis System for Event and Condition Assessment
INL	Idaho National Laboratory

INPO	Institute of Nuclear Power Operations
IORV	inadvertent open relief valve
ISI	in-service inspection
IST	in-service testing
LER	licensee event report
LERF	large early release frequency
LI	late injection
LOCA	loss-of-coolant accident
LOMFW	loss of main feedwater
LOOP	loss of offsite power
LPCI	low-pressure core injection
LPCS	low-pressure core spray
LPI	low-pressure injection
LPR	low-pressure recirculation
LTSBO	long-term station blackout
LWR	light-water reactor
LWRS	light water reactor sustainability
MCBE	multi-criterion benefit evaluation
MCR	main control room
MDP	motor-driven pump
ML	machine learning
MLOCA	medium loss-of-coolant
MOC	middle of the cycle
MOV	motor-operated valve
MSIV	main steam isolation valves
MSPI	mitigating system performance index
NEI	Nuclear Energy Institute
NOED	notice of enforcement discretion
NOV	notice of violation
NPL	natural language processing
NPP	nuclear power plant
NPSH	net positive suction head
NPSHA	available net positive suction head
NPSHR	required net positive suction head
NRC	Nuclear Regulatory Commission

NUREG	nuclear regulatory report
O&M	operation and maintenance
OpE	operating experience
OS	overstress
PCT	peak clad temperature
PI	performance index
PORV	power-operated relief valve
PRA	probabilistic risk assessment
PWR	pressurized water reactor
PWROG	PWR Owners Group
PZR	pressurizer
R&D	research and development
RA	risk assessment
RAVEN	Risk Analysis and Virtual Control Environment
RBPI	risk-based performance indicator
RCIC	reactor core isolation cooling
RCP	reactor coolant pump
RCS	reactor coolant system
RELAP5-3D	Reactor Excursion and Leak Analysis Program 5–3D
RES	(NRC's Office of) Nuclear Regulatory Research
RFO	refueling outage
RHR	residual heat removal
RISA	risk-informed systems analysis
ROM	reduced order model
ROP	reactor oversight process
RPS	reactor protection system
RPV	reactor pressure vessel
SAPHIRE	Systems Analysis Programs for Hands-on Integrated Reliability Evaluations
SBO	station blackout
SDP	significance determination process
SG	steam generator
SGP	steam generator pump
SLCS	standby liquid control system
SLOCA	small loss-of-coolant accident
SORV	stuck-open relief valve

SP	suppression pool
SPAR-H	standardized plant analysis risk – human reliability analysis
SRV	safety relief valve
SSU	safety system unavailability
STSBO	short-term station blackout
TBV	turbine bypass valve
TDP	turbine-driven pump
TH	thermal hydraulic
TM	testing and maintenance
TRANS	general transient
TS	technical specification
TSSD	technical specification-required reactor shutdown
UA	unavailability
UAI	unavailability index
UR	unreliability
URI	unreliability index
U.S.	United States
UTS	ultimate tensile strength
VSS	vapor suppression
WW	wetwell

1. INTRODUCTION

This report documents the activities performed by the Idaho National Laboratory (INL) during fiscal year (FY) 2021 for the U.S. Department of Energy (DOE) Light Water Reactor Sustainability (LWRS) Program, Risk-Informed Systems Analysis (RISA) Pathway as part of Enhanced Resilient Plant (ERP) project (Idaho National Laboratory, 2018). The LWRS Program is a research and development (R&D) program that develops methods to support safe and economical long-term management and operation of existing nuclear power plants (NPPs), and investigates new technologies to address enhanced plant performance, economics, and safety. With the continuing economic challenges faced by NPPs, the LWRS Program has redirected some of its R&D efforts to consider how to leverage the results from other ongoing R&D activities to improve the economic performance of LWRs in current and future energy markets. The RISA Pathway is one of the primary technical areas of R&D under the LWRS Program. This pathway supports decision-making related to economics, reliability, and safety by providing integrated plant system analysis and solutions through collaborative demonstrations to enhance economic competitiveness of operating NPPs. The purpose of RISA Pathway R&D is to support plant owner-operator decisions to improve economics and reliability and to maintain the high levels of safety of current NPPs over periods of extended plant operations. The goals of the RISA Pathway are:

- To demonstrate risk assessment methods coupled to safety margin quantification that can be used by decision-makers as a part of their margin recovery strategies
- To apply the "RISA toolkit" to enable more accurate representations of safety margins for the long-term benefit of nuclear assets.

One of the research efforts under the RISA Pathway is the ERP system analysis, which supports the DOE and industry initiatives targeting improvements of the safety and economic performance of the current fleet of NPPs such as accident-tolerant fuel (ATF), diverse and flexible coping strategy (FLEX), passive cooling system designs, and advanced battery technologies. The concept of ERP refers to a NPP that is enhanced with various industry initiatives such as those described above. The objective of the ERP research effort is to use the RISA methods and toolkit in industry applications, including methods development and early demonstration of technologies, in order to enhance existing reactors' safety features (both active and passive) and to substantially reduce operating costs through risk-informed approaches.

The ERP R&D efforts in FY 2021 are focused on three industry initiatives, including ATF, FLEX, and advanced battery technology with extended capacity. One focus area of the ATF efforts is to extend the FY 2020 analyses (Ma, et al., 2020) on a generic boiling water reactor (BWR). The same analysis process and analysis tools as in the FY 2020 work were used with two near-term ATF cladding (i.e., Iron-Chromium-Aluminum [FeCrAl] cladding and Chromium [Cr]-coated cladding) designs under four types of postulated scenarios, including general transient, loss of main feedwater (LOMFW), small loss-of-coolant accident (SLOCA), and inadvertent open relief valve (IORV).

Another focus area of the ATF efforts is to conduct a benchmark study between two probabilistic risk assessment (PRA) models—one is the generic pressurized water reactor (PWR) SAPHIRE model used in the FYs 2018 and 2019 ATF analyses under the ERP project (Ma, et al., 2018; Ma, Z. et al., 2019a; Ma, Z., et al., 2019b), and the other is the plant-specific PRA model of a reference PWR plant in U.S.. The benchmark study was motivated by mutual interests of the ERP team and the reference plant. The reference plant is interested in whether the plant-specific PRA models are sufficiently similar to the generic SAPHIRE models used in the existing ATF analyses conducted under the ERP project. If similar enough, the reference plant could then use as many insights as possible from the existing ERP ATF work and avoid having to incorporate ATF into plant-specific PRA models to obtain separate risk insights. The ERP team is also interested in comparing the generic SAPHIRE models against the plant-specific PRA models to evaluate whether the model differences would affect the ATF analysis results. An agreement was reached between the ERP team and the reference plant to conduct a benchmark study between the generic SAPHIRE model and a representative plant-specific PRA model. A third-party consulting company, Jensen Hughes, was subcontracted to conduct the benchmark study.

The FLEX efforts are focused on continued development of a dynamic approach for FLEX human reliability analysis (HRA) with Event Modeling Risk Assessment using Linked Diagrams (EMRALD) (Prescott, Smith, & Vang, 2018). The efforts on the advanced battery technology include a risk impact analysis and an economic impact analysis of deploying batteries with extended capacity at a generic BWR plant. Besides the above three industry-initiative-focused analyses, the work of optimizing mitigating system performance index (MSPI) through advanced artificial intelligence (AI) and machine learning (ML) techniques is also planned under the ERP project and some preliminary work is done in the FY 2021.

The remaining sections of the report are organized as below: Section 2 presents the analysis tools used in this work; Section 3 provides a description for a generic RELAP5-3D BWR model used in this work and presents the model improvements made in the FY 2021; Sections 4 to 7 provide risk-informed analyses of different accident scenarios for two near-term ATF designs; Section 8 presents the benchmark study between the generic PWR SAPHIRE model and a plant-specific PRA model; Section 9 introduces the dynamic HRA approach for FLEX; Section 10 presents the risk and economic impact analyses for the advanced battery technology; Section 11 introduces the MSPI and the preliminary plan of the MSPI optimization process; and Section 12 provides a summary and the future work planning for the ERP project.

2. RISK-INFORMED ANALYSIS TOOLS

This section provides summarized descriptions of the computational tools used in the report. Although most of them were introduced in FYs 2018, 2019, and 2020 (Ma, et al., 2018; Ma, et al., 2019a; Ma, et al., 2019b; Ma, et al., 2020), the tools are described here in order for this report to be independent and complete.

2.1 SAPHIRE

SAPHIRE is a probabilistic risk and reliability assessment software tool developed and maintained by the INL for the U.S. Nuclear Regulatory Commission (NRC) (Smith & Wood, 2011). SAPHIRE can be used to model NPP response to both internal hazards (for example general transients, loss of offsite power [LOOP], loss of feedwater, etc.), and external hazards (e.g., seismic, fire, external flooding, and high wind). SAPHIRE 8, the current version, can be used to develop Level 1 PRA for core damage frequency (CDF) quantification, Level 2 PRA for containment failure and release category frequency (including large early release frequency [LERF]) evaluation for severe accidents in which core damage (CD) has occurred, and limited Level 3 PRA for release consequence analysis. SAPHIRE 8 is a powerful PRA software that has both the basic PRA modeling capabilities such as creating event trees (ETs) and fault trees (FTs), defining and assigning basic event failure data, linking and solving ETs and FTs, documenting and reporting the results and the advanced capabilities such as integrated Level 1 and Level 2 PRA analysis, performing sensitivity and uncertainty analyses, and conducting specialized analyses for the NRC's Accident Sequence Precursor Program (U.S. Nuclear Regulatory Commission, 2020) and Significance Determination Process (U.S. Nuclear Regulatory Commission, 2020). Figure 2-1 shows the graphic user interface for SAPHIRE 8.

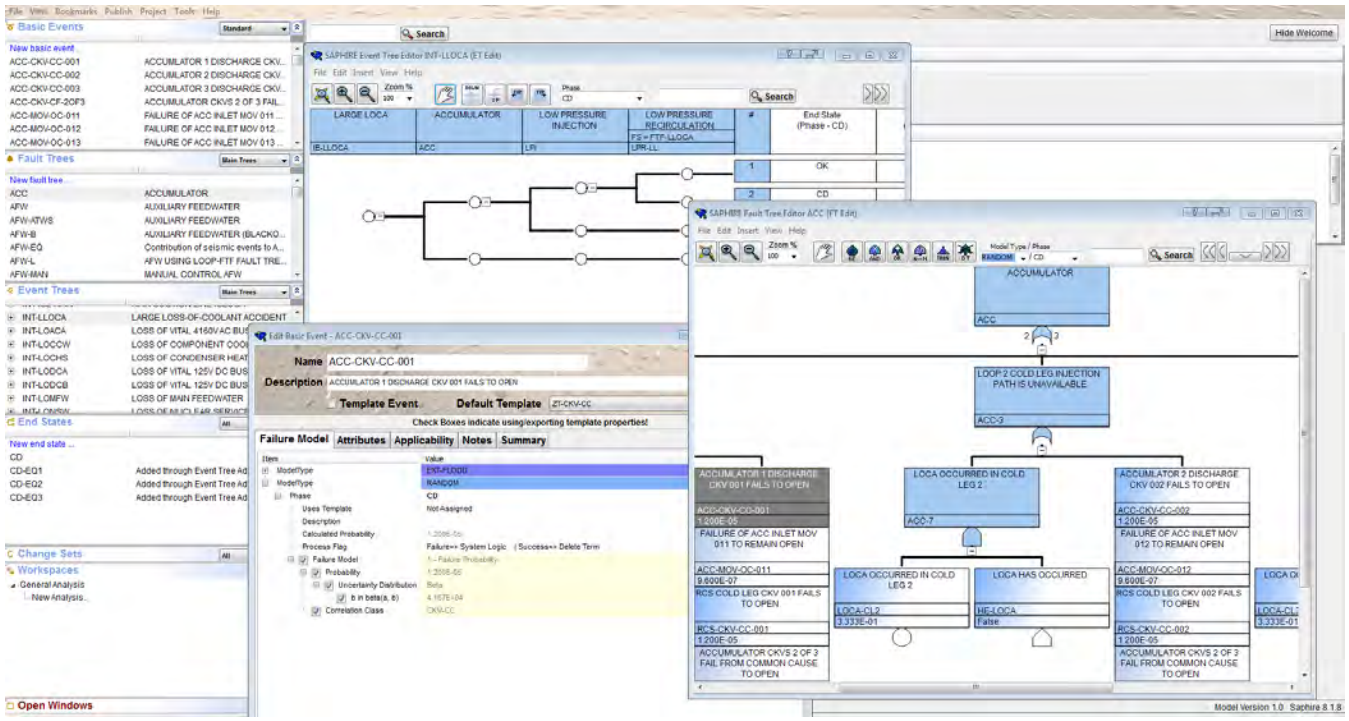

Figure 2-1. SAPHIRE 8 Graphic User Interface.

2.2 RELAP5-3D

RELAP5-3D code (RELAP5-3D Code Development Team, 2018) is the INL-developed best-estimate system thermal hydraulic (TH) code of the RELAP5 family. It is capable of performing transient simulations of light-water reactor systems during normal and accidental conditions (station blackout [SBO], both large and small loss-of-coolant accidents [LOCAs], anticipated transient without scram, loss of feedwater, main steam line break, etc.). RELAP5-3D has also been successfully used for modeling and simulations of the following systems: fusion reactors, space reactors, gas and liquid metal reactors, and cardiovascular systems.

The code solves a non-homogeneous and non-equilibrium model (unequal velocities and unequal temperatures) for the two-phase flow using a fast, partially implicit numerical scheme. RELAP5-3D differs from the other RELAP5 versions thanks to a multi-dimensional TH, a 3D neutron kinetic modeling capability, and an extensive library of different fluids properties. The code's development and validation are based on an extensive set of experimental data and its applicability to best estimate plus uncertainty technology (Schultz, 2015). In the ERP activities, the code is applied for the calculations of various accident scenarios for generic PWR and BWR designs. Simulations are run inside the code applicability range (i.e., until the code predicts the onset of the extensive fuel damage). The applicability range of RELAP5-3D is shown in Figure 2-2.

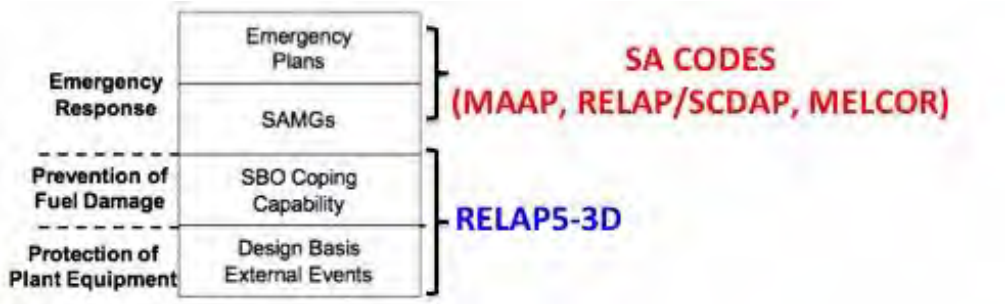

Figure 2-2. RELAP5-3D Role in LOOP and SBO Calculations.

References to the applicability of RELAP5 codes in simulating the above scenarios can be found in the open literature, for example (Prosek & Cizelj, 2013) and (Matev, 2006). Taking SBO and LOCA for instance, the clad temperature failure criteria reported in Table 2-1 were adopted. It should be noted for ATF, there are still not available fuel failure criteria. Therefore, for ATF it was decided to adopt the oxide shell failure temperatures as fuel failure criterion (Robb, Howell, & Ott, 2017). For Zircaloy, the established criterion for the emergency core cooling system (ECCS) from 10 Code of Federal Regulations (CFR) Part 50.46 (U.S. Nuclear Regulatory Commission, 2017) is that peak clad temperature (PCT) should not exceed 1477 K. However, for the purpose of having consistent comparisons, the fuel failure criterion for Zircaloy is also set as the oxide shell failure temperature.

Table 2-1. Failure Criteria for Different Fuel Clads.

Clad Type	Failure Criteria	
	LOCA	SBO
Zircaloy	PCT>2100 K	PCT>2100 K
ATF - FeCrAl	PCT>1804 K	PCT>1804 K
ATF – Cr-coated	PCT>1804 K	PCT>1804 K

Concerning ATF modeling and simulation, it should be noted MELCOR (Gauntt, et al., 2005), MAAP (EPRI, 2012), and TRACE (U.S. Nuclear Regulatory Commission, 2012) codes have been utilized previously to estimate the performance of various candidate ATF designs including FeCrAl and Cr-coated cladding materials. For instance, Wu and Shirvan (Wu & Shirvan, 2019) used TRACE to analyze near-term ATF claddings under BWR short-term and long-term SBO accidents. (Wang, Dailey, & Corradini, 2019) used MELCOR to evaluate the performance of ATF and reactor core isolation cooling (RCIC). In order to perform an effective study of the ATF candidate with the RELAP5-3D code for a BWR, additional code modifications to the oxidation model had to be implemented in FY 2020. The following paragraphs provide a description of the new oxidation model.

The capability of modeling a thin coating layer to the outside of fuel cladding was added to RELAP5-3D in this project. This coding change affects cylindrical heat structures for the fuel rods and rectangular heat structures for the fuel channels. The coating layer in the ATF designs is meant to protect the fuel cladding from oxidizing and degrading under high-temperature conditions. This oxidation reaction is of concern because it weakens the Zirconium cladding and also releases additional heat, which can increase the temperature in the reactor. The coating is designed to react instead of the cladding. A slow-reacting coating material should protect the cladding in the reactor and lengthen the lifetime of the reactor.

Note the change in outer fuel radius does not affect the flow geometry in the reactor core. The additional thickness in the cladding does not contribute to the heat conduction through the cladding. This change will protect the outer layer of the cladding from oxidation, the amount of heat generated due to the chemical reaction will be added to the heat structure, and the amount of chemical reaction product generated will be calculated.

A correlation developed by (Cathcart & et al., 1977) is used to model the metal-water reaction model in RELAP5-3D which uses a parabolic rate law. This default correlation was developed for the Zirconium-steam reaction. The code has been generalized to allow the user to model coolant-structure chemical interactions for which the parabolic rate law applies. The Cathcart correlation used in RELAP5-3D to calculate the thickness of the cladding converted to oxide is shown in Equation (2-1).

$$\Delta r^{n+1} = \left[(\Delta r^{n})^2 + (K\Delta t)e^{-(\Delta E/RT)}\right]^{1/2} \quad (2\text{-}1)$$

where:

$(\cdot)^{n+1}$	=	New time value
$(\cdot)^{n+1}$	=	Old time value
K	=	Reaction rate constant (9.166 x 10-7 m2/s, derived from the Cathcart model)
Δt		Time step size (s)
ΔE	=	Activation energy (35,890 cal/mole for the Cathcart model)
R	=	Gas constant (1.986 cal/K-mole)
T	=	Cladding temperature (K)

The amount of heat added (Q) to the outer surface of the cladding due to oxidation is calculated as follows.

$$Q = \rho\pi[(r_o - \Delta r^{n})^2 - (r_o - \Delta r^{n+1})^2]\frac{H}{W} \quad (2\text{-}2)$$

where:

r_o	=	Initial radius of unreacted cladding (cladding outer radius)
ρ	=	Cladding density (6,500 kg/m3 for Zirconium)
H	=	Reaction heat release (5.94 x 108 J/(kg-mole))
W		Molecular weight of cladding (91.22 kg/(kg-mole) for Zirconium)

Finally, the total hydrogen mass generated by the metal-water reaction is calculated by multiplying the mass of Zirconium reacted by the ration of the molecular weight of 4 hydrogen atoms to 1 Zirconium atom.

For the coating, the calculation of the thickness of the coating converted to oxide matches what is done for the cladding. The user can enter an initial coating thickness, material density, activation energy, reaction rate constant, reaction heat release, coating material molecular weight, and the molecular weight of the reaction product (typically hydrogen) divided by the coating material molecular weight.

At higher temperatures, the oxidation parameters can change significantly for both coated cladding and other ATF cladding types (e.g., full FeCrAl cladding). To account for this, additional input was added. The user can input a threshold temperature at which a transition occurs, followed by the usual input of material density, activation energy, reaction rate constant, reaction heat release, coating material molecular weight (although this should be a constant), and the molecular weight of the reaction product divided by the coating material molecular weight. Additional input was also added to allow the user to specify a transition temperature for the base-cladding or the full ATF cladding (FeCrAl). However, this option only allows the user to input a transition reaction rate constant.

The logic path for the metal-water reaction coding is shown in Figure 2-3, one potential logic path described here. When a coating layer is applied to the cladding, the coding first checks if the coating has oxidized through the entire thickness. If that is the case, the code will switch to performing the metal-water reaction calculations for the cladding material only. If the clad has broken, the metal-water reaction will be calculated for both the inner and outer surfaces of the cladding. If the outer surface heat structure temperature is greater than the specified

transition temperature, then the coding will switch to using the high-temperature parameters for the calculations. Other logic paths behave as shown in the figure.

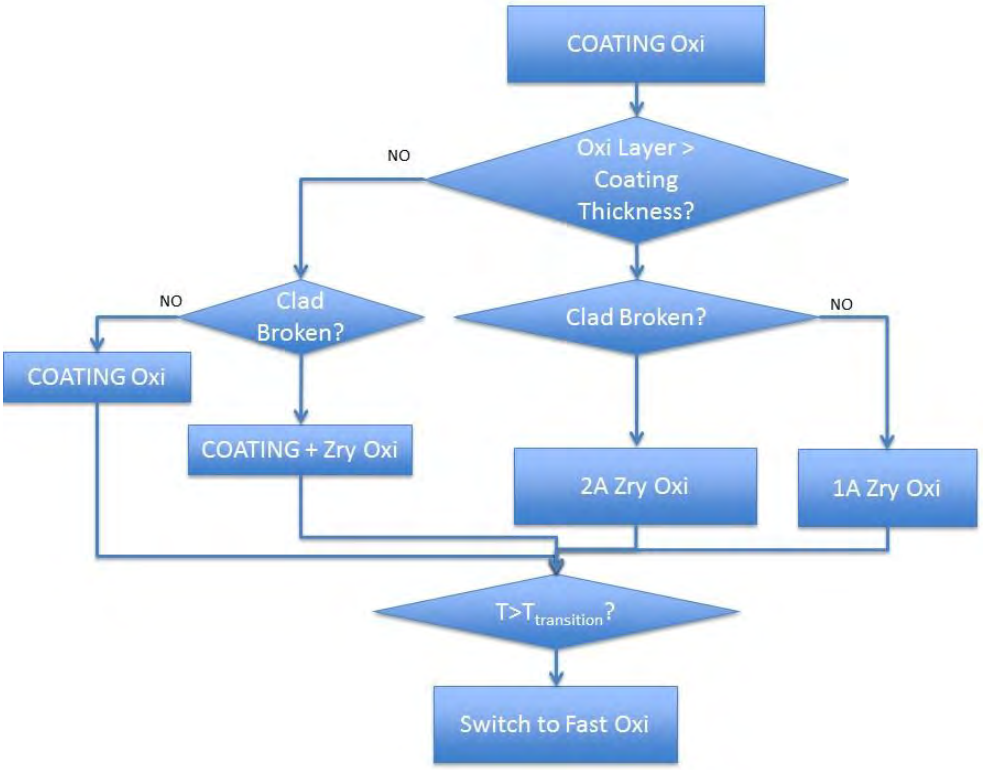

Figure 2-3. Logic Path for the Metal-Water Reaction Model Coding.

The changes to the input are as follows:

1CCCG002 Card, Coating Metal-Water Reaction Control	
W1(R)	Initial unreacted coating thickness on cladding's outer surface (m, ft).
W2(R)	Coating material density (kg/m^3). This quantity is optional, if not entered or 0.0 the default value for Zirconium (6,500 kg/m^3) is used.
W3(R)	Coating activation energy (cal/mole). This quantity is optional, if not entered or 0.0 the default value for the Cathcart model (35,890 cal/mole) is used.
W4(R)	Coating reaction rate constant (variable K) (m^2/s). This quantity is optional, if not entered or 0.0 the default value for the Cathcart model (2.252 x 10^{-6} m^2/s) is used.
W5(R)	Coating reaction heat release (J/kg-mole). This quantity is optional, if not entered or 0.0 the default value for the Zirconium-Steam reaction (5.94 x 10^8 J/kg-mole) is used.
W6(R)	Coating material molecular weight (kg/kg-mole). This quantity is optional, if not entered or 0.0 the default value for Zirconium (91.22 kg/kg-mole) is used.
W7(R)	Molecular weight of reaction product divided by Word 6. This quantity is optional, if not entered or 0.0 the default value for the Zirconium-Steam reaction (0.0442) is used.

W8(R)	Inner surface coating oxidation (for rectangular geometries only). To activate this option a real value greater than zero must be entered. Note that W8 of the 1CCCG003 Card must also be used to activate this option.
1CCCG005 Card, High-Temperature Coating Metal-Water Reaction Control	
W1(R)	Coating material transition temperature (K, F).
W2(R)	Coating material density (kg/m^3). This quantity is optional, if not entered or 0.0 the default value for Zirconium (6,500 kg/m^3) is used.
W3(R)	Coating activation energy (cal/mole). This quantity is optional, if not entered or 0.0 the default value for the Cathcart model (35,890 cal/mole) is used.
W4(R)	Coating reaction rate constant (variable K) (m^2/s). This quantity is optional, if not entered or 0.0 the default value for the Cathcart model (2.252×10^{-6} m^2/s) is used.
W5(R)	Coating reaction heat release (J/kg-mole). This quantity is optional, if not entered or 0.0 the default value for the Zirconium-Steam reaction (5.94×10^8 J/kg-mole) is used.
W6(R)	Coating material molecular weight (kg/kg-mole). This quantity is optional, if not entered or 0.0 the default value for Zirconium (91.22 kg/kg-mole) is used.
W7(R)	Molecular weight of reaction product divided by Word 6. This quantity is optional, if not entered or 0.0 the default value for the Zirconium-Steam reaction (0.0442) is used.
1CCCG003 Card, Cladding Metal-Water Reaction Control	
W8(R)	Initial oxide thickness on cladding's inner surface (m, ft). This quantity is optional for rectangular heat structures. This word must be entered to activate the calculation of the oxide thickness on the inner surface of a rectangular heat structure. The code sets this value to 0.0 for cylindrical or spherical heat structures. To activate this option a value less than or greater than zero must be entered. When less than zero, the initial oxide thickness is set to 0.0 m. When a value greater than zero is entered, the initial oxide thickness is the specified value. If 0.0 is entered, this option is ignored.
W9(R)	Cladding material transition temperature (K, F).
W10(R)	Cladding reaction rate constant (variable K) (m^2/s) at high-temperatures. This quantity is optional, if not entered or 0.0 the default value for the Cathcart model (2.252×10^{-6} m^2/s) is used.

2.3 EMRALD

EMRALD (Prescott, Smith, & Vang, 2018) is a dynamic PRA tool being developed at INL based on three-phase discrete event simulation. Traditional PRA modeling techniques are effective for many scenarios, but it is hard to capture time dependencies and any dynamic interactions using conventional techniques. EMRALD modeling methods are designed around traditional methods yet enable an analyst to probabilistically model sequential procedures and see the progression of events through time that caused the outcome. Compiling the simulation results can show probabilities or patterns of time-correlated failures.

An open communication protocol using the Extensible Messaging and Presence Protocol (XMPP) allows for easy coupling with other engineering tools. This coupling allows for direct interaction between the PRA model and physics-based simulations, so that simulated events can drive the PRA model and sampled PRA parameters can affect the simulation environment. The capabilities included in EMRALD permit PRA models to more easily and realistically account for the dynamic conditions associated with the progression of plant transient and accident sequences including accounting for the occurrence of modeled operator actions taken to mitigate the event.

3. GENERIC RELAP5-3D BWR MODEL

This section introduces the generic RELAP5-3D BWR model used in the report. Although most of the model details were introduced in FY 2020 (Ma, et al., 2020), they are described here from Section 3.1 to Section 3.4 in order for this report to be independent and complete. Also, the RELAP5-3D plant model for the generic BWR used in FY-20's analysis is improved to better simulate phenomena occurring during transient events. The model improvements are presented in Section 3.5.

The generic RELAP5-3D BWR model used in this study is based on a GE BWR/4 design with Mark I containment, representative of the U.S. BWR fleet and is shown in Figure 3-1 (U.S. Nuclear Regulatory Commission, 2012). The rated thermal power for this generic BWR is 3,293 MWth with 764 fuel assemblies (or bundles) in the core. The reactor pressure vessel (RPV), jet pumps, separator/dryer unit, main steam lines, main feedwater lines, recirculation loops, and the safety relief valves (SRVs) are modeled. Figure 3-2 shows the RELAP5-3D nodalization diagram for the generic BWR plant model. The base model can simulate the TH parameters of the primary side and of some parts of the containment. The reference base model with Zircaloy-clad was modified to include FeCrAl and Cr-coated as additional cladding material based on parameters from (Holzwarth & Stamm, 2002) and (Field, Snead, Yamamoto, & Terrani, 2017).

Table 3-1. Major Parameters for the Generic BWR.

	Value (SI Unit)
Rated Thermal Power (MWth)	3,293
Number of Fuel Assemblies (Bundles)	764
Core Mass Flow Rate (Kg/s)	11510
RPV Dome Normal Operating Pressure (MPa)	7.02
Feedwater Mass Flow Rate (Kg/s)	1681.3
Recirculation pump flow (Kg/s)	4278.6
Core mass flow rate (Kg/s)	11065.1
Bypass flow (Kg/s)	1266.2
Steam mass flow rate (Kg/s)	1681.3
Feedwater Temperature (K)	464.394
Feedwater Water Pressure (MPa)	7.2
RPV Inner Diameter (m)	6.38
RCIC Rated Flow (Kg/s)	37.8

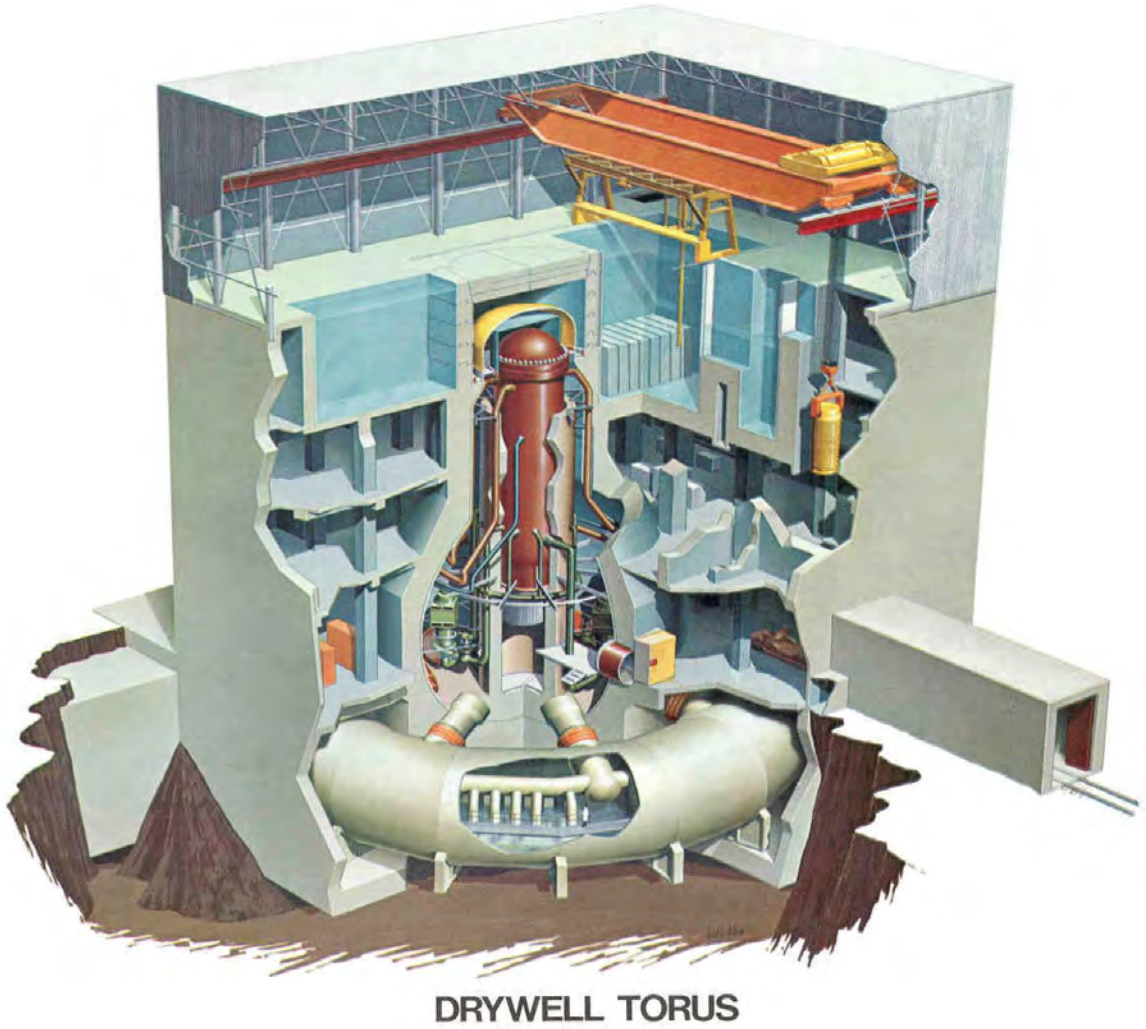

Figure 3-1. Cutaway Drawing of a BWR Mark I Containment Showing the Configuration of RPV, Recirculation Loop, Drywell, and Suppression Pool Torus (U.S. Nuclear Regulatory Commission, 2012).

The RELAP5-3D model developed for analyzing transient events is based on an input deck describing:

- RPV
- Main feedwater line
- Main steam line
- Jet pumps
- Recirculation loops
- Reactor core
- Steam separator
- Steam dryer
- Automatic depressurization system (ADS)
- SRVs

- High-pressure core injection (HPCI)
- RCIC
- Core spray (CS)
- Low-pressure core injection (LPCI)
- Firehose injection
- Control rod drive hydraulic system (CRDHS)
- Standby liquid control system (SLCS)
- Wetwell (WW)
- Drywell (DW)
- Vent lines from WW to DW.

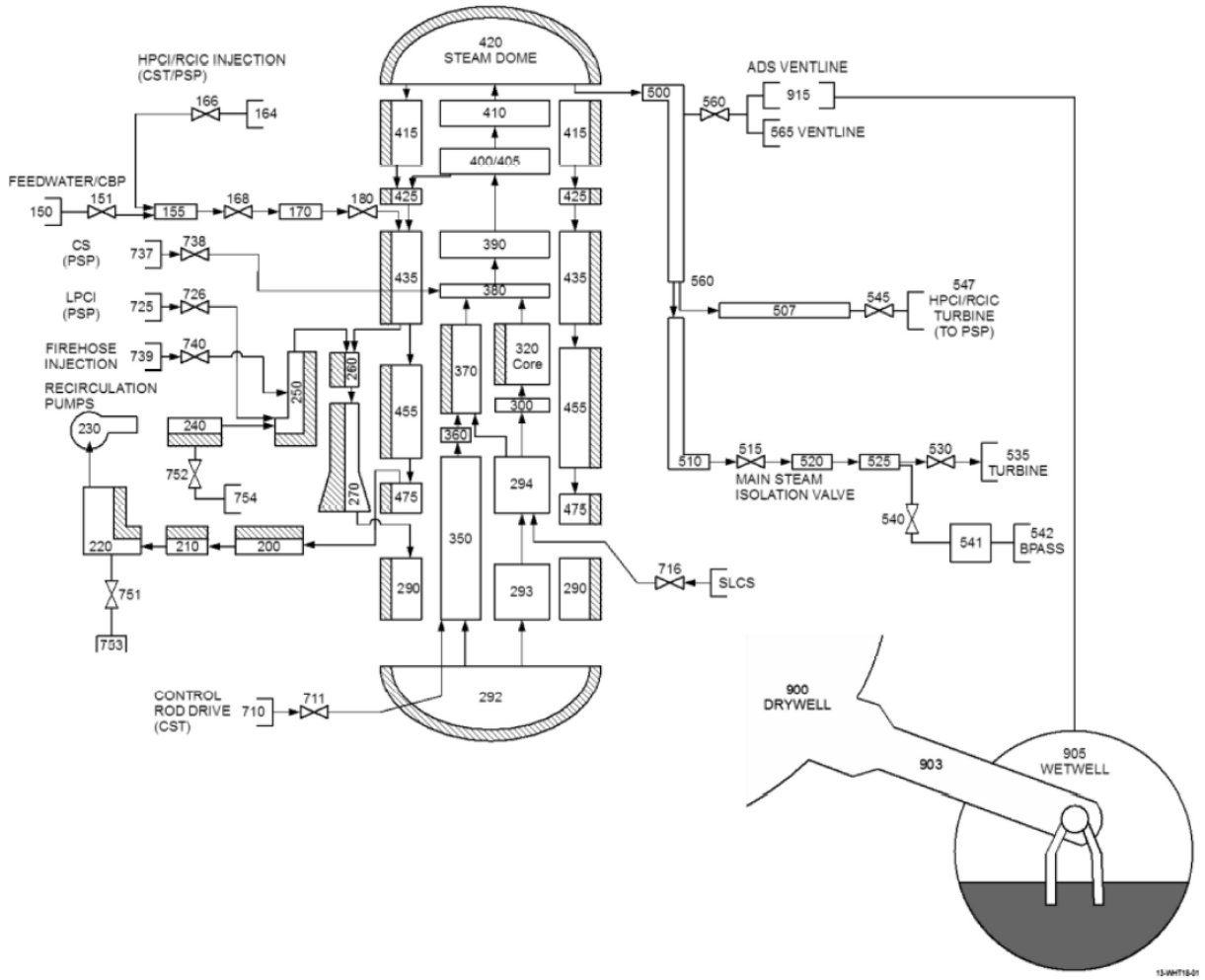

Figure 3-2. RELAP5-3D Nodalization Diagram.

3.1 TH Components

The modeling of the RPV includes the downcomer, lower plenum, core, upper plenum, standpipes, separator, dryer, and steam dome. The downcomer is modeled with a series of "Annulus" component. The steam separator unit is modeled with the "Simple Separator" component. The recirculation loops are lumped into one loop, and it includes a jet pump, a recirculation pump with pipes from pump suction/discharge. The recirculation pumps and jet pumps allow the operator to vary coolant flow through the core and hence change the power of the nuclear reactor. The jet pump components are located in the region between the core shroud and the vessel wall submerged in coolant. In order to limit the number of penetrations into the reactor vessel, the recirculation loops also serve as the residual heat removal (RHR) system. When the reactor is shut down, the core will continue to generate decay heat, which is removed by bypassing the turbine and dumping the steam directly to the condenser. RHR system provides shutdown cooling when pressure decreases to approximately 0.45 MPa.

The main feedwater lines are lumped into one. The feedwater systems are modeled using a series of "Pipe" components connected by junctions. The flow rates in the main feedwater line are controlled to maintain the desired downcomer water level in the RPV. High-pressure safety systems such as HPCI and RCIC will inject coolant through the main feedwater line. Finally, the main steam lines are lumped into one from three original steam lines. The main steam line has one main steam isolation valve (MSIV), turbine bypass valve (TBV), and turbine stop valve with the turbine modeled with boundary conditions (BCs).

The generic BWR model also includes a Mark I containment which consists of a DW, a WW, and vacuum breakers. The WW represents the suppression pool (SP) and the vapor space above it, which jointly form the torus in a typical BWR-4 design. The DW contains steam or liquid released from SBO, LOCA, etc. and minimizes radioactive leakage.

The WW is essentially a large tank of water which resides within containment of some BWR designs. WW refers to a pressure vessel which contains both a water pool and a non-condensable gas space. The WW water pool is commonly referred to as an SP because excess steam is condensed into this pool in order to suppress possible overpressure events. The SP is also called a suppression chamber or a pressure SP. It contains a large volume of fresh water and serves as heat sink for SRV discharged steam and exhaust steam from turbines in the high-pressure safety systems (i.e., HPCI and RCIC). The WW plays a vital safety role in SBO and other BWR accident scenarios in that it condenses released high-temperature steam vented from the DW to reduce containment pressure and provides a backup source of water for safety injection systems (the initial default is condensate storage tank [CST]). Steam can vent through the SRVs and/or the RCIC turbine exhaust into the WW where it condenses. The RCIC pump suction line draws water near the bottom of the WW pool to supply makeup water to the core. The steam injection and condensation taking place in the WW create momentum-induced mixing and buoyancy-induced thermal stratification. These two opposing phenomena determine the thermodynamic conditions of the WW and have a large effect on the overall performance of the RCIC System.

3.2 Safety Systems

The safety systems mainly involve coolant injection into RPV to prevent fuel damage under accident conditions and they can be categorized into high-pressure and low-pressure safety systems. In a typical BWR/4 plant, high-pressure safety systems include HPCI, RCIC, and ADS. Low-pressure safety systems include LPCI, low pressure CS, Firewater, SLCS, and CRDHS.

The RCIC system, as shown in Figure 3-3, provides makeup water to the RPV for core cooling when it is isolated from the secondary plant and the normal water supply to the RPV is lost and as a standby system for safe shutdown of the plant. It consists of a steam-driven turbine, turbine-driven pump, piping, and valves that are necessary to deliver core makeup water to the RPV at operating and accident conditions. The RCIC turbine is driven by high-pressure steam from the main steam lines, and the exhaust is discharged to the SP. The RCIC pump supplies makeup coolant from the CST or alternatively from the SP once the CST is drained to the reactor

via the main feedwater lines. CST contains a large volume of fresh water that can be used to cool the core. The RCIC system is nearly passive with the exception of requiring battery for control function. The functionality of RCIC is determined by a combination of factors, including the availability of direct current (DC) power, heat capacity temperature limits, RPV water level, and RPV pressures. When DC power is available, RCIC water injection is initiated automatically with a low-core water level signal or manually by the plant operator, and it is stopped automatically with a high-core water level signal or manually by the plant operator. When DC power is not available, RCIC can also be blackstarted and blackrun.

After a normal reactor shutdown, the RCIC turbine is driven by decay heat-generated steam and exhausts to the WW. The RCIC operates in this way until the vessel pressure and temperature are reduced sufficiently to the point the RHR system can come into operation. The RCIC system is actuated when: (1) the RPV is isolated from the main turbine and condenser, (2) SBO occurs and other systems are not available, or (3) feedwater flow is disrupted, and high pressure prohibits shutdown cooling system action. The RCIC system operates for a wide range of system pressures from normal operating pressure (~1135 psig) down to 150 psig. It is noted RCIC is not considered as a part of the ECCS and does not have an LOCA function; however, it does play an important safety role. LOCA accidents usually depressurize the RPV quickly, thereby disabling the RCIC system.

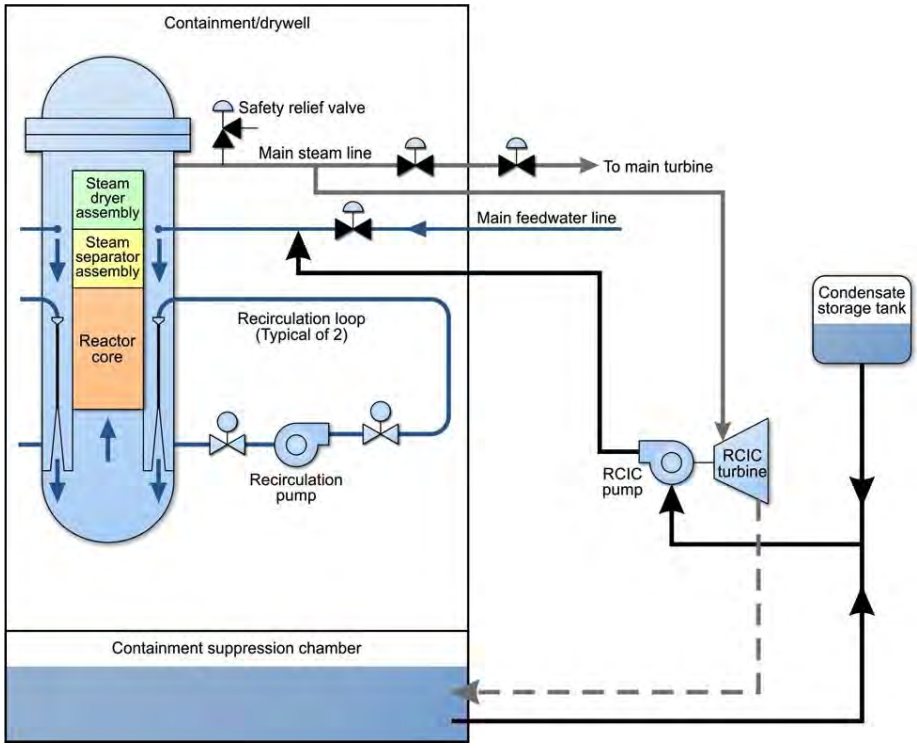

Figure 3-3. Schematic Illustration of RCIC System (U.S. Nuclear Regulatory Commission, 2012).

The HPCI system works in a similar way with RCIC, but it provides greater water injection rate (about 10 times greater than that of RCIC). It consists of a steam turbine-driven pump, valves and valve operators, and associated piping, including that from the normal and alternate pump suction sources and the pump discharge up to the penetration of the main feedwater line. It is a single-train system actuated by either a low reactor water level or a high-DW pressure. Just like RCIC, HPCI initially operates in an open loop mode, taking suction from the CST. When the level in the CST reaches a low-level setpoint, the HPCI system is aligned to the SP. HPCI is an independent ECCS system that requires no auxiliary AC power to provide makeup water to the core under small to intermediate size LOCA accidents. The main difference between HPCI and RCIC is the operation of HPCI will

rapidly depressurize the RPV due to its large steam release rate, while the steam-driven turbines of HPCI rely on high-pressure steam to operate.

There are 13 SRVs connected on the steam exit pipe of the main steam line. SRVs can be manually controlled with DC power to limit the RPV pressure in a prescribed range or obtain the controlled depressurization of the reactor. Following a normal reactor shutdown, or reactor scram under accident scenarios, the decay heat continues to generate steam, albeit at a reduced rate. The turbine bypass system diverts the steam to the condenser if the RPV is not isolated from the secondary plant, or the steam will be vented to the SP through operation of the SRVs when the RPV is isolated. Among the 13 SRVs, five valves also serve in the ADS which can be employed to complete depressurizing the RPV in a short period of time. Once the RPV is completely depressurized by ADS, no core cooling is available unless AC power is recovered.

Low-pressure ECCS systems such as low-pressure safety injection, low-pressure core spray (LPCS), and firewater can be aligned to the RPV to inject coolant to the core when AC power is available, and the RPV is depressurized. LPCI is the dominant mode of the RHR system. It takes water from the SP and discharges to the RPV to maintain the coolant inventory at a relatively low pressure. LPCS is capable of pumping water from the SP and spray it on top of fuel assemblies.

3.3 Reactor Core Modeling

The reactor core modeling consists of flow channels simulating the coolant flow within the fuel assembly channel boxes and heat structures attached to flow channels simulating the heat transfer within the fuel rods. There are two independent TH channels representing the coolant flow in the core—one hot channel and one average channel. The hot channel represents the flow in the fuel assembly with highest power and the average channel represents the flow for the remaining 763 fuel assemblies.

The fuel design used in the core modeling represents a state-of-the-art fuel design for BWRs based on publicly available GE14 design data. Figure 3-4 shows the side view of the GE14 fuel assembly design. The fuel assembly geometry is a 10×10 lattice. The cross-sectional view of the fuel assembly is shown in Figure 3-5. The basic fuel rod is comprised of a column of right circular cylinder fuel pellets enclosed by a cladding tube and sealed gas-tight by plugs inserted in each end of the cladding tube. The fuel pellets consist of sintered uranium-dioxide (UO2) or UO2-gadolinia solid solution ((U,Gd)O2) with a ground cylindrical surface, flat ends, and chamfered edges. Each full-length UO2 fuel rod may include natural enrichment UO2 pellets at each end of the fuel pellet column. The fuel rod cladding tube is comprised of Zircaloy-2 with a metallurgically bonded inner Zirconium layer. Each fuel rod includes a plenum at the top of the fuel rod to accommodate the release of gaseous fission products from the fuel pellets. This gas plenum includes a compression spring to minimize fuel column movement during fuel assembly shipping and handling operations while permitting fuel column axial expansion during operation. The GE14 fuel assembly contains 14 fuel rods, which are reduced in length relative to the remaining fuel rods. These rods are called part length rods. Fuel rods are internally pressurized with helium to reduce the compressive hoop stress induced in the cladding tube by the coolant pressure and to improve the fuel to cladding heat transfer. With the absence of known data, the fuel rod internal pressure is assumed to be 1 MPa.

Table 3-2. Fuel Parameters (Nuclear Engineering International, 2007)

Parameters	Values
Bundle assembly lattice	10 x 10
Number of full-length rods	78
Number of part length rods	14
Number of water rods	2
Active fuel length (cm)	368.91
Part length rod length (cm)	213.36
Rod to rod pitch (cm)	1.295

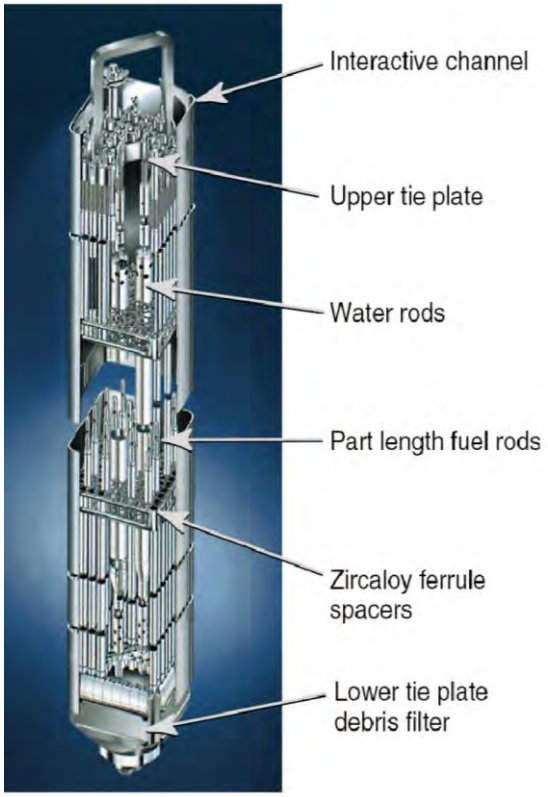

Figure 3-4. Side View of GE14 Fuel Assembly (U.S. Nuclear Regulatory Commission, 2011)

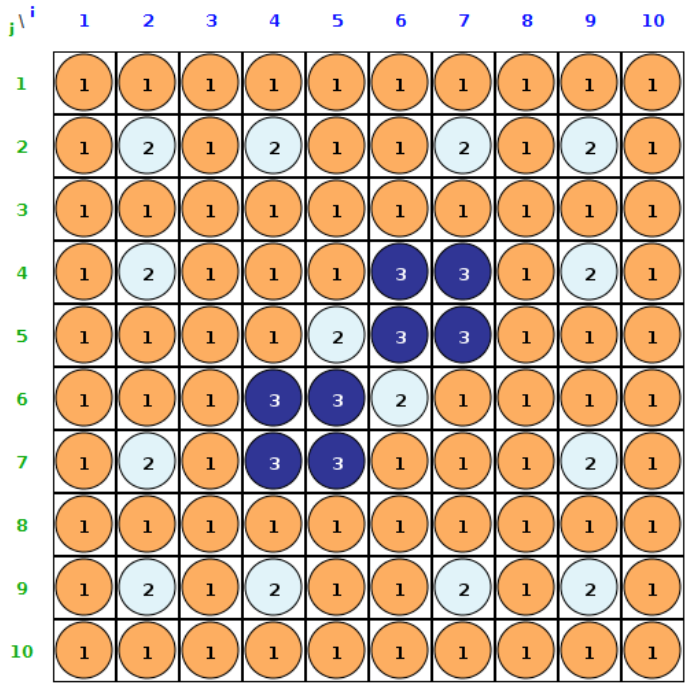

Figure 3-5. Cross-sectional View of the 10×10 Fuel Assembly Design. 1 Denotes Fuel Length Rods, 2 Denotes Part Length Rods, and 3 Denotes Water Rods.

Since the reactor core has 764 fuel assemblies, with 92 fuel rods within each assembly, the total number of fuel rods in the core is 70,288, which renders tracking individual fuel rods impractical in systems transient analyses. Therefore, homogenization techniques would be used to lump fuel rods and flow channels into manageable number. Different homogenization approaches are used for thermal fluid dynamics calculations for the two-phase flow in the fuel assemblies than for the heat conduction and clad oxidation calculations in the fuel rods. For the thermal fluid dynamics calculations, two flow channels are built to simulate the active flow within the fuel assemblies—the hot channel and the average channel. The hot channel represents the active flow within the hot assembly and the average channel represents the active flow in the remaining assemblies of the core. Hot assembly is the assembly with highest assembly power in the core.

For heat conduction and clad oxidation calculations, three sets of heat structures are built—one set represents the hot rod (highest power rod) in the hot assembly, another set represents the remaining 91 fuel rods in the hot assembly, and the third set represents the average of all the fuel rods in the remaining 763 fuel assemblies.

These homogenization approaches are reasonable as they: (1) greatly speedup the simulation time and (2) capture the flow behaviors in the hot channel as well as the temperature profiles and oxidation behaviors in the hot rod. As a result, heat structures for the hot rod in the hot assembly and the heat structures for the remaining fuel rods in the hot assembly are attached to the flow in the hot channel, as shown in Figure 3-6. Analogously, the heat structures for all the fuel rods in the remaining 763 assemblies are lumped into one set and are attached to the flow in the average channel, as shown in Figure 3-7.

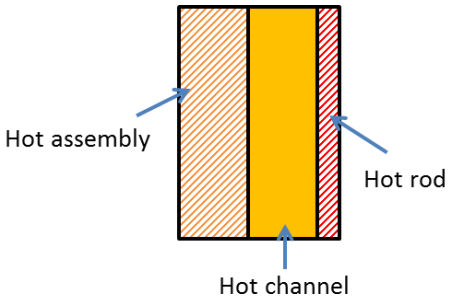

Figure 3-6. Schematic Illustration of the Heat Structure Mapping for the Hot Assembly and its Hot Rod with the Hot Channel.

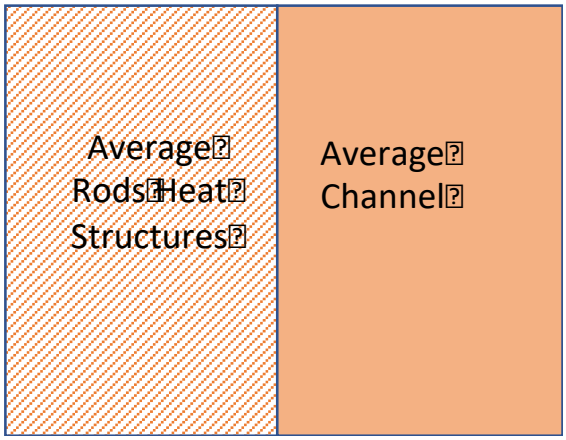

Figure 3-7. Schematic Illustration of the Heat Structure Mapping for the Average Assemblies and the Average Flow Channel.

The neutron energy spectrum can vary during an operation cycle to generate and utilize more plutonium from the non-fissile U-238 by changing the void fraction in the core through control of the core coolant flow rate. This operation method, which is called a spectral shift operation, is practiced in BWRs to save natural uranium. The core power shapes, as a function of cycle burnup state, have significant impact on the temperature distributions in the core. For a typical BWR core, the power shapes tend to be bottom-peaked near the beginning of the cycle (BOC). As the cycle depletion progresses, the power shapes gradually evolve into cosine shape near the middle of the cycle (MOC). Toward the end of the cycle (EOC), the power shapes tend to be top-peaked. In this analysis, operating conditions, in the form of maximum power verses exposure envelopes for GE14, are postulated which cover the conditions anticipated during normal steady-state operation and accident conditions. An example power-exposure envelope is shown in Figure 3-8, which is reproduced from the Global Nuclear Fuel's licensing topical report for GE14 fuel rod thermal-mechanical design report (Global Nuclear Fuel, 2006). The power shapes, shown in Figure 3-8, represent the maximum power verses exposure envelopes that cover conditions anticipated during normal steady-state operation and anticipated operational occurrences. The fuel rod axial power shape is changed three times during each cycle, BOC, MOC, EOC, and simulates the distribution effects of burnup. The three power shapes should provide bounding conditions for the evolving power shapes in the cycle.

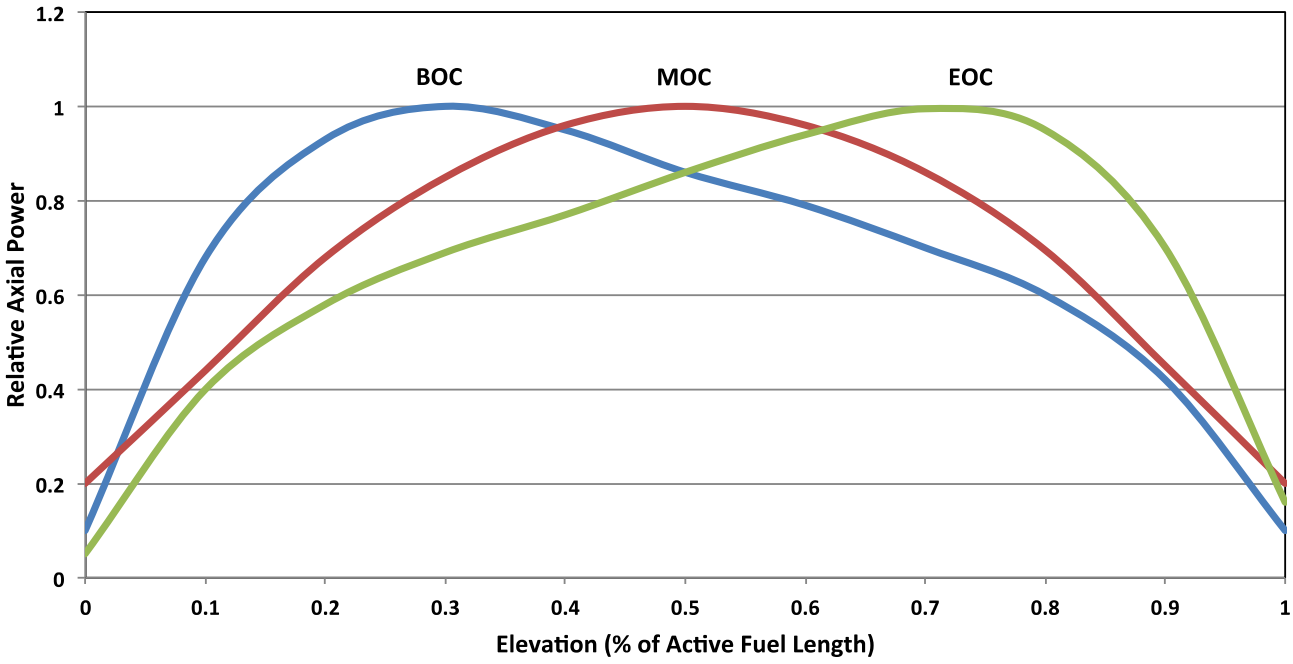

Figure 3-8. Core Axial Power Shapes Used in the RELAP5-3D Calculations (Global Nuclear Fuel, 2006).

3.4 Fuel Rod Geometry and Cladding Oxidation Kinetics

The specific fuel rod parameters used are shown in Table 3-3. The Zircaloy cladding is the baseline fuel design cladding. The outer radius of the fuel rod is identical for Zry and FeCrAl. For the Cr-coated cladding design, 15 microns in thickness of Cr-coating is applied to the outside surface of the baseline Zircaloy cladding; therefore, the outer radius of the Cr-coated cladding is 0.015 mm thicker than that of Zry and FeCrAl. Due to the higher neutron absorption rate of FeCrAl cladding, the thickness of FeCrAl cladding is reduced to half of the Zircaloy cladding. The pellet diameter is increased to keep the plenum gap size the same as the baseline fuel design with Zircaloy cladding.

Table 3-3. Fuel Rod Geometry for Reference and ATF Fuel Designs.

Cladding Type	Pellet Outer Radius (cm)	Cladding Inner Radius (cm)	Cladding Outer Radius (cm)
Zircaloy	0.438	0.45	0.513
Zircaloy + Cr-coating	0.438	0.45	0.5145
FeCrAl	0.4695	0.4815	0.513

The RELAP5-3D input deck uses the special cards developed for simulating the oxidation kinetics of ATF (both coated and non-coated clads). The ATF oxidation parameters were obtained from selected publications and implemented in the RELAP5-3D input deck. The main parameters for the oxidation kinetics and the fuel pin geometries are reported in Table 3-4.

For the FeCrAl clad, a transition temperature of 1773 K was selected. When the code calculates such temperature, the oxidation kinetics parameters are switched to the stainless-steel oxidation parameter (i.e., rapid oxidation). The failure criterion for both Cr-coated and FeCrAl is the PCT reaching 1804 K. Additional to performing heat conduction and oxidation calculations in a fuel rod, RELAP5-3D performs a simplified clad

deformation calculation. The empirical model included in RELAP5-3D was taken from the FRAP-T6 code. The purpose of the model is to consider a possible plastic deformation of the clad during an accident condition. The model can inform the user of a possible cladding rupture and of a possible flow blockage due to the hydraulic channel flow area reduction. Further investigation by specialized fuel pin mechanics codes, such as BISON, are needed if extensive plastic deformation or rupture of the clad are detected.

Table 3-4. RELAP5-3D Parameters for the Cladding Oxidation Kinetics.

Parameter	Cladding Type		
	Zry	Cr-coated	FeCrAl
Reaction Rate Constant (m^2 Metal/s)	9.166E-7	1.409E-5	2.444E-5
Reaction Heat Release (J/Kg-mole)	5.94E+8	6.48E+7	6.73E+7
Activation Energy (cal/mole)	35,890	66,890	82,218
Clad Density (kg/m^3)	6,500	7,190	6,860
Clad Molecular Weight (kg/kg-mole)	91.22	51.99	53.96
Ratio Molecular Weight Reactant/Clad	0.042	0.058	0.112

3.5 RELAP5-3D Generic BWR Plant Model Improvement

The RELAP5-3D plant model for the generic BWR used in FY-20's analysis is improved to better simulate the phenomena going on in the transients. The improvements are important for the scenarios involving the operations of the low-pressure safety injection systems such as CS and LPCI.

3.5.1 Steady-State Model Changes

The original model resulted in an unrealistic amount of liquid flowing from the WW to the DW during steady-state calculations and after the SRVs open. The WW originally is modeled with a pipe with 10 control volumes, and that model was later changed to a pipe with two control volumes. The two control volume torus model was used in the FY-20's analysis for SBO and MLOCA. In this work, this was improved by changing the WW model from a pipe with two control volumes to a pipe with three control volumes. The first volume was initially filled with liquid and represented the first five control volumes in the original ten-celled model. This first control volume was the same in both the two-celled and three-celled WW models. The second volume in the two-celled model, which was initially filled with gas, was divided into two volumes in the three-celled model. The second control volume in the three-celled model represents the sixth volume in the original ten-celled model. The third volume in the three-celled model represents control volumes sixth through tenth in the original ten-celled model. In addition, vent valves are modeled explicitly with Valve 906, which now connects the bottom of Volume 90503 in the WW with the bottom of the DW, Volume 90001. The vent valves alleviate the effects of WW pressurization during extended discharge through the SRVs. There are 12 18-inch swing check valves that open if the WW pressure exceeds the DW pressure by 0.5 psig. No attempt was made to model the opening and closing of the check valves. Valve 906 was assumed to stay open after it is opened. The input area of Valve 906 was 0.0858 ft^2. The following shows the input changes to the WW and vent valves between the WW and the DW.

```
*------------------------------------------------------------------------
9050000 torus  pipe
9050001 3
* vol_area
9050101 0.0  3
* Junc_area
9050201 10858.92 1
9050202 10578.45 2
* vol_length
9050301 15.0  1
9050302 3.0  2
9050303 12.0  3
* vol
9050401 126761.00 1
9050402 43108.9  2
9050403 94510.1  3
9050601 90.0  3
9050801 0.00015 0.0 3
9050901 0.0 0.0 2
9051001 00  3
9051101 1000  2
9051201 3 14.7 90.0 0.0 0.0 0.0 1
9051202 4 14.7 90.0 1.0 0.0 0.0 2
9051203 4 14.7 90.0 1.0 0.0 0.0 3
9051300 0
9051301 0.0 0.0 0.0 2
*
9060000 "wetvent" valve
9060101 905030001 900000000 0.0858 0. 0. 0100 1. 1.
9060201 0  0.0 0.0  0.0
9060300 trpvlv
9060301 565
```

Trip 565 was added to control the opening of the WW vent valves.

```
0000565 time 0  ge null 0 1.0e6 n * wetwell vent valve open
```

The trip is set so that the valves would not open during the steady-state calculation. The trip setpoint is changed to a mechanistic value in the transient calculation. The DW is pressurized so that its pressure is between 1.1 and 1.3 psia higher than the pressure of the WW. A time-dependent volume and single junction are connected to the drywell to maintain its pressure at 14.7 + 1.3 = 16.0 psia. At the end of the steady-state calculation, the DW and WW pressures are 16.0 and 16.3 psia, respectively. The WW pressure is higher than desired because the vent line (Component 903) is connected at the top of the fourth cell in the original ten-cell model but is connected to the top of the first cell in the current model, which corresponds to an elevation of the top of the fifth cell in the original model. The elevation change of the fifth cell in the original model is 3 ft which corresponds to hydrostatic head of about 1.3 psia. Thus, connecting the vent line at the correct elevation would reduce the WW pressure resulting in a better calculation of the differential pressure between the DW and the WW.

```
*
* dummy control volume to maintain drywell pressure at steady state
*
9070000 "dummy" tmdpvol
9070101 1.e6 1. 0.0 0. 0. 0.
9070102 0.0 0.0 00
9070200 4
9070201 0. 16.0 70. 0.
*
9080000 "dummy" sngljun
9080101 907010000 900010003 0.0 0.0 0.0 00100
9080201 0.0 0.0 0.0    *jc
```

The original model contains a control system that uses a heat source in the WW to conserve energy. The control system assumes the flow through the SRVs is steam. The same mass flow is added as liquid to the WW using Time-dependent Junction 916. Control Variable 906 then calculates the difference in the energy flowing from the reactor coolant system (RCS) and that entering the WW. This control variable is then applied as a heat source in Heat Structure Geometry 9051. This approach conserves both the mass flow and energy transfer to the WW if pure steam flows from the RCS. However, in the transients emergency core coolant (ECC) fills the reactor vessel enough that some liquid flows through the SRVs for a period of time. The existing control system assumes only steam flows through the SRVs and does not conserve energy when some liquid flows through the valves. The control system is revised to account for the possibility of liquid flow. Control Variable 904 calculates the specific enthalpy of the liquid entering the WW through Junction 916. Control Variable 906 calculates the difference in energy entering the WW and that leaving the RCS through Junction 560. The use of the flenth minor edit variable, which is the gas mass flow rate times the gas specific enthalpy plus the liquid mass flow rate times the liquid specific enthalpy, accounts for the actual state of the fluid leaving through Junction 560, regardless if the fluid is vapor, liquid, or a mixture of the two. The time-dependent junction, control system, and WW heat structure are probably used to get around thermodynamic property failures that could occur due to condensation in the WW.

```
* energy of the fluid leaving the RCS (assumes liquid entering the wetwell)
20590300 workin div 1.0 0.0 1
20590301 rhof 915010000 p 905010000
20590400 enthin sum 1.0 0.0 1
20590401 0.0 1.0 uf 915010000 1.0 cntrlvar 903
20590500 energin mult 1.0 0.0 0
20590501 mflowj 560000000 cntrlvar 903
20590600 energdif sum 1.0 0.0 0
20590601 0.0 1.0 flenth 560000000 -1.0 cntrlvar 905
```

The SRV flow in the original model discharges to Time-dependent Volume 815, which is assumed to be at atmospheric pressure. However, the pressure in the containment (WW and DW) increases substantially during the transient because of the steam discharge into the WW. The reactor coolant pressure decreases significantly after ADS actuation. Eventually, the flow through the SRVs unchokes and the differential pressure between the RCS and the WW becomes relatively small. The RCS and containment pressures are uncoupled in the current model, which is appropriate when the flow is choked but is not appropriate when the flow is unchoked. The two pressures should be closely coupled after ADS actuation. In preliminary transient calculations, the RCS pressure was at times more than 100 psi below the containment pressure whereas it should have been a little above containment pressure. To get around this unphysical result, the pressure in the time-dependent volume receiving the effluent of the SRV valves was coupled to the pressure of the WW. Time-dependent Volume 815 was changed to Time-dependent Volume 920 which referenced the pressure in Volume 90503. The thermodynamic state was changed

to pure steam rather than an air mixture to avoid code failures due to non-condensable appearance in the event of reverse flow from the time-dependent volume. The inputs needed to accomplish these changes are shown below.

```
*
* couple the rcs and containment pressures after ads
*
5600000 "safety" valve   *models 13 valves
5600101 500010000 920000000 1.1154 0. 0. 0100 1. 1.
5600201 0  0.0 0.0  0.0
5600300 srvvlv
5600301 044   *** 84% normal steam at set point.
*
*Not used for station blackout, it's a closed system other than CST injection
*
9200000 "ventline" tmdpvol
9200101 1.e6 1.0 0.0 0.0 0.0 0.0
9200102 0.000005 0.0 00
9200200 2 0 p 905030000
9200201 14.7 14.7 1.0
9200202 150. 150. 1.0
```

3.5.2 Transient Model Changes

Various trips were revised. The minimum volume of the CST is 300,000 gallons according to the BWR Simulator Training manual (GSE). The mass of water in the CST available for ECC injection is approximately MCST = 300,000 gal × $1ft^3$/ 7.48052 gal × $(0.3048 ft/m)^3$ × 1000 kg/m^3 = 1.136E6 kg. This value was included in Trip 501 to determine when the CST is empty.

```
0000501 cntrlvar 941   gt null 0 1.136e6 l *CST empty
```

According to Table B-2 of NUREG/CR-4165 (Dallman, et al., 1987), the WW SP water level varies between 175.25 and 181.25 inches. According to Page 20 of NUREG/CR-4165 (Dallman, et al., 1987), the suction of the high-pressure injection (HPI) system pumps switches from the CST to the WW after the WW level reaches 181.25 inches. The water level in the WW at the end of the steady-state calculation is 4.5726 m. The switch to WW injection is modeled when the WW level has increased by 6 inches from the steady value or 4.5726m + 6 inches x 0.0254 (m/inch) = 4.7250 m, which is reflected in Trip 402. The bearings in the HPI pumps are assumed to fail when the fluid temperature in the SP reaches 361 K (190ºF) based on Page 20 of NUREG/CR-4165 (Dallman, et al., 1987). This value is reflected in Trip 502.

```
0000402 cntrlvar 924 ge null 0 4.7250 l -1.0  *torus level has increased 6.00
inches from steady state
0000502 tempf 905010000 gt null 0 190.0
```

The design pressure of the DW and the WW is 56 psig per Page 2 of NUREG/CR-4165 (Dallman, et al., 1987). Trip 503 determines when the DW pressure exceeds its design value of 56 + 14.7 = 70.70 psia. The CS pumps are assumed to fail if the design pressure is exceeded.

```
0000503 p  900010000 gt null 0 70.70 l *greater than design pressure
```

The HPI logic is described below. The HPI is activated if the downcomer level drops below the lo-lo level (level 2) of 39.67 ft (see Trip 508). The HPI pumps are assumed to trip if the downcomer level exceeds 48.50 ft based on Table A 7 of NUREG/CR-4165 (Dallman, et al., 1987). Trip 507 simulates the high-level trip. The HPI initially takes suction from the CST but then switches to the WW when the WW level increases by 6 inches from

the steady value as described previously. The bearings in the HPI pumps are assumed to fail when the fluid temperature in the WW reaches 190ºF based on Page 20 of NUREG/CR-4165 (Dallman, et al., 1987). This value is reflected in Trip 502. The HPI also stops if the CST is empty, the containment exceeds its design pressure, or the pumps are manually tripped. The manual trip is simulated by setting Trip 509 to false. HPI flow occurs when Trip 613 is true. Time-dependent Volume 964 is used to simulate the switch from CST temperature to WW SP temperature.

```
0000402 cntrlvar 924 ge null 0 4.7250 l -1.0  *torus level has increased 6.00
inches from steady state
0000501 cntrlvar 941   gt null 0 1.136e6 l *CST empty
0000502 tempf 905010000 gt null 0 190.0 l
0000503 p  900010000 gt null 0 70.70 l *greater than design pressure
0000507 cntrlvar 008   ge null 0 48.5 n *high level
0000508 cntrlvar 008   le null 0 39.67 n *lo-lo level
0000509 time,0    le null 0 1440000. n *manual

*hpi logic
0000603  508  or  604 n
0000604  603  and  -507 n
0000610  604  and  509 n
0000611  610  and  -501 n * CST not empty
0000612  611  and  -502 n * Torus temp not high
0000613  612  and  -503 n * Containment not failed, hpis allowed

************************************************************************
* re-input hpi-src for switchover; code apparently cannot refer to a
* lower component number
************************************************************************
1640000 "c.s.tank" delete
9640000 "hpi-src" tmdpvol
9640101 1.e6  1.0  0.0  0.  90.  1.
9640102 0.0  0.0  00
9640200 3   402  tempf  905010000
9640201 70.0  70.7  70.0  *cst p & t
9640202 303.0  70.7  303.0  *max torus temp at design pressur
*
1660000 hpi tmdpjun *#5000 gpm, 5450000 conjugate
1660101 964000000 155000000 1.1175
1660200 0   613          *trip
1660201 0.  0.   0.  0.
*1660202 25.  1.196816 0.0  0.0 *# fsar ramp time
1660202 25.  11.1649 0.0  0.0 *# fsar ramp time

* hpi/rcic flow in gpm
20516600 "hpi/rci" div  15851.339 0.0  1
20516601 rhof 964010000 mflowj 166000000

20593800 "notswch" tripunit 1.0  0.0  1 * hpi switchover has not occurred
20593801   -502
20593900 "hpifcst" mult  1.0  0.0  1 * kg/s
20593901 cntrlvar 938 mflowj 166000000
* sum of ecc flows
20594000 "tecc" sum 1.0 0.0 1  * kg/s
20594001 0.0  1.0 cntrlvar 939  * rcic/hpci
20594002   1.0 mflowj 726000000 * lpci
```

```
20594003   1.0 mflowj 738000000 * core spray
```

Components 907 and 908, which are used to obtain the desired initial drywell pressure in the steady-state calculation, are deleted in the transient calculation. Control Variables 921 through 923 are also re-entered to that the integrals could be used for transient mass balances. Trip 565 is re-entered to input a mechanistic value for the transient calculation. According to Page B4 of NUREG/CR-4165 (Dallman, et al., 1987), the vacuum relief valves in the WW open if the WW pressure exceeds the DW pressure by 0.5 psi. According to Page B4 of NUREG/CR-4165 (Dallman, et al., 1987), the DW is pressurized by about 1.2 psi compared to the WW during normal operation. The differential pressure between the WW and the DW changes from about −1.2 psi during normal operation to 0.5 psi when the vent valves open for a total change of 1.7 psi. The calculated DW and WW pressures at steady state are 16.000 and 16.325 psi. The calculated differential pressure at steady state is 0.325 psi. Thus, the vacuum relief valves are assumed to open at a differential pressure of 0.325 + 1.7 = 2.025 psi.

```
*
* reset containment parameters
*
9070000 "dummy" delete
9080000 "dummy" delete
*
20592100 "srvflow" integral 1.0   0.0   0 0
20592101 mflowj 916000000        * (kg)
20592200 "to-dryw" integral -1.0   0.0   0 0
20592201 mflowj 900010000        * (kg)
20592300 "vent"  integral 1.0   0.0   0 0
20592301 mflowj 906000000        * (kg)
*
0000402 cntrlvar 924 ge null 0 4.7250 l -1.0  *torus level has increased 6.00
inches from steady state
0000565 p 905030000 ge p 900010000 2.025 l -1.0 *dp has increased by 1.7 psi from
steady state
```

Time-dependent Junction 925 and Time-dependent Volume 930 are added to the model to remove the same amount of water from the WW as was injected by the HPI and CS and LPCI systems when they are drawing suction from the WW. The flow area of the junction was arbitrarily set to that of the CS (Junction 738). Control Variable 939 calculates the flow rate removed from the WW by the HPI and core spray/LPCI in SI units (kg/s). A factor of 2.2046 lbm/kg was added to the second words of Cards 9250201 and 9250202 to account for the conversion from SI to British units. Control Variables 931 through 934 are used to calculate the amount of core spray that comes from the WW and the amount that comes from the CST. Control Variables 935 through 937 calculate the amount of HPI that comes from the WW and CST. The total ECC flow rate from the torus and the CST are calculated in Control Variables 939 and 940, respectively. The control system currently assumes all the low-pressure injection comes from the WW. The integrated mass flows from the CST and torus are calculated with Control Variables 941 and 942, respectively. Control Variable 941 is used in Trip 501 to determine when the CST is empty. Trip 403 determines if the core spray pumps take suction from the torus or the CST. The core spray/LPCI pumps take suction from the WW SP if Trip 403 is true. They take suction from the CST if Trip 403 is false.

```
************************************************************************
*
* Actually remove flow from the suppression pool when ECC pumps take suction from
the suppression pool
*
9250000 "eccftor" tmdpjun *
9250101 905010001 930000000 1.7044
9250200 1   0  cntrlvar 939 * conversion from kg/s to lbm/s built into the table
9250201 0.0  0.0  0.0  0.0
9250202 10000. 22046. 0.0  0.0
*
9300000 "eccsink" tmdpvol
9300101 1.e6  1.  0.0  0.  0.  0.
9300102 0.0  0.0  00
9300200 3
9300201 0.0  70.7  70.0

20593100 "csfmtor" tripunit 1.0  1.0  1 * cs takes suction from torus
20593101    403
20593200 "csfmcst" sum  1.0  0.0  1 * cs takes suction from cst
20593201 1.0  -1.0 cntrlvar 931
20593300 "csm-tor" mult  1.0  0.0  1 * cs mass flow from torus, kg/s
20593301 cntrlvar 931 mflowj 738000000
20593400 "csm-cst" mult  1.0  0.0  1 * cs mass flow from cst, kg/s
20593401 cntrlvar 932 mflowj 738000000
*
20593500 "notswch" tripunit 1.0  0.0  1 * hpi switchover has not occurred
20593501   -402
20593600 "hpiswch" sum  1.0  0.0  1 * hpi switchover has occurred
20593601 1.0  -1.0 cntrlvar 935
20593700 "hpifcst" mult  1.0  0.0  1 * hpi flow from cst, kg/s
20593701 cntrlvar 935 mflowj 166000000
20593800 "hpiftor" mult  1.0  0.0  1 * hpi flow from torus, kg/s
20593801 cntrlvar 936 mflowj 166000000
* sum of ecc flows from torus
20593900 "tecctor" sum 1.0 0.0 1  * kg/s
20593901 0.0  1.0 cntrlvar 938  * rcic/hpci
20593902   1.0 mflowj 726000000 * lpci (assumes lpci always comes from torus)
20593903   1.0 cntrlvar 933  * core spray
* sum of ecc flows from cst
20594000 "tecccst" sum 1.0 0.0 1  * kg/s
20594001 0.0  1.0 cntrlvar 937  * rcic/hpci
20594002         * lpci (assumes lpci always comes from torus)
20594003   1.0 cntrlvar 934  * core spray
*
20594100 "iecccst" integral 1.0 0.0 1  * integrated flow from cst, kg
20594101 cntrlvar 940
*
20594200 "iecctor" integral 1.0 0.0 1  * integrated flow from torus, kg
20594201 cntrlvar 940

0000403 time  0 ge null 0 -1.0 l 0.0  *spray suction from suppression pool
```

4. RISK-INFORMED ATF ANALYSIS OF BWR GENERAL TRANSIENT SCENARIOS

The risk-informed analysis of near-term ATF designs for BWR general transient scenarios is presented in this section. The BWR general transient SAPHIRE model and scenarios are presented in Section 4.1. The RELAP5-3D analyses of ATF designs for the general transient scenarios are presented in Section 4.2. The analysis results are summarized in Section 4.3.

4.1 BWR General Transient SAPHIRE Model and Scenarios

The generic BWR general transient SAPHIRE model starts with the occurrence of a general plant transient. The model includes a main event tree TRANS (general transient) and four transfer trees including 1SORV (one stuck-open SRV), 2SORVS (two stuck-open SRVs), ATWS (anticipated transients without scram), and LOOP. The event tree structures are shown from Figure 4-1 to Figure 4-6.

The ETs are quantified with SAPHIRE 8 using a truncation level of 1E-12 per reactor year. There are 236 CD sequences with a total general-transient-induced CDF of 3.89E-06 per reactor year. Among the 236 CD sequences, 68 sequences have non-zero (or non-truncated) CDF; 13 sequences have greater-than-0.1% contribution to total general-transient-induced CDF with a sum of 98.8% of total TRANS CDF. The 13 sequences are shown in Table 4-1.

Table 4-1. BWR General Transient Sequences with Greater-Than-0.1% CDF Contribution.

No.	BWR TRANS Sequence	CDF	Group	RELAP5 Scenario
1	TRANS:71	2.76E-06	TRANS	TRANS-1
2	TRANS:10	4.56E-07	TRANS	TRANS-2
3	TRANS:45	2.75E-07	TRANS	TRANS-3
4	TRANS:72-55	1.14E-07	SORV	TRANS-SORV-1
5	TRANS:72-23	3.75E-08	SORV	TRANS-SORV-2
6	TRANS:72-35	2.68E-08	SORV	TRANS-SORV-3
7	TRANS:72-28	6.13E-09	SORV	TRANS-SORV-4
8	TRANS:74-34	5.02E-08	LOOP	TRANS-LOOP-1
9	TRANS:74-09	3.06E-08	LOOP	TRANS-LOOP-2
10	TRANS:74-35-21	2.97E-08	LOOP	TRANS-LOOP-3
11	TRANS:74-37-03-17	1.28E-08	SBO	TRANS-SBO-1
12	TRANS:75-05	3.39E-08	ATWS	TRANS-ATWS-1
13	TRANS:75-10	9.13E-09	ATWS	TRANS-ATWS-2

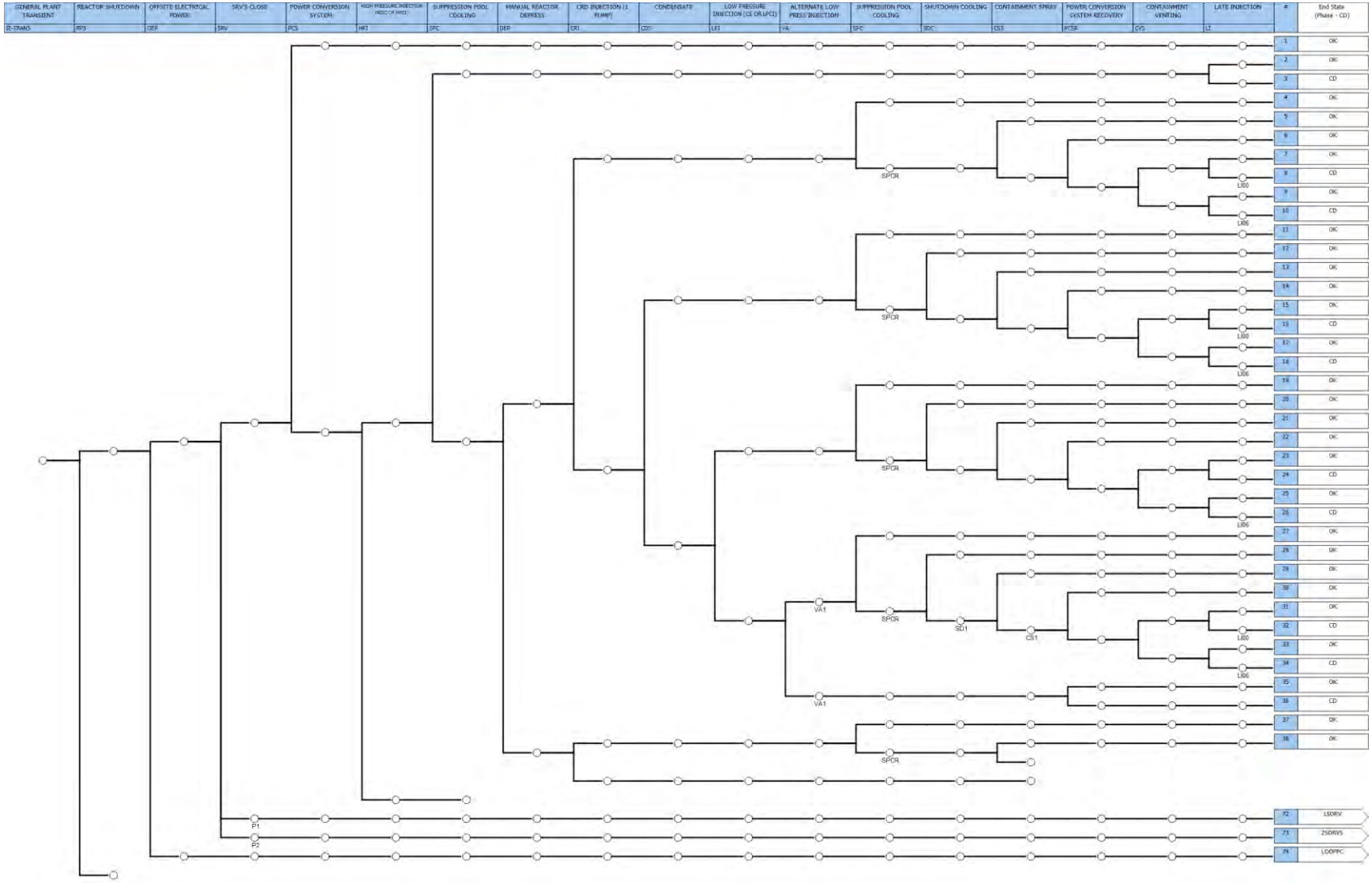

Figure 4-1. Generic BWR TRANS Event Tree (First Half).

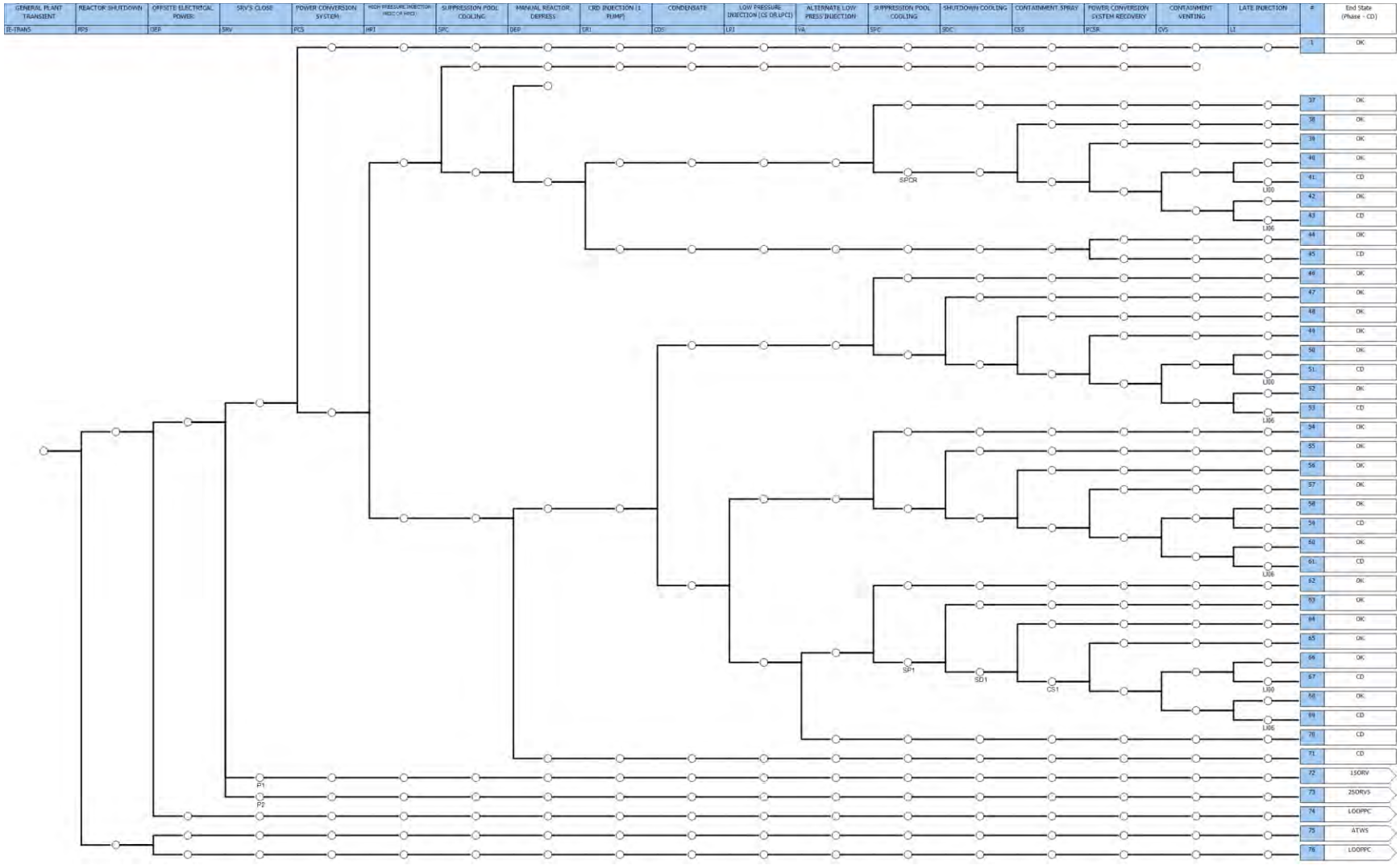

Figure 4-2. Generic BWR TRANS Event Tree (Second Half).

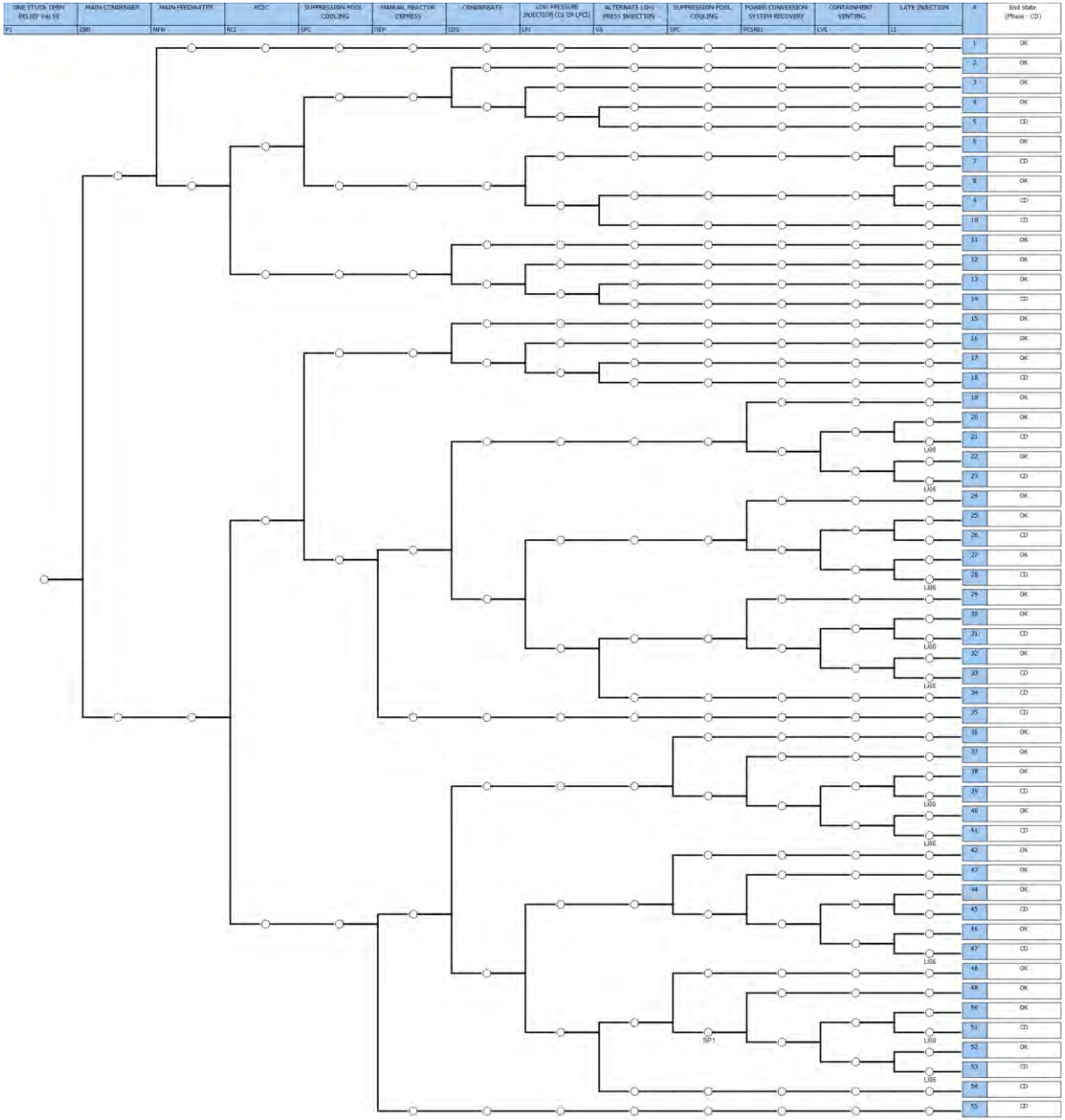

Figure 4-3. Generic BWR 1SORV Event Tree.

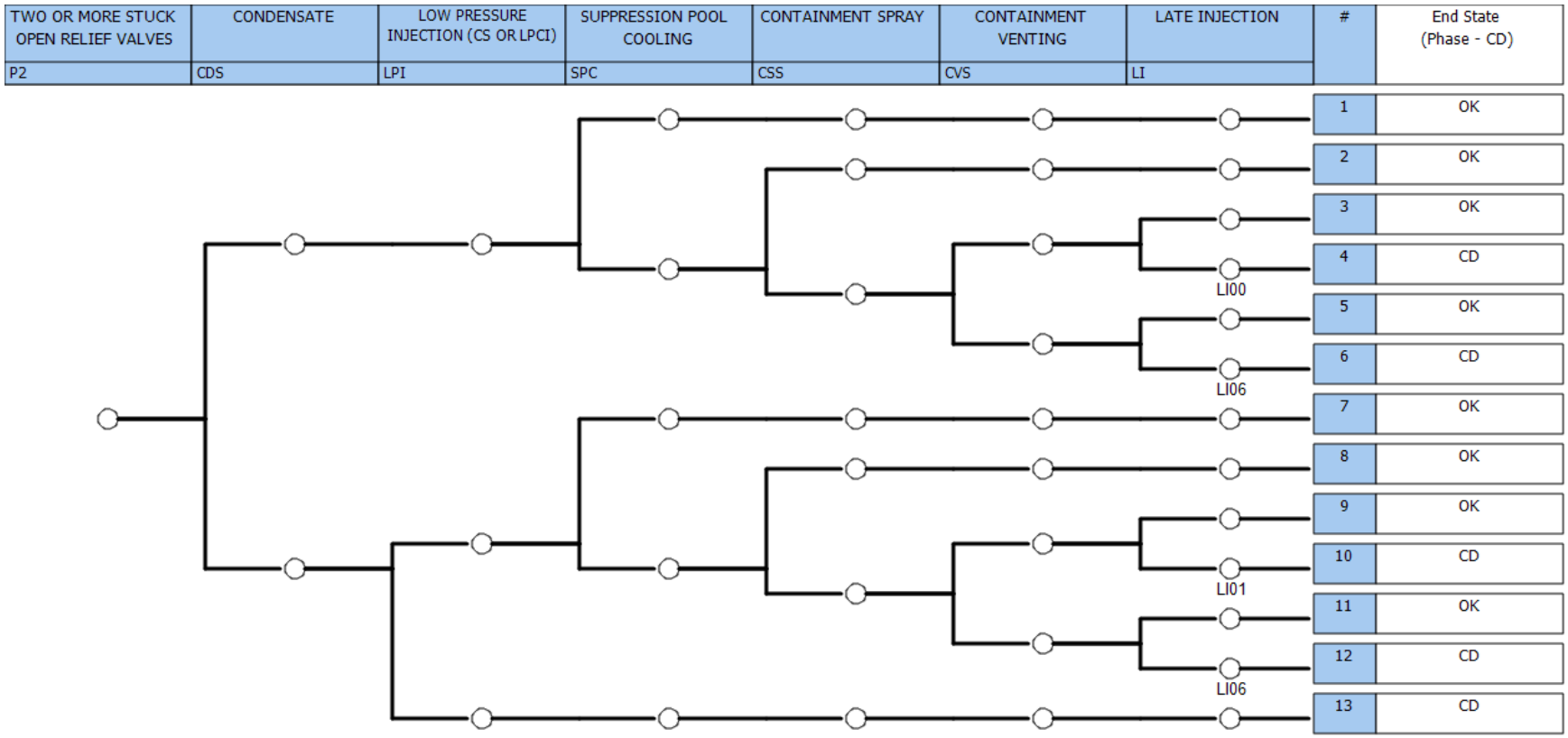

Figure 4-4. Generic BWR 2SORVS Event Tree.

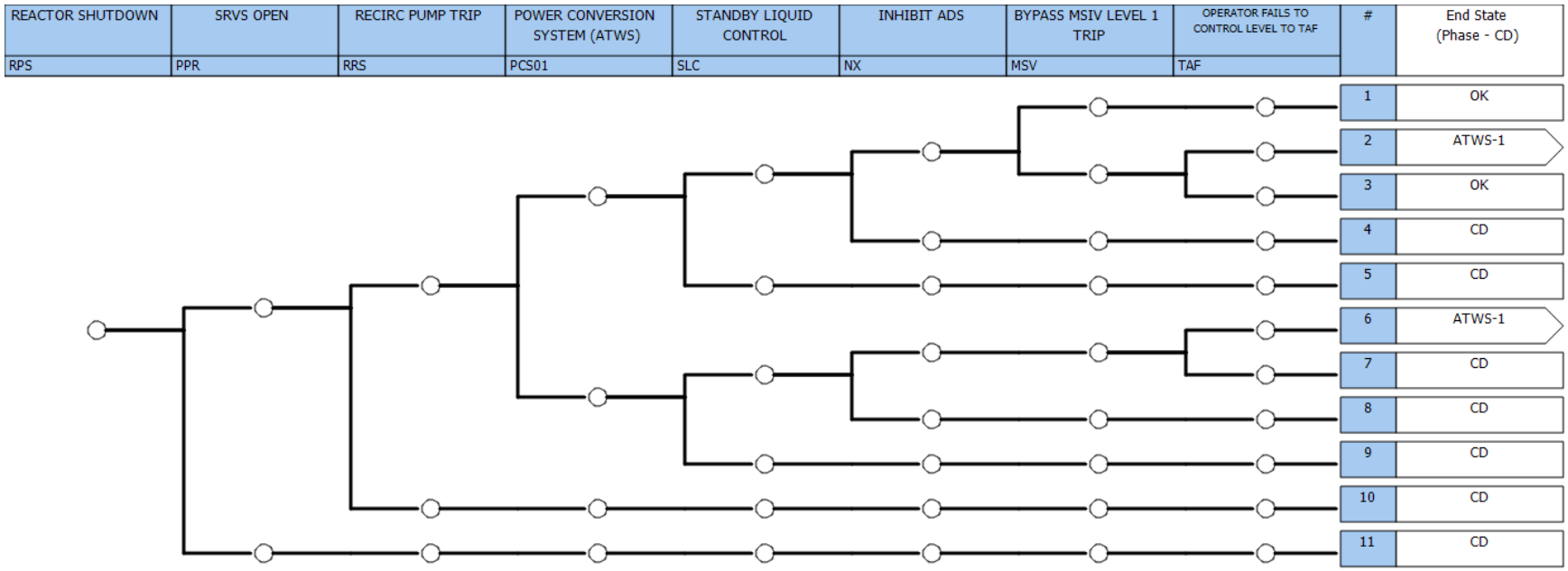

Figure 4-5. Generic BWR ATWS Event Tree.

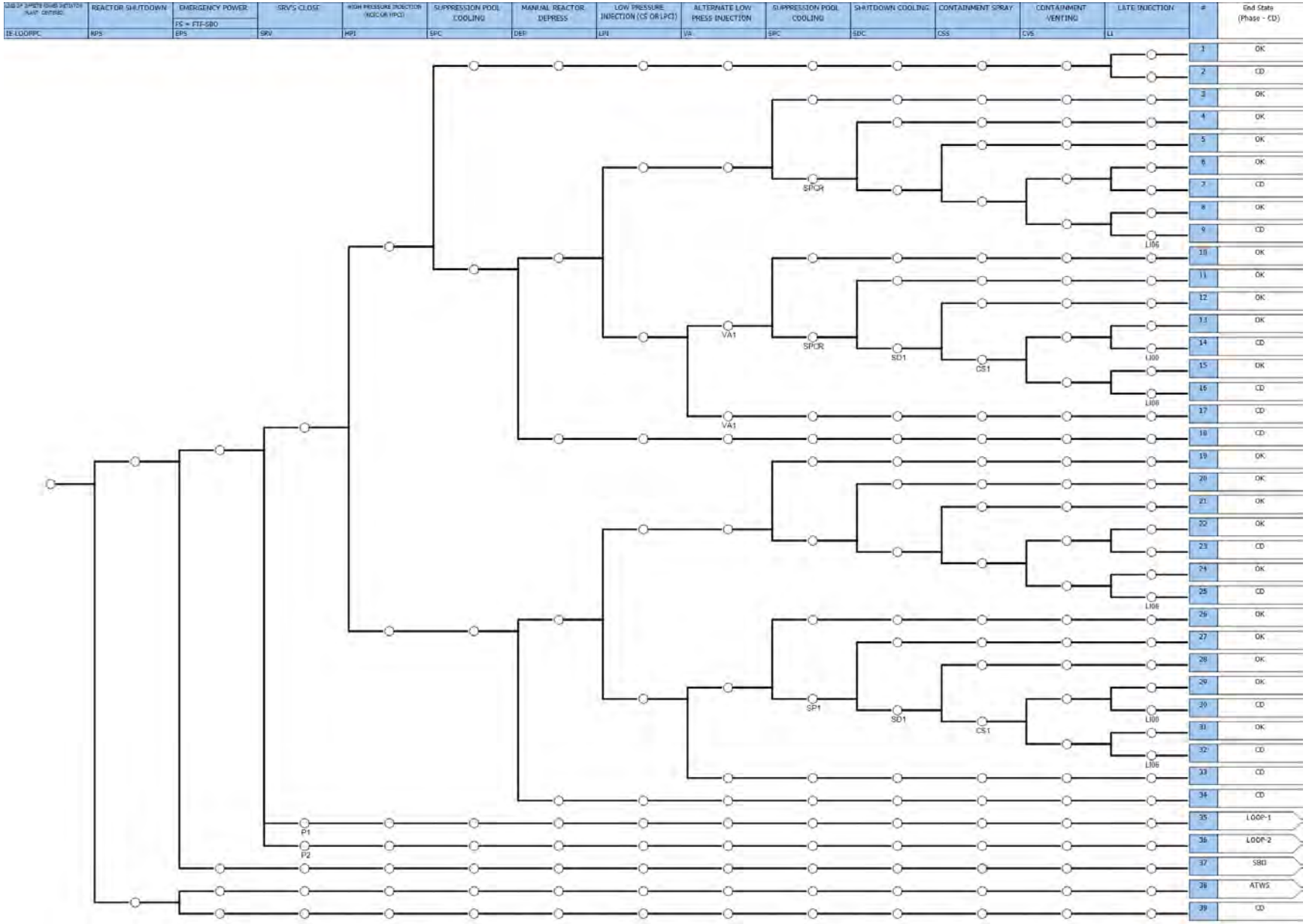

Figure 4-6. Generic BWR LOOP Event Tree.

The 13 sequences can be grouped into four categories:

- Three TRANS scenarios with no further transfer, TRANS-1 to TRANS-3
- Four SORV scenarios transferred from general plant transient, TRANS-SORV-1 to TRANS-SORV-4
- Three LOOP scenarios and one station blackout (SBO) scenario transferred from general plant transient, TRANS-LOOP-1 to TRANS-LOOP-3 and TRANS-SBO-1
- Two ATWS scenarios transferred from general plant transient, TRANS-ATWS-1 and TRANS-ATWS-2.

Two TRANS-LOOP scenarios (TRANS-LOOP-1 and TRANS-LOOP-3) are the same as scenarios TRANS-1 and TRANS-SORV-1, respectively, except for their sources of AC power—the LOOP scenarios use emergency power and the TRANS and TRANS-SORV scenarios use offsite power. As this difference will not lead to difference in RELAP5-3D modeling, the two TRANS-LOOP scenarios can be enveloped by the TRANS and TRANS-SORV scenarios. Also, the TRANS-SBO scenario can be enveloped by the SBO-1 scenario analyzed in FY 2020 (Ma, et al., 2020). The TRANS-LOOP/SBO scenarios, except for scenario TRANS-LOOP-2, are thus excluded and not passed on to RELAP5-3D analysis.

Besides the remaining 10 sequences selected based on PRA-estimated risk significance, four sequences (including TRANS-4, TRANS-SORV-5, TRANS-ATWS-3, and TRANS-ATWS-4) are selected for RELAP5-3D analysis either based on Jensen Hughes' recommendations or to make the selected accident spectrum more complete by including a scenario with two stuck-open SRVs. Hence, a total of 14 general transient scenarios were developed for RELAP5-3D analysis with short descriptions provided in Table 4-2 and detailed mitigating system statuses provided from Table 4-3 to Table 4-6.

Table 4-2. BWR General Transient Scenarios Selected for RELAP5-3D Analysis: Scenario Description.

No.	RELAP5 Scenario	Scenario Description[a]
1	TRANS-1	General transient, RCS inventory control failed (no HPI or DEP)
2	TRANS-2	General transient, containment heat removal failed
3	TRANS-3	General transient, RCS inventory control failed (no DEP)
4	TRANS-4	General transient, RCS inventory control failed (no LPI)
5	TRANS-SORV-1	1 stuck-open SRV, RCS inventory control failed (no HPI or DEP)
6	TRANS-SORV-2	1 stuck-open SRV, containment heat removal failed (using condensate system for RCS inventory control)
7	TRANS-SORV-3	1 stuck-open SRV, RCS inventory control failed (no DEP)
8	TRANS-SORV-4	1 stuck-open SRV, containment heat removal failed (using LPI for RCS inventory control)
9	TRANS-SORV-5	2 stuck-open SRVs, containment heat removal failed
10	TRANS-LOOP-1[b]	LOOP, containment heat removal failed
11	TRANS-ATWS-1	ATWS, reactivity control failed
12	TRANS-ATWS-2	ATWS, power control failed
13	TRANS-ATWS-3	ATWS, RCS inventory control failed (no DEP)
14	TRANS-ATWS-4	ATWS, RCS inventory control failed (no LPI)

a. Acronyms include: DEP = manual reactor depressurization, HPI = high-pressure coolant injection, which can be achieved using HPCI or RCIC, LPI = low-pressure coolant injection, which can be achieved using LPCI or core spray.

b. Renumbered from scenario TRANS-LOOP-2 in Table 4-1.

- **TRANS-1:** A general transient initiating event (IE) occurs, reactor automatically shuts down, AC power is available, all SRVs are successfully opened and reclosed, but power conversion system (PCS) fails. HPI fails to maintain RCS inventory. Neither does DEP succeed to allow LPI. CD occurs.

- **TRANS-2:** A general transient IE occurs, reactor automatically shuts down, AC power is available, all SRVs are successfully opened and reclosed, but PCS failed. RCS inventory is successfully maintained initially through HPI and later through DEP plus control rod drive injection. However, CD occurs due to failure of decay heat removal.
- **TRANS-3:** A general transient IE occurs, reactor automatically shuts down, AC power is available, all SRVs are successfully opened and reclosed, but PCS failed. HPI initially succeeds to maintain RCS inventory but finally fails from inadequate lube oil cooling as a result of pump suction from overheated SP. Neither does DEP succeed to allow LPI. CD occurs.
- **TRANS-4:** This scenario is similar to TRANS-3, except that DEP succeeds but LPI fails.
- **TRANS-SORV-1:** A general transient IE occurs, reactor automatically shuts down, AC power is available, but one SRV is stuck-open, and PCS fails. Neither HPI nor DEP succeeds. CD occurs.
- **TRANS-SORV-2:** A general transient IE occurs, reactor automatically shuts down, AC power is available, but one SRV is stuck-open, and PCS fails. RCS inventory is successfully maintained initially through HPI and later through DEP plus condensate system injection. However, CD occurs due to failure of decay heat removal.
- **TRANS-SORV-3:** A general transient IE occurs, reactor automatically shuts down, AC power is available, but one SRV is stuck-open, and PCS fails. HPI initially succeeds to maintain RCS inventory but finally fails from inadequate lube oil cooling as a result of pump suction from overheated SP. Neither does DEP succeed to allow LPI. Then, CD occurs.
- **TRANS-SORV-4:** This scenario is similar to SORV-2 except RCS inventory is maintained through DEP plus LPI.
- **TRANS-SORV-5:** A general transient IE occurs, reactor automatically shuts down, AC power is available, but two SRVs are stuck-open. Condensate system injection succeeds to maintain RCS inventory, but CD still occurs due to failure of decay heat removal.
- **TRANS-LOOP-1:** A general transient IE occurs, reactor automatically shuts down, but offsite power is lost. AC power is still available using emergency power; all SRVs are successfully opened and reclosed, but suppression pool cooling (SPC) is lost. RCS inventory is successfully maintained, initially through HPI and later through DEP plus LPI. However, CD occurs due to failure of decay heat removal.
- **TRANS-ATWS-1:** A general transient IE occurs, reactor protection system (RPS) fails to trip reactor leading to an ATWS. A sufficient number of SRVs are opened. Recirculation pumps are tripped, and PCS succeeds, but standby liquid control fails to start. CD occurs due to failure of reactivity control.
- **TRANS-ATWS-2:** A general transient IE occurs, RPS fails to trip reactor leading to an ATWS. A sufficient number of SRVs are opened, but recirculation pumps are not tripped. CD occurs due to failure of power control.
- **TRANS-ATWS-3:** A general transient IE occurs, RPS fails to trip reactor, leading to an ATWS. A sufficient number of SRVs are opened. Both PCS and standby liquid control succeed, and ADS is inhibited. Operators fail to bypass MSIV Level 1 trip and as a result, MSIVs are closed, but operators succeed in tripping recirculation pumps and lowering water level to top of active fuel. But CD still occurs due to failure of DEP to allow LPI.
- **TRANS-ATWS-4:** This scenario is similar to TRANS-ATWS-3 except DEP succeeds and LPI fails.

Although general transients encompass a wide range of reactor trip initiators, two specific general transient initiators are worth investigating as suggested by Jensen Hughes including transient with turbine control valve (TCV) fast closure and transient with MSIV closure. Jensen Hughes further suggested two cases worth evaluating with different combinations of mitigating system states for transient with MSIV closure; these two suggested cases can be enveloped by scenarios TRANS-3 and TRANS-4. Jensen Hughes did not suggest specific cases for

transient with TCV fast closure. Based on the above recommendations, transient with TCV fast closure is used as the base case initiator for all the scenarios in RELAP5-3D analysis; for scenarios TRANS-3 and TRANS-4, two more additional RELAP5-3D analysis cases are conducted using transient with MSIV closure as the initiator.

Table 4-3. BWR General Transient Scenarios for RELAP-5 3D Analysis: Mitigating System Statuses (TRANS Scenarios).

RELAP5 TRANS Scenario	TRANS Main Event Tree														
#	Rx[a]	AC Power Available	Stuck-open SRVs	PCS Success	HPI Success	SPC Success	DEP Success	CRD[b] Injection Success	Condensate System Success	LPI Success	Alternative LPI Success	SPC Recovery	Containment Spray or Venting Success	PCS Recovery	Late Injection Success
TRANS-1	Trip	Yes	0	No	No		No								
TRANS-2	Trip	Yes	0	No	Yes	No	Yes	Yes				No	No	No	No
TRANS-3	Trip	Yes	0	No	Yes	No	No	No						No	
TRANS-4	Trip	Yes	0	No	Yes	No	Yes	No	No	No	No			No	

[a] Rx = reactor; [b] CRD = control rod drive

Table 4-4. BWR General Transient Scenarios for RELAP-5 3D Analysis: Mitigating System Statuses (TRANS-SORV Scenarios).

RELAP5 TRANS Scenario	TRANS Main Event Tree		SORV Transfer Event Tree												
#	Rx	AC Power Available	Stuck-open SRVs	Main Condenser Success	RCIC Success	SPC Success	DEP Success	Condensate System Success	LPI Success	PCS Recovery	SPC Success	Containment Spray Success	Containment Venting Success	Late Injection Success
TRANS-SORV-1	Trip	Yes	1	No	No		No							
TRANS-SORV-2	Trip	Yes	1	No	Yes	No	Yes	Yes		No			No	No
TRANS-SORV-3	Trip	Yes	1	No	Yes	No	No							
TRANS-SORV-4	Trip	Yes	1	No	Yes	No	Yes	No	Yes	No			No	No
TRANS-SORV-5	Trip	Yes	2					Yes			No	No	No	No

Table 4-5. BWR General Transient Scenarios for RELAP-5 3D Analysis: Mitigating System Statuses (TRANS-LOOP Scenario).

RELAP5 TRANS Scenario	TRANS Main Event Tree		LOOP Transfer Event Tree									
#	Rx	AC Power Available	Stuck-open SRVs	HPI Success	SPC Success	DEP Success	LPI Success	SPC Recovery	Shutdown Cooling Success	Containment Spray Success	Containment Venting Success	Late Injection Success
TRANS-LOOP-1	Trip	Yes	0	Yes	No	Yes	Yes	No	No	No	No	No

Table 4-6. BWR General Transient Scenarios for RELAP-5 3D Analysis: Mitigating System Statuses (TRANS-ATWS Scenarios).

RELAP5 TRANS Scenario	TRANS Main Event Tree		ATWS Transfer Event Tree									
#	Rx	AC Power Available	SRVs Open	Recirculation Pump	PCS Success	Standby Liquid Control Success	Inhibit ADS	Bypass MSIV Level 1 Trip	Lower Level to Top of Active Fuel	DEP Success	LPI Success	Alternative LPI Success
TRANS-ATWS-1	No trip	Yes	Yes	Trip	Yes	No						
TRANS-ATWS-2	No trip	Yes	Yes	No trip								
TRANS-ATWS-3	No trip	Yes	Yes	Trip	Yes	Yes	Yes	No	Yes	No		
TRANS-ATWS-4	No trip	Yes	Yes	Trip	Yes	Yes	Yes	No	Yes	Yes	No	No

4.2 BWR General Transient RELAP5-3D Analysis

The RELAP5-3D analyses are subdivided into two broad categories—general transients with reactor scram and ATWS. Section 4.2.1 presents the results for the transients with reactor scram and Section 4.2.2 presents the results for ATWS.

It is noted due to the spectral shift operations of BWRs; the axial power shapes tend to be bottom peaked near the BOC, cosine shaped in the MOC, and top peaked in the EOC. In the previous RELAP5-3D simulations of SBO and medium loss-of-coolant accident (MLOCA) scenarios (Ma, et al., 2020), bottom-peaked, cosine, and top-peaked power shapes were used to represent the operating state at BOC, MOC, and EOC, respectively. The results obtained, such as the gain in time to CD (coping time gain) and the reduction of hydrogen production, were similar for the two ATF designs with Cr-coated and FeCrAl claddings using the three power shapes. As a result, in the analyses for general transients and subsequent analysis for other transients, only the bottom-peaked power shapes were used in the calculations to represent the entire cycle.

4.2.1 General Transients with Reactor Scram

Ten transient scenarios (No. 1 to 10 in Table 4-2) with reactor scram are analyzed and the results are presented in this section.

4.2.1.1 TRANS-1

In this scenario, it is assumed a general transient IE causes the reactor to automatically shut down. AC power is available, however, the HPI systems fail to start. SRVs are successfully opened and reclosed to keep the system pressure within a predefined range. The PCS fails so all steam is guided to the SP in the WW where it condenses. It is further assumed the ADS fails such that LPI system is not able to inject water to the RPV. With the absence of water injection into the RPV from HPI and LPI systems after the transient starts, the reactor coolant in the core boils off fairly quickly and causes fuel failure in less than one and a half hours. Figure 4-7 shows the RPV dome pressure, which indicates the system pressure is maintained within the operating range. Figure 4-8 shows the mass flow rate through the SRVs. Figure 4-9 shows the RPV downcomer water during the transient and Figure 4-10 shows the PCT comparisons.

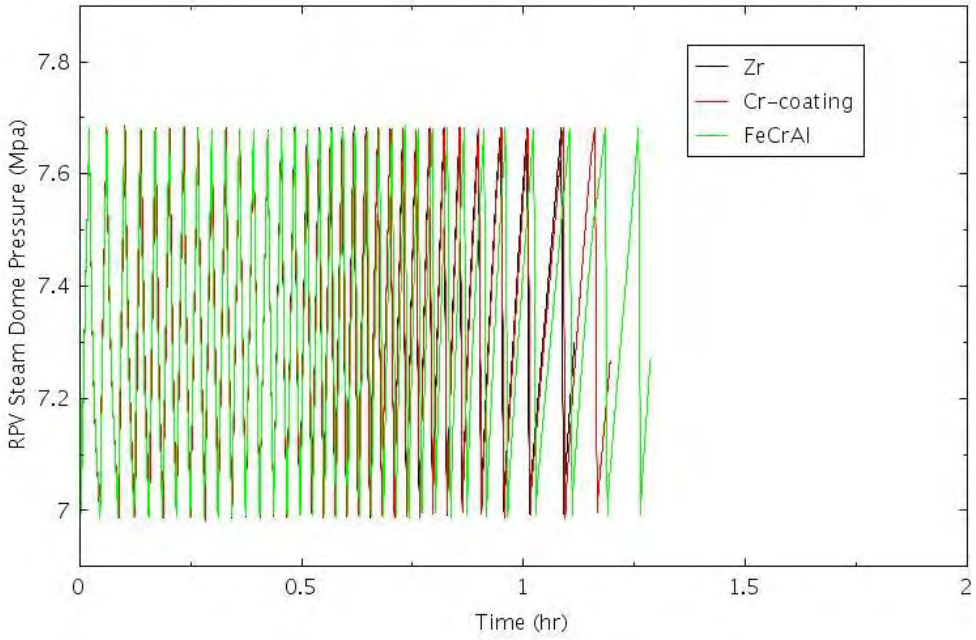

Figure 4-7. RPV Dome Pressure for TRANS-1.

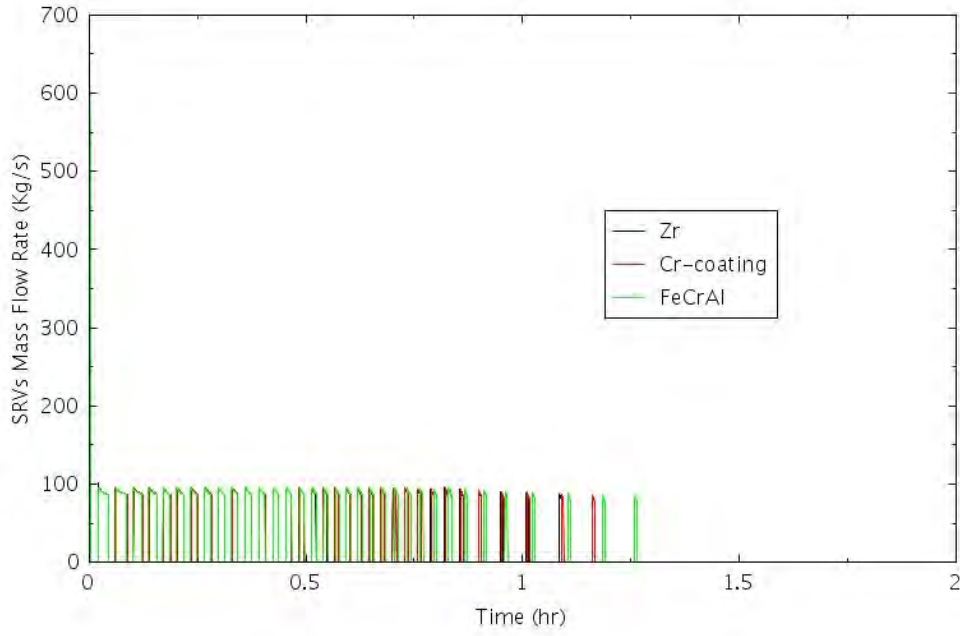

Figure 4-8. Mass Flow Rate Through SRVs for TRANS-1.

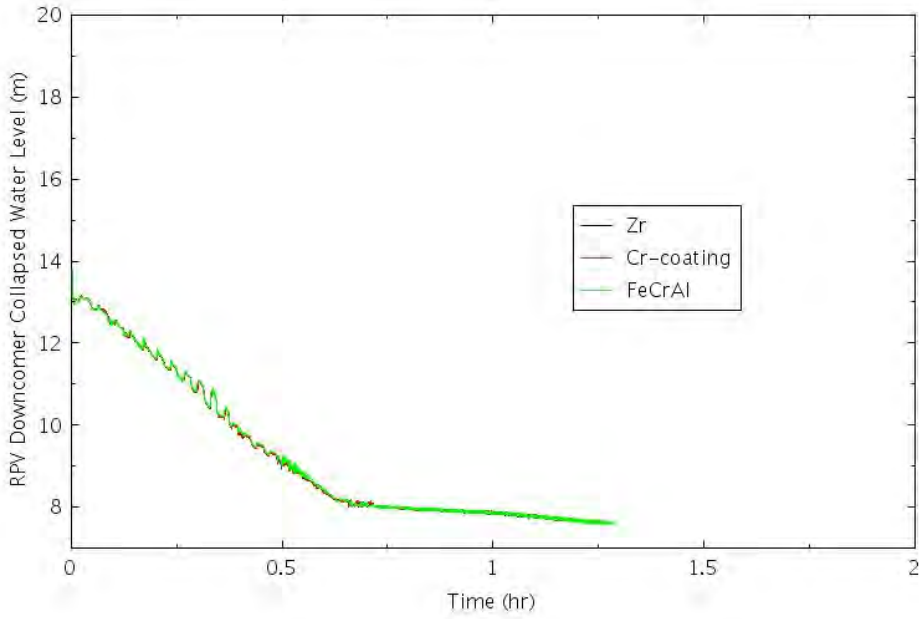

Figure 4-9. RPV Downcomer Water Level for TRANS-1.

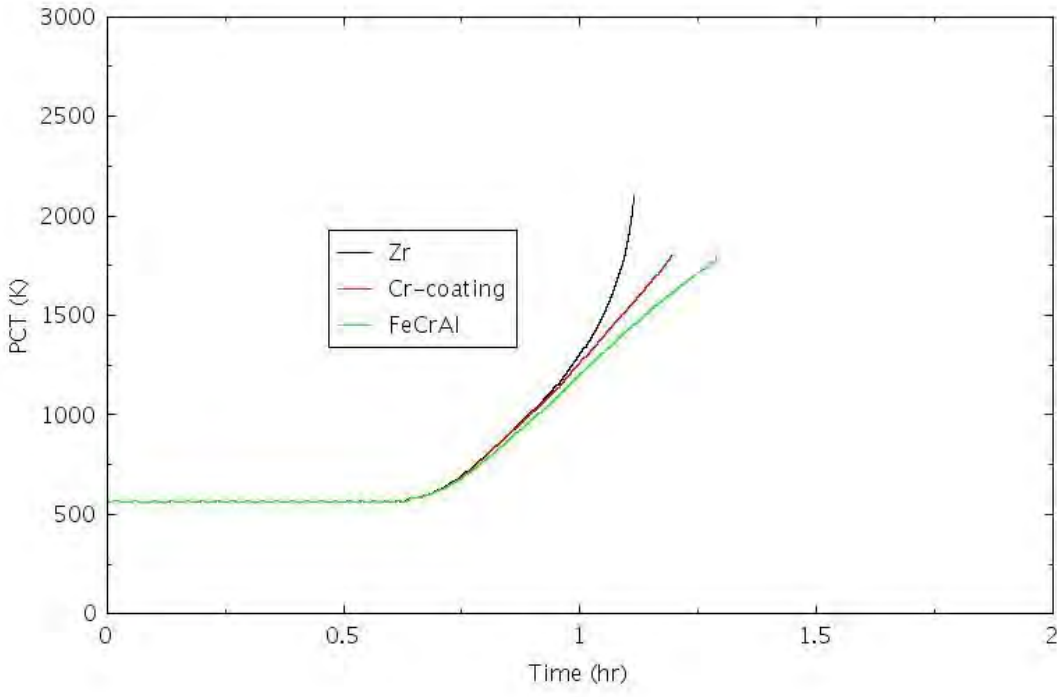

Figure 4-10. PCT for TRANS-1.

4.2.1.2 TRANS-2

In this scenario, it is assumed a general transient IE causes the reactor to automatically shut down. AC power is available, and all SRVs are successfully opened and reclosed. The PCS failed so all steam is guided to the SP where it condenses. The HPI systems successfully start; however, it is assumed HPI stops injecting water into the RPV once the SP temperature reaches 361 K (190°F). Figure 4-11 shows the HPI mass flow rate. Once the HPI stops injecting water into the RPV, the RPV downcomer water level, as shown in Figure 4-12, gradually decreases. Once the water level decrease to the Level 1 set point, the RPV is depressurized. Figure 4-13 shows the RPV dome pressure. The SRV mass flow rate is shown in Figure 4-14. The CRD injection system is a high-pressure system. It is able to inject water into the reactor core directly under both high-pressure and depressurized conditions. Once the HPI stops injecting water into the RPV, the CRD flow is not able to provide enough coolant into the RPV to prevent the RPV water level from decreasing, as shown in Figure 4-12. The decreasing water level in the RPV and core eventually leads to fuel failure after about 10 hours into the transient. The CRD flow rate is assumed to at 7.07 Kg/s (112 GPM). The CRD flow rate is shown in Figure 4-15. The SP water temperature is shown in Figure 4-16, and the containment drywell pressure is shown in Figure 4-17. Figure 4-18 shows the comparison of PCT for the Zr cladding and ATF claddings.

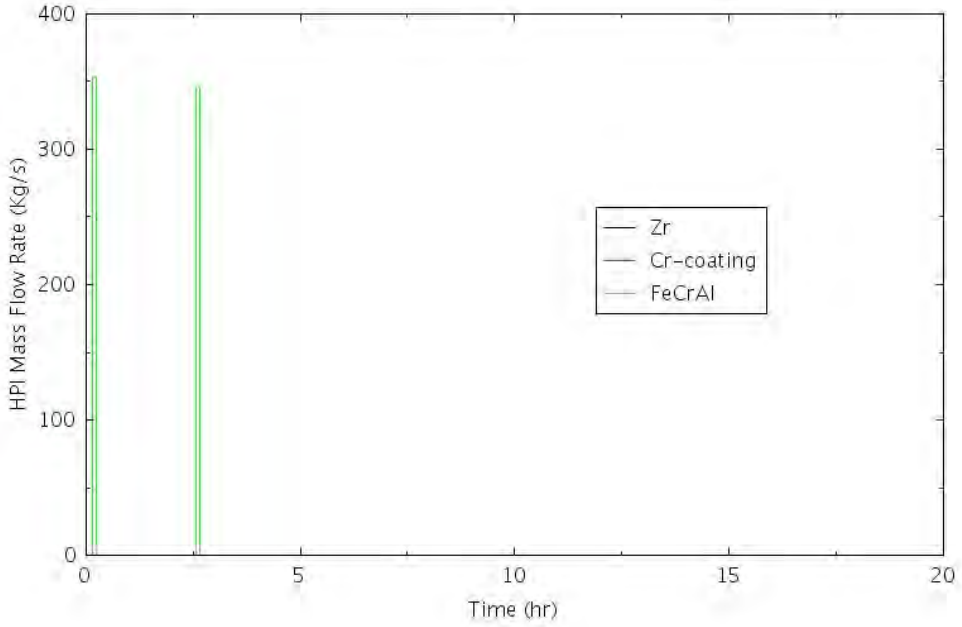

Figure 4-11. HPI Mass Flow Rate for TRANS-2.

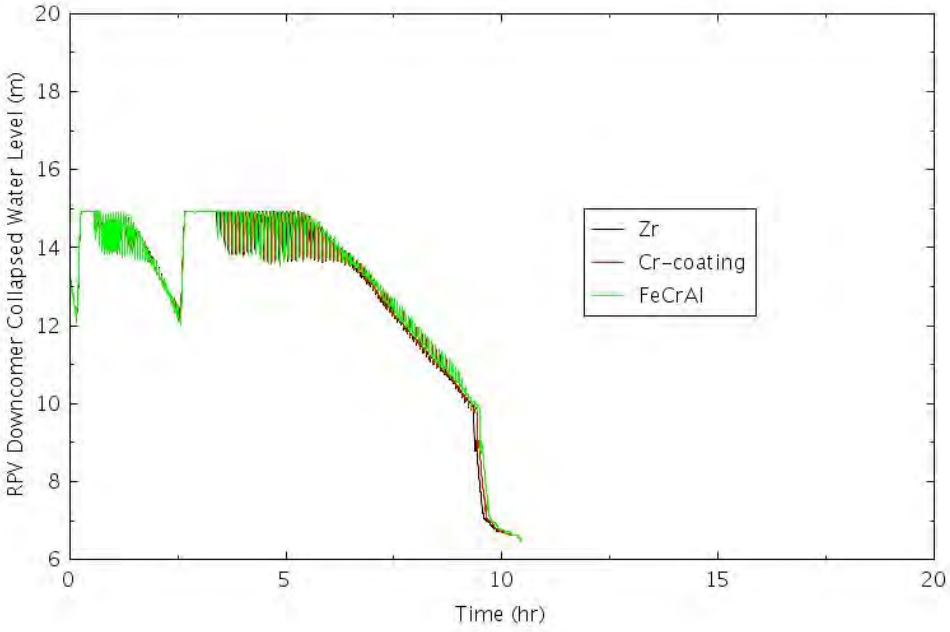

Figure 4-12. RPV Downcomer Collapsed Water Level for TRANS-2.

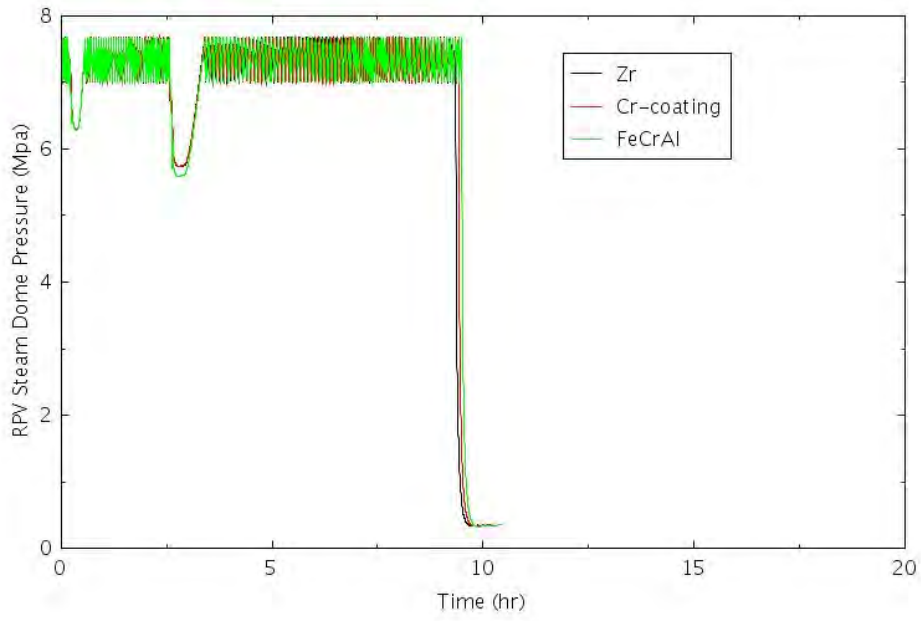

Figure 4-13. RPV Dome Pressure for TRANS-2.

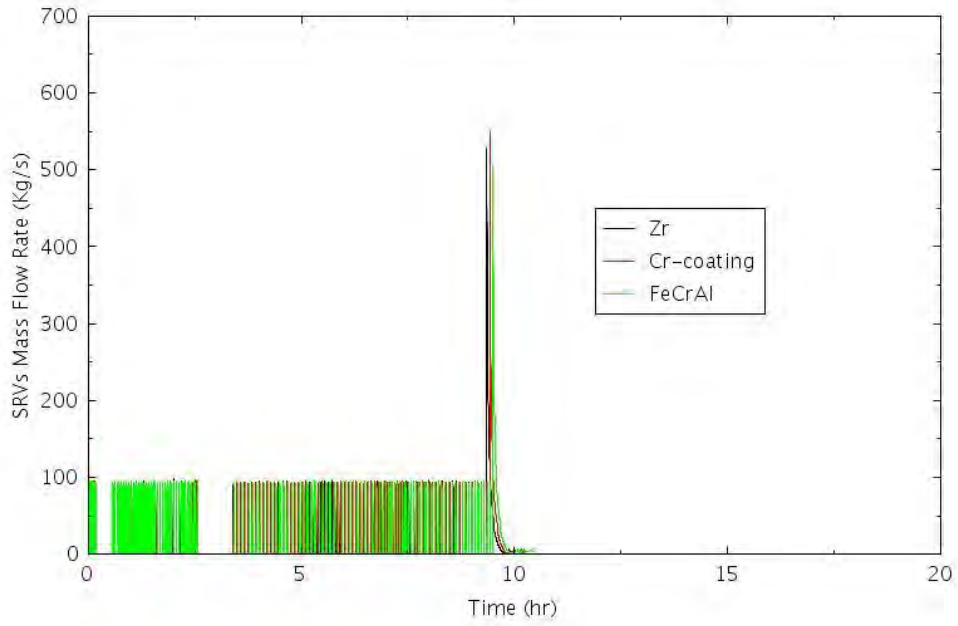

Figure 4-14. Mass Flow Rate Through SRVs for TRANS-2.

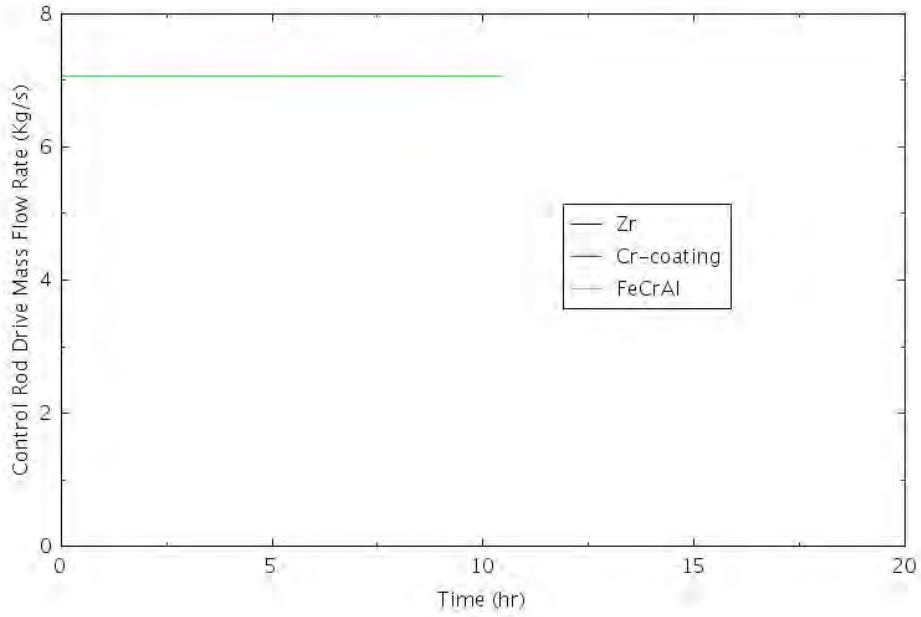

Figure 4-15. CRDHS Mass Flow Rate for TRANS-2.

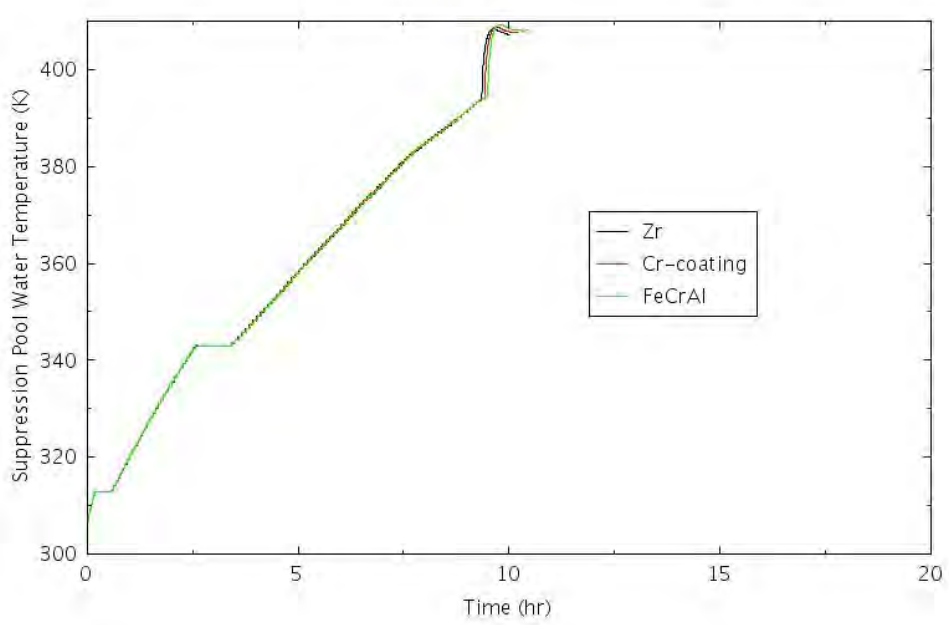

Figure 4-16. SP Water Temperature for TRANS-2.

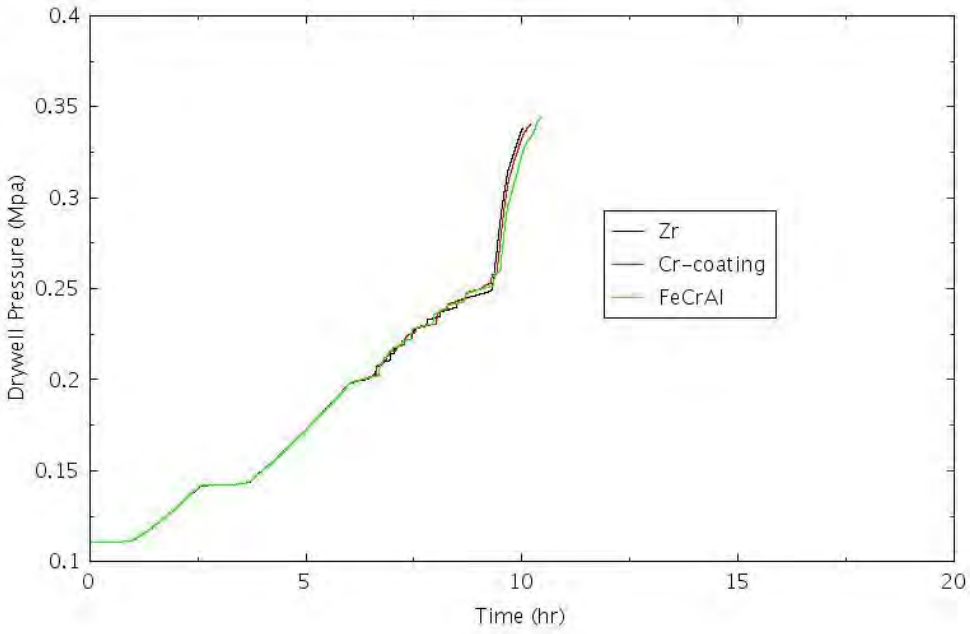

Figure 4-17. Containment Drywell Pressure for TRANS-2.

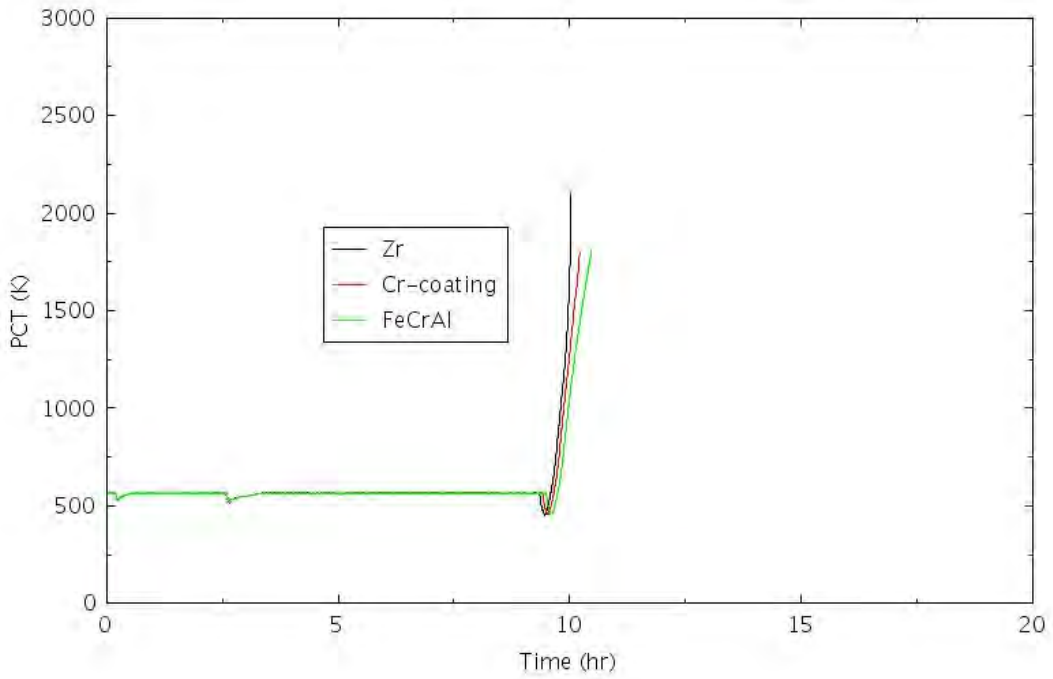

Figure 4-18. PCT Comparison for TRANS-2.

4.2.1.3 TRANS-3

In this scenario, it is assumed a general transient IE causes the reactor to automatically shut down. AC power is available, and the HPI systems successfully start and are able to maintain the RCS inventory for several hours. SRVs are successfully opened and reclosed to keep the system pressure within a predefined range. The PCS fails so all steam is guided to the SP where it condenses. Due to overheating of the SP water, the pump suction fails due to inadequate lube oil cooling. In this simulation, it is assumed the pump suction fails once the SP temperature reaches 361 K (190°F). It is further assumed the ADS fails to actuate such that LPI system is not able to inject water to the RPV. With the absence of water injection into the RPV after HPI stops injecting water into the RPV, the core continues to boil off and the reactor core eventually becomes uncovered which leads to fuel failure. Fuel failure happens at about 8 hours after the event onset for this transient. Figure 4-19 shows the HPI mass flow rate. HPI works for close to 4 hours. HPI injection is able to maintain the RPV water level for over 5 hours before it starts to decrease, as shown in Figure 4-20. The RPV dome pressure is shown in Figure 4-21, and it indicates the system pressure is maintained close to the operating range for the duration of transient. Figure 4-22 shows the mass flow rate through the SRVs. Figure 4-23 shows the SP water temperature. Figure 4-24 shows the PCT comparisons.

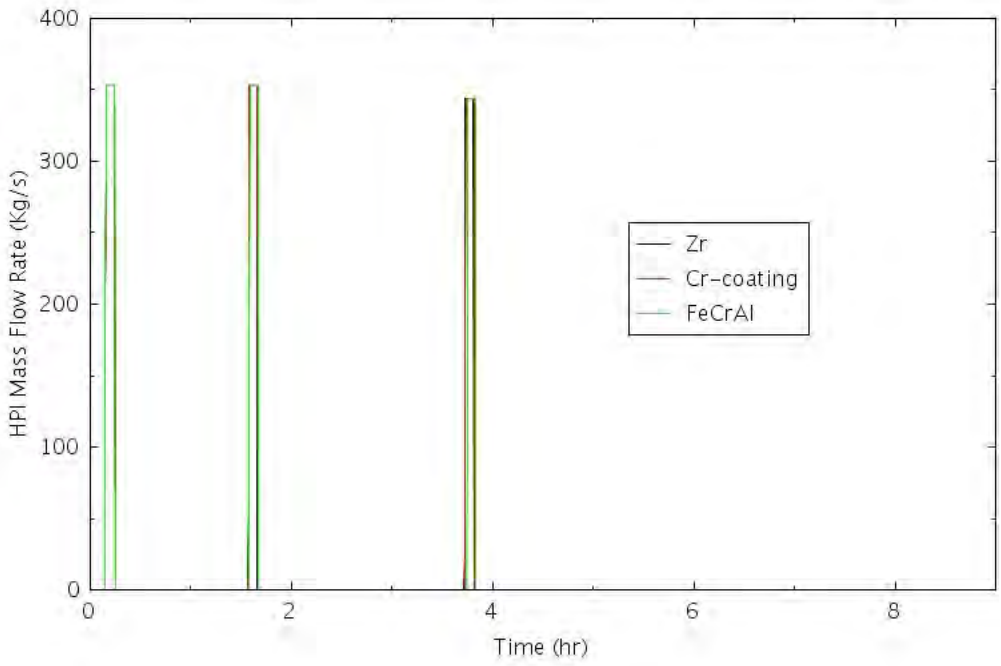

Figure 4-19. HPI Flow for TRANS-3.

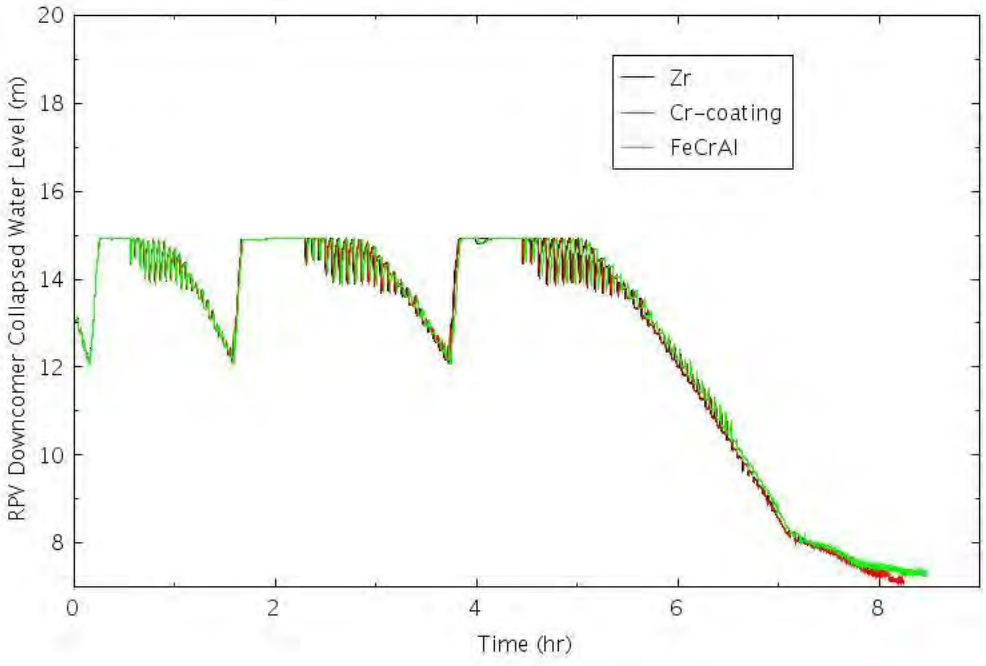

Figure 4-20. RPV Downcomer Collapsed Water Level for TRANS-3.

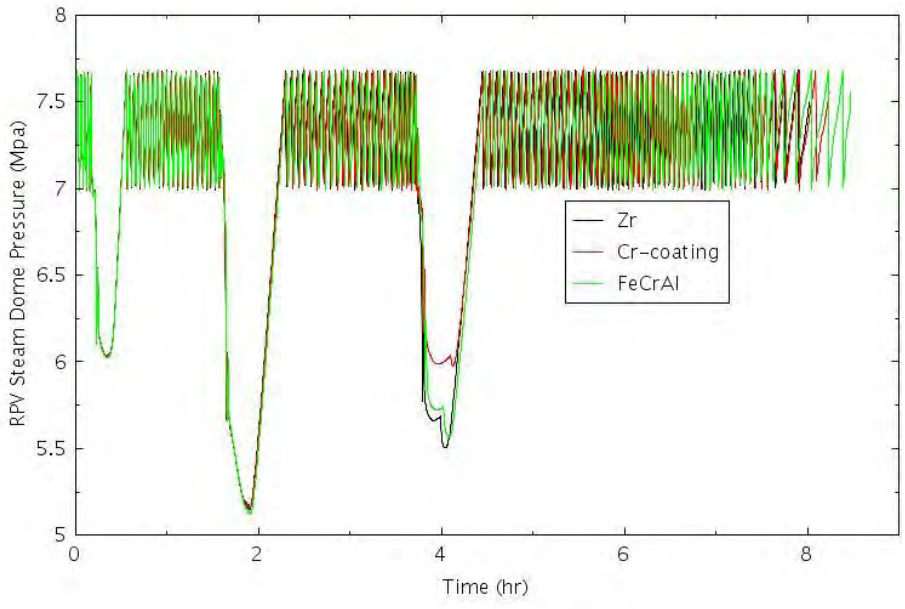

Figure 4-21. Dome Pressure for TRANS-3.

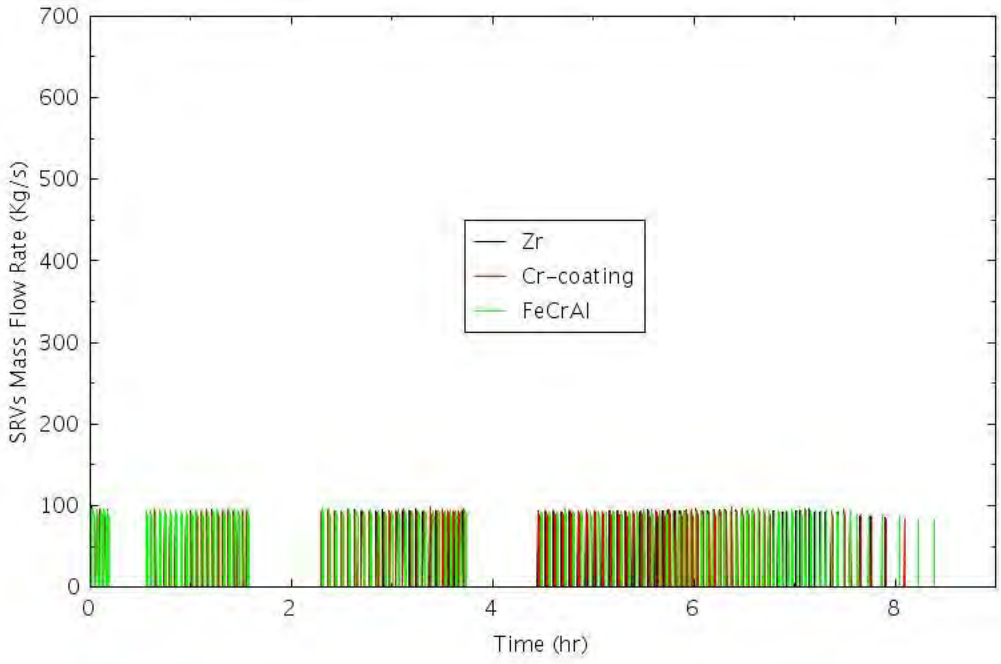

Figure 4-22. SRV Flow Rate for TRANS-3.

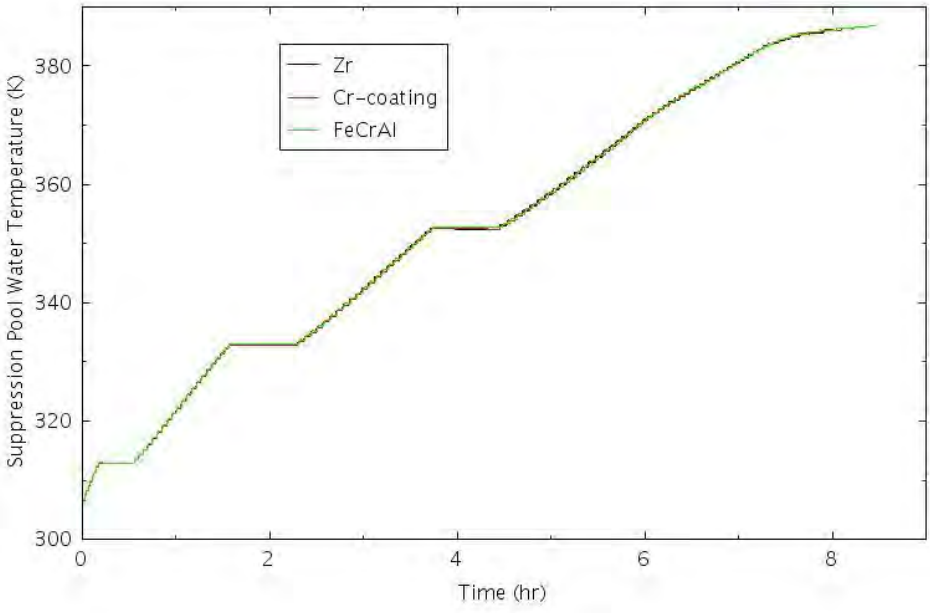

Figure 4-23. SP Water Temperature for TRANS-3.

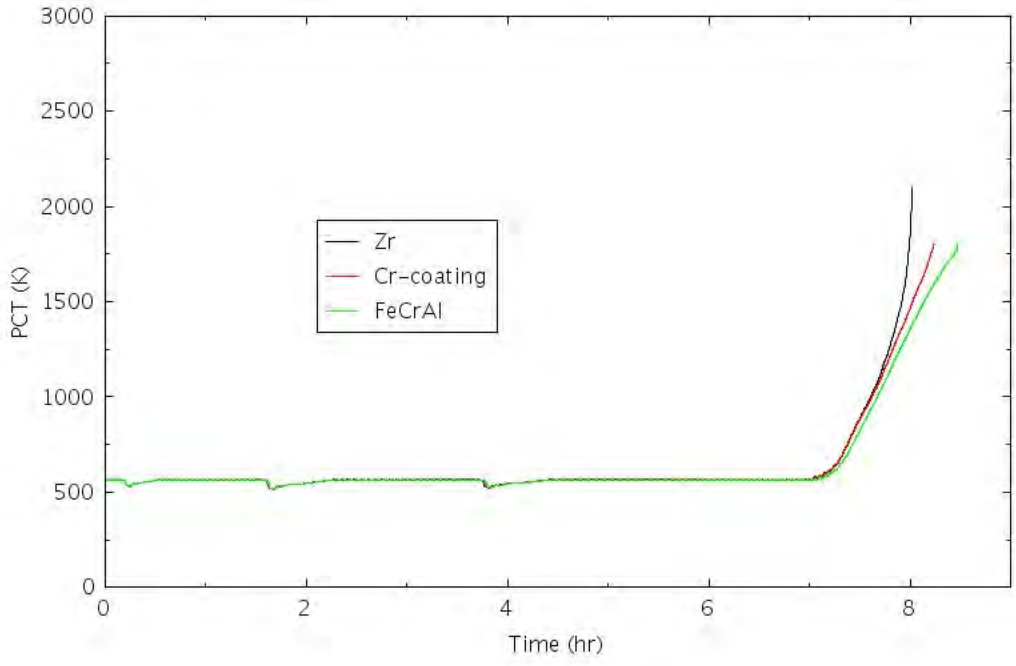

Figure 4-24. PCT for TRANS-3.

4.2.1.4 TRANS-4

In this scenario, it is assumed a general transient IE causes the reactor to automatically shut down. AC power is available, and the HPI systems successfully start and are able to maintain the RCS inventory for several hours. SRVs are successfully opened and reclosed to keep the system pressure within a predefined range. The PCS failed so all steam is guided to the SP where it condenses. Due to overheating of the SP water, the pump suction fails due to inadequate lube oil cooling. In the RELAP5-3D simulation for this scenario, it is assumed the pump suction fails once the suppression temperature reaches 361 K (190°F). It is further assumed when the pump suction fails, the RPV is depressurized; however, the LPI system fails to inject water into the RPV. With the absence of water injection into the RPV, the core continues to boil off and the reactor core eventually becomes uncovered which leads to fuel failure. Fuel failure happens at about 7 hours after the event onset for this transient. Figure 4-25 shows the HPI mass flow rate. HPI works for close to 4 hours. HPI injection is able to maintain the RPV water level for over 5 hours before it starts to decrease, as shown in Figure 4-26. Once the pump suction fails, the RPV is manually depressurized, the RPV dome pressure is shown in Figure 4-27. Figure 4-28 shows the mass flow rate through the SRVs. Figure 4-29 shows the SP water temperature. Figure 4-30 shows the PCT comparisons for Zr cladding and the ATF claddings.

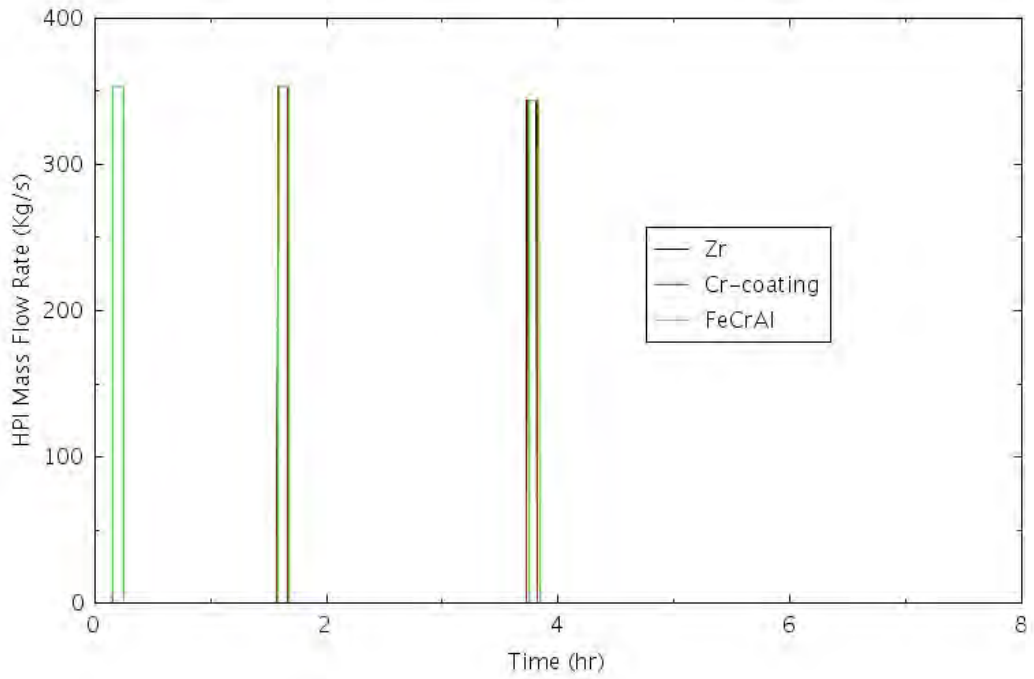

Figure 4-25. HPI Mass Flow Rate for TRANS-4.

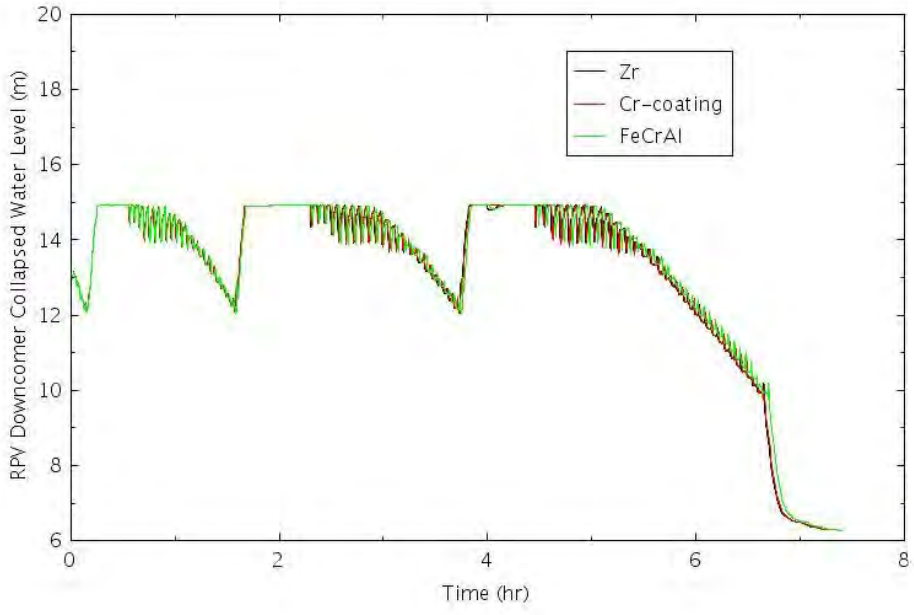

Figure 4-26. RPV Downcomer Collapsed Water Level for TRANS-4.

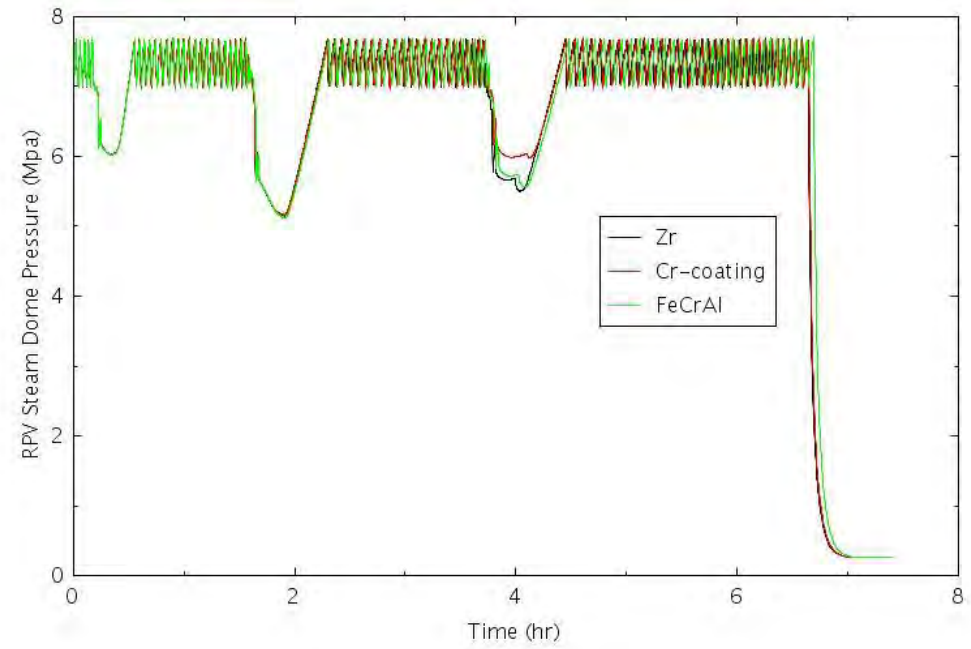

Figure 4-27. RPV Dome Pressure for TRANS-4.

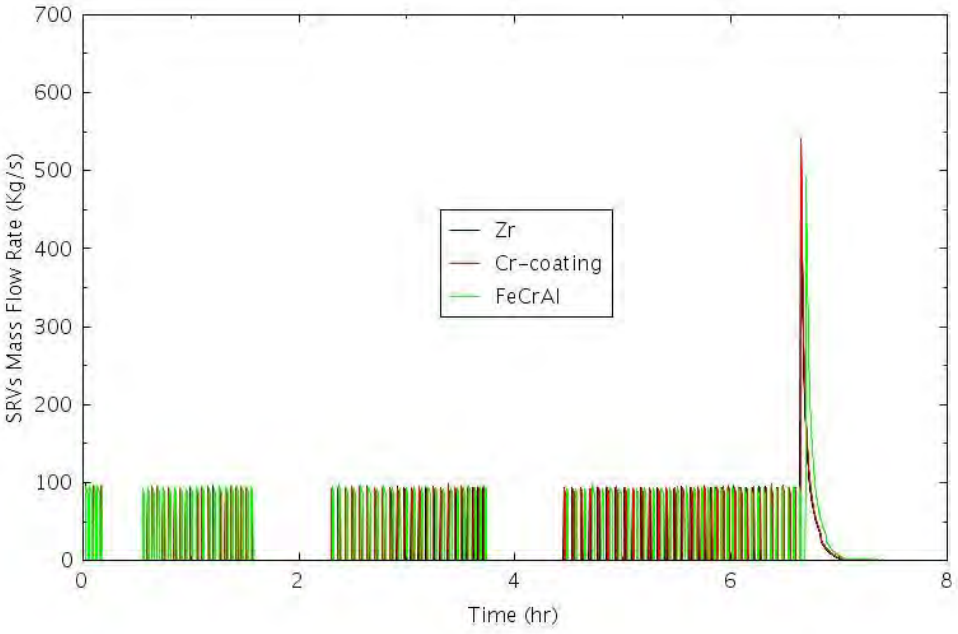

Figure 4-28. Mass Flow Rates Through SRVs for TRANS-4.

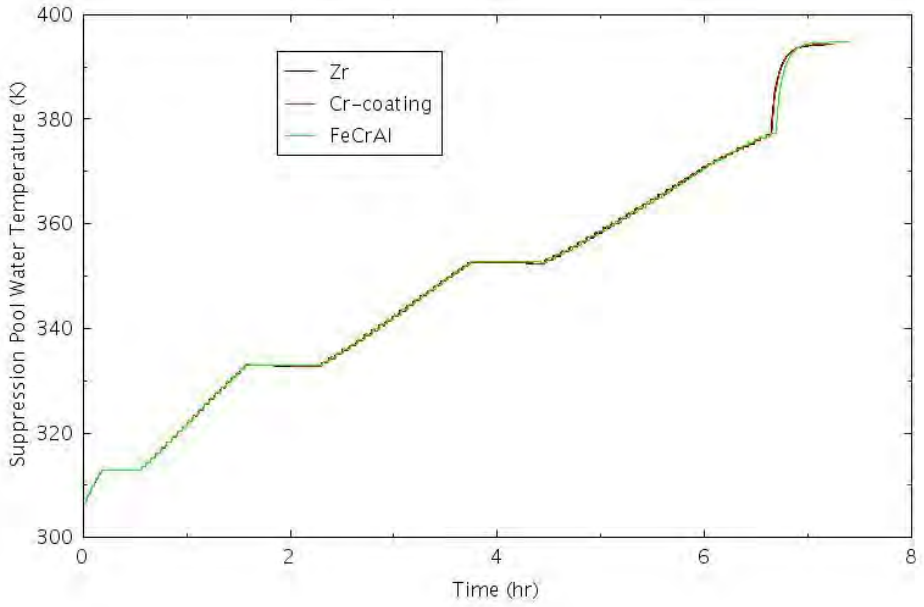

Figure 4-29. SP Water Temperature for TRANS-4.

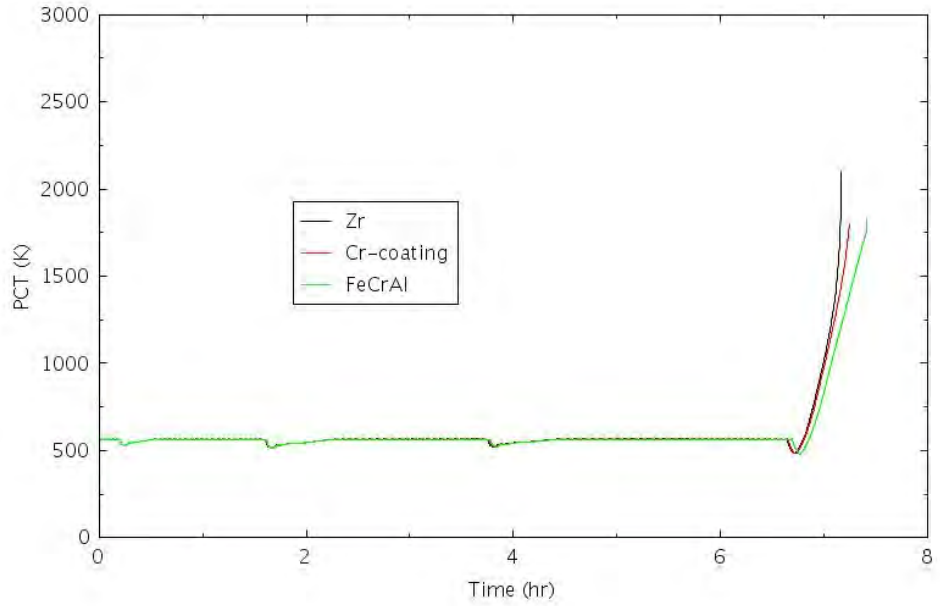

Figure 4-30. PCT Comparison for TRANS-4.

4.2.1.5 TRANS-SORV-1

In this scenario, it is assumed a general transient IE causes the reactor to automatically shut down. AC power is available, however, the HPI systems fails to start. One SRV is stuck once it is opened due to the increase in system pressure after the initiation of the transient. As the result of one stuck-open SRV, the system pressure starts to decrease rapidly. The PCS fails so all steam is guided to the SP where it condenses. It is further assumed the ADS fails to actuate such that the low-pressure injection system is not able to inject water to the RPV. With the absence of makeup water from either the HPI or LPI system, the coolant in the reactor core boils off rapidly and leads to CD in about 1 hour after the event onset. Figure 4-31 shows the RPV dome pressure, which indicates the system pressure decreases rapidly with the stuck-open SRV. Figure 4-32 shows the mass flow rate through the SRVs. Figure 4-33 shows the RPV downcomer water during the transient, and Figure 4-34 shows the PCT comparisons for the Zr cladding and the ATF claddings.

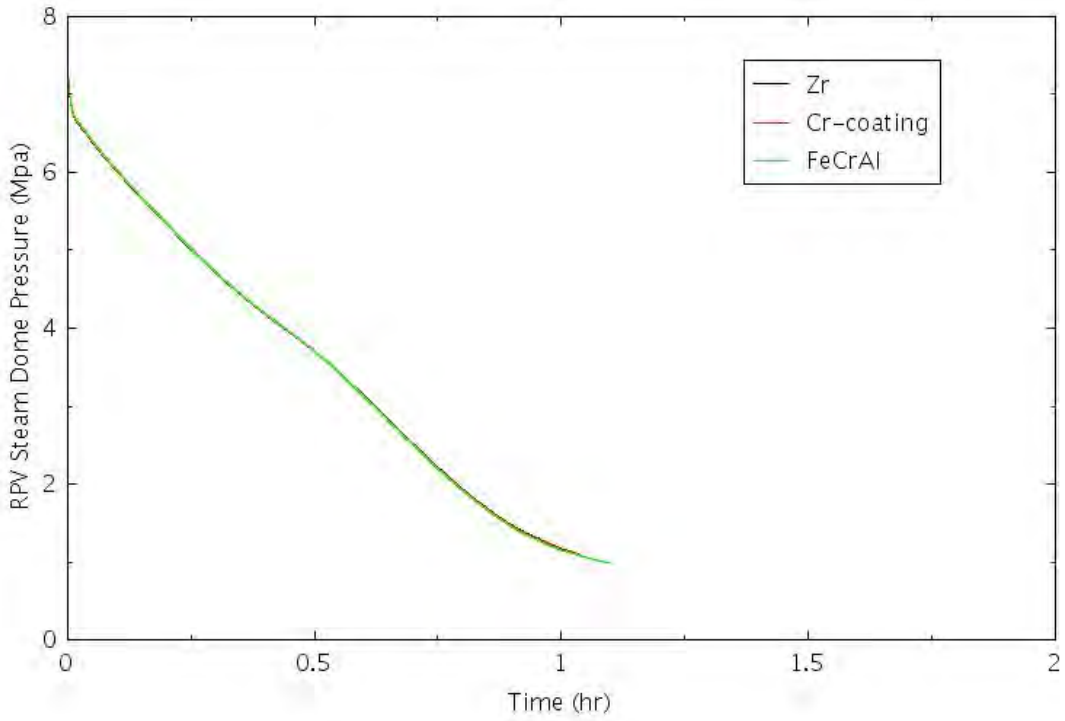

Figure 4-31. RPV Dome Pressure for TRANS-SORV-1.

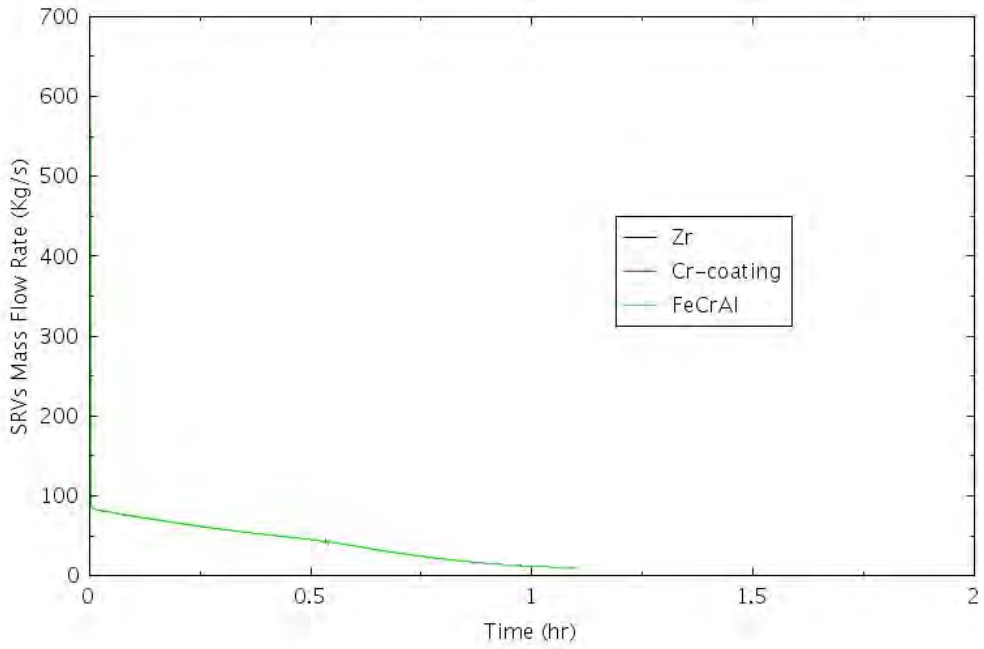

Figure 4-32. SRV Mass Flow Rate for TRANS-SORV-1.

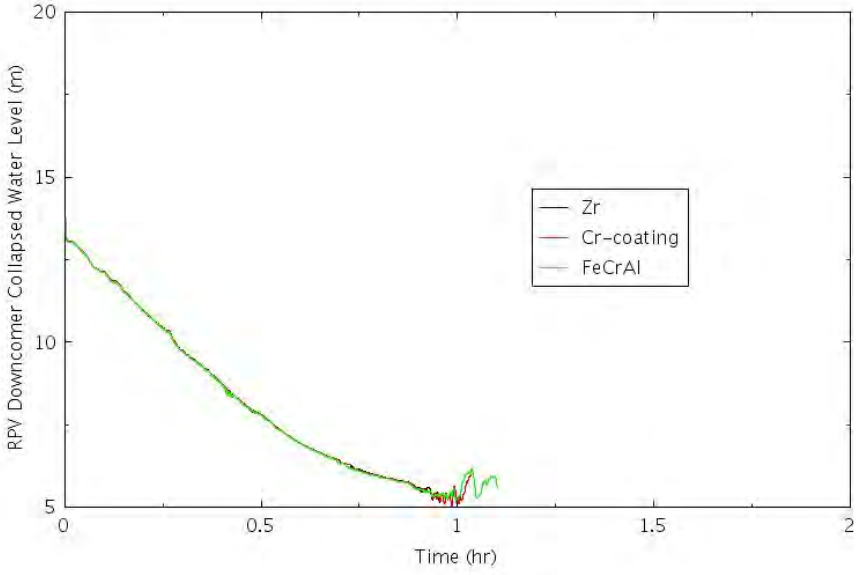

Figure 4-33. RPV Downcomer Collapsed Water Level for TRANS-SORV-1.

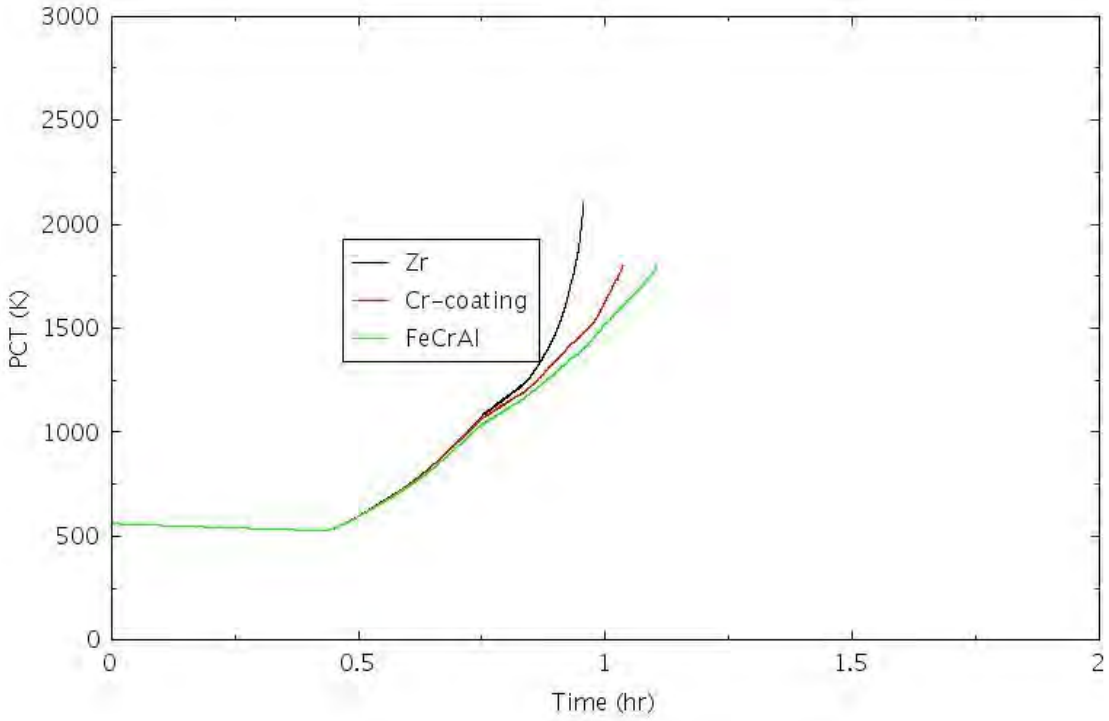

Figure 4-34. PCT for TRANS-SORV-1.

4.2.1.6 TRANS-SORV-2

In this scenario, it is assumed a general transient IE causes the reactor to automatically shut down. AC power is available, and one SRV is stuck-open once the valve is lifted open by the initial rise of the system pressure. The PCS failed so all steam is guided to the SP where it condenses. The HPI system successfully starts; however, it stops injecting water into the RPV once the SP temperature reaches 361 K (190°F). Once the HPI system ceases to inject water into the RPV, the RPV water level starts to decrease. Once the water level reaches the Level 1 water level set point, the CS system starts to inject water into the RPV. It is further assumed once the containment DW pressure reaches its design pressure of 0.49 MPa (70.7 psia), the CS injection stops to inject water into the RPV. With the loss of water injection into the RPV, the coolant in the core continues to boil off and the reactor core eventually becomes uncovered which leads to fuel failure. The fuel failure happens in less than 15 hours. Figure 4-35 shows the HPI mass flow rate. Figure 4-36 shows the CS injection mass flow rate. With the high-mass flow rate of the CS injection, the RPV water level is raised up quickly as shown in Figure 4-37. The CS injection is stopped once the water level reaches the high-water level set point to avoid the flooding of the main steam line. The CS system is not started again before the drywell pressure reaches its design value of 0.49 MPa. The containment drywell pressure and temperature are shown in Figure 4-38 and Figure 4-39, respectively. The mass flow rate through the SRVs is shown in Figure 4-40. It can be seen steam flows out of the SRVs continuously during the transient leading to the depressurization of the RPV. The RPV dome pressure is shown in Figure 4-41. With the stuck-open SRV, the RPV pressure initially decreases rapidly. With the water injection from HPI initially and later from CS, the RPV dome pressure rises a bit but still stays in the low range. The PCT comparisons are shown in Figure 4-42.

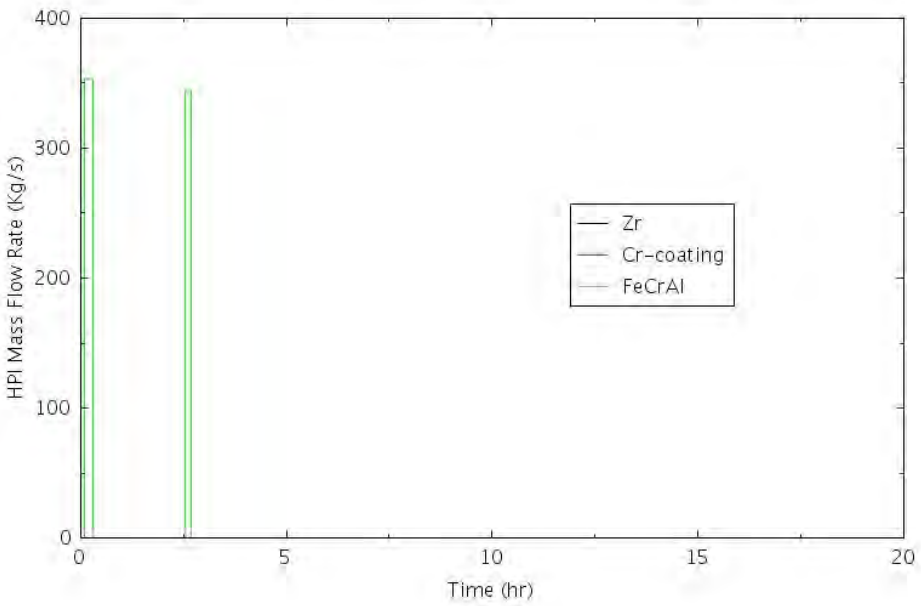

Figure 4-35. HPI Mass Flow Rate for TRANS-SORV-2.

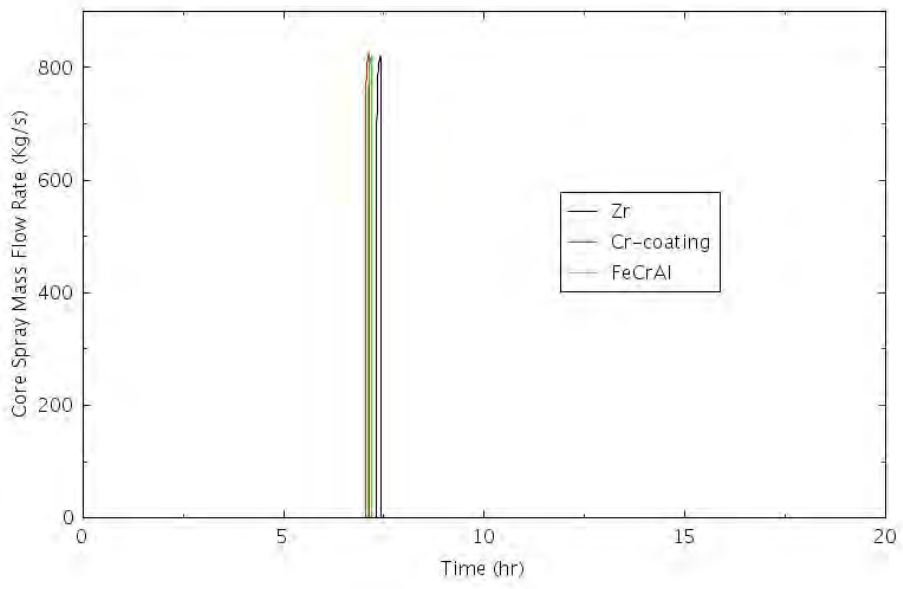

Figure 4-36. CS Mass Flow Rate for TRANS-SORV-2.

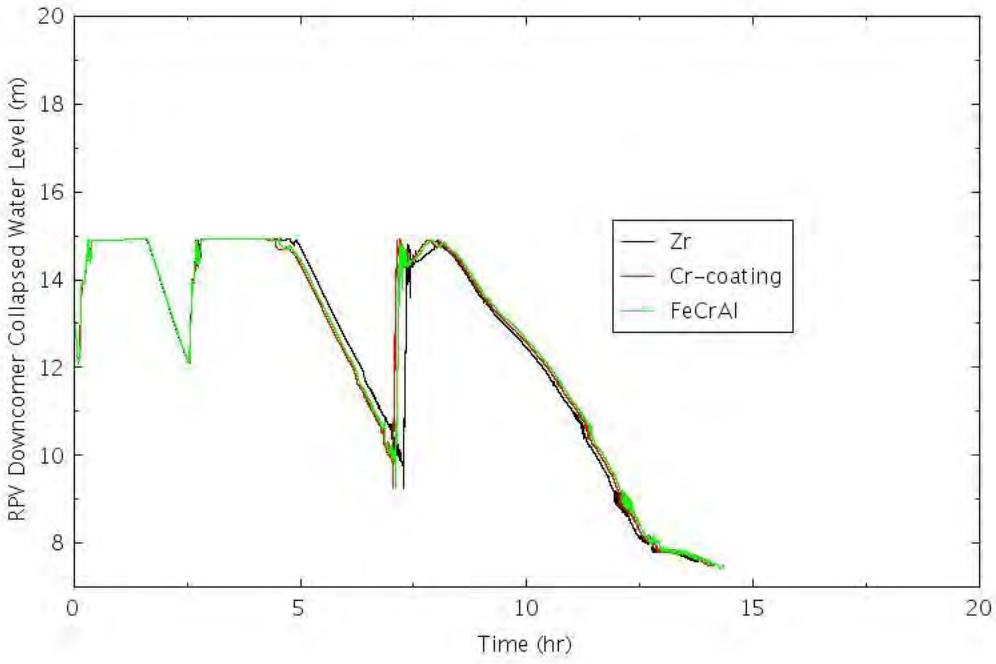

Figure 4-37. RPV Downcomer Collapsed Water Level for TRANS-SORV-2.

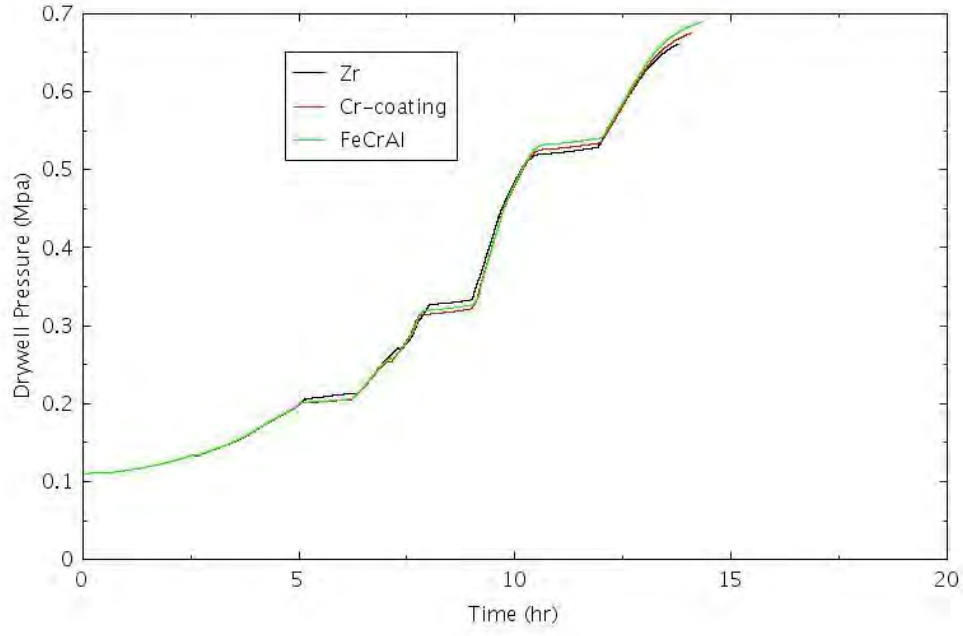

Figure 4-38. Containment Drywell Pressure for TRANS-SORV-2.

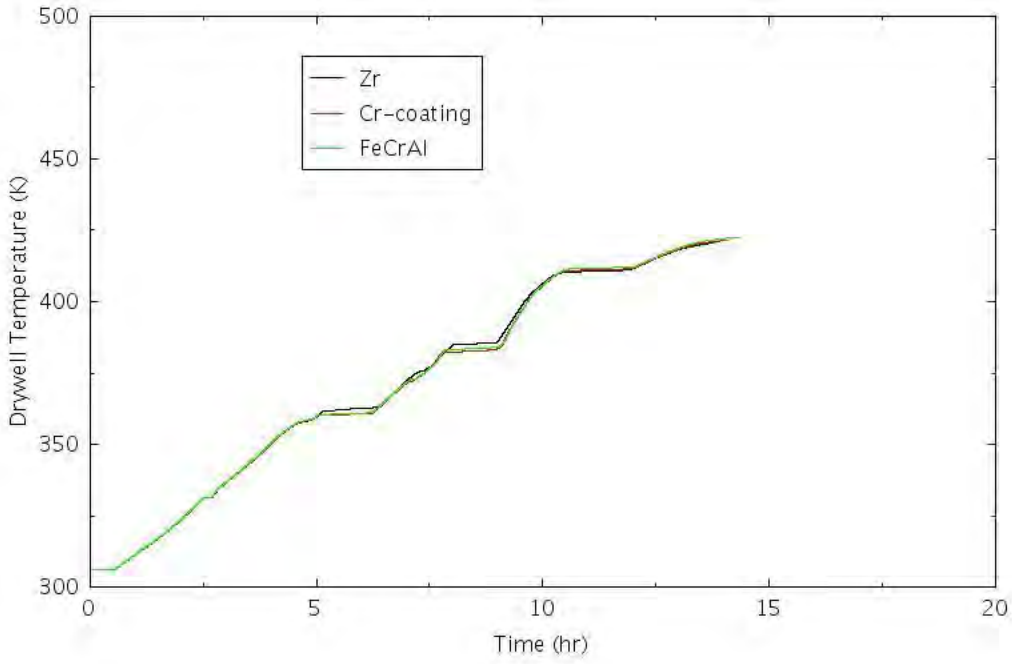

Figure 4-39. Containment Drywell Temperature for TRANS-SORV-2.

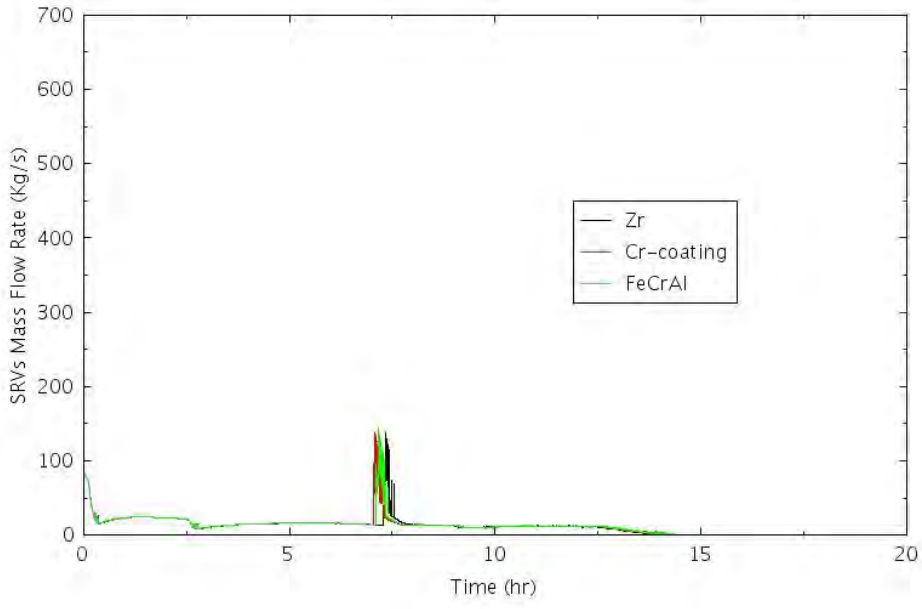

Figure 4-40. Mass Flow Rate Through SRVs for TRANS-SORV-2.

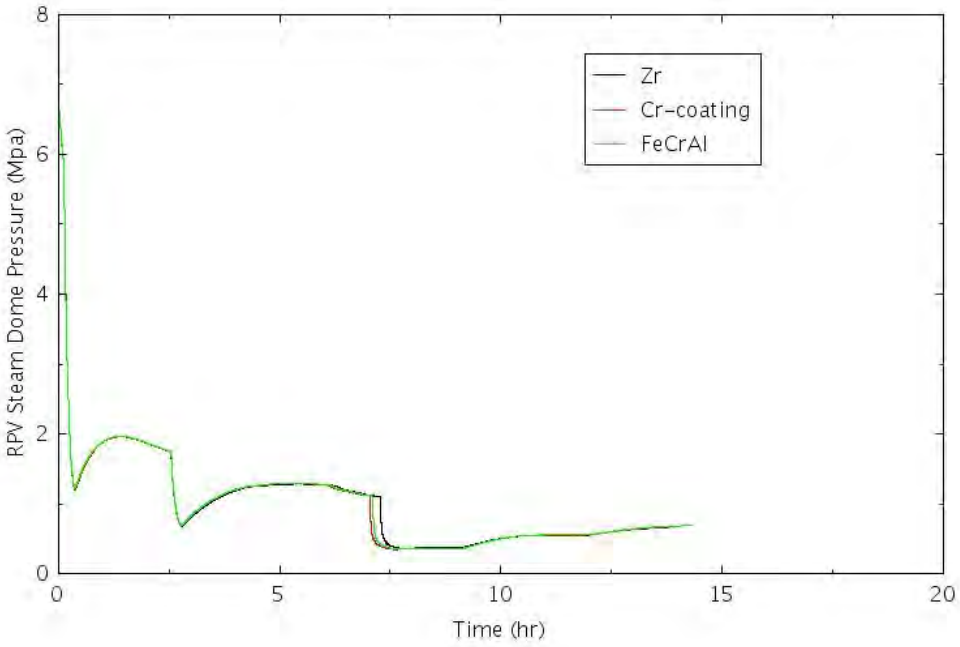

Figure 4-41. RPV Dome Pressure for TRANS-SORV-2.

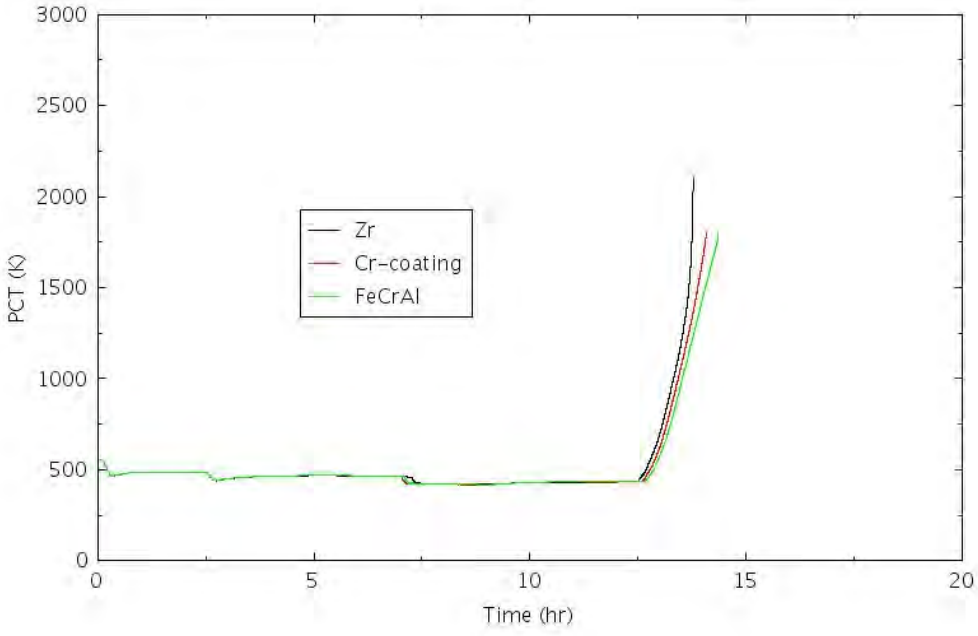

Figure 4-42. PCT Comparison for TRANS-SORV-2.

4.2.1.7 TRANS-SORV-3

In this scenario, it is assumed a general transient IE causes the reactor to automatically shut down. AC power is available, and the HPI systems successfully start and are able to maintain the RCS inventory for several hours. It is further assumed one SRV is stuck-open once it is opened initially. The PCS fails so all steam is guided to the SP where it condenses. Due to overheating of the SP water, the pump suction fails due to inadequate lube oil cooling. It is assumed the pump suctions fails when the SP temperature reaches 361 K (190°F). It is further assumed there is no manual depressurization, and the LPCI system fails to inject water to the RPV. With the loss of water injection into the RPV, the coolant in the core continues to boil off and the reactor core eventually becomes uncovered which leads to fuel failure after about 8 hours into the transient. Figure 4-43 shows the mass flow rate through the stuck-open SRV. It can be seen steam flows out of the stuck-open SRV continuously during the transient leading to the depressurization of the RPV. Figure 4-44 shows the RPV dome pressure, which indicates with the stuck-open of one SRV, the RPV pressure initially decreases rapidly. With intermittent water injection from HPI, the RPV dome oscillates in a low range. The HPI water injection mass flow rate is shown in Figure 4-45. The HPI is turned on and off twice within the first 3 hours. After it is assumed overheating of the suppression water results in the failure of the suction pump due to inadequate lube oil cooling, the SP temperature is shown in Figure 4-46. As the HPI water injection ceases and with no water injection from LPCI, the water level in the RPV decreases precipitously due to coolant boiling off. The RPV downcomer collapsed water level is shown in Figure 4-47. The PCT comparisons are shown in Figure 4-48.

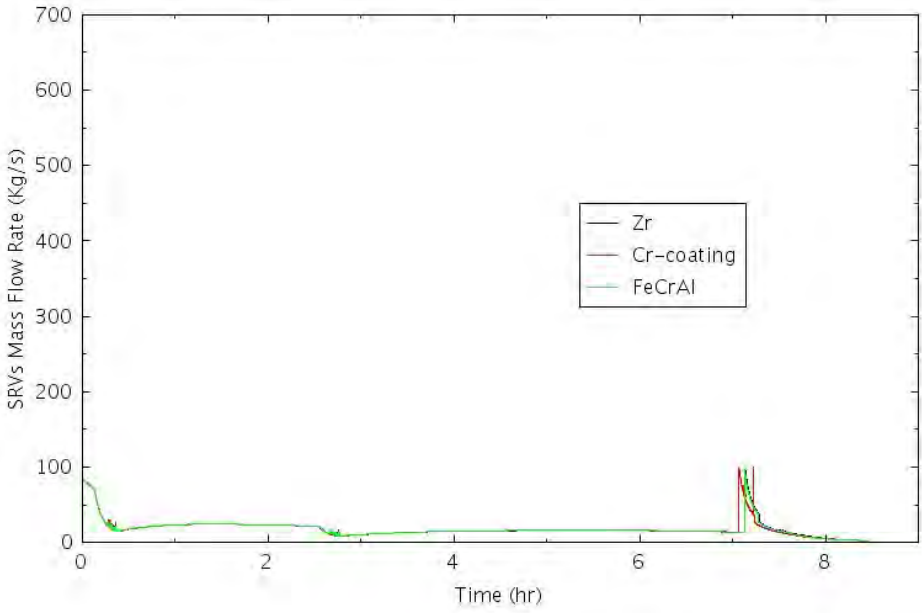

Figure 4-43. Mass Flow Rate Through SRVs for TRANS-SORV-3.

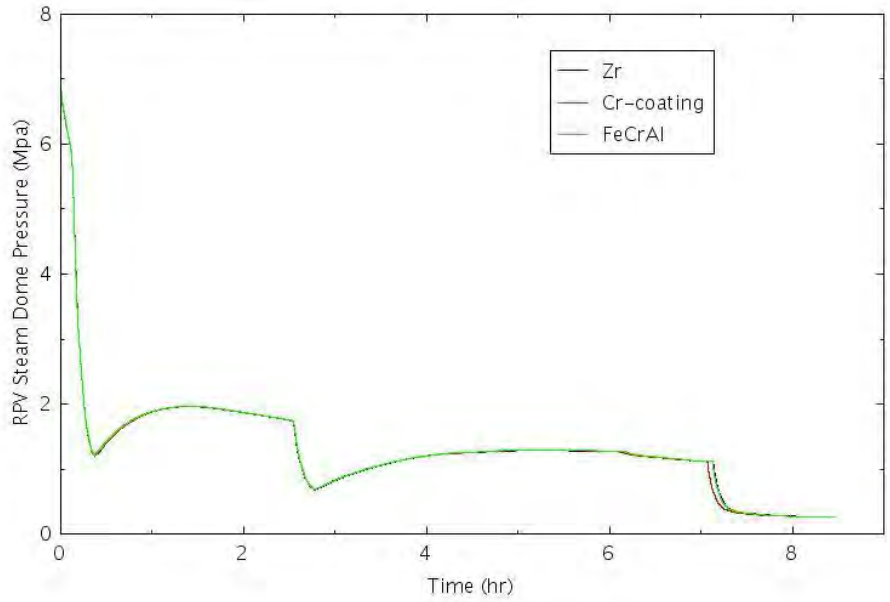

Figure 4-44. RPV Dome Pressure for TRANS-SORV-3.

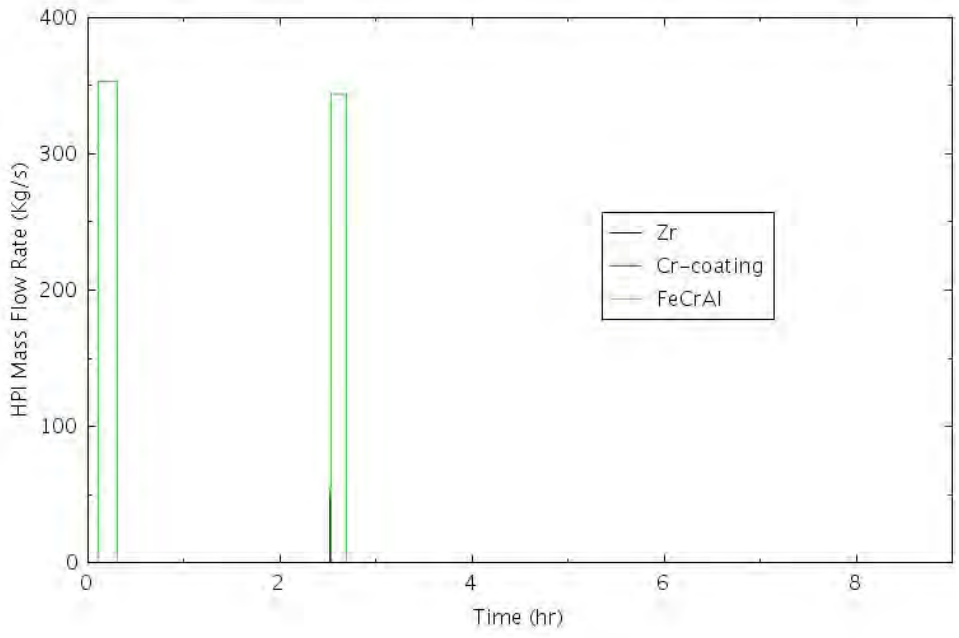

Figure 4-45. HPI Mass Flow Rate for TRANS-SORV-3.

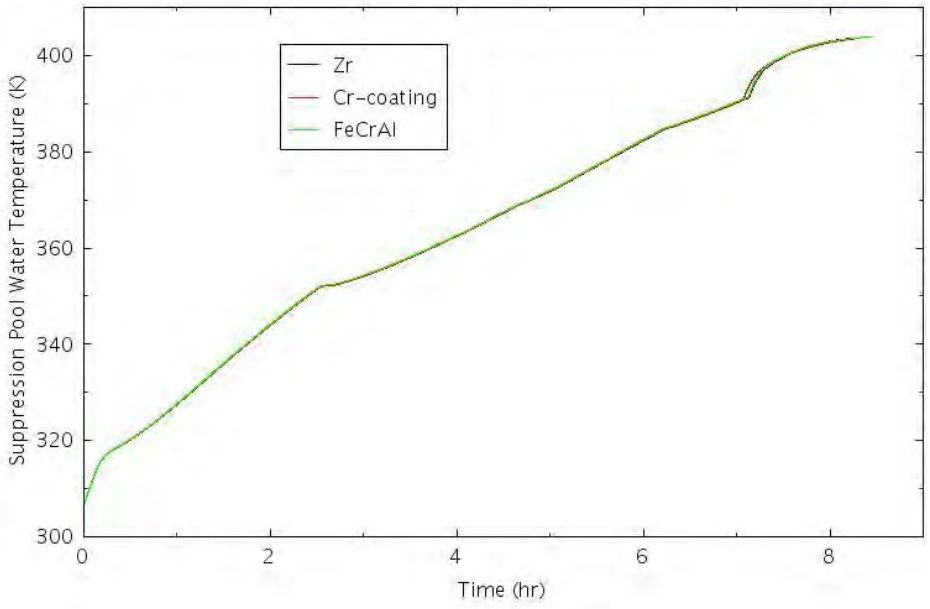

Figure 4-46. SP Water Temperature During TRANS-SORV-3.

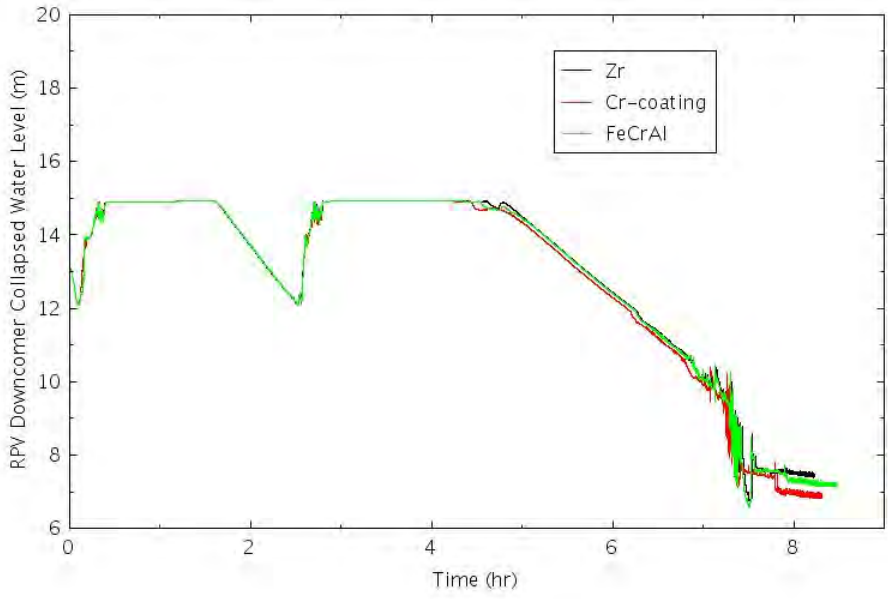

Figure 4-47. RPV Downcomer Collapsed Water Level for TRANS-SORV-3.

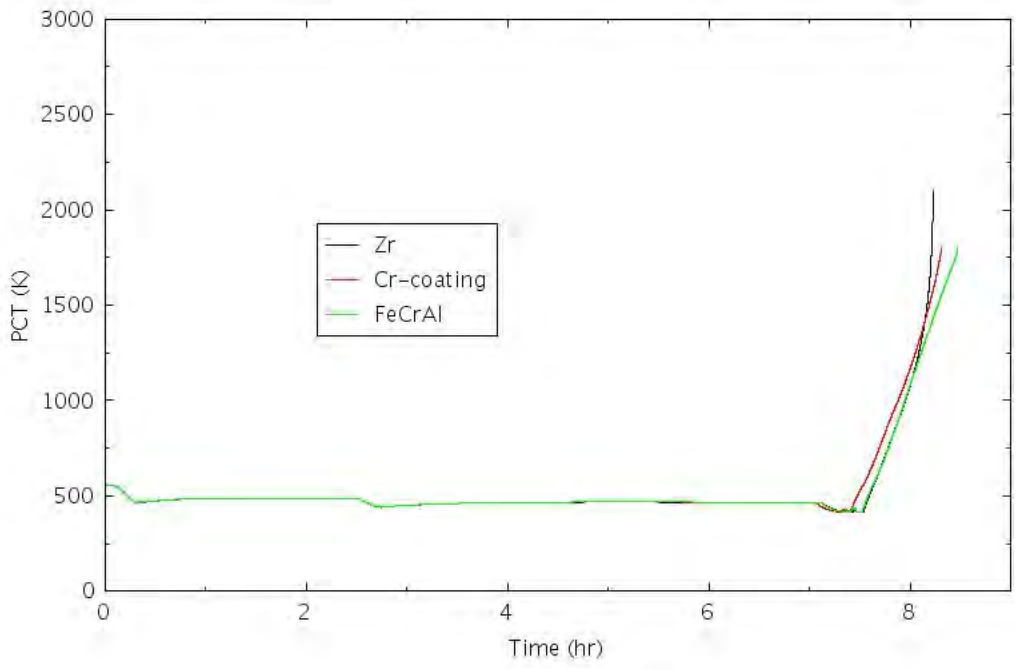

Figure 4-48. PCT Comparison During TRANS-SORV-3.

4.2.1.8 TRANS-SORV-4

In this scenario, it is assumed a general transient IE causes the reactor to automatically shut down. AC power is available, and one SRV is stuck-open once the valve is lifted by the initial rise of the system pressure. The PCS fails so all steam is guided to the SP where it condenses. The HPI system successfully starts; however, it stops injecting water into the RPV once the SP temperature reaches 361 K (190°F). Once the HPI system ceases to inject water into the RPV, the RPV water level starts to decrease. Once the water level reaches the Level 1 water level set point, the LPCI system starts to inject water into the RPV. It is further assumed once the containment drywell pressure reaches its design pressure of 0.49 MPa (70.7 psia), the LPCI stops to inject water into the RPV. With the loss of water injection into the RPV, the coolant in the core continues to boil off and the reactor core eventually becomes uncovered leading to fuel damage at about 13 hours into the transient. Figure 4-49 shows the HPI mass flow rate. Figure 4-50 shows the low-pressure injection mass flow rate. With the high-mass flow rate of the LPCI injection, the RPV water level rises up quickly as shown in Figure 4-51. The low-pressure injection is stopped once the water level reaches high-water level set point to avoid the flooding of the main steam line. The LPCI is not started again before the drywell pressure reaches its design value of 0.49 MPa. The SP temperature is shown in Figure 4-52, and the drywell pressure is shown in Figure 4-53. The mass flow rate through the SRVs is shown in Figure 4-54. It can be seen steam flows out of the SRVs continuously during the transient leading to the depressurization of the RPV. The RPV dome pressure is shown Figure 4-55. With the stuck-open SRV, the RPV pressure initially decreases rapidly. With the water injection from HPI initially and later from LPCI, the RPV dome pressure rises a bit but still stays in the low range. The PCT comparisons are shown in Figure 4-56.

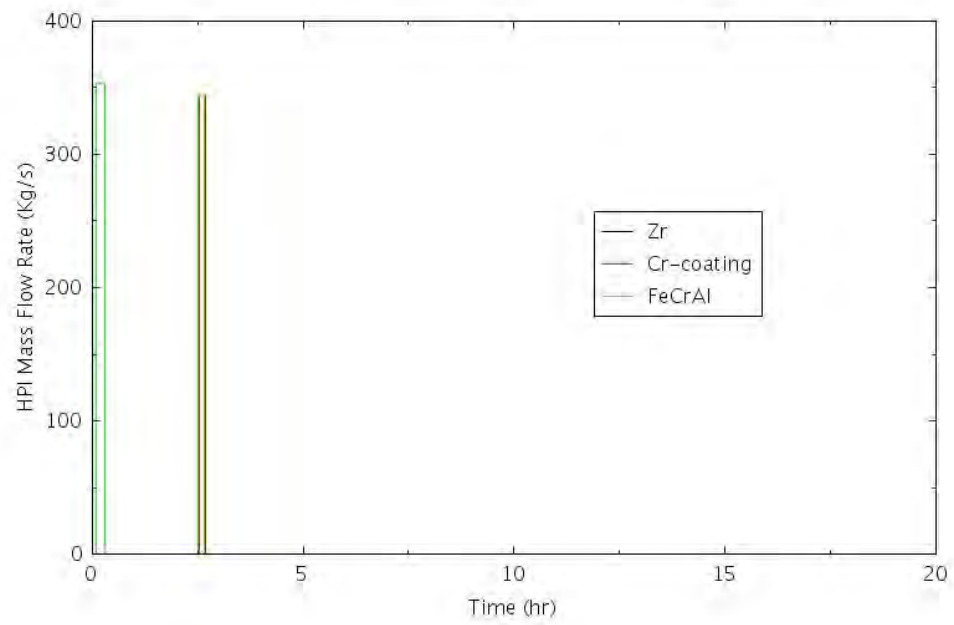

Figure 4-49. HPI Mass Flow Rate for TRANS-SORV-4.

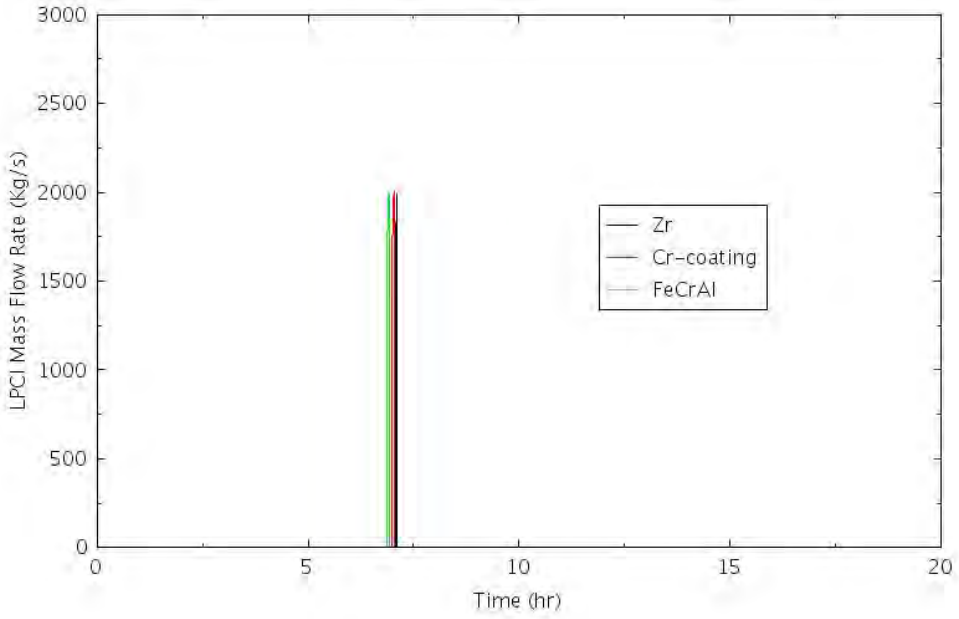

Figure 4-50. LPCI Mass Flow Rate for TRANS-SORV-4.

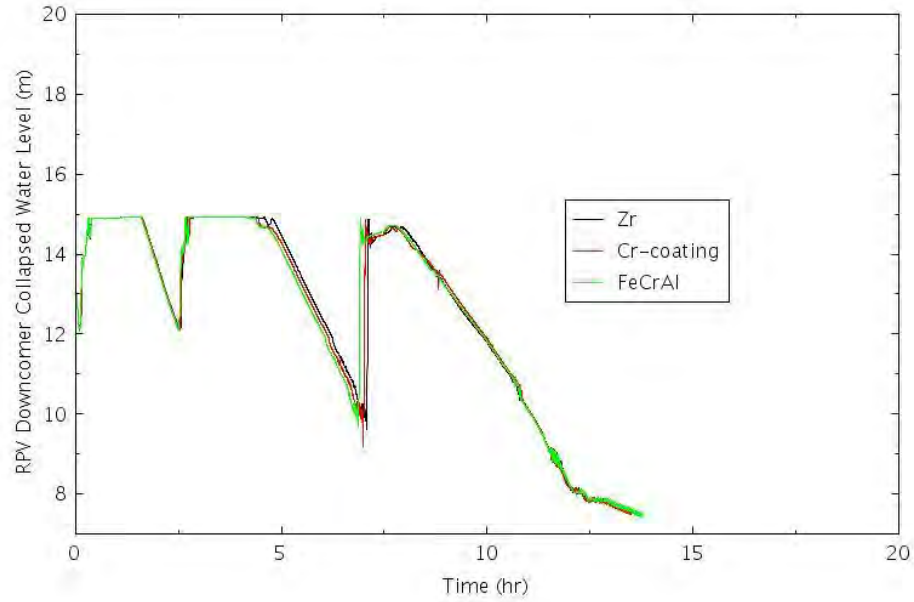

Figure 4-51. RPV Collapsed Water Level for TRANS-SORV-4.

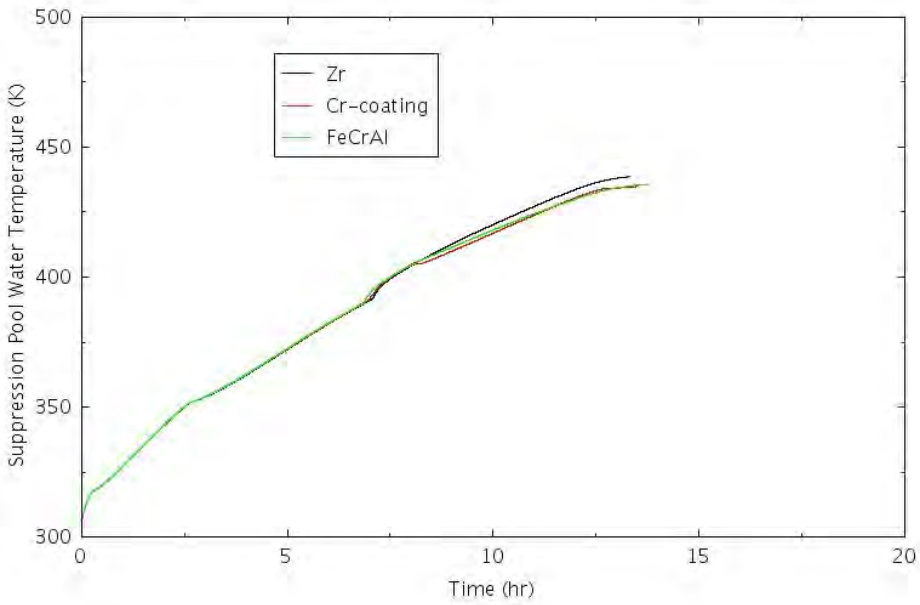

Figure 4-52. Containment WW Suppression Temperature for TRANS-SORV-4.

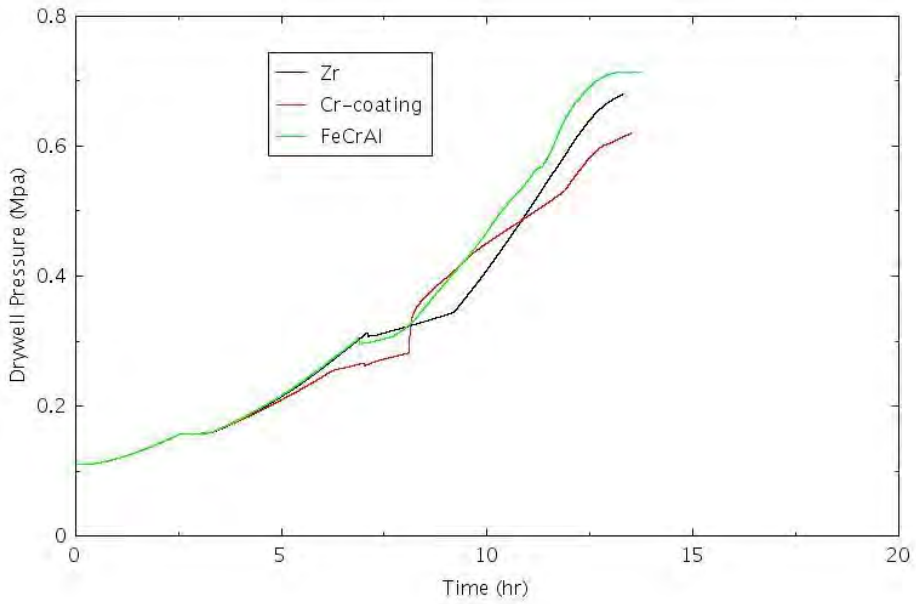

Figure 4-53. Containment DW Pressure for TRANS-SORV-4.

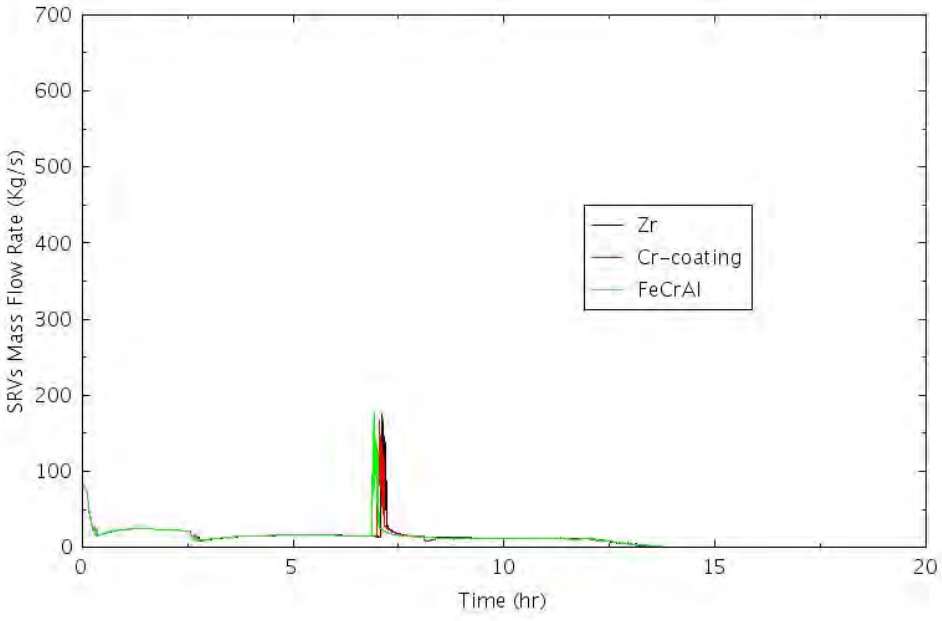

Figure 4-54. Mass Flow Rate Through SRVs for TRANS-SORV-4.

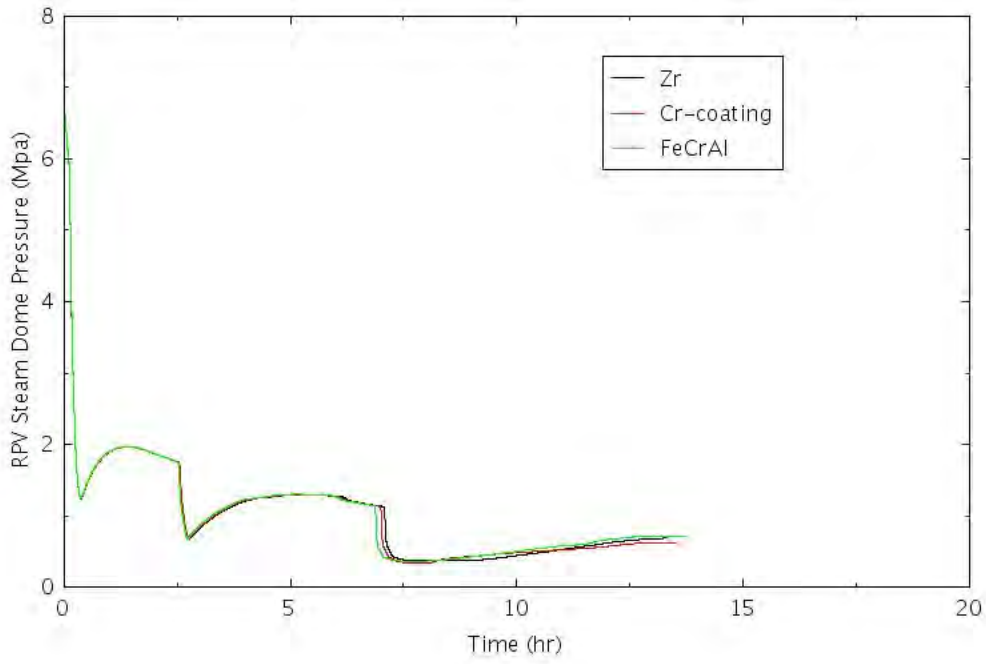

Figure 4-55. RPV Steam Dome Pressure for TRANS-SORV-4.

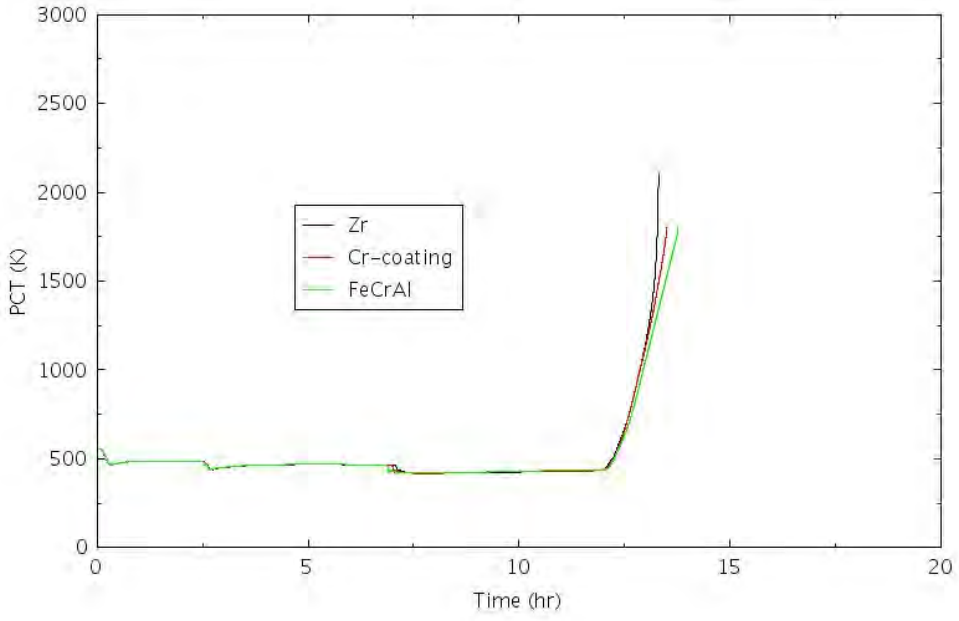

Figure 4-56. PCT Comparison for TRANS-SORV-4.

4.2.1.9 TRANS-SORV-5

In this scenario, it is assumed a general transient IE causes the reactor to automatically shut down. AC power is available, and two SRVs are stuck-open once they are lifted open by the initial rise of the system pressure. The PCS fails so all steam is guided to the SP where it condenses. The HPI system successfully starts; however, it stops injecting water into the RPV once the SP temperature reaches 361 K (190°F). With the two SRVs stuck-open, the low-pressure safety injection system is able to inject water into RPV once the system pressure is low enough. It is assumed the CS system is able to inject condensate water into RPV. Once the containment drywell pressure reaches 0.49 MPa (70.7 Psia), it is assumed the core spay system stops working. With the loss of water injection into the RPV, the core continues to boil off and the reactor core eventually becomes uncovered which leads to fuel damage. Figure 4-57 shows the HPI mass flow rate. Figure 4-58 shows the CS injection mass flow rate. With the high-mass flow rate of the CS injection, the RPV water level is raised up quickly as shown in Figure 4-59. The CS injection is stopped once the water level reaches high-water level set point to avoid the flooding of the main steam line. The CS system is not started again before the drywell pressure reaches its design value of 0.49 MPa. The containment WW SP temperature and DW pressure are shown in Figure 4-60 and Figure 4-61, respectively. The mass flow rate through the SRVs is shown in Figure 4-62. It can be seen steam flows out of the SRVs continuously during the transient leading to the depressurization of the RPV. The RPV dome pressure is shown in Figure 4-63. With the two SRVs stuck-open, the RPV pressure initially decreases rapidly. With the water injection from HPI initially and later from CS, the RPV dome pressure rises a bit but still stays in the low range. The PCT comparisons are shown in Figure 4-64.

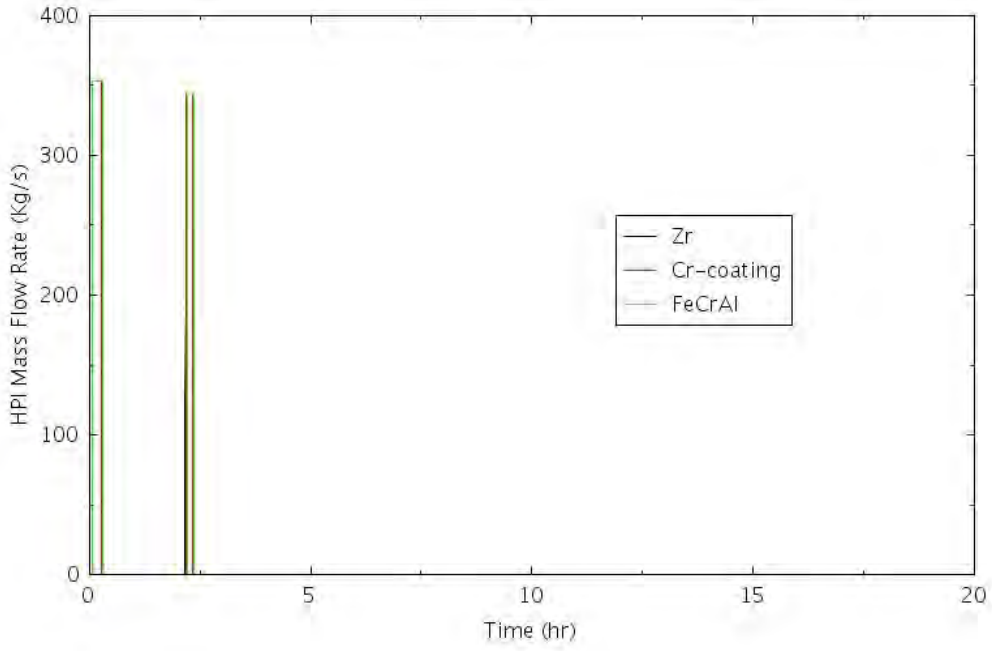

Figure 4-57. HPI Mass Flow Rate for TRANS-SORV-5.

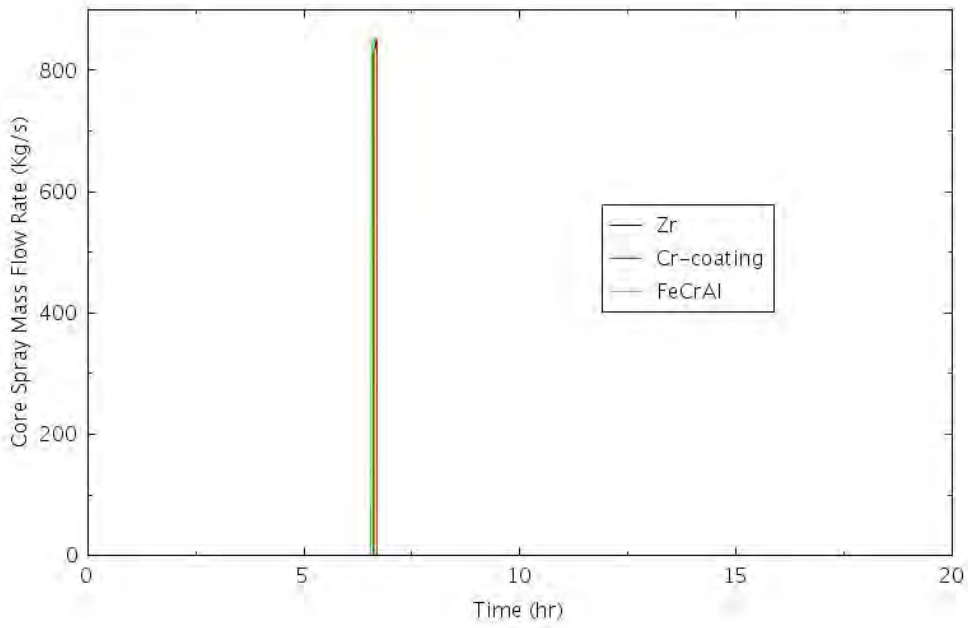

Figure 4-58. CS Mass Flow Rate for TRANS-SORV-5.

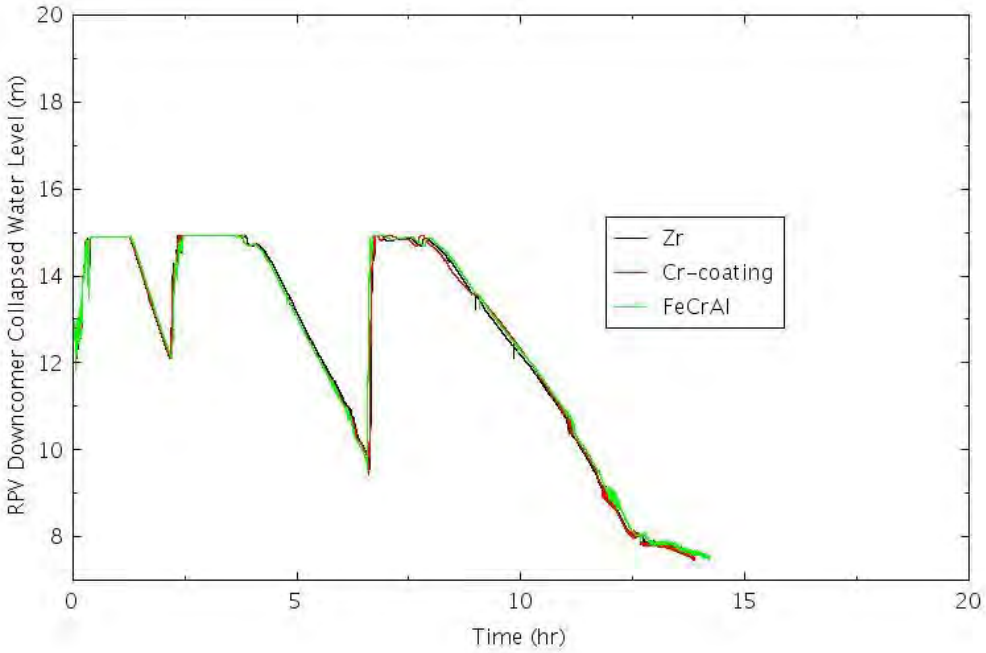

Figure 4-59. RPV Downcomer Collapsed Water Level for TRANS-SORV-5.

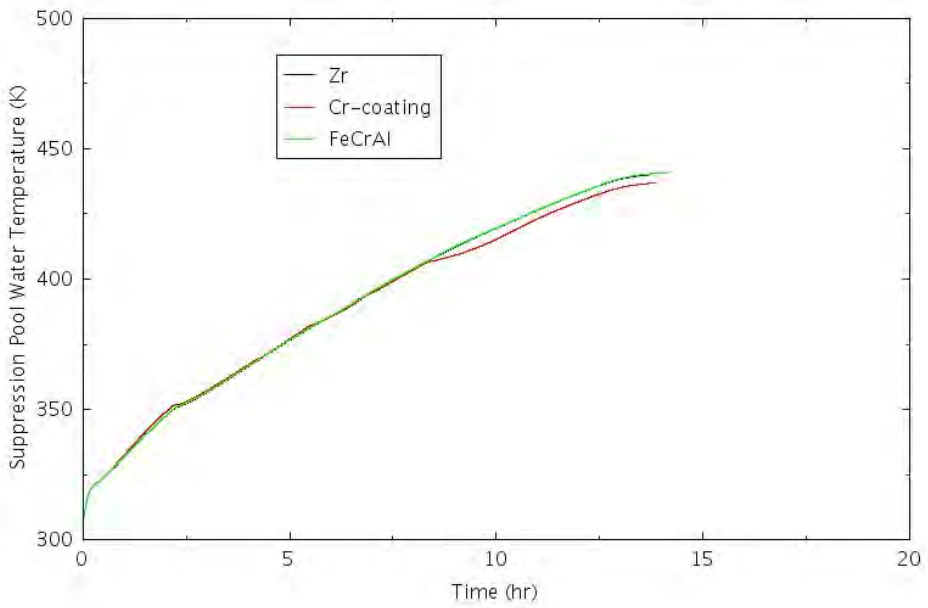

Figure 4-60. Containment WW SP Temperature for TRANS-SORV-5.

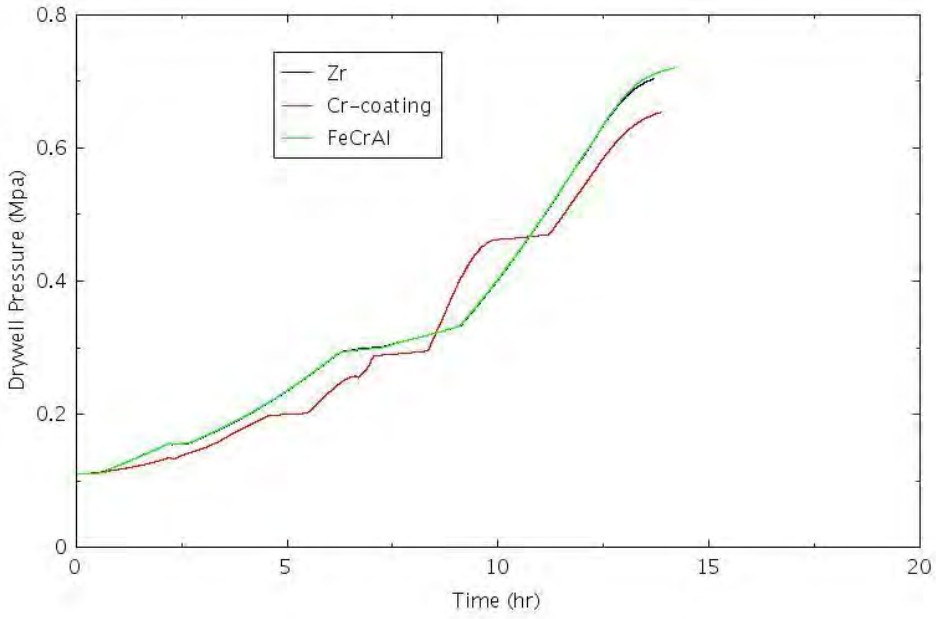

Figure 4-61. Containment DW Pressure for TRANS-SORV-5.

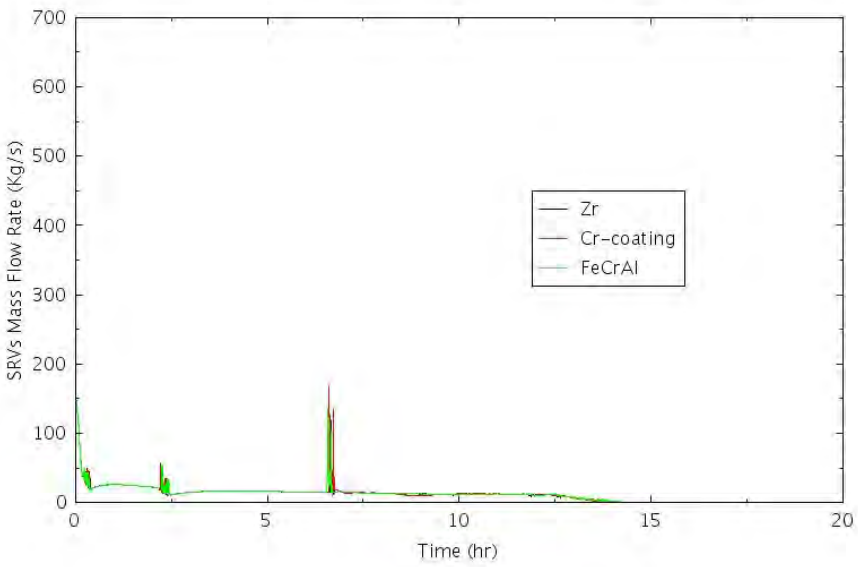

Figure 4-62. SRVs Mass Flow Rate for TRANS-SORV-5.

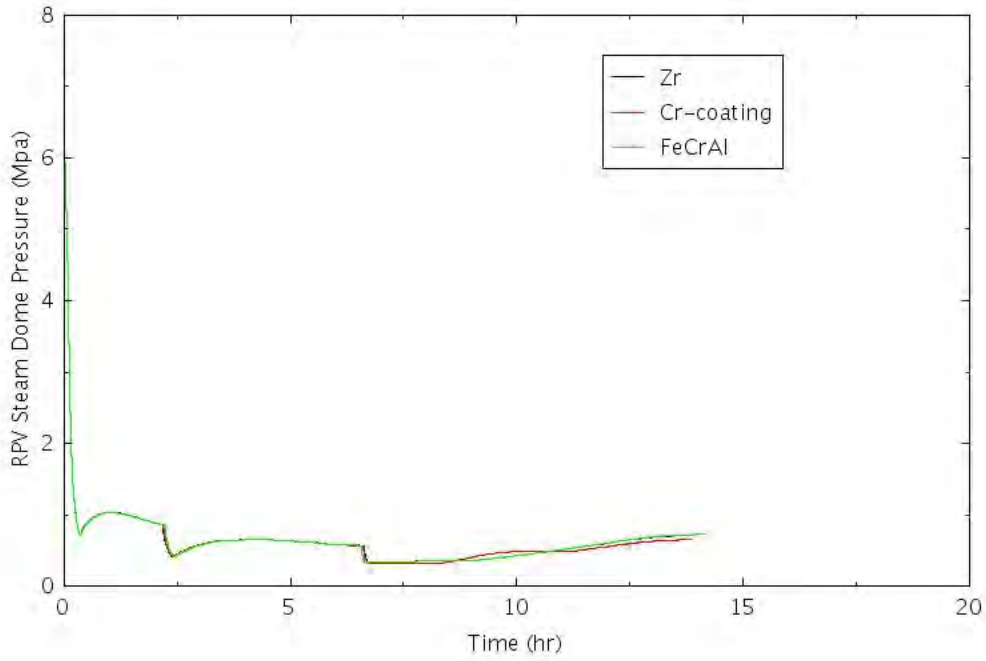

Figure 4-63. RPV Dome Pressure for TRANS-SORV-5.

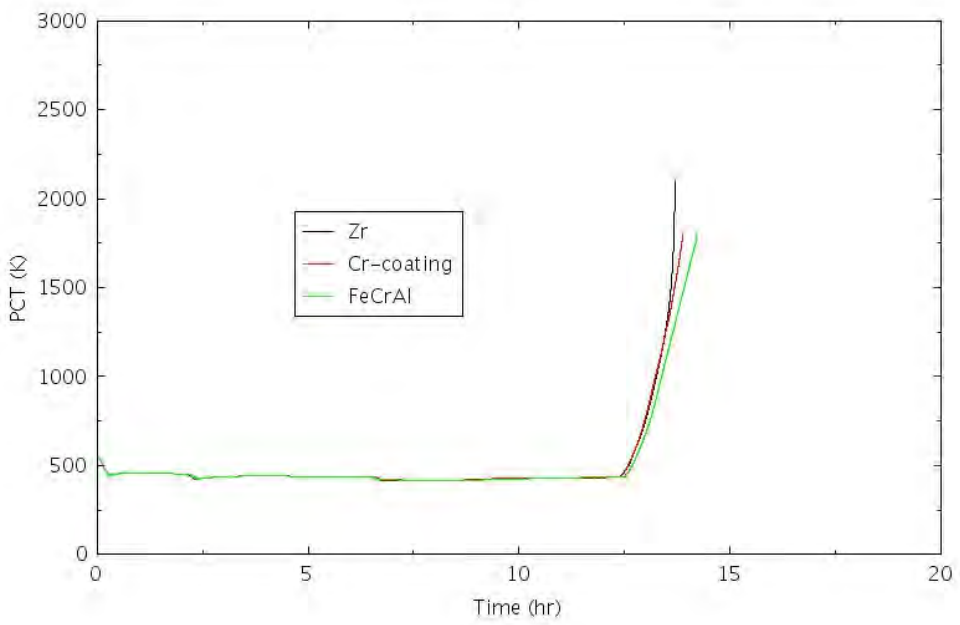

Figure 4-64. PCT Comparison for TRANS-SORV-5.

4.2.1.10 TRANS-LOOP-1

In this scenario, it is assumed a general transient IE occurs leading to the reactor automatically shutting down. The offsite power is lost, but the AC power is still available using the onsite emergency diesel power generator. All SRVs are successfully opened and reclosed depending on their respective set point values. RCS inventory is successfully maintained, initially through HPI system and later through manual depressurization to allow LPCI system to inject water into the RPV. In order to speed up the simulation time, it is assumed the HPI system stops injecting water into RPV once the SP water temperature reaches 361 K (190°F). After that, the RPV water level starts to decrease. Once the RPV downcomer water level reaches the Level 1 set point value, the RPV is depressurized such that LPCI system is able to inject water into the RPV. It is further assumed once containment drywell pressure reaches its design limit of 0.49 MPa (70.7 psia), the LPCI would stop injecting water due to the containment failure. Once the water injection stops, the coolant in the RPV boils off due the decay heat and leads to CD at about 19 hours into the transient. Figure 4-65 shows the HPI mass flow rate. Figure 4-66 shows the LPCI mass flow rate. Figure 4-67 shows the RPV downcomer collapsed water level. Figure 4-68 shows the RPV dome pressure. The manual depressurization of the RPV allows the LPCI system to inject water into the RPV. The large mass flow rate of LPCI allows the RPV water level to be restored quickly, as shown in Figure 4-67. The containment WW suppression temperature is shown in Figure 4-69, and the containment DW pressure is shown in Figure 4-70. Once the containment DW pressure reaches 0.49 MPa, the LPCI is not able to restart again and with the absence of makeup water to the RPV, the coolant in the core boils off due to the decay heat. Figure 4-71 shows the mass flow rates through SRVs, and Figure 4-72 shows the comparison of PCTs.

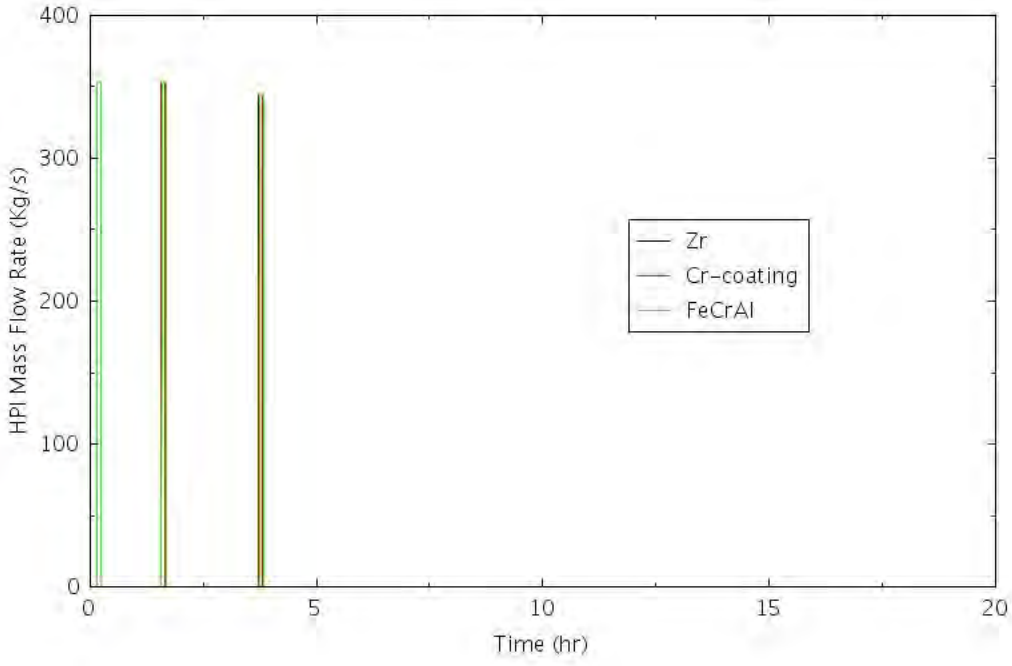

Figure 4-65. HPI Mas Flow Rate for TRANS-LOOP-1.

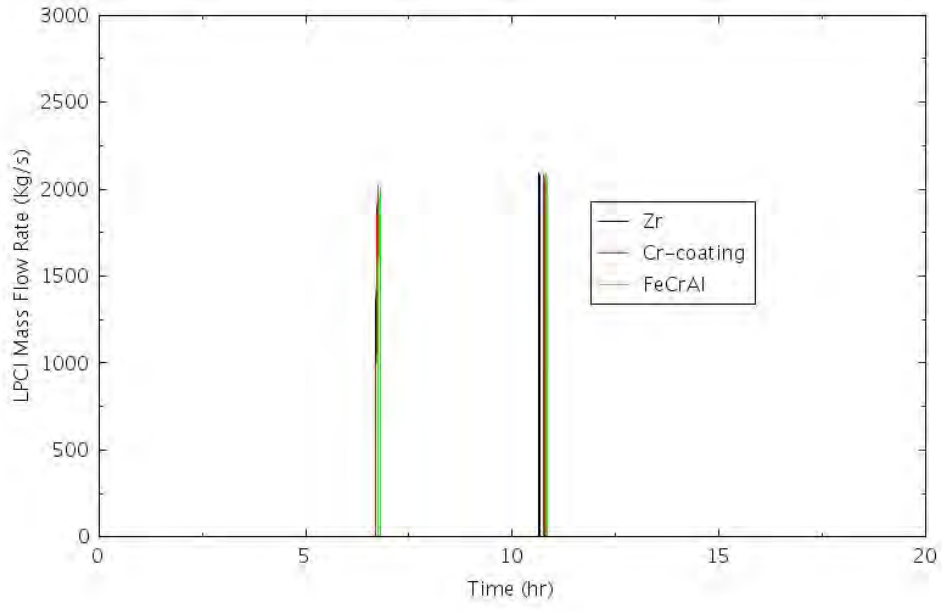

Figure 4-66. LPCI Mass Flow Rate for TRANS-LOOP-1.

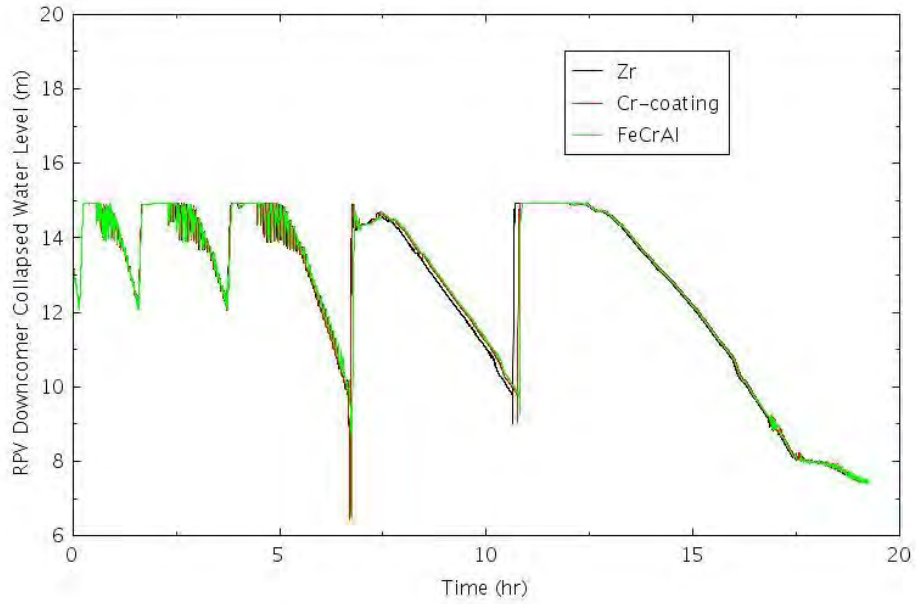

Figure 4-67. RPV Downcomer Collapsed Water Level for TRANS-LOOP-1.

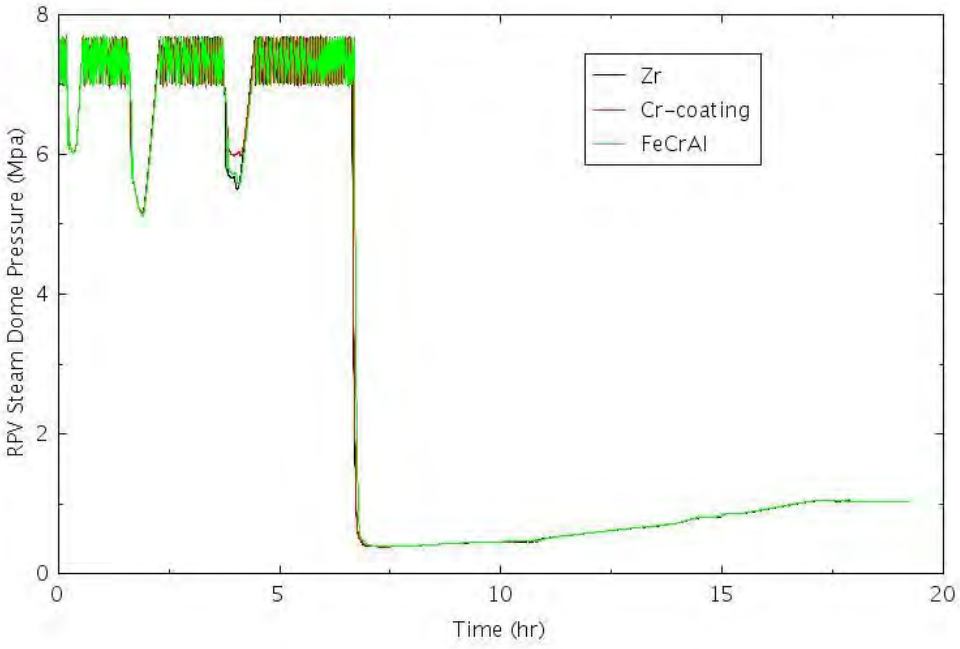

Figure 4-68. RPV Dome Pressure for TRANS-LOOP-1.

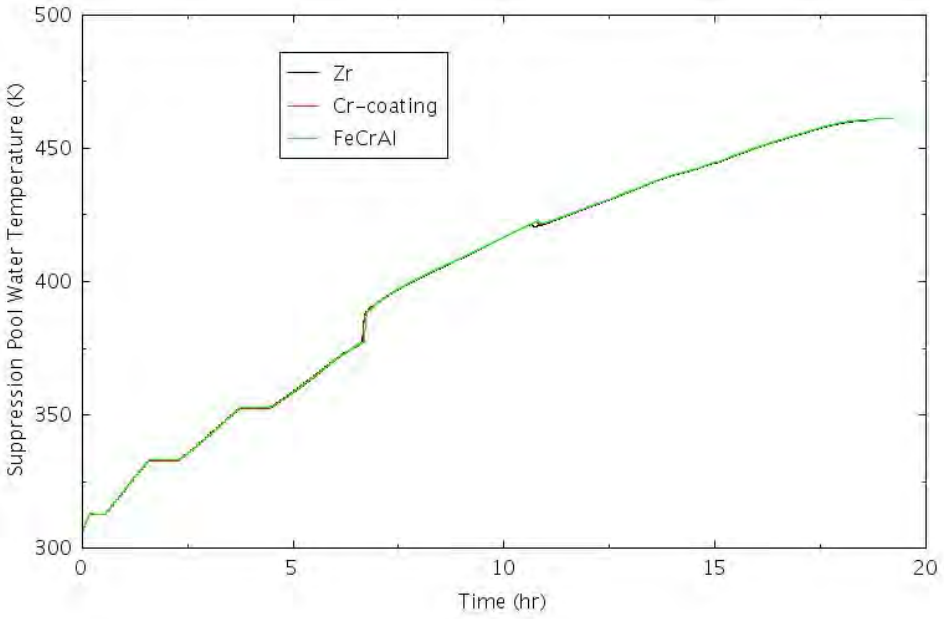

Figure 4-69. Containment WW Suppression Temperature for TRANS-LOOP-1.

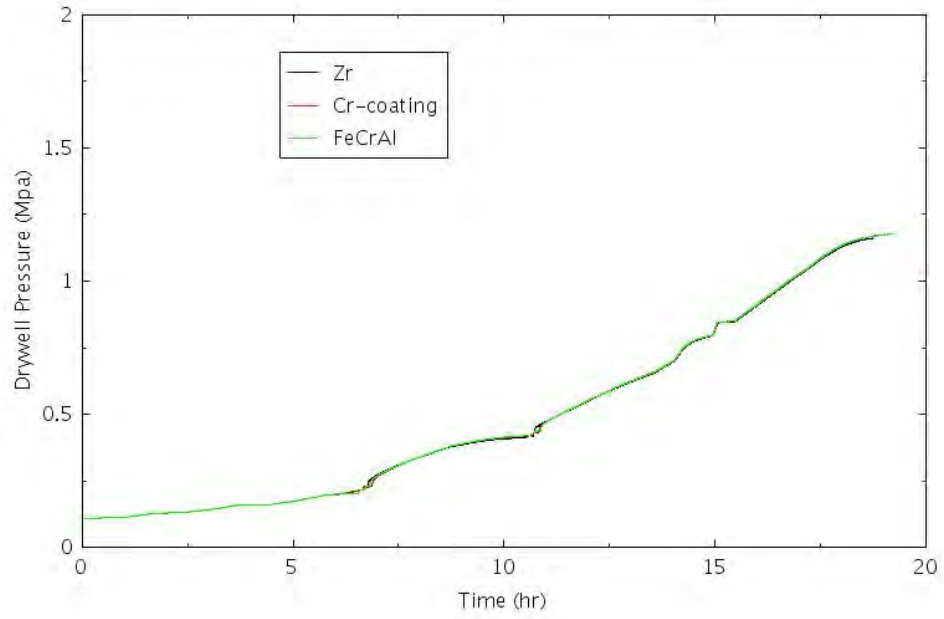

Figure 4-70. Containment DW Pressure for TRANS-LOOP-1.

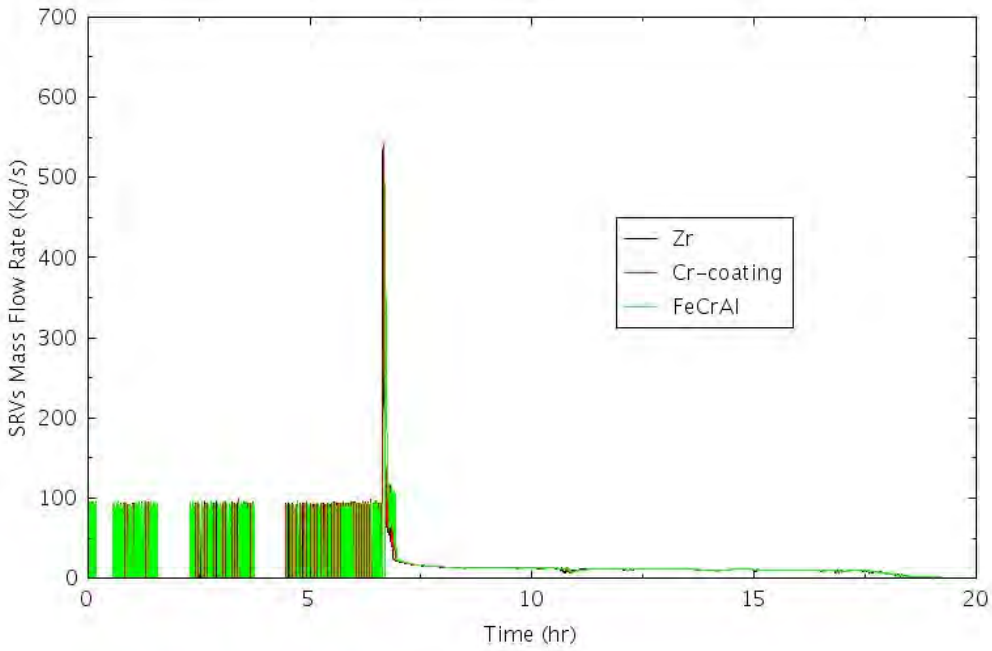

Figure 4-71. Mass Flow Rates through SRVs for TRANS-LOOP-1.

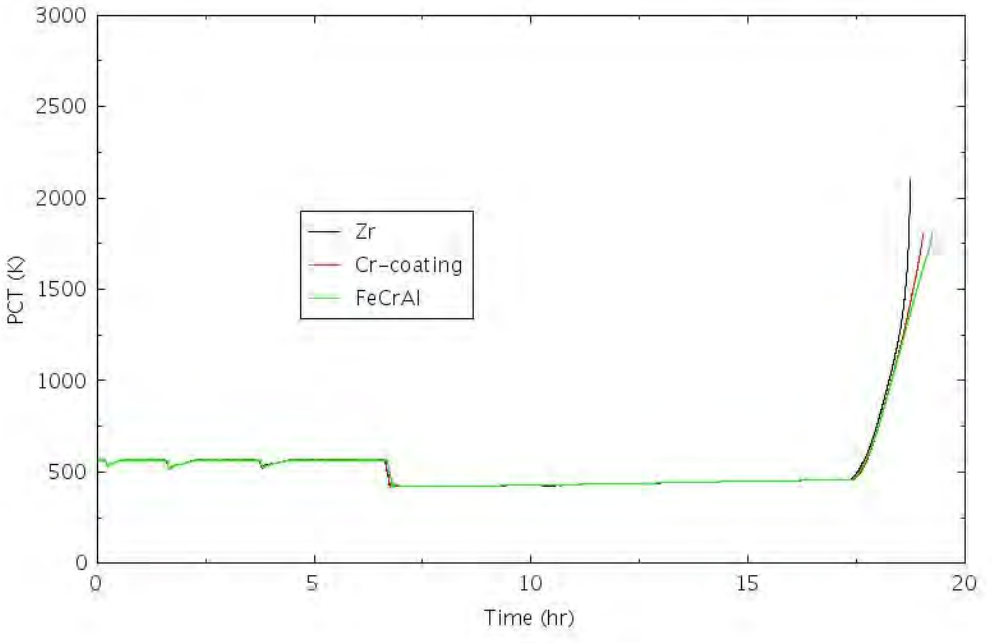

Figure 4-72. PCT Comparison for TRANS-LOOP-1.

4.2.2 Anticipated Transients Without Scram

The integrity of MARK I containments could be challenged by the consequences of a postulated transient such as MSIV closure followed by ATWS at full power. In this analysis, the inadvertent closure of the MSIVs is postulated to be the IE. In the simulations of ATWS transients, the plant is assumed to be at the nominal conditions before the accident. The MSIV closure begins at time zero. Scram signal occurs, but the reactor is postulated to fail to scram and results in ATWS. The MSIV valves close completely in about 3 seconds. The RPS fails to trip the reactor. The RPV pressure rises rapidly, collapsing core voids and thereby inserting positive reactivity and causing reactor power to rapidly rise initially. Rising fuel temperatures cause the negative Doppler reactivity to reduce the power. The rise in vessel dome pressure from steam generation in the core peaks at about 4 seconds. All 13 SRVs are then opened, and pressure begins to decrease. Once the low-pressure set points are reached, some of the SRVs are closed such that the system pressure stays within a predefined operating range. The steam from the SRVs is guided to the SP where it condenses. The feedwater controller is put into manual mode, and then, the feedwater flow is ramped down to zero after 120 seconds. It is further assumed the startup of the HPCI and RCIC systems is inhibited. The feedwater heaters are lost during this transient because they are shut off from the steam providing the necessary heat. This effect was represented in an approximate way only since the generic RELAP5-3D model used in the analysis does not include balance-of-plant systems. It is assumed the feedwater temperature will stay at its nominal temperature of 464.4 K for 30 seconds after the closure of the MSIV because of stored heat in the heater walls and the time required for the feedwater to be transported to the reactor vessel. Within 20 seconds, the feedwater temperature was ramped down to 321.7 K. Total cessation of feedwater flow into the vessel results in an immediate and rapid drop in downcomer liquid level.

4.2.2.1 TRANS-ATWS-1

In this scenario, it is assumed MSIV closure occurs at time zero, and the valves are fully closed at about 3 seconds as shown in Figure 4-73. The RPS fails to trip the reactor, leading to an ATWS. The reactor power initially rises and then starts to decrease as shown in Figure 4-74 and Figure 4-75. Figure 4-74 shows the reactor power during the entire transient, and Figure 4-75 provides zoomed in view of the reactor power change within the first 200 seconds of the transient. The feedback reactivity is shown in Figure 4-76 for the entire transient and Figure 4-77 for the zoomed in view of the feedback reactivity within the first 200 seconds of the transient. With the MSIV closure, the system pressure spikes rapidly. Figure 4-78 shows the RPV dome pressure for the entire transient, and Figure 4-79 provides a zoomed in view of the RPV pressure within the first 20 seconds of the transient. The system pressure spike causes the opening of all the SRVs, as shown in Figure 4-80 for the mass flow rates through the SRVs. It is further assumed the increase in system pressure also successfully trips the recirculation pumps. Recirculation pump trip occurs on high dome pressure at 7.826 MPa, and core flow is reduced to natural circulation conditions. This rapid decrease in flow also contributes to void formation in the core, supplying even more negative reactivity. The standby liquid control fails to start. Figure 4-81 shows the recirculation pump mass flow rate as a function of time. The feedwater flow is shown in Figure 4-82, and it ceases at 120 seconds. The feedwater temperature is shown in Figure 4-83. It is assumed feedwater heater works for 30 seconds, and the feedwater temperature drops to 321.8K at 50 seconds. The RPV collapsed water level is shown in Figure 4-84, and the water level drops precipitously once the feedwater flow stops. The decreasing water level in the RPV and core leads to fuel failure within 2,000 seconds after the initiation of the transient. Figure 4-85 shows the comparison of PCT for conventional fuel with Zircaloy cladding and ATF with Cr-coated and FeCrAl cladding.

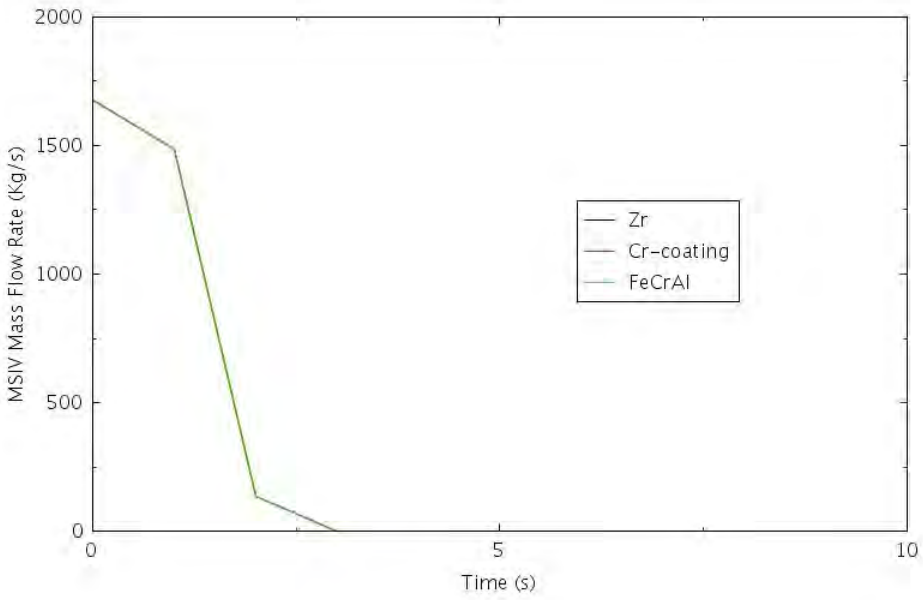

Figure 4-73. MSIV Mass Flow Rate for TRANS-ATWS-1.

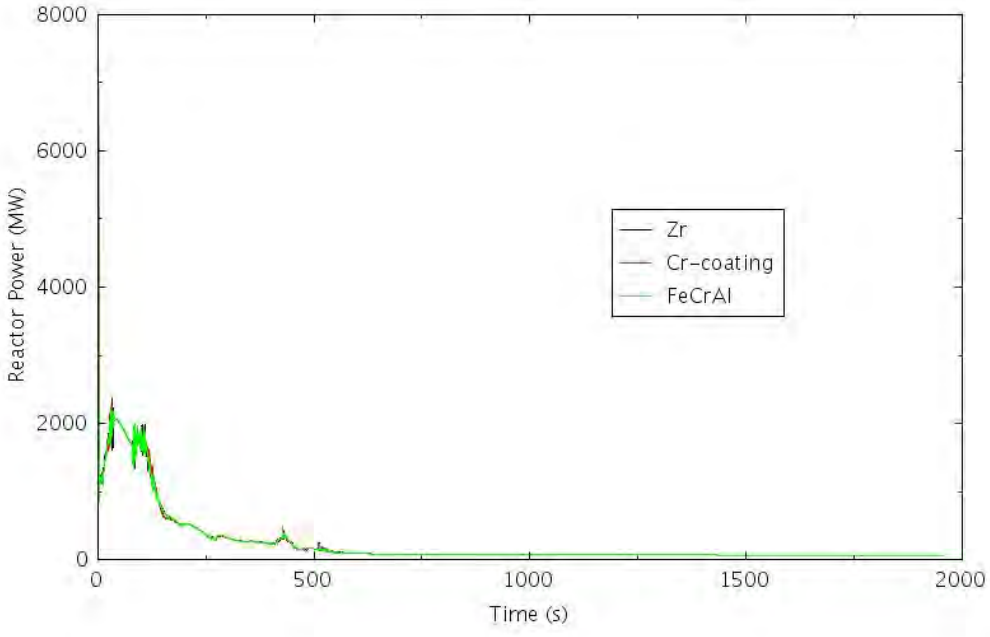

Figure 4-74. Reactor Power as a Function of Time for TRANS-ATWS-1.

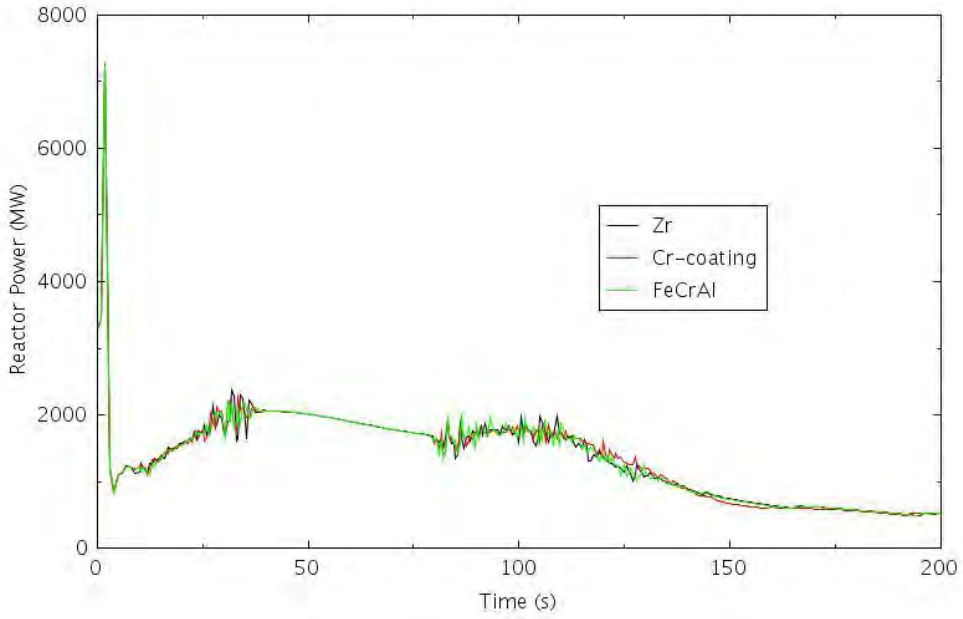

Figure 4-75. Reactor Power within 200 Seconds for TRANS-ATWS-1.

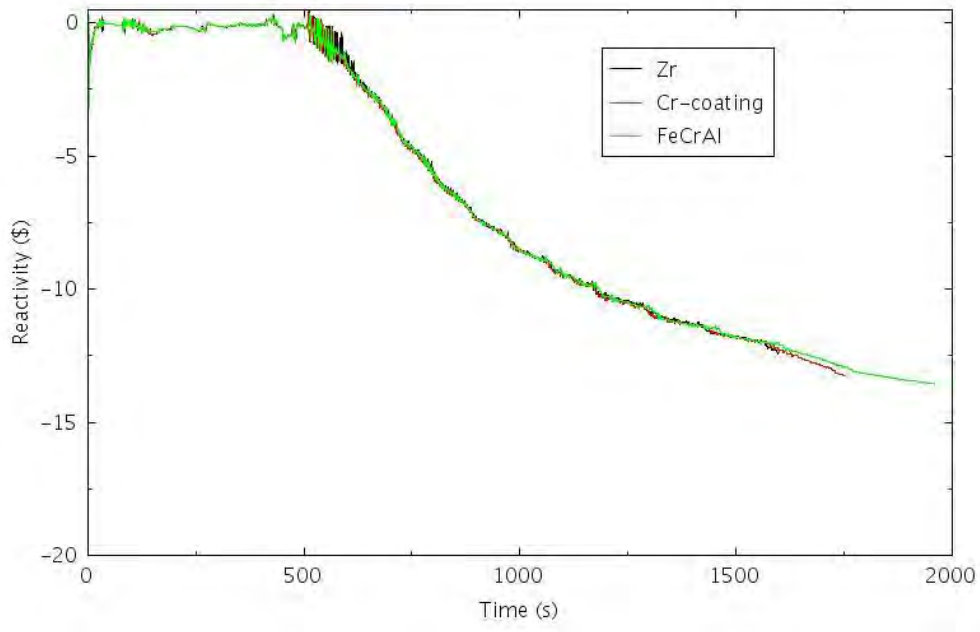

Figure 4-76. Feedback Reactivity as a Function of Time for TRANS-ATWS-1.

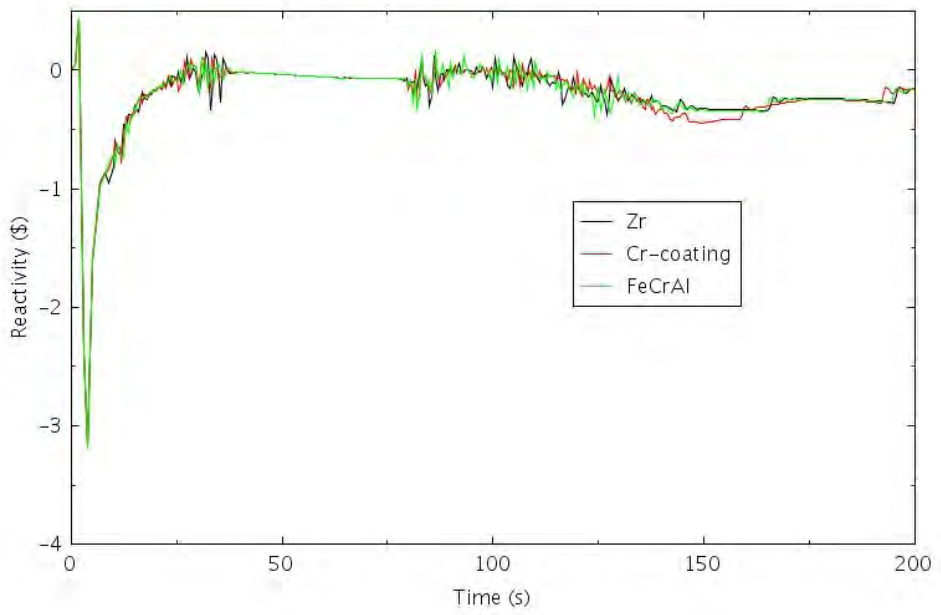

Figure 4-77. Feedback Reactivity within the First 200 Seconds for TRANS-ATWS-1.

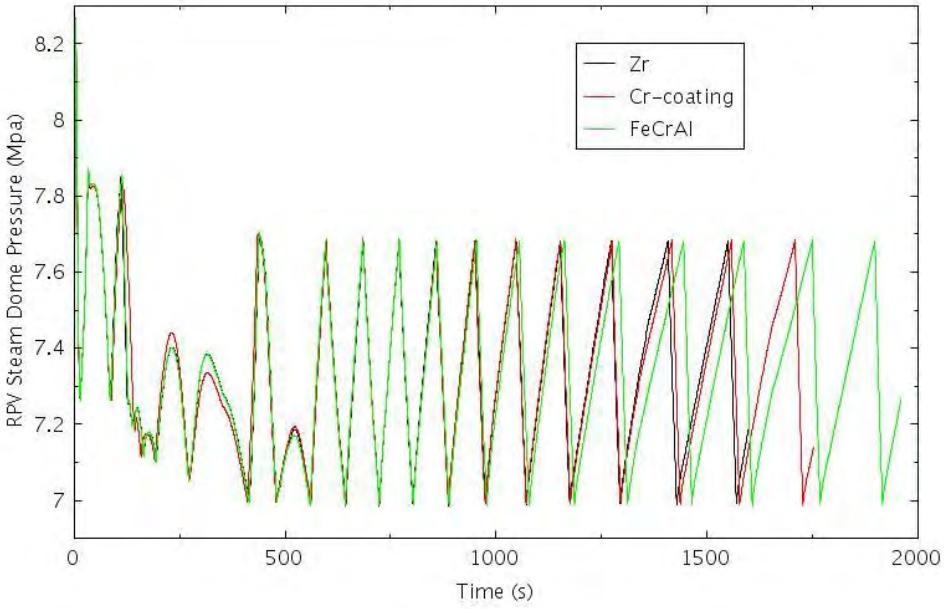

Figure 4-78. RPV Dome Pressure for TRANS-ATWS-1.

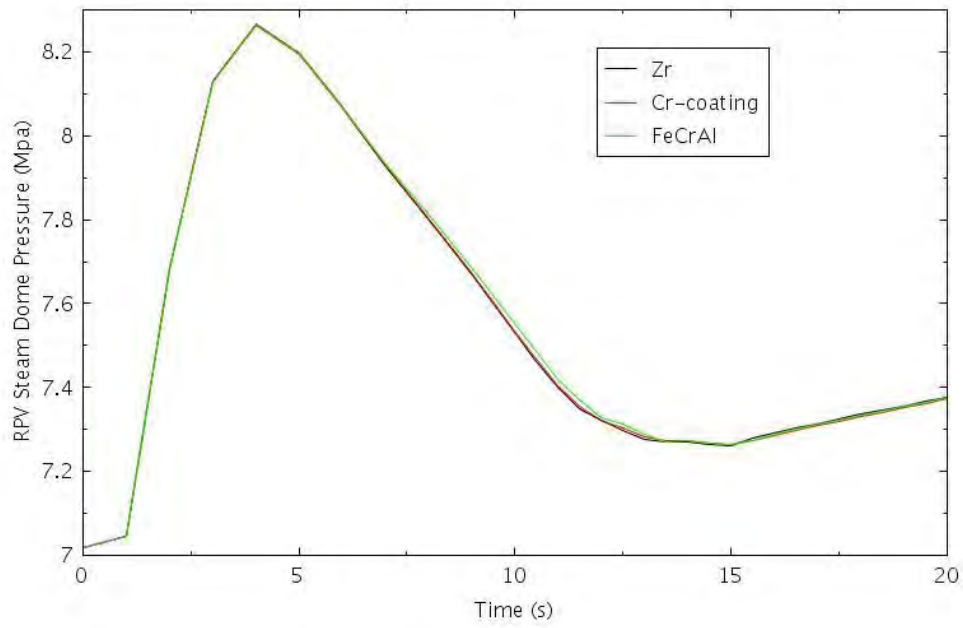

Figure 4-79. RPV Dome Pressure within the First 20 Seconds for TRANS-ATWS-1.

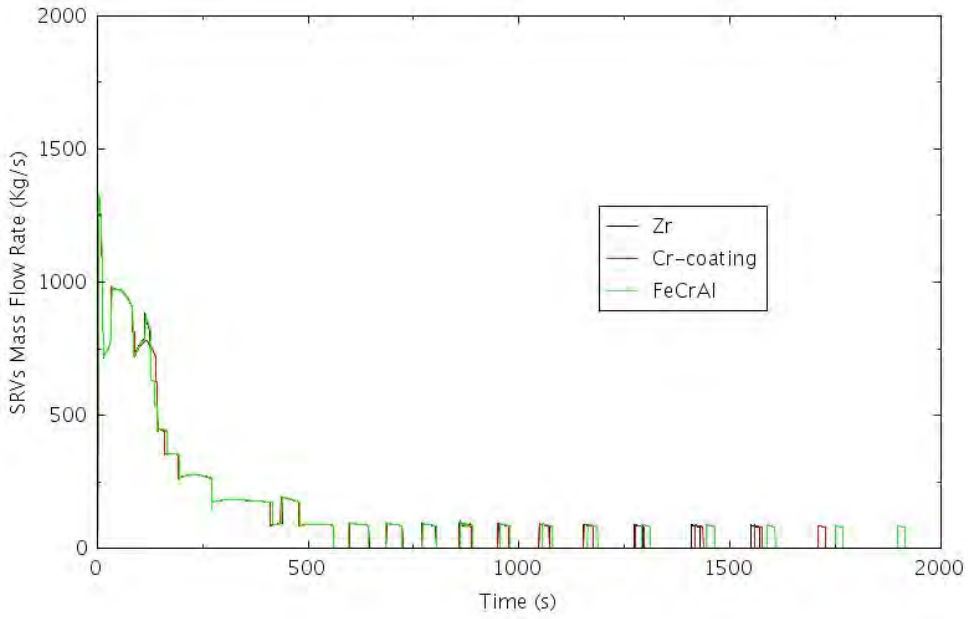

Figure 4-80. SRV Flow as a Function of Time for TRANS-ATWS-1.

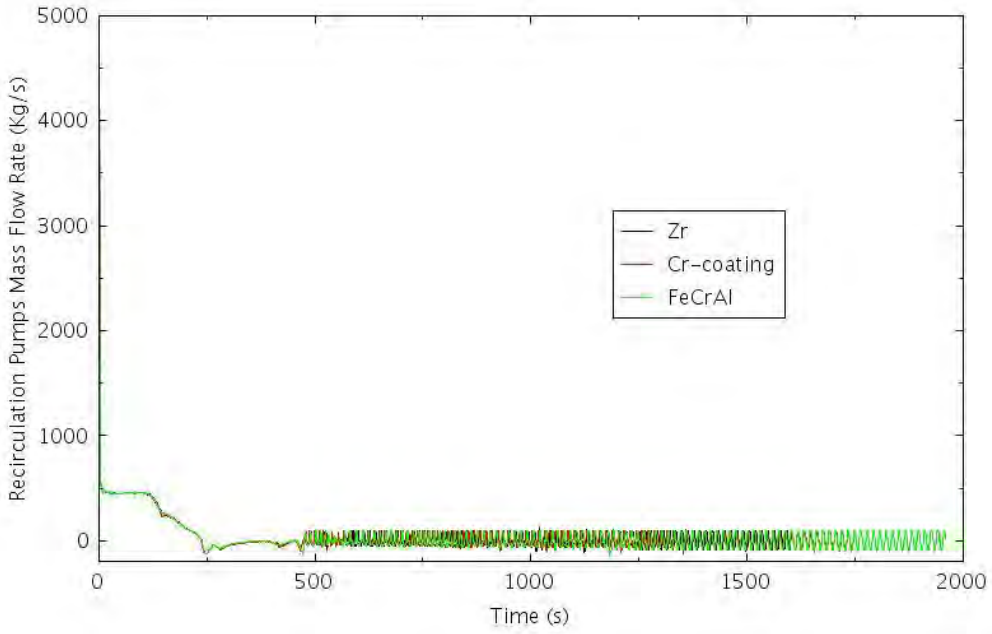

Figure 4-81. Recirculation Pump Mass Flow Rate as a Function of Time for TRANS-ATWS-1.

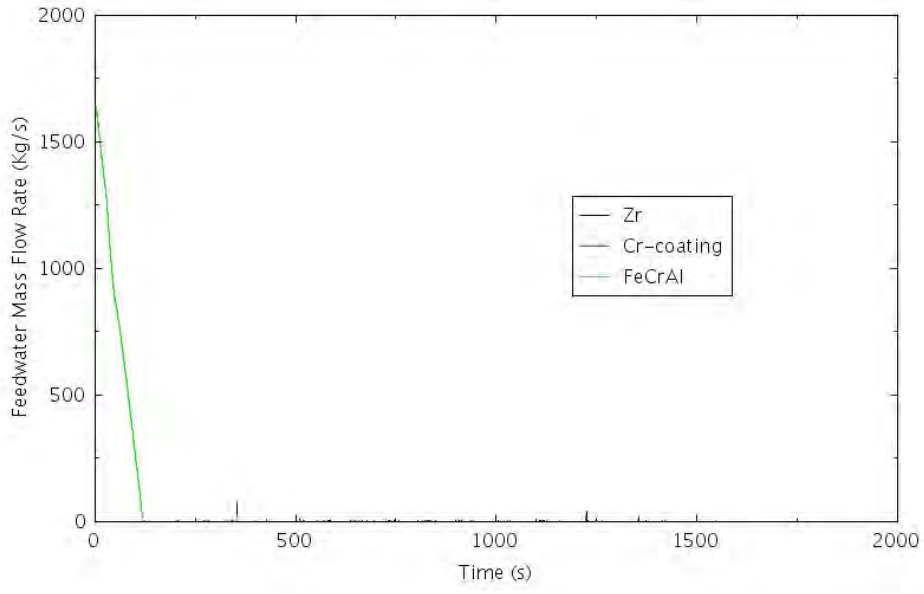

Figure 4-82. Feedwater Mass Flow Rate as a Function of Time for TRANS-ATWS-1.

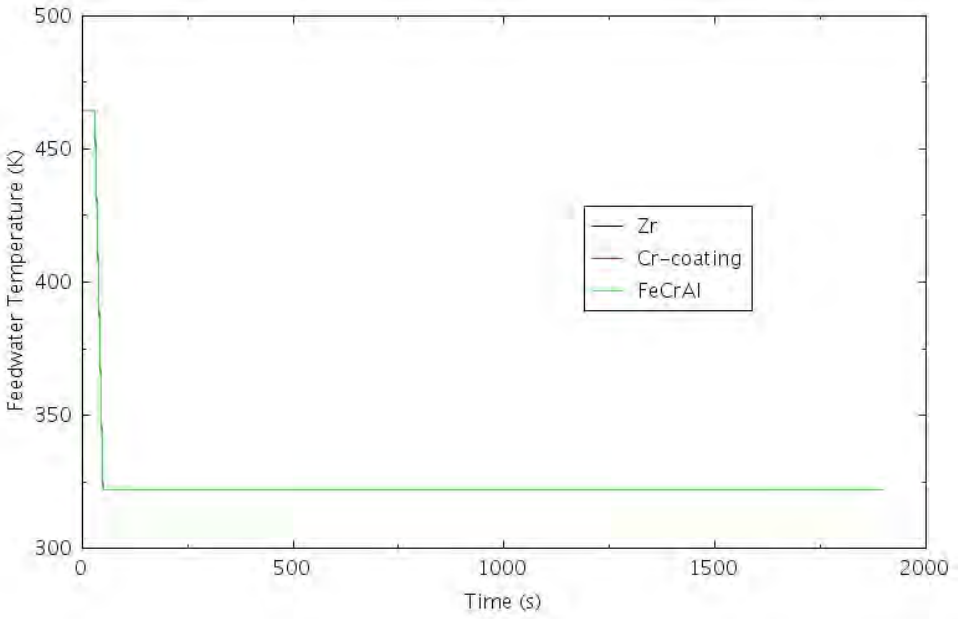

Figure 4-83. Feedwater Temperature as a Function of Time for TRANS-ATWS-1.

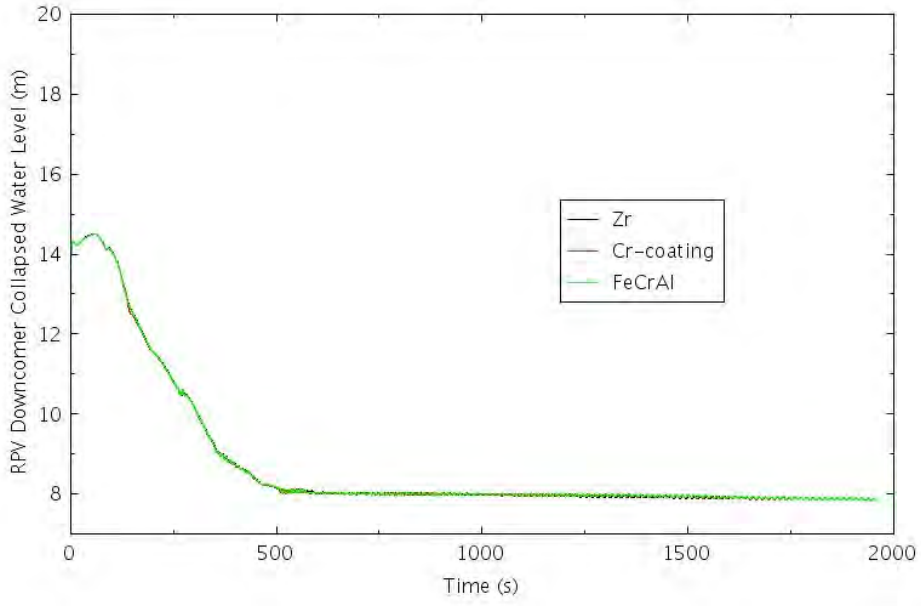

Figure 4-84. RPV Collapsed Water Level for TRANS-ATWS-1.

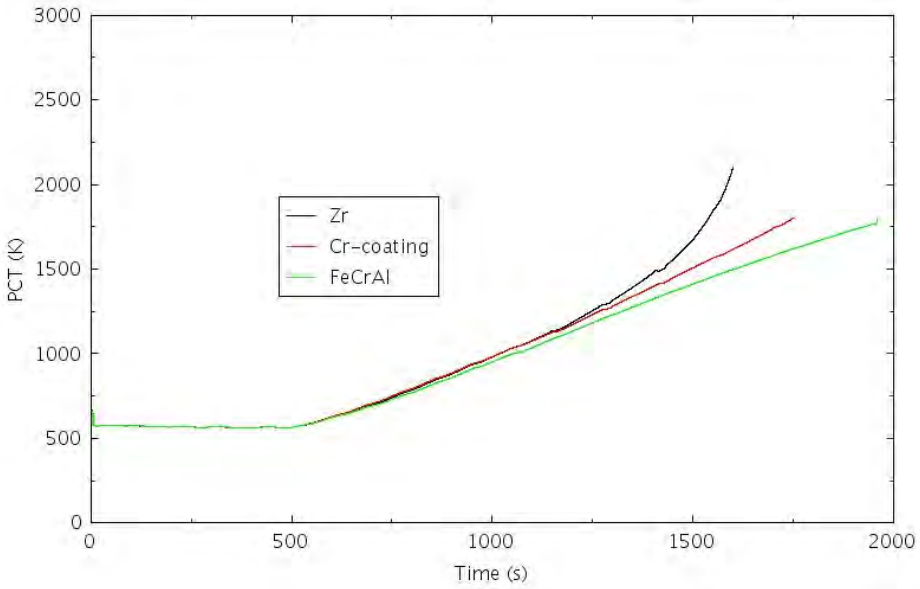

Figure 4-85. PCT as a Function of Time for TRANS-ATWS-1.

4.2.2.2 TRANS-ATWS-2

This scenario is similar to ATWS-1. The major difference is the recirculation pumps trip is assumed to fail under high-pressure conditions. Figure 4-86 shows the reactor power during the entire transient, and Figure 4-87 provides zoomed in view of the reactor power change within the first 200 seconds of the transient. The feedback reactivity is shown in Figure 4-88 for the entire transient and Figure 4-89 for the zoomed in view of the feedback reactivity within the first 200 seconds of the transient. With the closure of MSIV, the system pressure spikes rapidly. Figure 4-90 shows the RPV dome pressure for the entire transient. The system pressure spike causes the opening of all the SRVs, as shown in Figure 4-91, for the mass flow rates through the SRVs. However, the increase in system pressure fails to trip the recirculation pumps. Figure 4-92 shows the mass flow rate through the recirculation pumps during the entire transients. Even without tripping the recirculation pumps, the recirculation flow decreases rapidly, and this in turn reduces core flow through the reactor core. This rapid decrease in flow also contributes to void formation in the core supplying even more negative reactivity. The standby liquid control fails to start. The feedwater flow is shown in Figure 4-93, and it is assumed to cease at 120 seconds. The feedwater temperature is shown in Figure 4-94. It is assumed feedwater heater works for 30 seconds, and the feedwater temperature drops to 321.8K at 50 seconds. The RPV collapsed water level is shown in Figure 4-95, and the water level drops precipitously once the feedwater flow stops. Figure 4-96 shows the comparison of PCT for conventional fuel with Zircaloy cladding and ATF with Cr-coated and FeCrAl cladding.

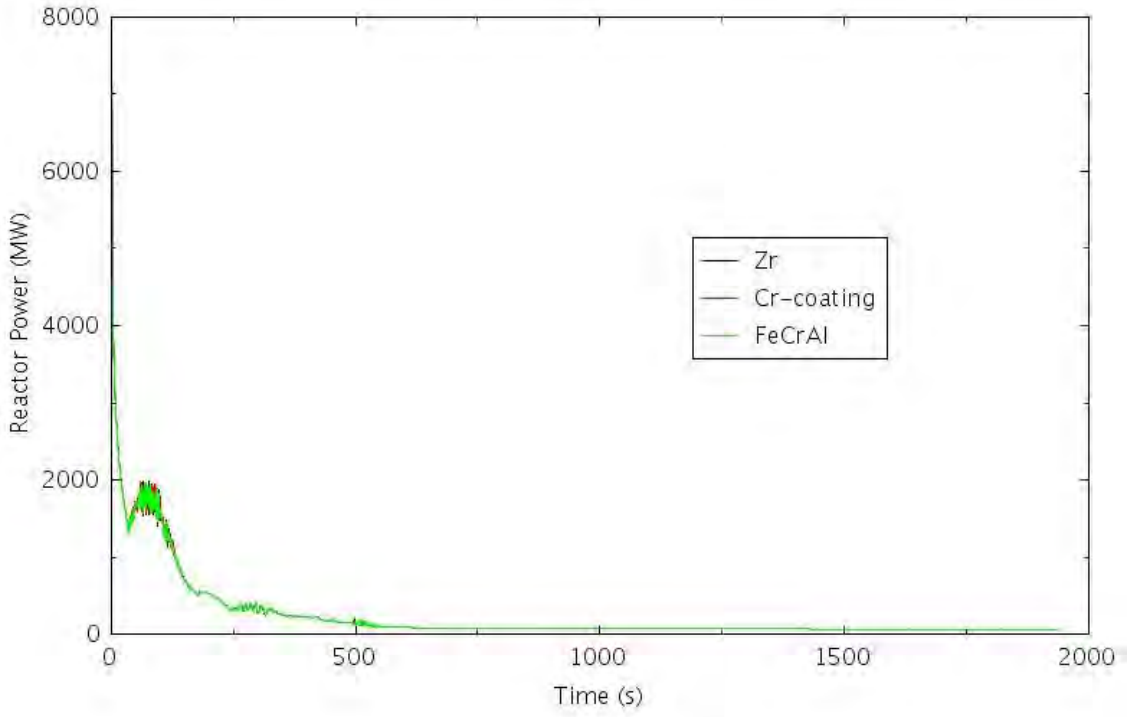

Figure 4-86. Reactor Power as a Function of Time for TRANS-ATWS-2.

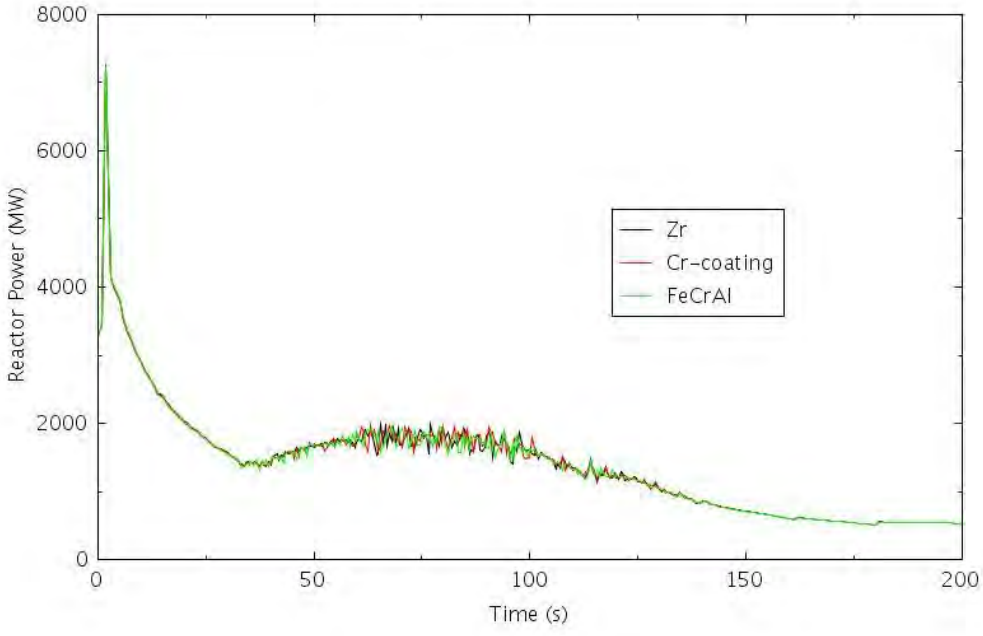

Figure 4-87. Reactor Power within the First 200 Seconds for TRANS-ATWS-2.

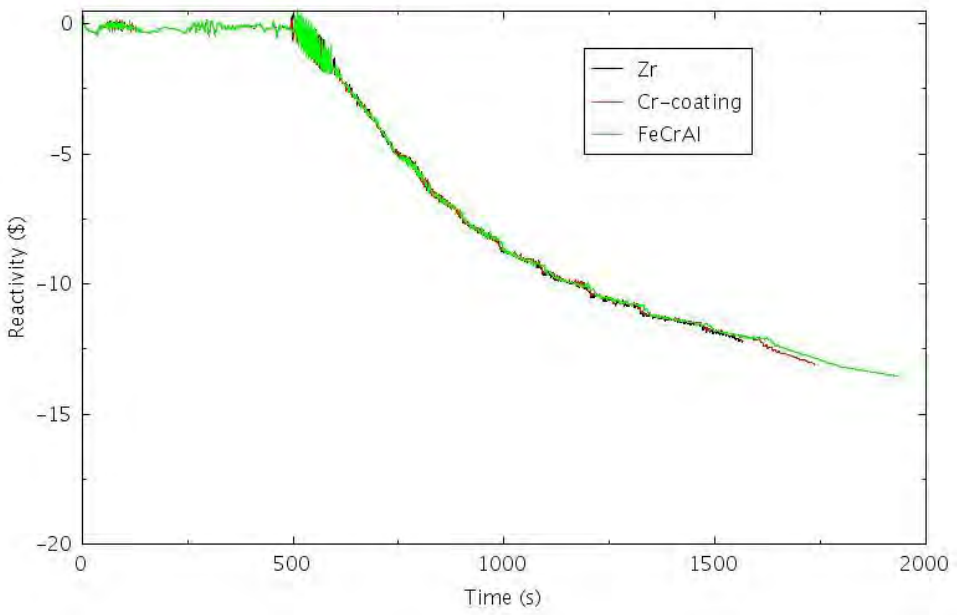

Figure 4-88. Feedback Reactivity as a Function of Time for TRANS-ATWS-2.

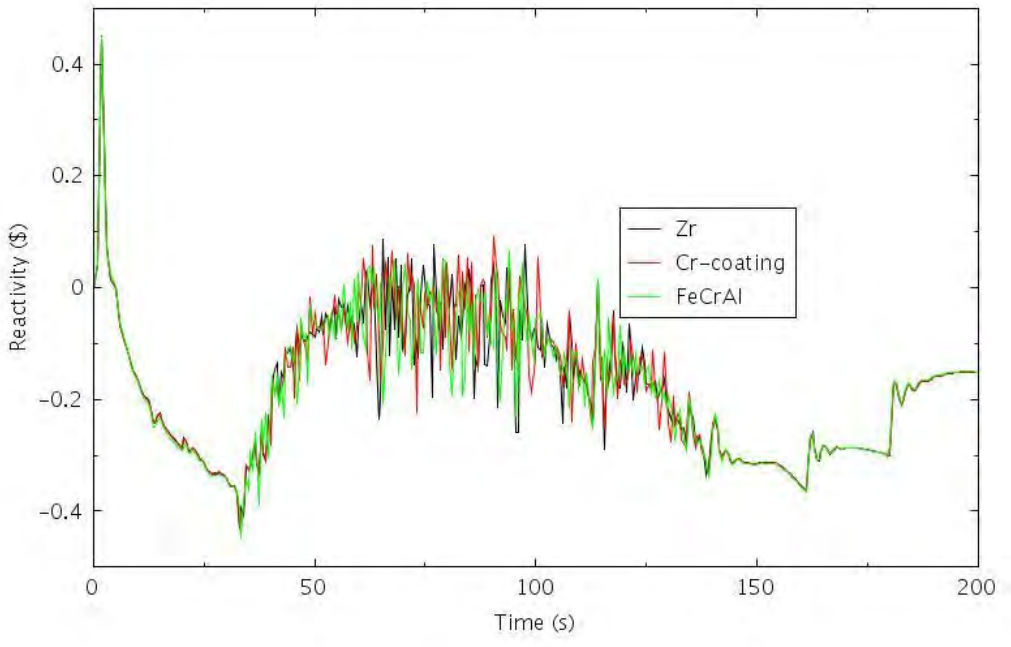

Figure 4-89. Feedback Reactivity for Within the First 200 Seconds for TRANS-ATWS-2.

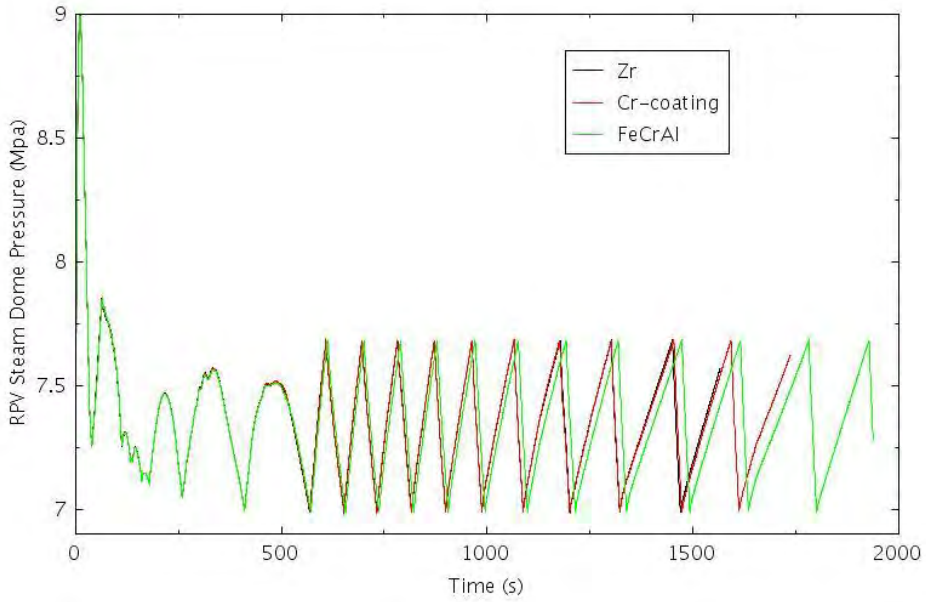

Figure 4-90. RPV Dome Pressure for TRANS-ATWS-2.

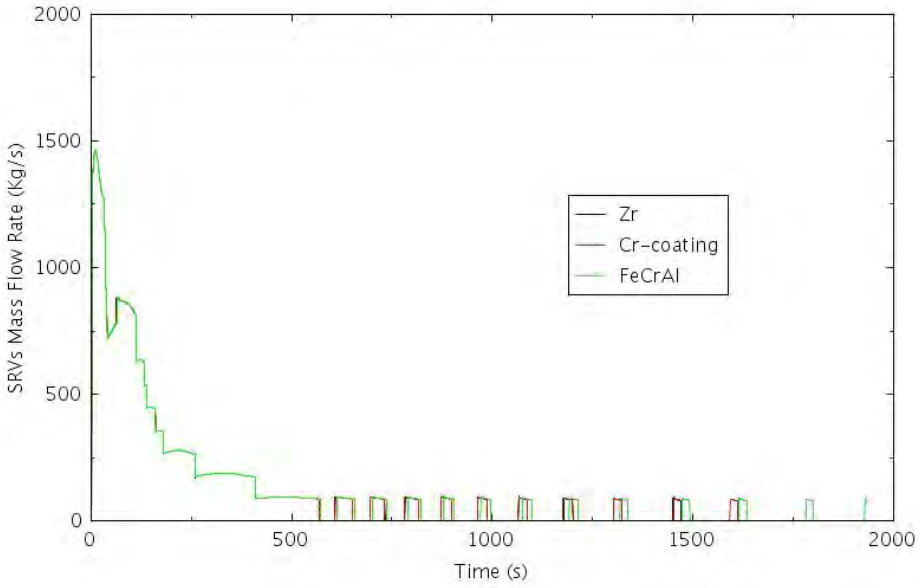

Figure 4-91. Mass Flow Rates Through SRVs as a Function of Time for TRANS-ATWS-2.

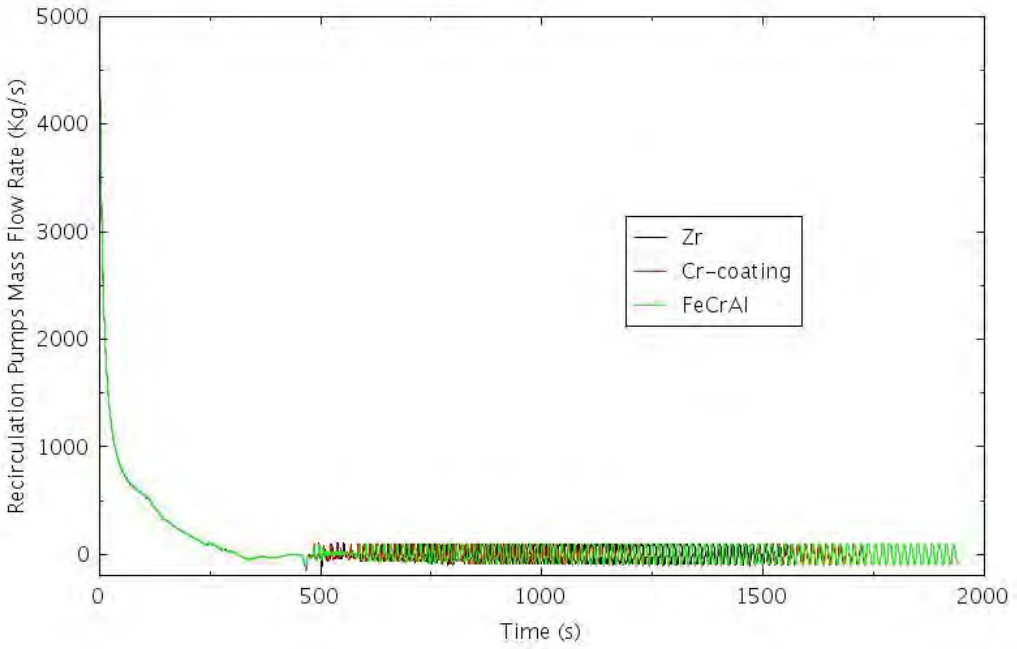

Figure 4-92. Recirculation Pumps Mass Flow Rate as a Function of Time for TRANS-ATWS-2.

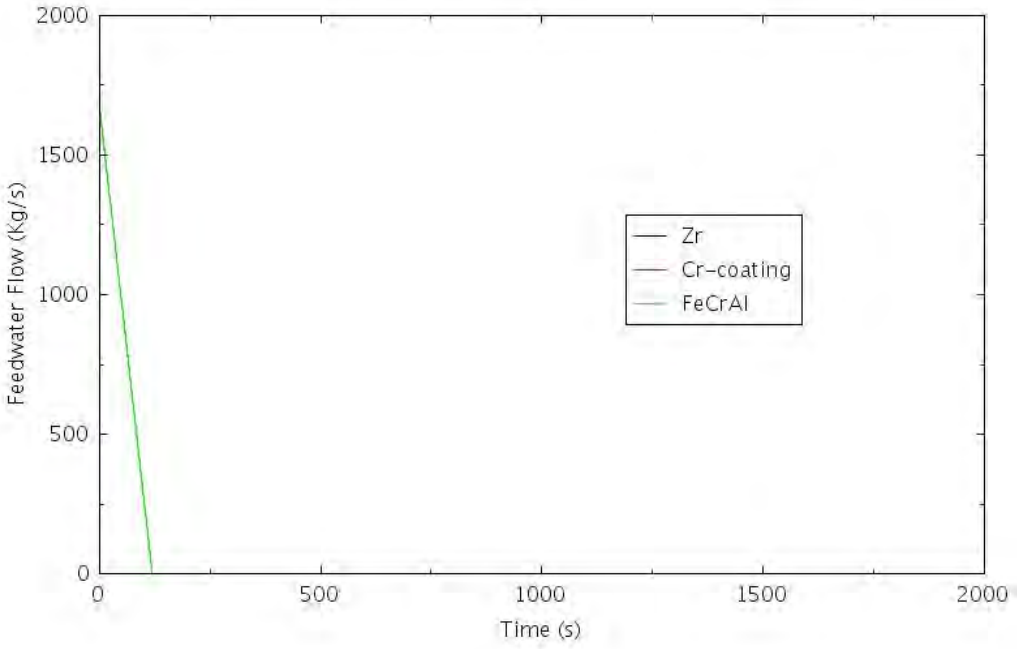

Figure 4-93. Feedwater Mass Flow Rate for TRANS-ATWS-2.

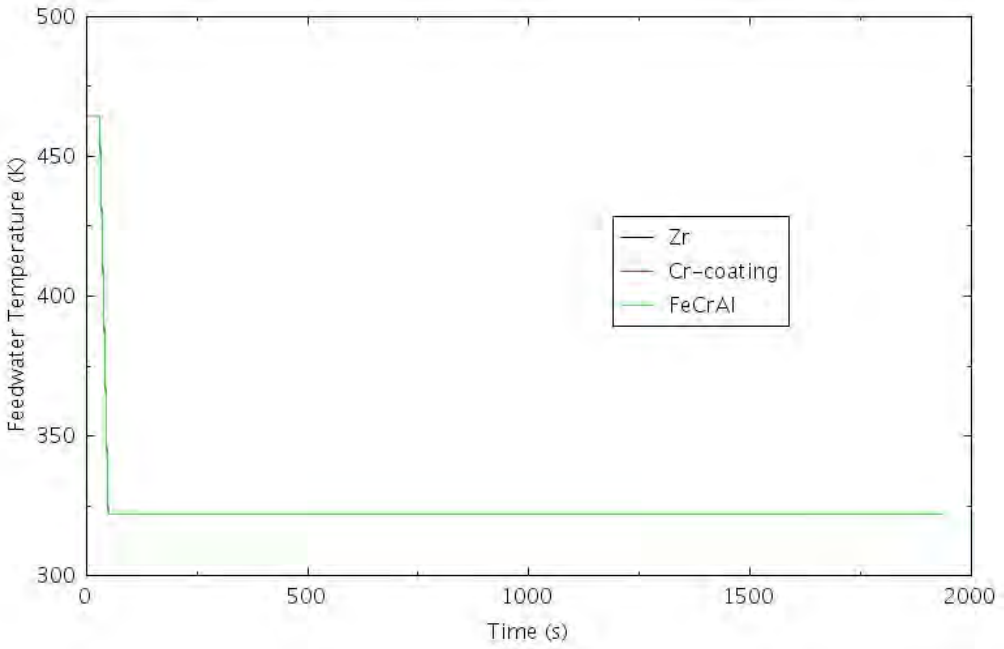

Figure 4-94. Feedwater Temperature for TRANS-ATWS-2.

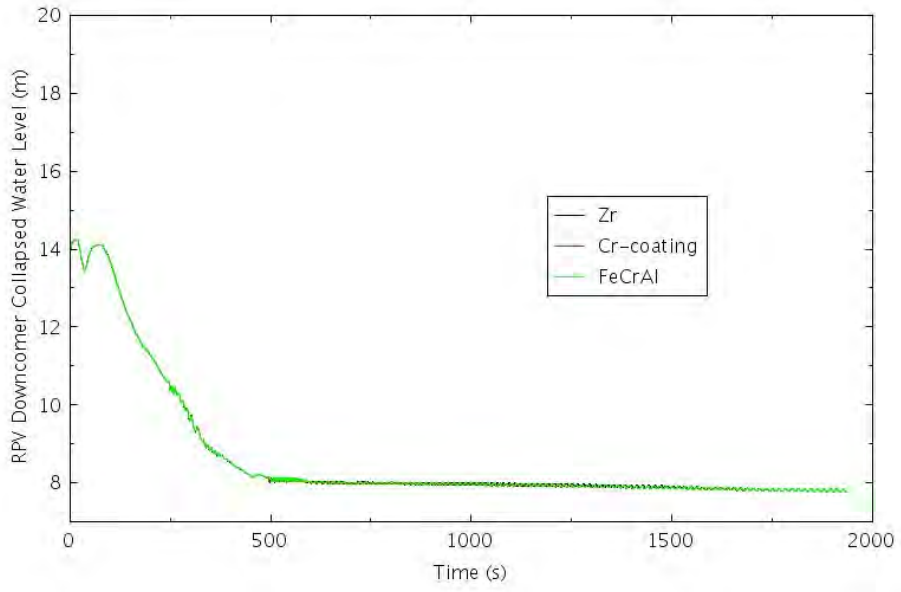

Figure 4-95. RPV Downcomer Collapsed Water Level for TRANS-ATWS-2.

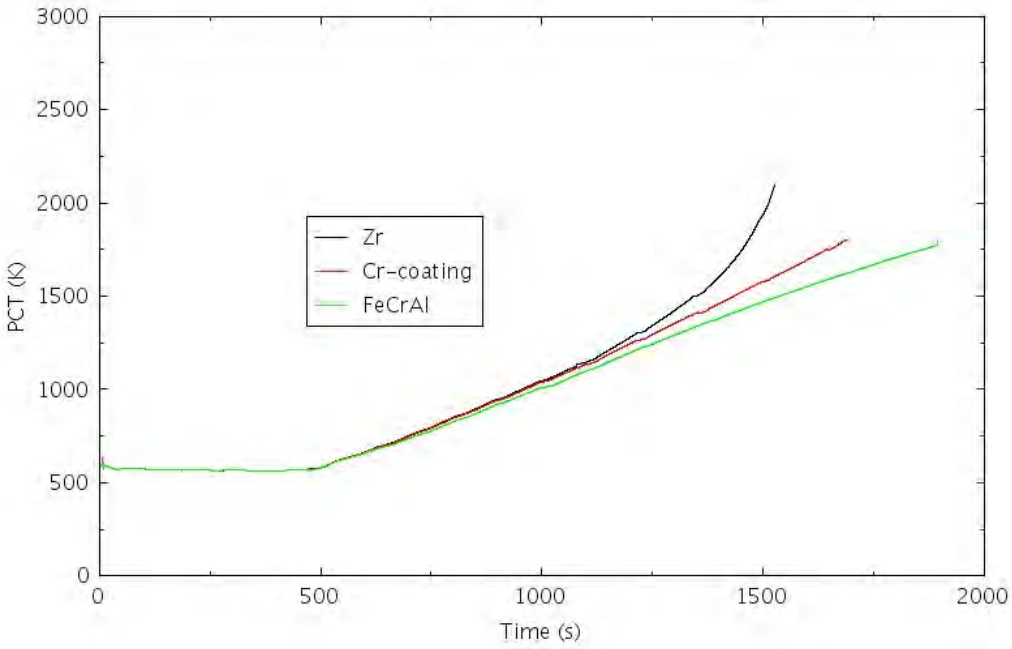

Figure 4-96. PCT for TRANS-ATWS-2.

4.2.2.3 TRANS-ATWS-3

In this scenario, it is assumed the MSIV closure occurs at time zero and the RPS fails to trip reactor, leading to an ATWS. However, it is further assumed in this scenario the SLCS is successfully started to inject boron into the reactor to shut down the reactor power. The reactor power initially rises and then starts to decrease as shown in Figure 4-97 and Figure 4-98. Figure 4-97 shows the reactor power during the entire transient, and Figure 4-98 provides zoomed in view of the reactor power change within the first 200 seconds of the transient. The feedback reactivity is shown in Figure 4-99 for the entire transient and Figure 4-100 for the zoomed in view of the feedback reactivity within the first 200 seconds of the transient. With the closure of MSIV, the system pressure spikes rapidly. Figure 4-101 shows the RPV dome pressure for the entire transient. The system pressure spike causes the opening of all the SRVs, as shown in Figure 4-102 for the mass flow rates through the SRVs. It is further assumed the increase in system pressure also successfully trips the recirculation pumps. Recirculation pump trip occurs on high dome pressure at 7.826 MPa, and core flow is reduced to natural circulation conditions. This rapid decrease in flow also contributes to void formation in the core supplying even more negative reactivity. Figure 4-103 shows the recirculation pump mass flow rate as a function of time. The feedwater flow is shown in Figure 4-104, and it ceases at 120 seconds. The feedwater temperature is shown in Figure 4-105. It is assumed feedwater heater works for 30 seconds, and the feedwater temperature drops to 321.8K at 50 seconds. The RPV collapsed water level is shown in Figure 4-106, and the water level drops precipitously once the feedwater flow stops. The boron concentration at the reactor core inlet is shown in Figure 4-107. Figure 4-108 shows the comparison of PCT for conventional fuel with Zircaloy cladding and ATF with Cr-coated and FeCrAl cladding.

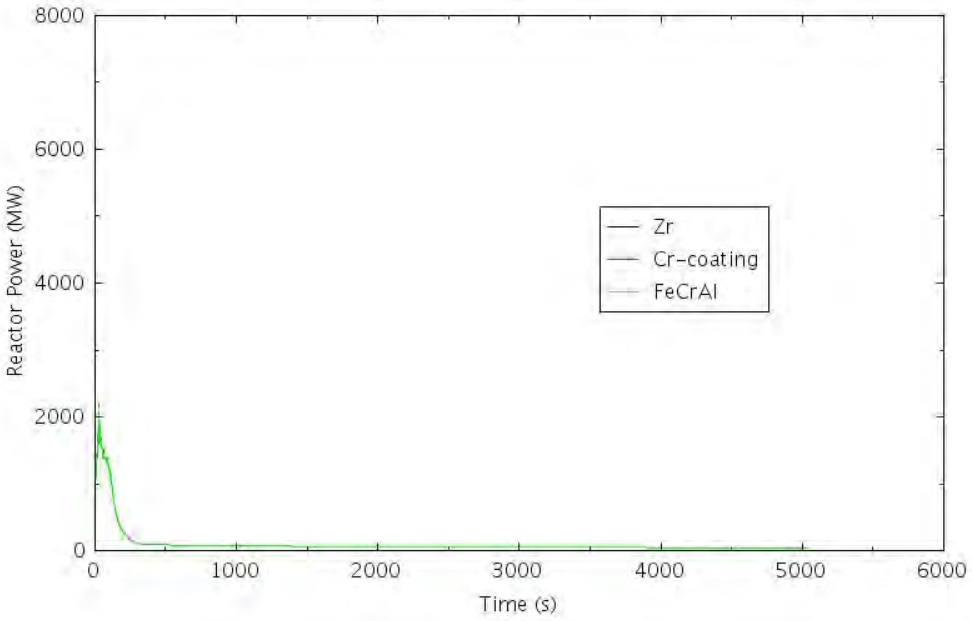

Figure 4-97. Reactor Power for TRANS-ATWS-3.

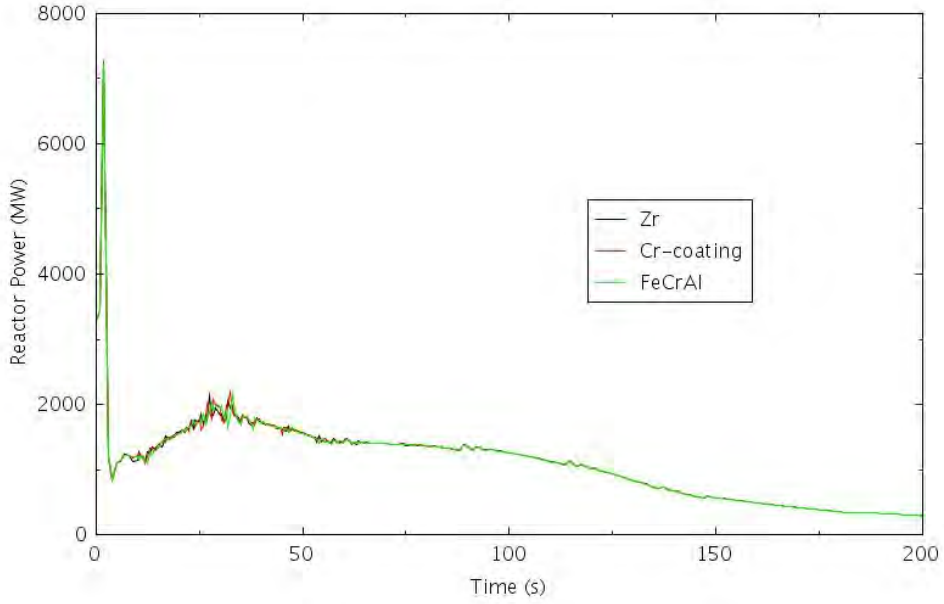

Figure 4-98. Reactor Power Within the First 200 Seconds for TRANS-ATWS-3.

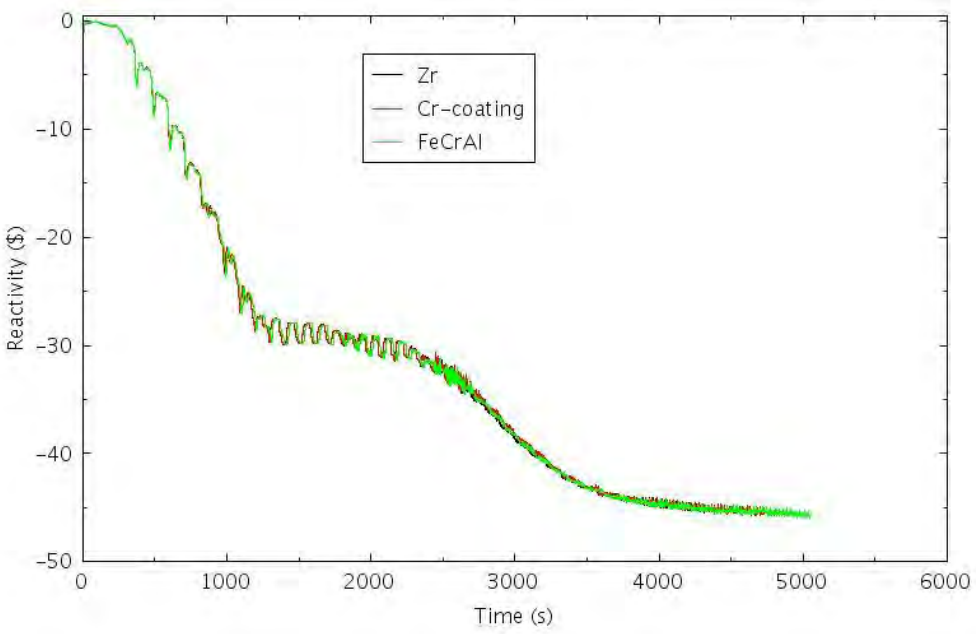

Figure 4-99. Feedback Reactivity for TRANS-ATWS-3.

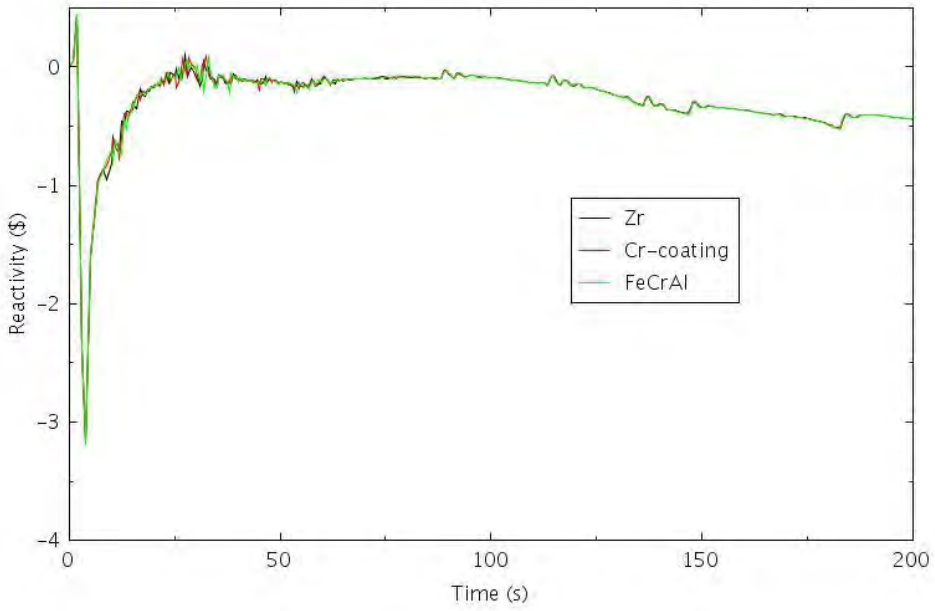

Figure 4-100. Feedback Reactivity Within the First 200 Seconds for TRANS-ATWS-3.

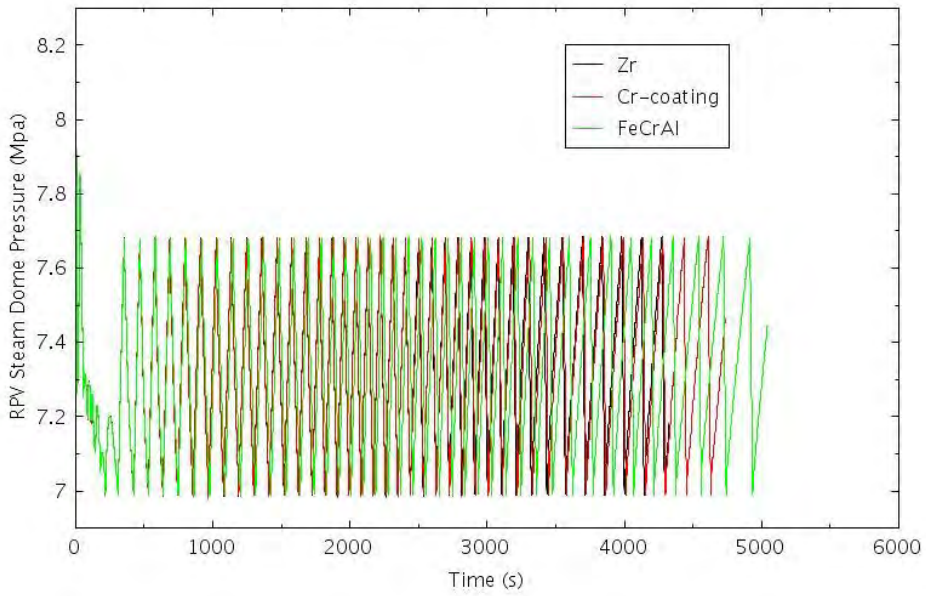

Figure 4-101. RPV Dome Pressure for TRANS-ATWS-3.

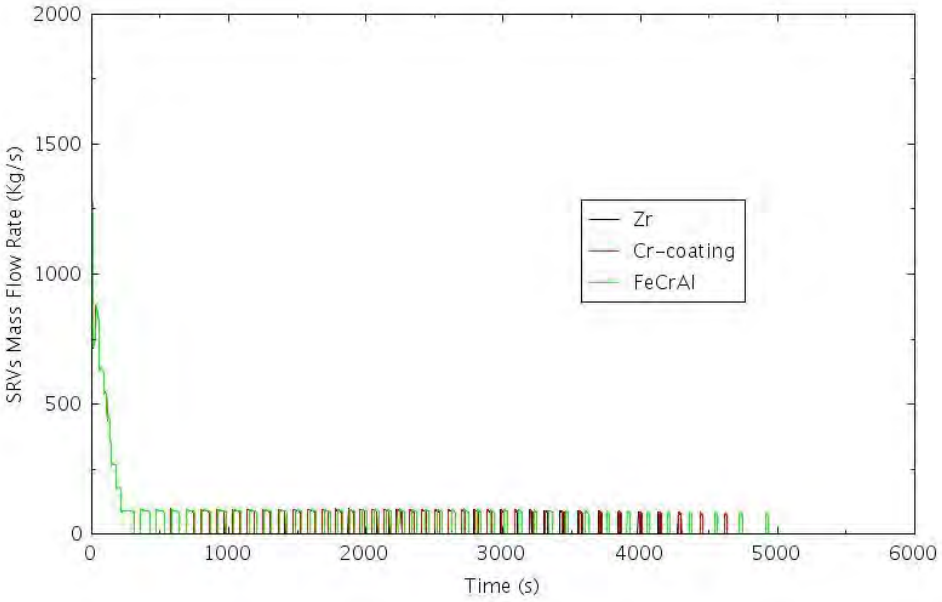

Figure 4-102. Mass Flow Rates through SRVs for TRANS-ATWS-3.

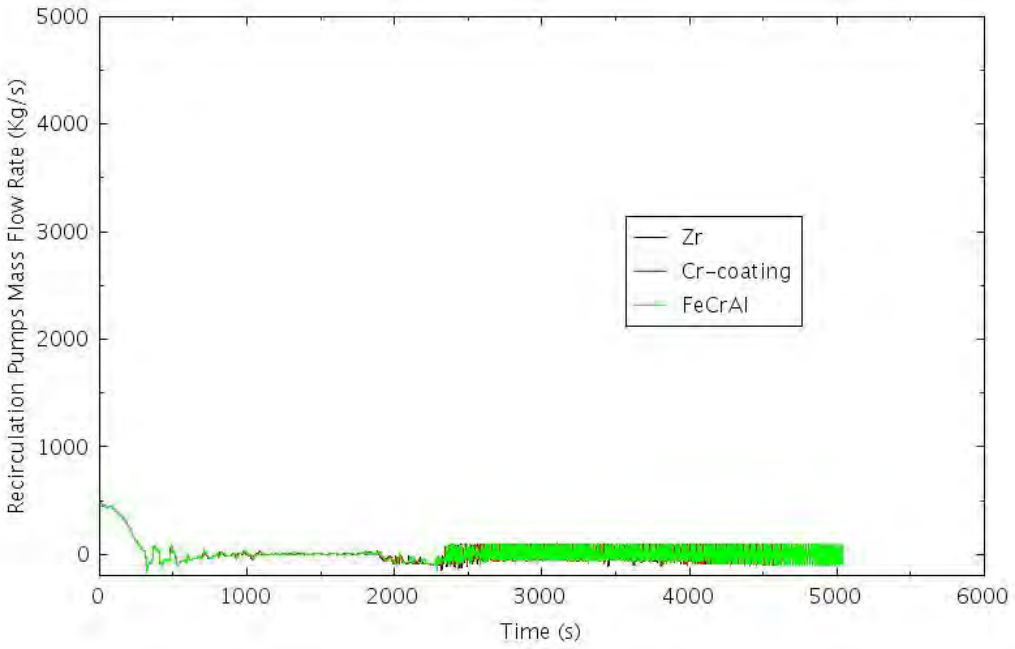

Figure 4-103. Recirculation Pumps Mass Flow Rate for TRANS-ATWS-3.

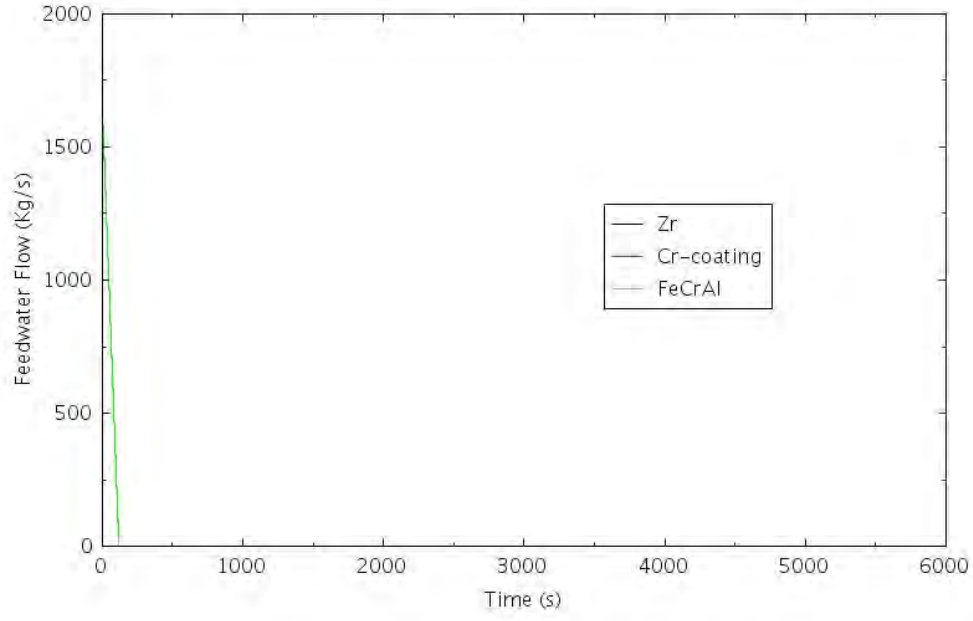

Figure 4-104. Feedwater Mass Flow Rate for TRANS-ATWS-3.

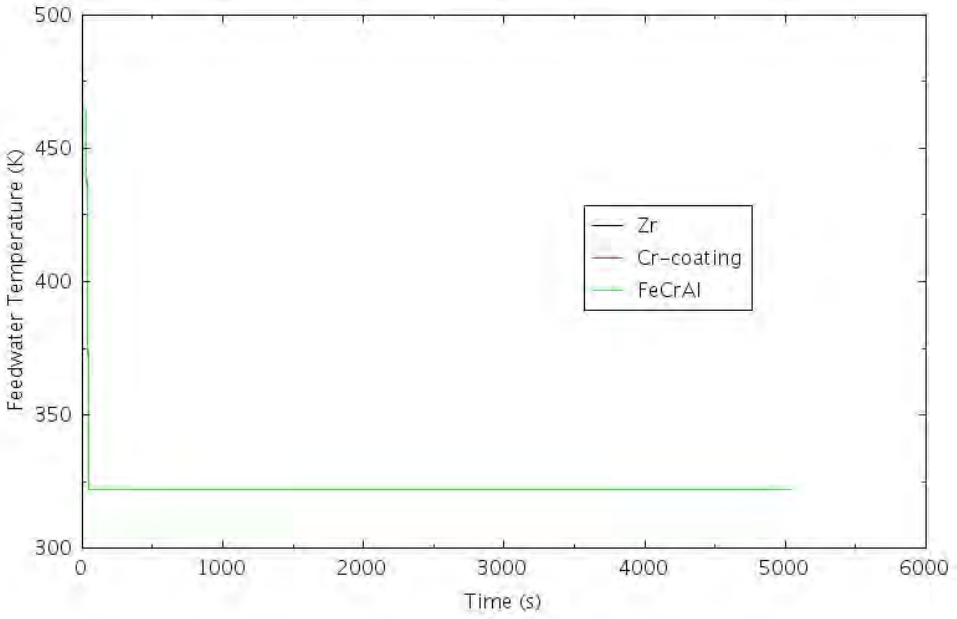

Figure 4-105. Feedwater Temperature for TRANS-ATWS-3.

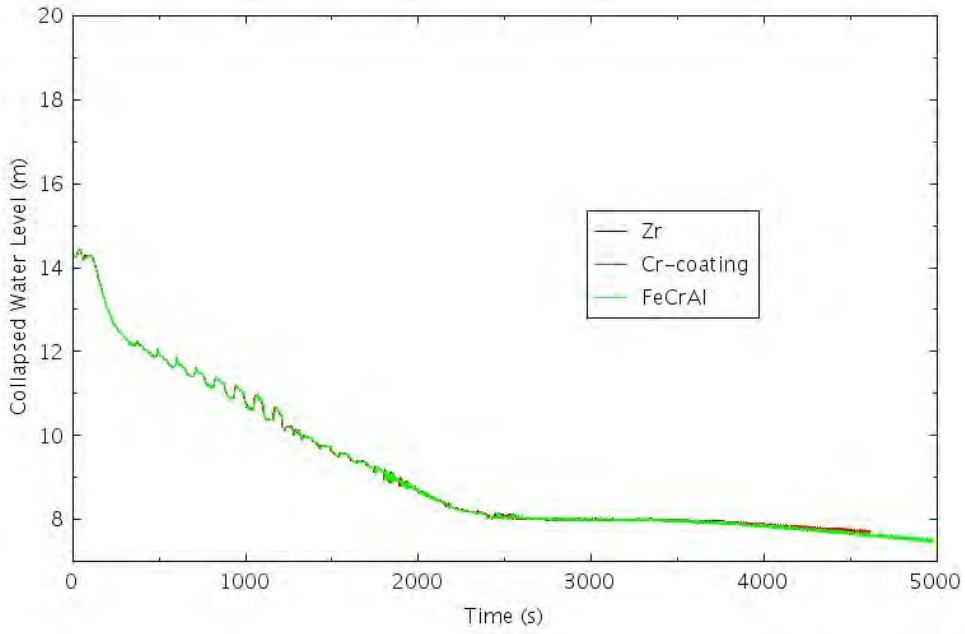

Figure 4-106. RPV Downcomer Collapsed Water Level for TRANS-ATWS-3.

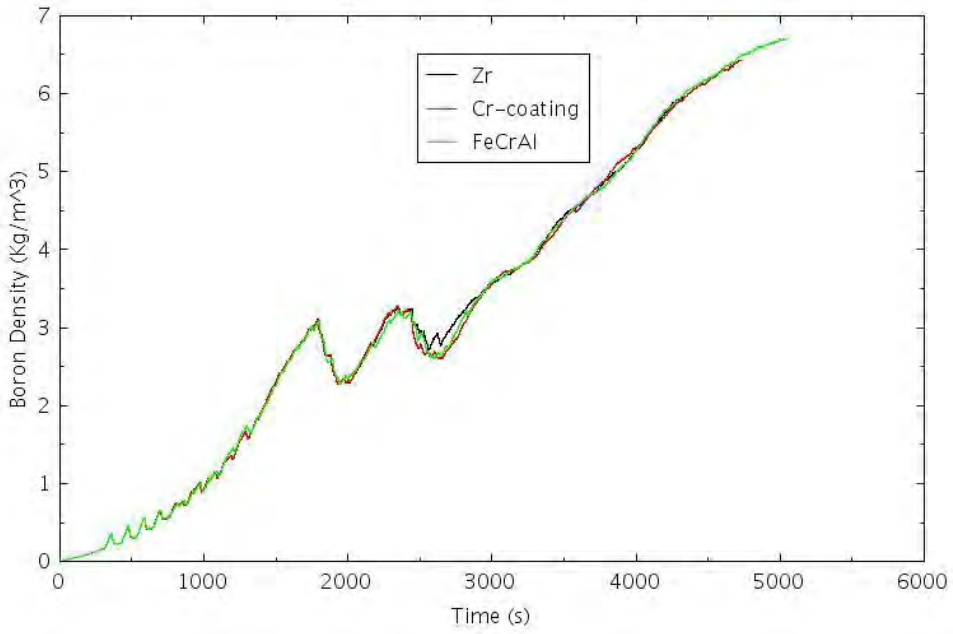

Figure 4-107. Boron Density at the Core Inlet for TRANS-ATWS-3.

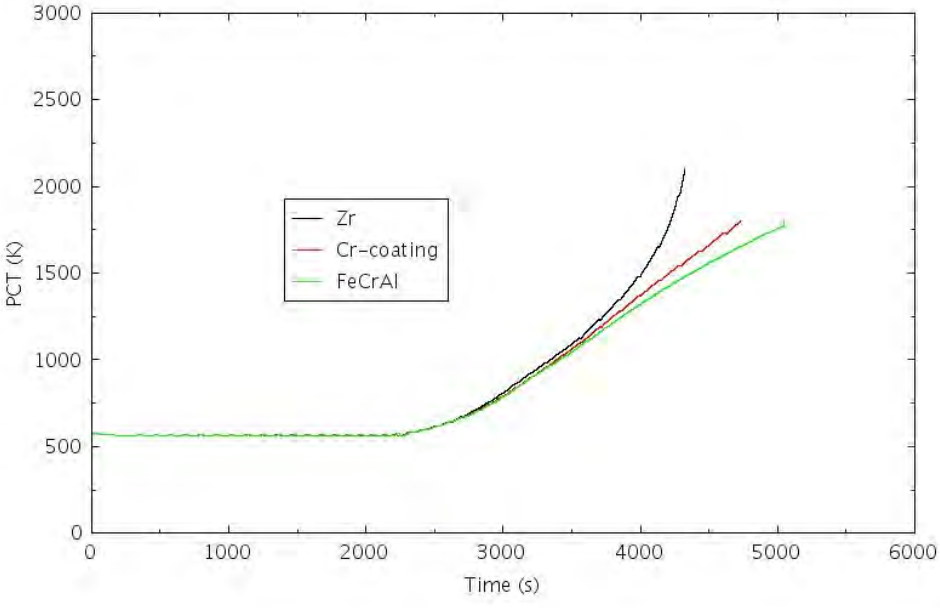

Figure 4-108. PCT for TRANS-ATWS-3.

4.2.2.4 TRANS-ATWS-4

This scenario is similar to ATWS-3 with the exception that depressurization of the primary system is successful, but low-pressure injection fails to start. The depressurization occurs when the RPV water level decrease to the Level 1 water level setpoint. Figure 4-109 shows the reactor power during the entire transient, and Figure 4-110 provides zoomed in view of the reactor power change within the first 200 seconds of the transient. The feedback reactivity is shown in Figure 4-111 for the entire transient. As shown in Figure 4-111, the feedback reactivity becomes less negative after 2,040 seconds. This is caused by the dry-out in the reactor core and boron precipitation. With the closure of MSIV, the system pressure spikes rapidly. Figure 4-112 shows the RPV dome pressure for the entire transient. The initial system pressure spike causes opening of all the SRVs, as shown in Figure 4-113 for the mass flow rates through the SRVs. Figure 4-112 also shows the depressurization of the RPV. It is further assumed the initial increase in system pressure also successfully trips the recirculation pumps. Recirculation pump trip occurs on high dome pressure at 7.826 MPa, and core flow is reduced to natural circulation conditions. This rapid decrease in flow also contributes to void formation in the core supplying even more negative reactivity. Figure 4-114 shows the recirculation pump mass flow rate as a function of time. The feedwater flow is shown in Figure 4-115, and it ceases at 120 seconds. The feedwater temperature is shown in Figure 4-116. It is assumed feedwater heater works for 30 seconds, and the feedwater temperature drops to 321.8K at 50 seconds. The RPV collapsed water level is shown in Figure 4-117, and the water level drops precipitously once the feedwater flow stops. The boron concentration at the reactor core inlet is shown in Figure 4-118. Figure 4-119 shows the comparison of PCT for conventional fuel with Zircaloy cladding and ATF with Cr-coated and FeCrAl cladding.

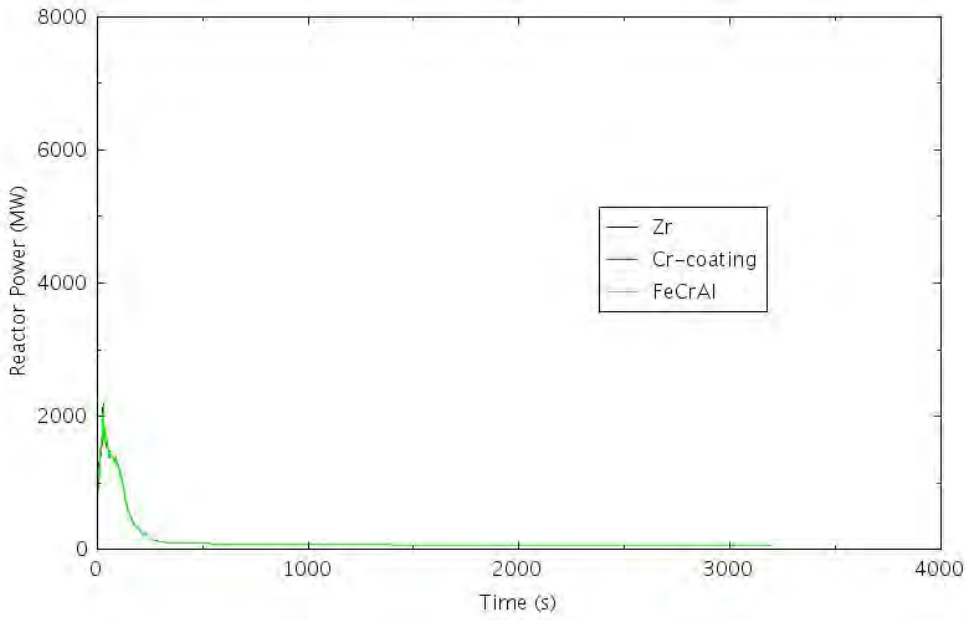

Figure 4-109. Reactor Power for TRANS-ATWS-4.

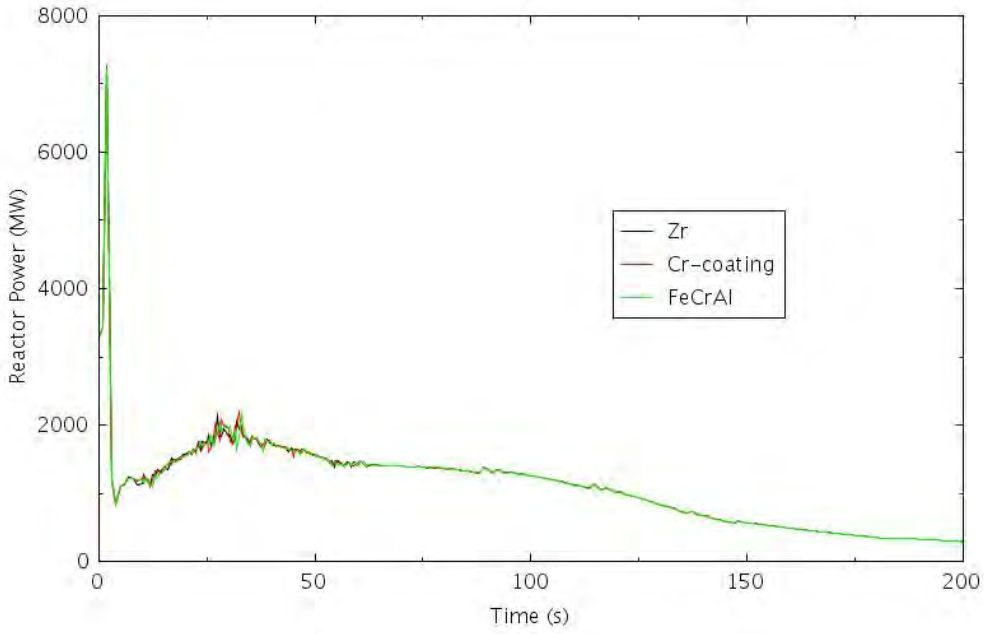

Figure 4-110. Reactor Power Within the First 200 Seconds for TRANS-ATWS-4.

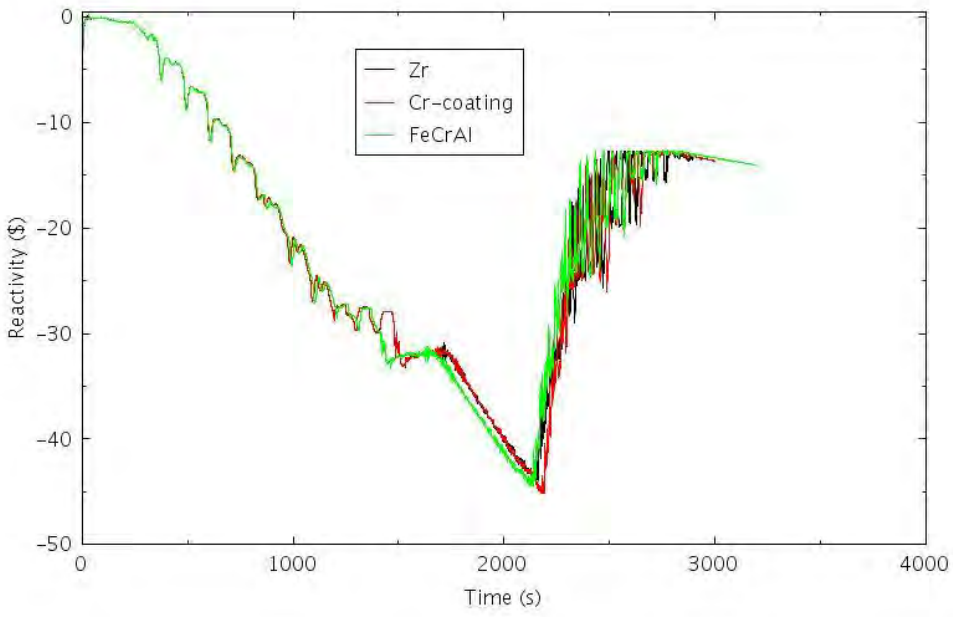

Figure 4-111. Reactivity for TRANS-ATWS-4.

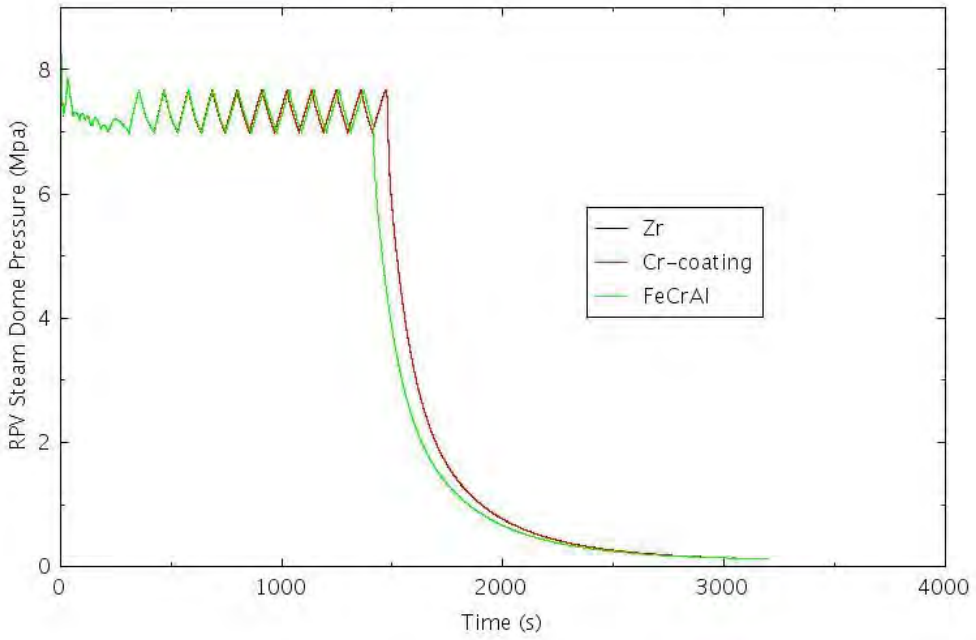

Figure 4-112. RPV Dome Pressure for TRANS-ATWS-4.

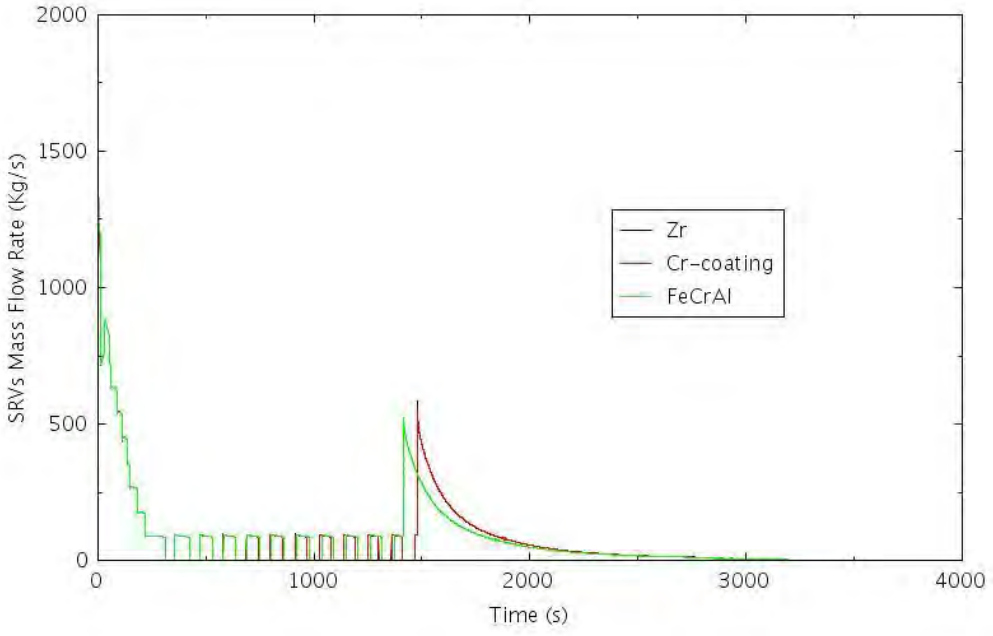

Figure 4-113. Mass Flow Rates through SRVs for TRANS-ATWS-4.

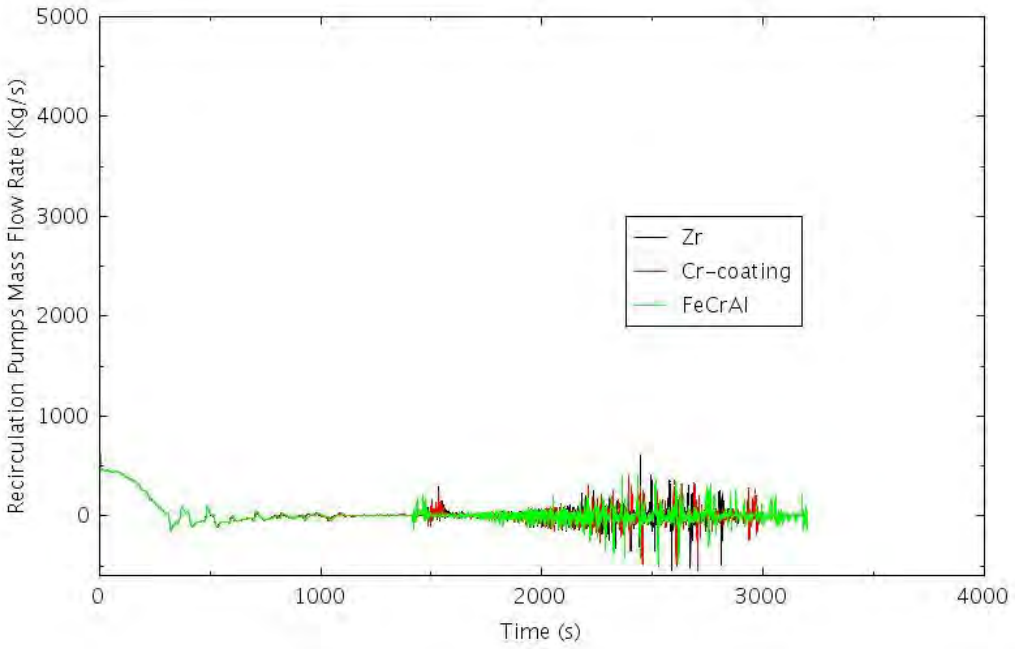

Figure 4-114. Recirculation Pumps Mass Flow Rate for TRANS-ATWS-4.

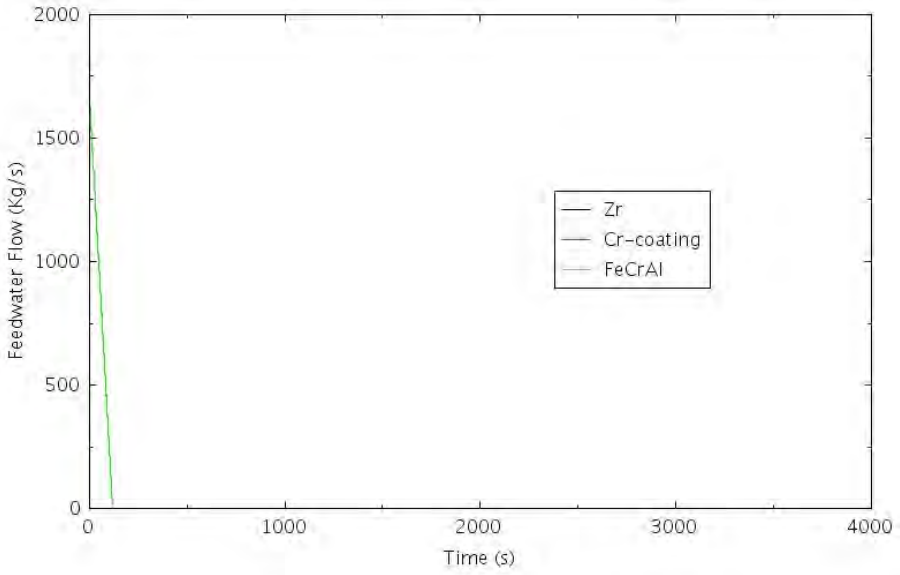

Figure 4-115. Feedwater Mass Flow Rate for TRANS-ATWS-4.

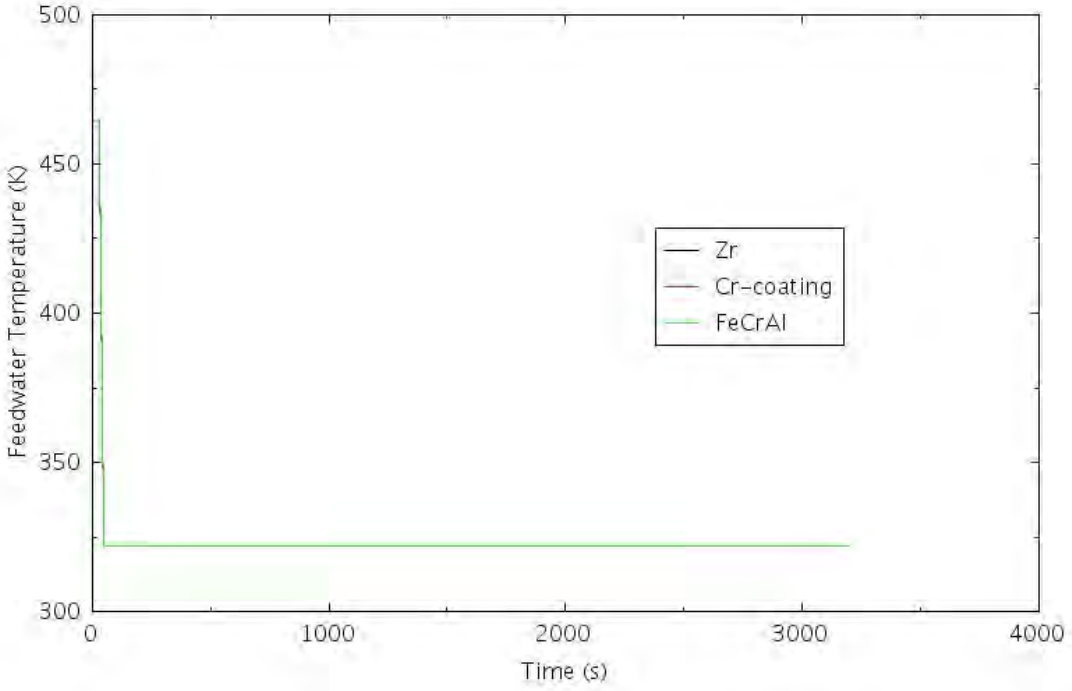

Figure 4-116. Feedwater Temperature for TRANS-ATWS-4.

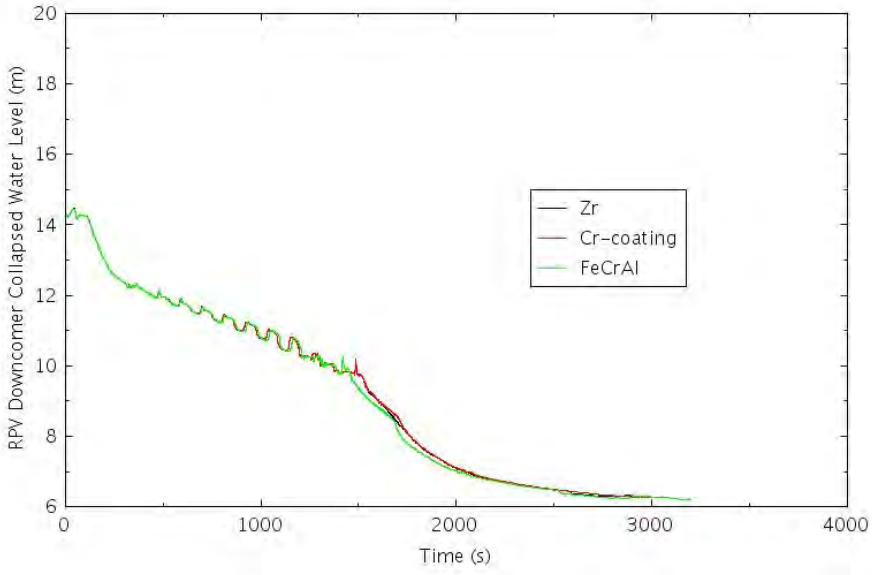

Figure 4-117. RPV Downcomer Collapsed Water Level for TRANS-ATWS-4.

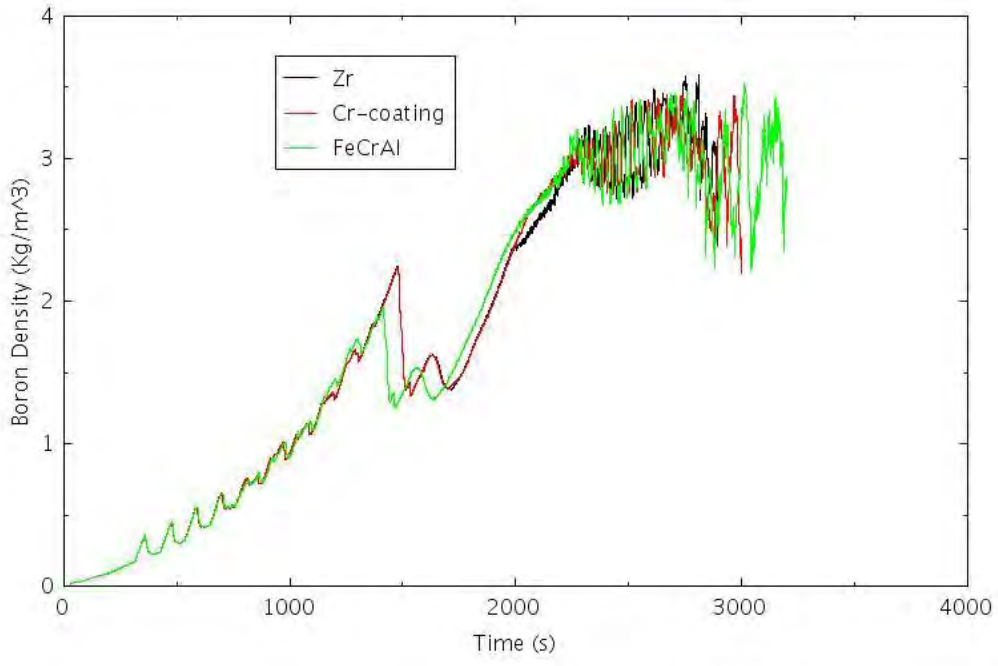

Figure 4-118. Boron Concentration at the Core Inlet for TRANS-ATWS-4.

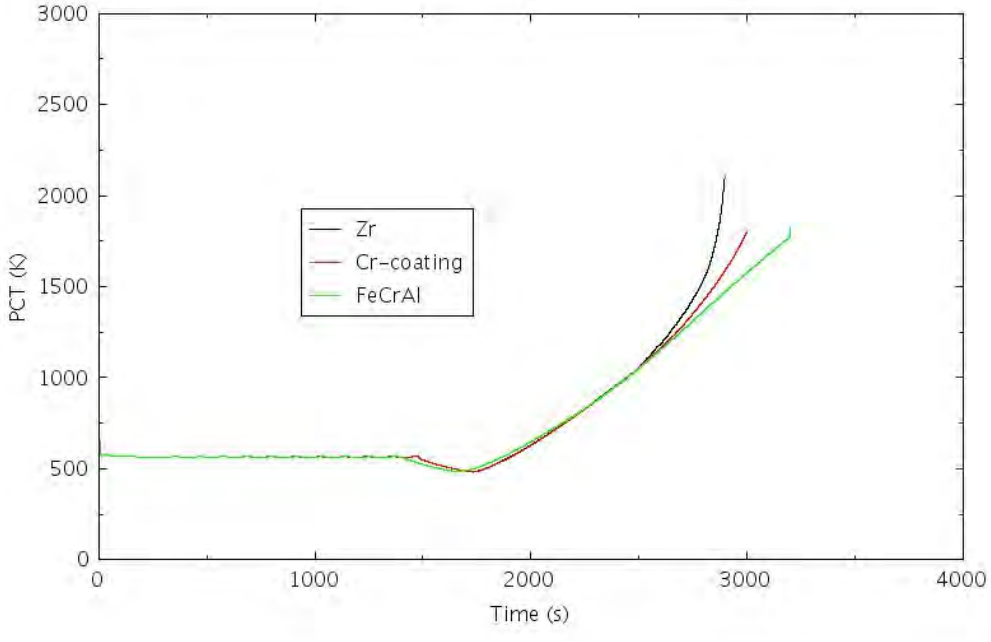

Figure 4-119. PCT for TRANS-ATWS-4.

4.3 Summary of BWR General Transient Analyses

4.3.1 Results for General Transients with Scram

Table 4-7 compares the times to CD for ATF designs (FeCrAl and Cr-coated claddings) with those for existing Zircaloy-clad design in different general transient scenarios with reactor scram. The table shows the gain of coping time, or the delay of time to CD, is less than or equal to 30 minutes for most scenarios. For FeCrAl, a gain of coping time ranges from 10 to 35 minutes. For Cr-coated cladding, a gain of coping time ranges from 5 to 19 minutes. With only a marginal increase of the time to core damage with FeCrAl and Cr-coated against the conventional Zry-cladding design based on the RELAP5-3D simulation results, the risk-benefit on behalf of CDF as the risk metrics would be very small and it is not quantified.

However, the RELAP5-3D simulation results show the clear benefit in adopting ATF due to much less hydrogen produced at the time of CD. Table 4-8 compares the hydrogen production for ATF designs (FeCrAl and Cr-coated claddings) with that for existing Zircaloy-clad design in different general transient scenarios. The table shows the hydrogen production can be a few times lower for the Cr-coated cladding and up to two orders of magnitude lower for FeCrAl cladding than with Zircaloy cladding cases.

Table 4-7. Comparison of Time to CD with ATF Designs for General Transients with Reactor Scram.

Scenario	Scenario Description	Time to CD t_{CD} (hh:mm)					
		Zry	Cr-coated	Δt	Zry	FeCrAl	Δt
TRANS-1	Reactor trip, no HPI, no DEP	1:07	1:12	0:05	1:07	1:17	0:10
TRANS-2	Reactor trip, AC, HPI, DEP, Control Rod Drive Injection, no Containment HR	10:02	10:13	0:11	10:02	10:27	0:25
TRANS-3	Reactor trip, AC, HPI, no DEP	8:01	8:14	0:13	8:01	8:28	0:27
TRANS-4	Reactor trip, AC, HPI, DEP, no LPI	7:10	7:15	0:05	7:10	7:25	0:15
TRANS-SORV-1	Reactor trip, AC, 1 SRV Open, no HPI, no DEP	0:57	1:02	0:05	0:57	1:06	0:09
TRANS-SORV-2	Reactor trip, AC, 1 SRV Open, DEP, CS, no Containment HR	13:46	14:05	0:19	13:46	14:21	0:35
TRANS-SORV-3	Reactor trip, AC, 1 SRV Open, no DEP, no LPCI	8:14	8:19	0:05	8:14	8:28	0:14
TRANS-SORV-4	Reactor trip, AC, 1 SRV Open, DEP, LPCI, no Containment HR	13:18	13:30	0:12	13:18	13:46	0:28
TRANS-SORV-5	Reactor trip, AC, 2 SRVs Open, DEP, CS, no Containment HR	13:42	13:53	0:11	13:42	14:13	0:31
TRANS-LOOP-1	Reactor trip, LOOP, AC, HPI, DEP, LPCI, no Containment HR	18:44	19:02	0:18	18:44	19:14	0:30

Table 4-8. Comparison of H_2 Productions with ATF Designs for General Transients with Reactor Scram.

Scenario	Scenario Description	Total H_2 (kg)			H_2 %	
		Zry	Cr-coated	FeCrAl	Cr-coated	FeCrAl
TRANS-1	Reactor trip, no HPI, no DEP	21.2	5.6	0.4	26.6	1.9

Scenario	Scenario Description	Total H_2 (kg)			H_2 %	
		Zry	Cr-coated	FeCrAl	Cr-coated	FeCrAl
TRANS-2	Reactor trip, AC, HPI, DEP, Control Rod Drive Injection, no Containment HR	13.6	2.6	0.2	18.8	1.2
TRANS-3	Reactor trip, AC, HPI, no DEP	31.2	6.0	0.6	19.4	1.9
TRANS-4	Reactor trip, AC, HPI, DEP, no LPI	9.0	1.5	0.1	16.2	1.1
TRANS-SORV-1	Reactor trip, AC, 1 SRV Open, no HPI, no DEP	51.1	5.4	0.5	10.5	1.0
TRANS-SORV-2	Reactor trip, AC, 1 SRV Open, DEP, CS, no Containment HR	20.4	5.2	0.3	25.3	1.7
TRANS-SORV-3	Reactor trip, AC, 1 SRV Open, no DEP, no LPCI	12.2	3.3	0.2	27.3	1.5
TRANS-SORV-4	Reactor trip, AC, 1 SRV Open, DEP, LPCI, no Containment HR	18.4	5.0	0.3	26.9	1.8
TRANS-SORV-5	Reactor trip, AC, 2 SRVs Open, DEP, CS, no Containment HR	18.2	11.2	0.3	61.6	1.8
TRANS-LOOP-1	Reactor trip, LOOP, AC, HPI, DEP, LPCI, no Containment HR	21.2	5.6	0.4	26.6	1.9

4.3.2 Results for ATWS Scenarios

Table 4-9 compares the times to CD for ATF designs (FeCrAl and Cr-coated claddings) with those for existing Zircaloy-clad design in different ATWS scenarios. The table shows the gain of coping time, or the delay of time to CD, is less than 12 minutes for all scenarios. For FeCrAl, a gain of coping time ranges from 5 to 12 minutes. For Cr-coated cladding, a gain of coping time ranges from 2 to 7 minutes. With only a marginal increase of the time to core damage with FeCrAl and Cr-coated against the conventional Zry-cladding design based on the RELAP5-3D simulation results, the risk-benefit on behalf of CDF as the risk metric would be very small and it is not quantified.

Similar to the results obtained from the analyses for general transients with reactor scram, the RELAP5-3D simulation results show the clear benefit in adopting ATF due to much less hydrogen produced at the time of CD. Table 4-10 compares the hydrogen production for ATF designs (FeCrAl and Cr-coated claddings) with that for existing Zircaloy-clad design in different ATWS scenarios. The table shows the hydrogen production can be a few times lower for the Cr-coated cladding and up to two orders of magnitude lower for FeCrAl cladding than with Zircaloy cladding cases.

Table 4-9. Time to CD Comparison for ATWS Scenarios with ATF Designs.

Scenario	Scenario Description	Time to CD t_{CD} (hh:mm)					
		Zry	Cr-coated	Δt	Zry	FeCrAl	Δt
TRANS-ATWS-1	No trip, AC, SRVs Open, Recirc Pump Trip, No SLCS, No ADS, No DEP, No LPI	0:27	0:29	0:03	0:27	0:33	0:06
TRANS-ATWS-2	No trip, AC, SRVs Open, No Recirc Pump Trip, No SLCS, No ADS, No DEP, No LPI	0:26	0:29	0:03	0:26	0:32	0:06
TRANS-ATWS-3	No trip, AC, SRVs Open, Recirc Pump Trip, SLCS, No ADS, No DEP, No LPI	1:12	1:19	0:07	1:12	1:24	0:12
TRANS-ATWS-4	No trip, AC, SRVs Open, Recirc Pump Trip, SLCS, ADS, DEP, No LPI	0:48	0:50	0:02	0:48	0:53	0:05

Table 4-10. Comparison of H_2 Productions for ATWS Scenarios with ATF Designs.

Scenario	Scenario Description	Total H_2 (kg)			H_2 %	
		Zry	Cr-coated	FeCrAl	Cr-coated	FeCrAl
TRANS-ATWS-1	No trip, AC, SRVs Open, Recirc Pump Trip, No SLCS, No ADS, No DEP, No LPI	20.8	3.0	0.2	14.4	1.0
TRANS-ATWS-2	No trip, AC, SRVs Open, No Recirc Pump Trip, No SLCS, No ADS, No DEP, No LPI	19.2	2.9	0.2	15.1	1.0
TRANS-ATWS-3	No trip, AC, SRVs Open, Recirc Pump Trip, SLCS, No ADS, No DEP, No LPI	26.8	4.8	0.3	18.0	1.3
TRANS-ATWS-4	No trip, AC, SRVs Open, Recirc Pump Trip, SLCS, ADS, DEP, No LPI	19.7	7.4	0.1	37.3	0.7

5. RISK-INFORMED ATF ANALYSIS OF BWR LOSS OF MAIN FEEDWATER SCENARIOS

The risk-informed analysis of near-term ATF designs for BWR LOMFW scenarios is presented in this section. The BWR LOMFW model and scenarios are presented in Section 5.1. The RELAP5-3D analyses of ATF designs for the LOMFW scenarios are presented in Section 5.2. The analysis results are summarized in Section 5.3.

5.1 BWR LOMFW SAPHIRE Model and Scenarios

The generic BWR LOMFW SAPHIRE model starts with the occurrence of LOMFW. The model includes a main event tree LOMFW and four transfer trees including 1SORV, 2SORVS, ATWS, and LOOP. The structures of the main event tree and the transfer trees are the same (except containing different IEs) as those of the general transient scenarios and thus not provided again in this section.

The ETs were quantified with SAPHIRE 8 using a truncation level of 1E-12 per reactor year. There are 236 CD sequences with a total LOMFW CDF of 9.47E-07 per reactor year. Among the 236 CD sequences, 52 sequences have non-zero (or non-truncated) CDF; 13 sequences have greater-than-0.1% contribution to total LOMFW CDF with a sum of 99.5% of total LOMFW CDF. The 13 sequences are shown in Table 5-1.

Table 5-1. BWR LOMFW Sequences with Greater-Than-0.1% CDF Contribution.

No.	BWR LOMFW Sequence	CDF	Group	RELAP5 Scenario
1	LOMFW:70	7.44E-07	LOMFW	LOMFW-1
2	LOMFW:09	1.42E-07	LOMFW	LOMFW-2
3	LOMFW:44	2.20E-08	LOMFW	LOMFW-3
4	LOMFW:71-55	9.11E-09	SORV	LOMFW-SORV-1
5	LOMFW:73-34	3.99E-09	LOOP	LOMFW-LOOP-1
6	LOMFW:74-07	3.62E-09	ATWS	LOMFW-ATWS-1
7	LOMFW:71-23	2.99E-09	SORV	LOMFW-SORV-2
8	LOMFW:74-09	2.72E-09	ATWS	LOMFW-ATWS-2
9	LOMFW:52	2.42E-09	LOMFW	LOMFW-4
10	LOMFW:73-09	2.42E-09	LOOP	LOMFW-LOOP-2
11	LOMFW:73-35-21	2.38E-09	LOOP	LOMFW-LOOP-3
12	LOMFW:71-35	2.15E-09	SORV	LOMFW-SORV-3
13	LOMFW:74-06-07	1.45E-09	ATWS	LOMFW-ATWS-3

The 13 sequences were grouped into four categories:

- Four LOMFW scenarios with no further transfer, LOMFW-1 to LOMFW-4
- Three SORV scenarios transferred from LOMFW, LOMFW-SORV-1 to LOMFW-SORV-3
- Three LOOP scenarios transferred from LOMFW, LOMFW-LOOP-1 to LOMFW-LOOP-3
- Three ATWS scenarios transferred from LOMFW, LOMFW-ATWS-1 to LOMFW-ATWS-3.

Two LOMFW-LOOP scenarios (LOMFW-LOOP-1 and LOMFW-LOOP-3) are the same as scenarios LOMFW-1 and LOMFW-SORV-1, respectively, except for their sources of AC power—the LOOP scenarios use emergency power, and the LOMFW and SORV scenarios use offsite power. As this difference will not lead to difference in RELAP5-3D modeling, the two LOOP scenarios can be enveloped by the LOMFW and SORV scenarios. The LOOP scenarios, except for scenario LOMFW-LOOP-2, are thus excluded and not passed on to RELAP5-3D analysis.

Besides the remaining 11 sequences selected based on PRA-estimated risk significance, one sequence (LOMFW-SORV-4) is added for RELAP5-3D analysis to make the selected accident spectrum more complete by including a scenario with two stuck-open SRVs. Hence, a total of 12 LOMFW scenarios were developed for RELAP5-3D analysis as shown in Table 5-2. It should also be noted that the plant responses of eight LOMFW scenarios are the same as those of several TRANS scenarios. The LOMFW scenarios and their corresponding TRANS scenarios and are shown in

Table 5-3.

Table 5-2. BWR LOMFW Scenarios Developed for RELAP5-3D Analysis.

No.	RELAP5 Scenario	Scenario Description
1	LOMFW-1	LOMFW, RCS inventory control failed (no HPI or DEP)
2	LOMFW-2	LOMFW, containment heat removal failed (using control rod drive injection for RCS inventory control)
3	LOMFW-3	LOMFW, RCS inventory control failed (no DEP)
4	LOMFW-4	LOMFW, containment heat removal failed (using condensate system for RCS inventory control)
5	LOMFW-SORV-1	1 stuck-open SRV, RCS inventory control failed (no HPI or DEP)
6	LOMFW-SORV-2	1 stuck-open SRV, containment heat removal failed
7	LOMFW-SORV-3	1 stuck-open SRV, RCS inventory control failed (no DEP)
8	LOMFW-SORV-4	2 stuck-open SRVs, containment heat removal failed
9	LOMFW-LOOP-1[a]	LOOP, containment heat removal failed
10	LOMFW-ATWS-1	ATWS, power control failed
11	LOMFW-ATWS-2	ATWS, reactivity control failed
12	LOMFW-ATWS-3	ATWS, RCS overfilled
a. Renumbered from scenario LOMFW-LOOP-2 in Table 5-1.		

Table 5-3. BWR LOMFW Scenarios and TRANS Scenarios with Same Plant Responses.

LOMFW Scenario	Corresponding TRANS Scenario
LOMFW-1	TRANS-1
LOMFW-2	TRANS-2
LOMFW-3	TRANS-3
LOMFW-SORV-1	TRANS-SORV-1
LOMFW-SORV-2	TRANS-SORV-2
LOMFW-SORV-3	TRANS-SORV-3
LOMFW-SORV-4	TRANS-SORV-5
LOMFW-LOOP-1	TRANS-LOOP-1

Since the eight LOMFW scenarios shown in

Table 5-3 have already been analyzed in the general transients. Only four scenarios are analyzed in this section, including LOMFWS-4, LOMFW-ATWS-1, LOMFW-ATWS-2, and LOMFW-ATWS-3. Short descriptions of these four scenarios are provided below and detailed mitigating system statuses provided in Table 5-4 and Table 5-5.

- **LOMFWS-4:** An LOMFW IE occurs, reactor automatically shuts down, AC power is available, and all SRVs are successfully opened and reclosed. Although HPI fails, RCS inventory is maintained through DEP plus condensate system injection. CD still occurs due to failure of decay heat removal.
- **LOMFW-ATWS-1:** An LOMFW IE occurs, RPS fails to trip reactor, leading to an ATWS. A sufficient number of SRVs are opened, and recirculation pumps are tripped. Standby liquid control succeeds to control reactivity, and ADS is inhibited. However, operators fail to lower water level in the RPV to top of active fuel. CD occurs due to failure of power control.

- **LOMFW-ATWS-2:** An LOMFW IE occurs, RPS fails to trip reactor, leading to an ATWS. A sufficient number of SRVs are opened, and recirculation pumps are tripped. But standby liquid control fails to start. CD occurs due to failure of reactivity control.
- **LOMFW-ATWS-3:** An LOMFW IE occurs, RPS fails to trip reactor, leading to an ATWS. A sufficient number of SRVs are opened, and recirculation pumps are tripped. Standby liquid control succeeds to control reactivity, and ADS is inhibited. Operators succeed in lowering RPV water level to top of active fuel for early power control. Both DEP and low-pressure coolant injection succeed in restoring RPV water level, but operators fail to control the injection, and CD occurs due to overfill.

Table 5-4. BWR LOMFW Scenarios for RELAP-5 3D Analysis: Mitigating System Statuses (LOMFW Scenario).

RELAP5 LOMFW Scenario	LOMFW Main Event Tree									
#	Rx	AC Power Available	Stuck-open SRVs	HPI Success	DEP Success	Condensate System Success	SPC Success	Containment Spray or Venting Success	PCS Recovery	Late Injection Success
LOMFW-4	Trip	Yes	0	No	Yes	Yes	No	No	No	No

Table 5-5. BWR LOMFW Scenarios for RELAP-5 3D Analysis: Mitigating System Statuses (LOMFW-ATWS Scenarios).

RELAP5 LOMFW Scenario	LOMFW Main Event Tree	ATWS Transfer Event Tree								
#	Rx	AC Power Available	SRVs Open	Recirculation Pump	Standby Liquid Control Success	Inhibit ADS	Lower Level to Top of Active Fuel	DEP Success	LPI Success	Restore RPV Level and Prevent Overfill
LOMFW-ATWS-1	No trip	Yes	Yes	Trip	Yes	Yes	No			
LOMFW-ATWS-2	No trip	Yes	Yes	Trip	No					
LOMFW-ATWS-3	No trip	Yes	Yes	Trip	Yes	Yes	Yes	Yes	Yes	No

5.2 BWR LOMFW RELAP5-3D Analysis

The RELAP5-3D analyses are grouped in two categories: LOMFW with reactor scram and LOMFW-initiated ATWS. The analysis in the previous section indicates for the LOMFW with reactor scram transients, only the LOMFWS-4 scenario needs to be analyzed using RELAP5-3D, and the results are presented in Section 5.2.1. The other eight scenarios for LOMFW with reactor scram have already been analyzed in the general transients. For the LOMFW-initiated ATWS scenarios, all three scenarios, LOMFW-ATWS-1, LOMFW-ATWS-2, and LOMFW-ATWS-3, are analyzed, and results are presented in Section 5.2.2.

5.2.1 LOMFW with Reactor Scram

The results from the RELAP5-3D analyses for the LOMFWS-4 scenario are presented in Section 5.2.1.1.

5.2.1.1 LOMFW-4

In this scenario, an LOMFW IE occurs, the reactor power is automatically shut down. AC power is available, and all the SRVs are successfully opened and closed. It is further assumed HPI system fails to start. As a result, the RPV water level starts to decrease after the initiation of the event. The RPV downcomer collapsed water level is shown in Figure 5-1. Once the RPV water level decrease to the Level 1 set point value, the RPV is manually depressurized. Figure 5-2 shows the RPV dome pressure. Once the RPV is depressurized, the CS system is assumed to start successfully to inject water into the RPV. The CS injection mass flow rates are shown in Figure 5-3. It is assumed when the containment drywell pressure, as shown in Figure 5-4, reaches design limit of 0.49 MPa (70.7 psia), the CS system pump loses suction and stops to inject water into the RPV. With the absence of makeup water to the RPV, the coolant in the core boils off due to decay heat and leads to fuel failure. Figure 5-5 shows the mass flow rates through SRVs, and Figure 5-6 shows the comparison of PCTs.

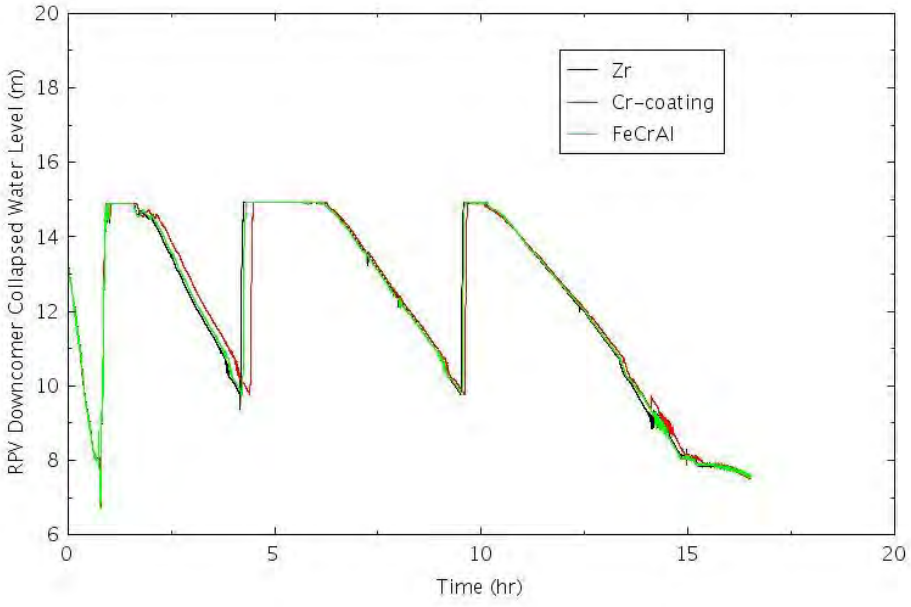

Figure 5-1. RPV Downcomer Water Level for LOMFW-4.

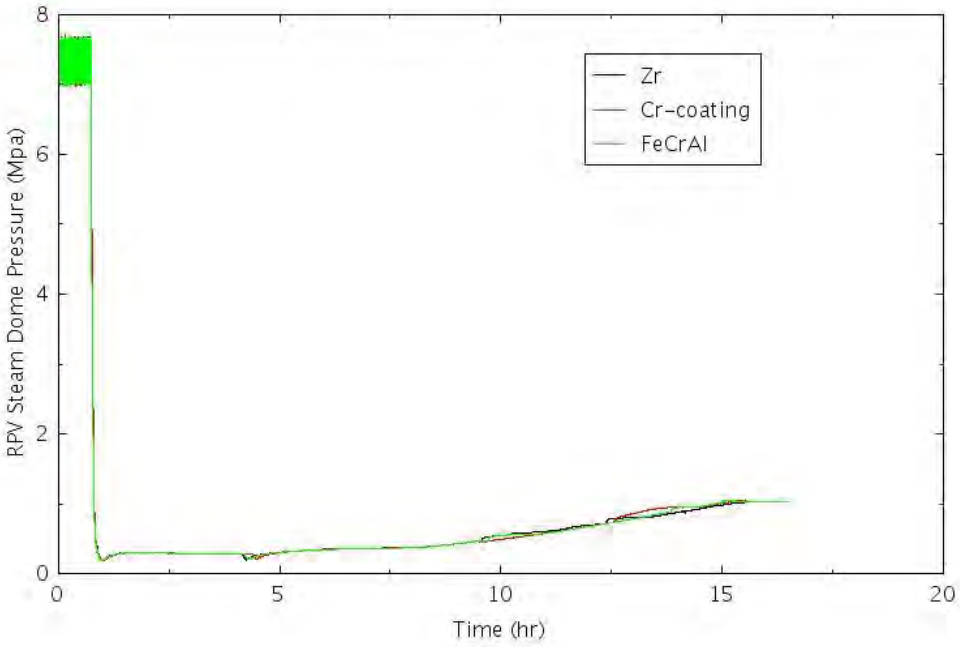

Figure 5-2. RPV Dome Pressure for LOMFW-4.

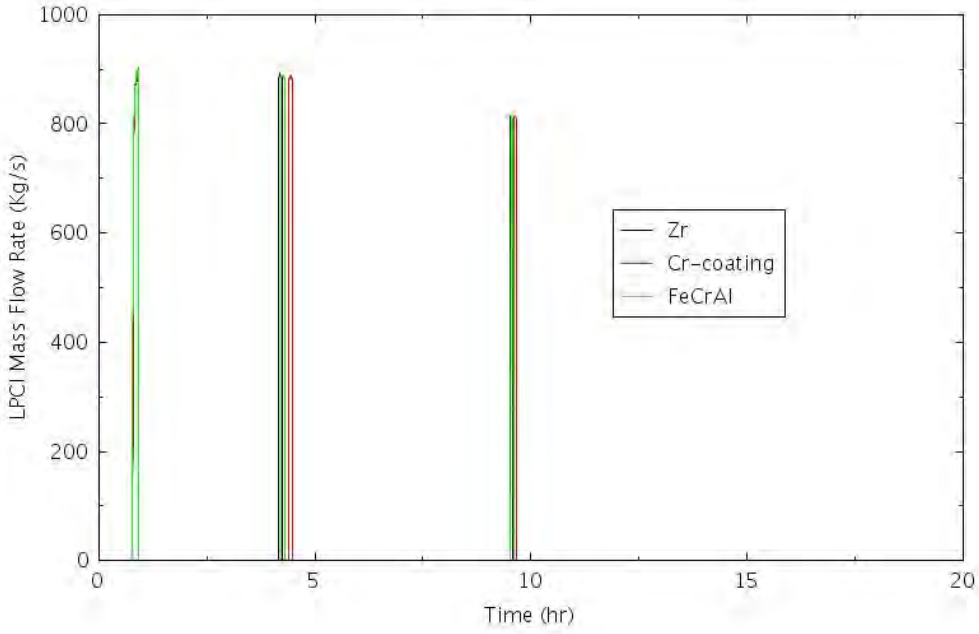

Figure 5-3. CS Injection Mass Flow Rate for LOMFW-4.

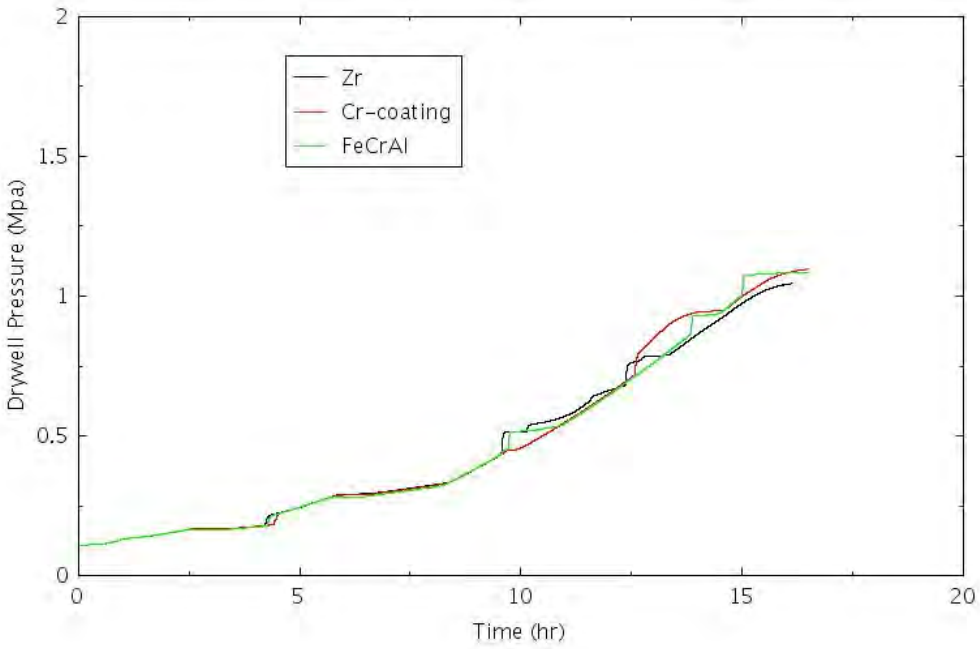

Figure 5-4. Containment DW Pressure for LOMFW-4.

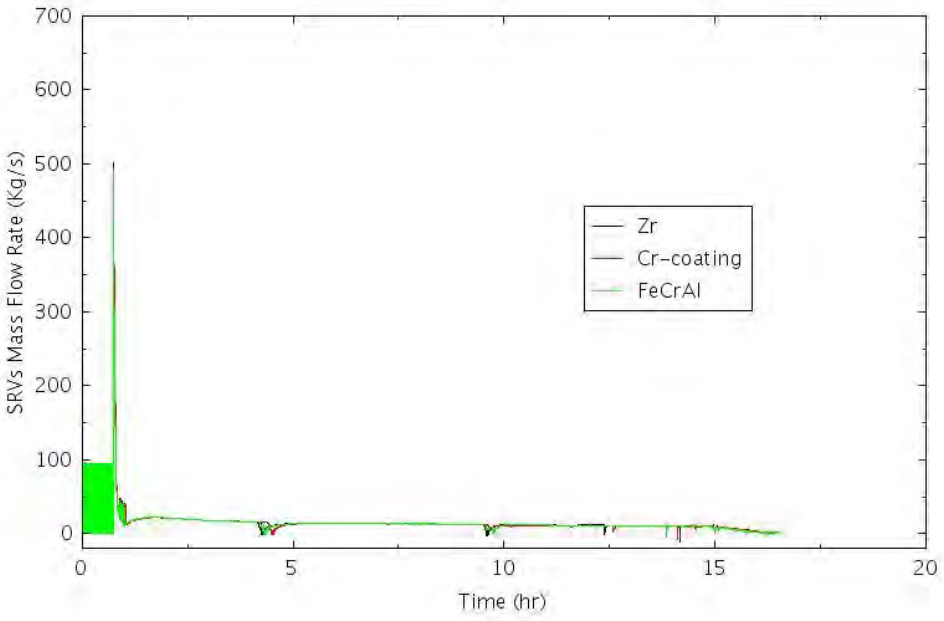

Figure 5-5. Mass Flow Rates through SRVs for LOMFW-4.

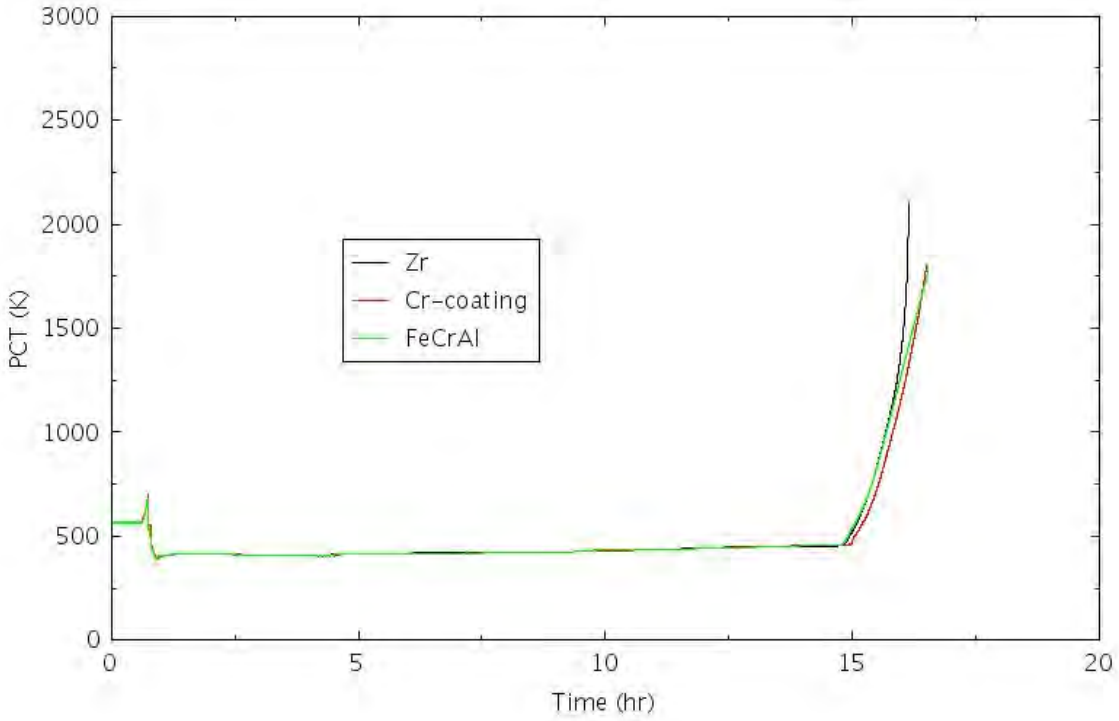

Figure 5-6. PCT Comparison for LOMFW-4.

5.2.2 LOMFW-Initiated ATWS

The three ATWS scenarios initiated by the LOMFW are analyzed in this section.

5.2.2.1 LOMFW-ATWS-1

In this scenario, it is assumed LOMFW occurs at time zero, and the feedwater flow ceases at about 3 seconds as shown in Figure 5-7. The RPS fails to trip reactor, leading to an ATWS. The LOMFW and recirculation pump trip greatly reduce the coolant flow in the core which leads to increased voiding in the core. Figure 5-8 shows the recirculation pump flow. Figure 5-9 shows the void fraction in the middle of the core for the hot channel, and Figure 5-10 shows the void fraction in the middle core for the hot channel for the first 50 seconds. As shown in Figure 5-10, the void fraction in the core increases rapidly following the initiation of the LOMFW flow which introduces negative feedback reactivity as shown in Figure 5-11 for the entire of the transient and Figure 5-12 for the first 200 seconds. The negative feedback reactivity promptly deceases reactor power as shown in Figure 5-13 for the duration of the transient and Figure 5-14 for the first 200 seconds of the transient. Since the SLCS starts successfully, the boron concentration at the core inlet is shown in Figure 5-15. The RPV dome pressure is shown in Figure 5-16. It can be seen the system pressure initially dropped due to the flow imbalance between LOMFW flow and the loss of inventory through the main steam line. The MSIV stays open, as shown in Figure 5-17, until 530 seconds when the water level drops to the Level 1 setpoint at which the MSIV closes. After the MSIV closes, the system pressure increases, and the SRVs start to cycle to keep the system pressure within a predefined operating range, as shown in Figure 5-18. The RPV collapsed water level is shown in Figure 5-19, and the water level drops precipitously once the feedwater flow stops. Figure 5-20 shows the comparison of PCT for conventional fuel with Zircaloy cladding and ATF with Cr-coated and FeCrAl cladding.

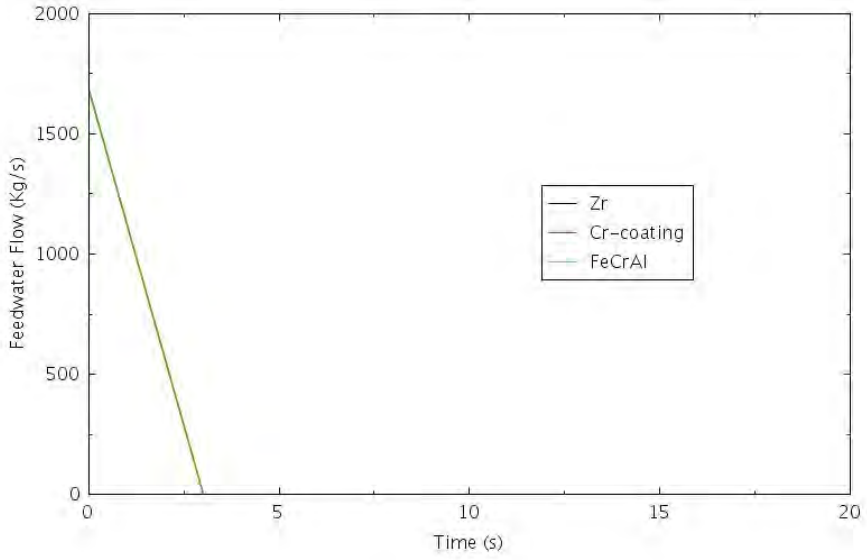

Figure 5-7. Main Feedwater Mass Flow Rate for LOMFW-ATWS-1.

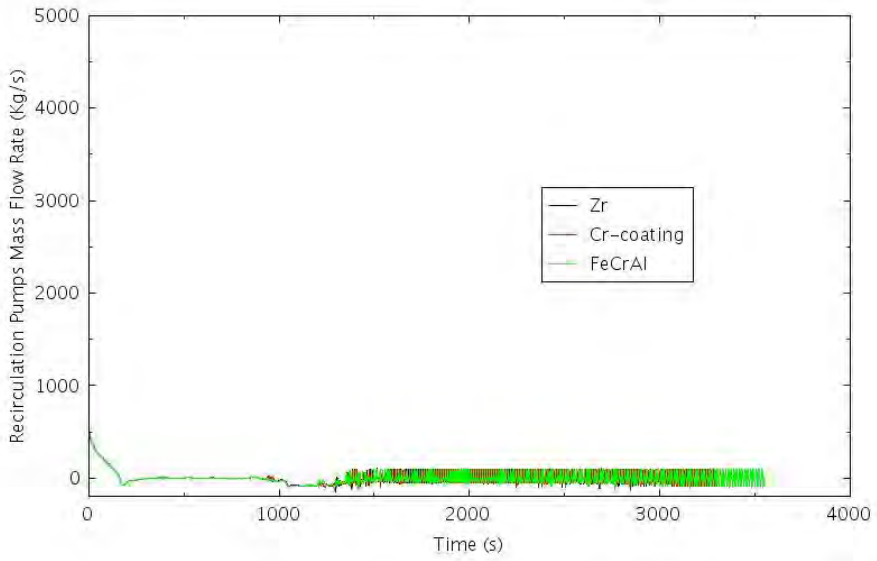

Figure 5-8. Recirculation Pumps Mass Flow Rate for LOMFW-ATWS-1.

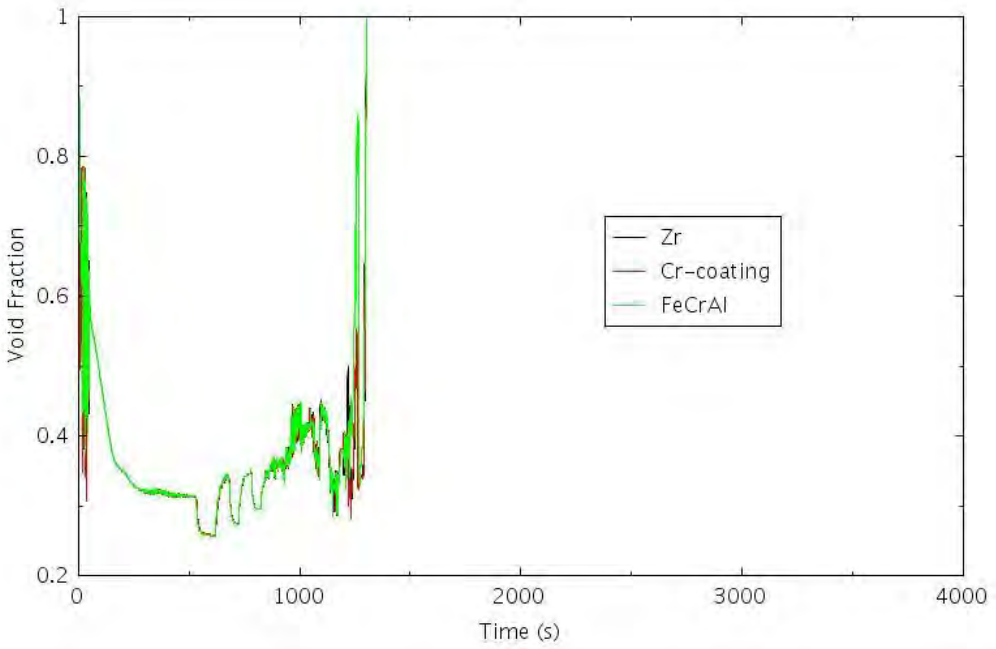

Figure 5-9. Void Fraction in the Middle of the Core in the Hot Channel for LOMFW-ATWS-1.

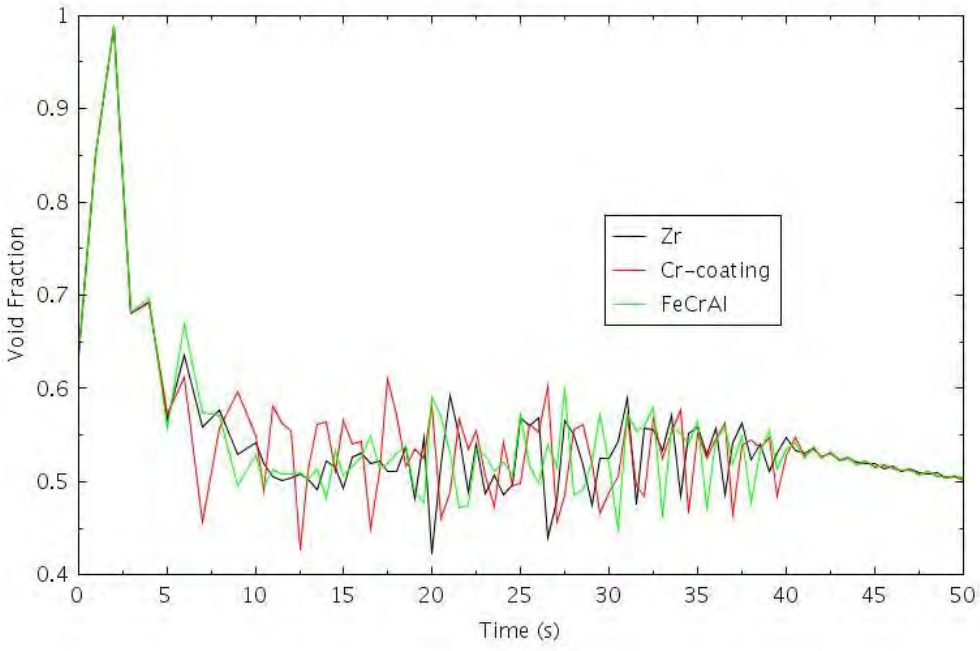

Figure 5-10. Void Fraction in the Middle of the Core in the Hot Channel for LOMFW-ATWS-1.

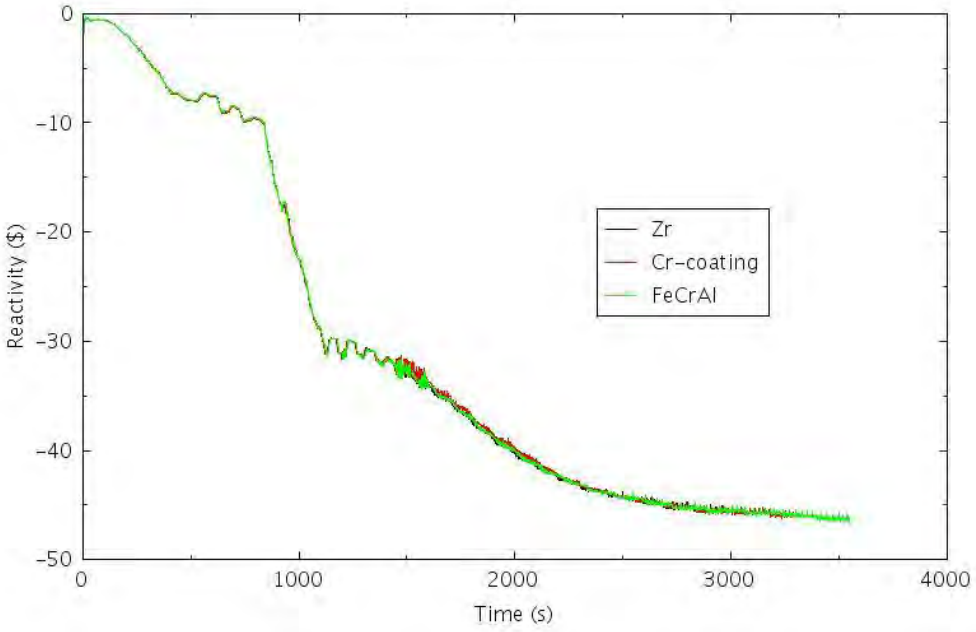

Figure 5-11. Reactivity for LOMFW-ATWS-1.

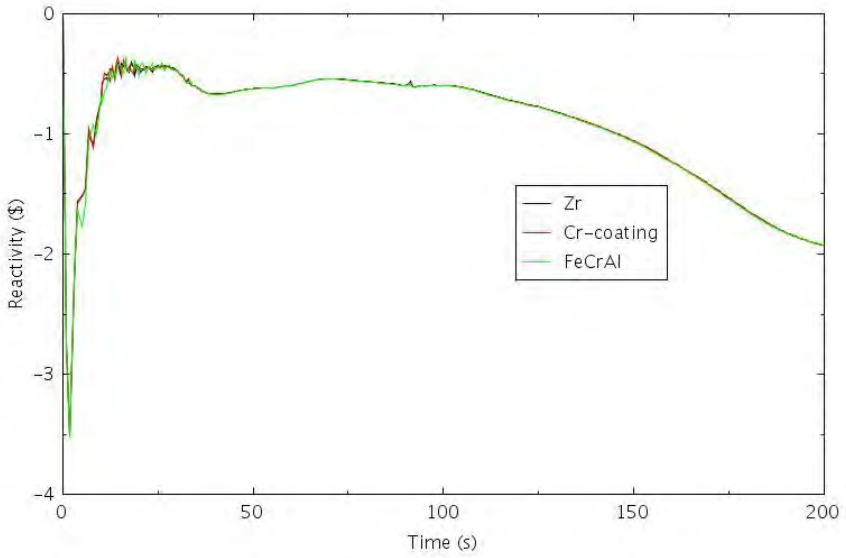

Figure 5-12. Reactivity During the First 200 Seconds of LOMFW-ATWS-1.

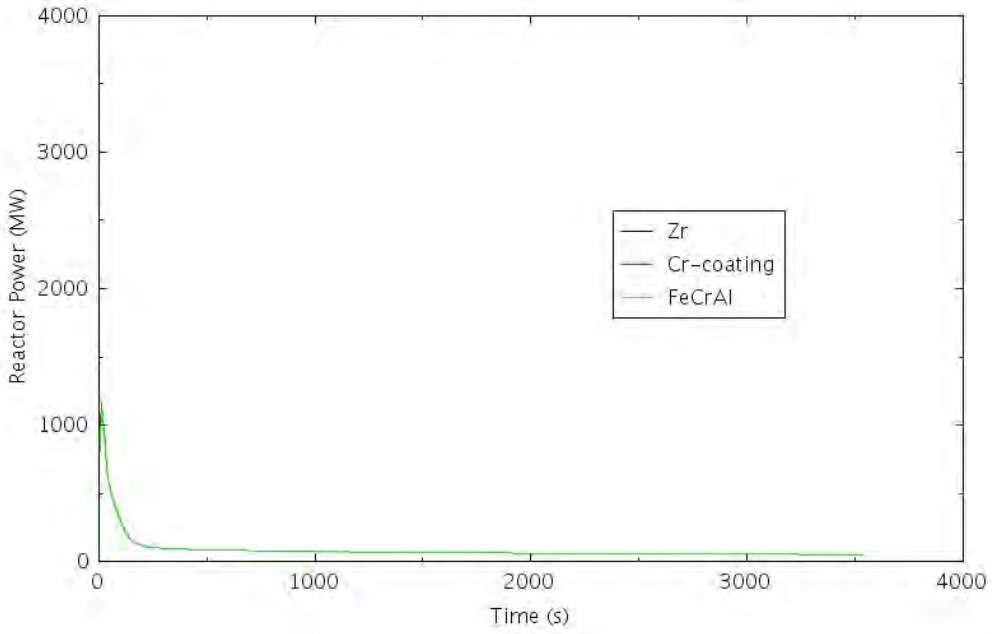

Figure 5-13. Reactor Power for LOMFW-ATWS-1.

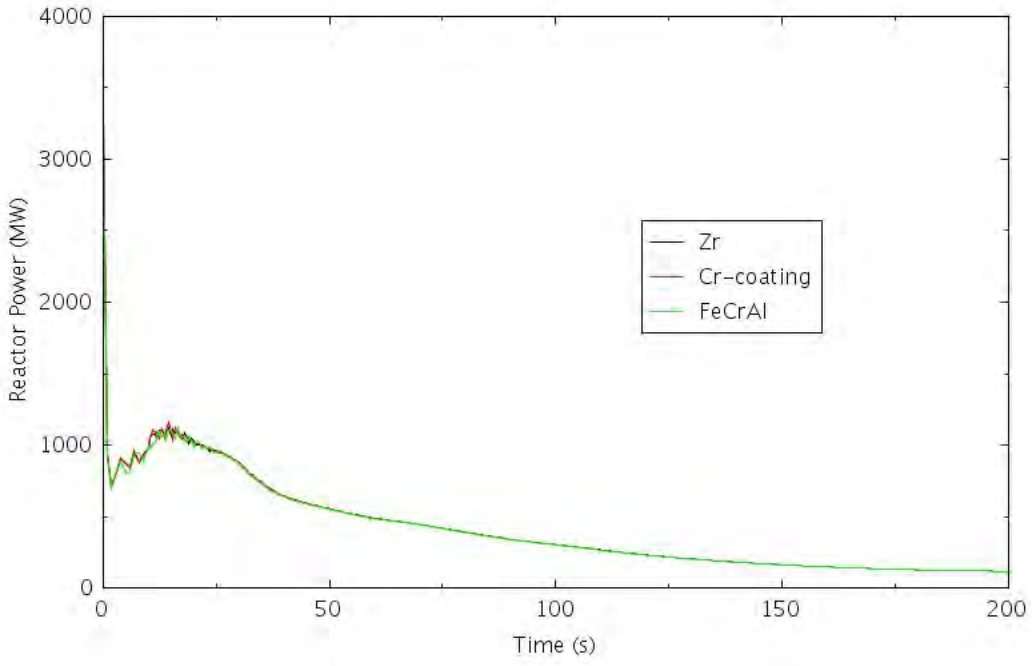

Figure 5-14. Reactor Power for LOMFW-ATWS-1.

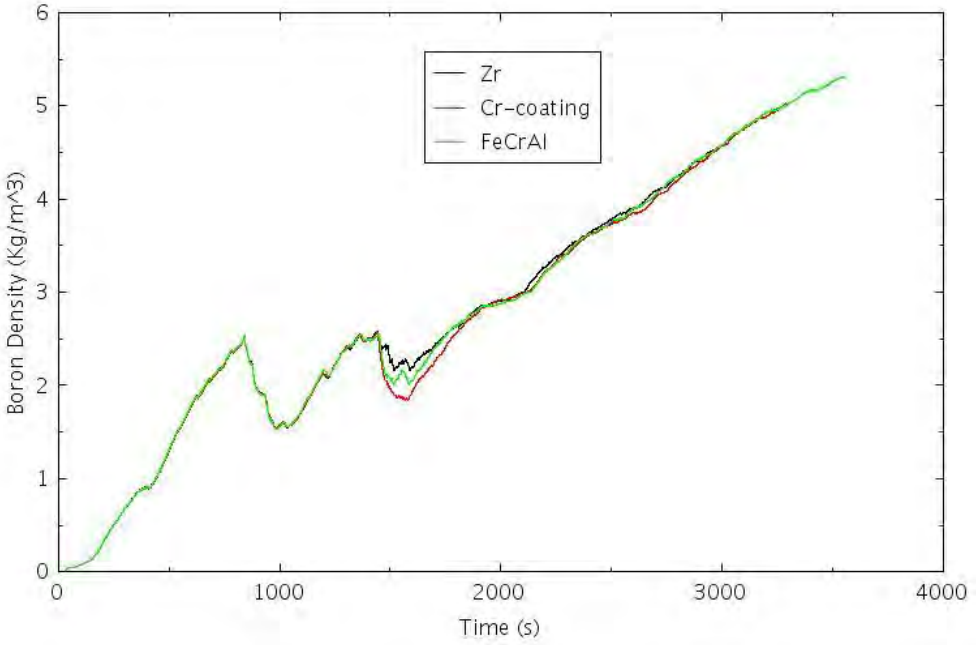

Figure 5-15. Boron Concentration at the Core Inlet for LOMFW-ATWS-1.

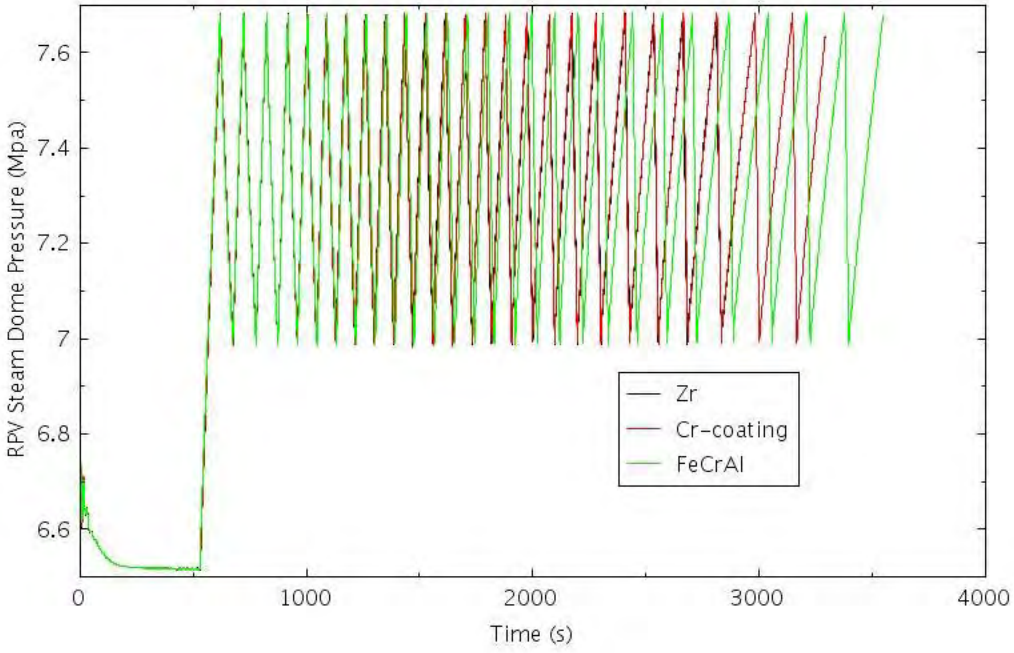

Figure 5-16. RPV Dome Pressure for LOMFW-ATWS-1.

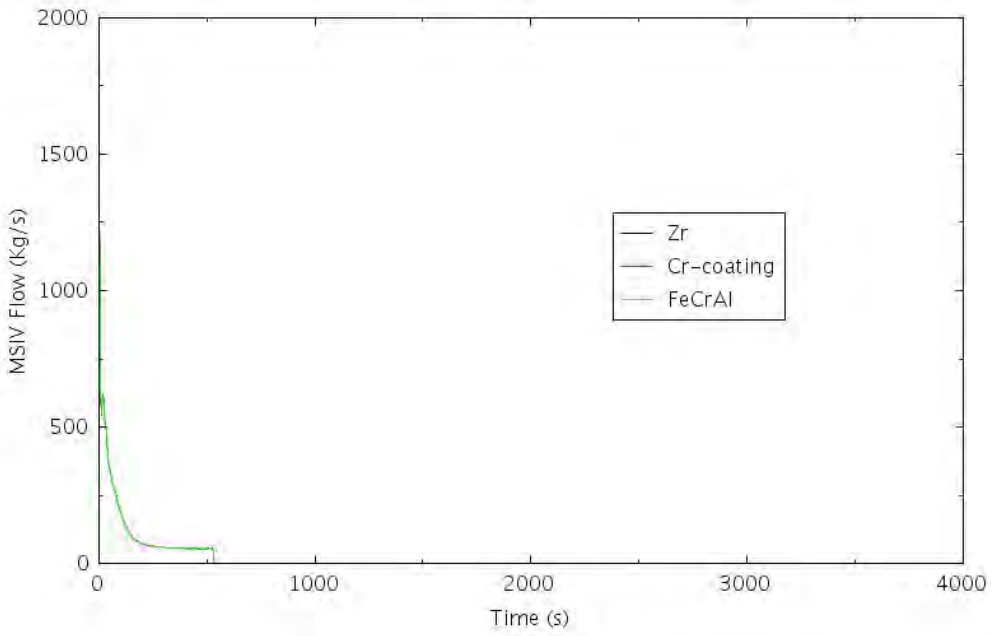

Figure 5-17. MSIV Mass Flow Rate for LOMFW-ATWS-1.

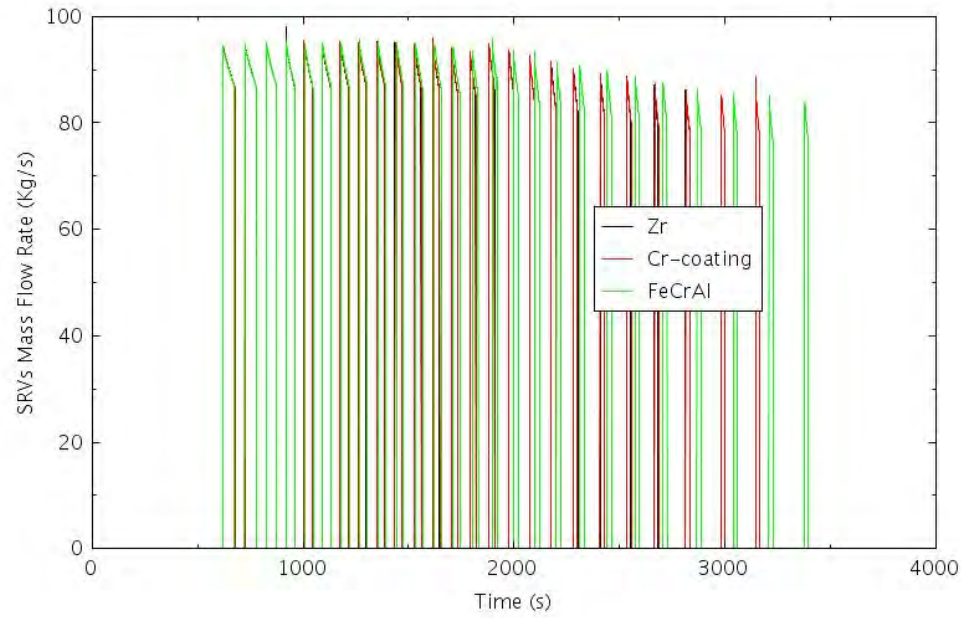

Figure 5-18. SRVs Mass Flow Rate as a Function of Time for LOMFW-ATWS-1.

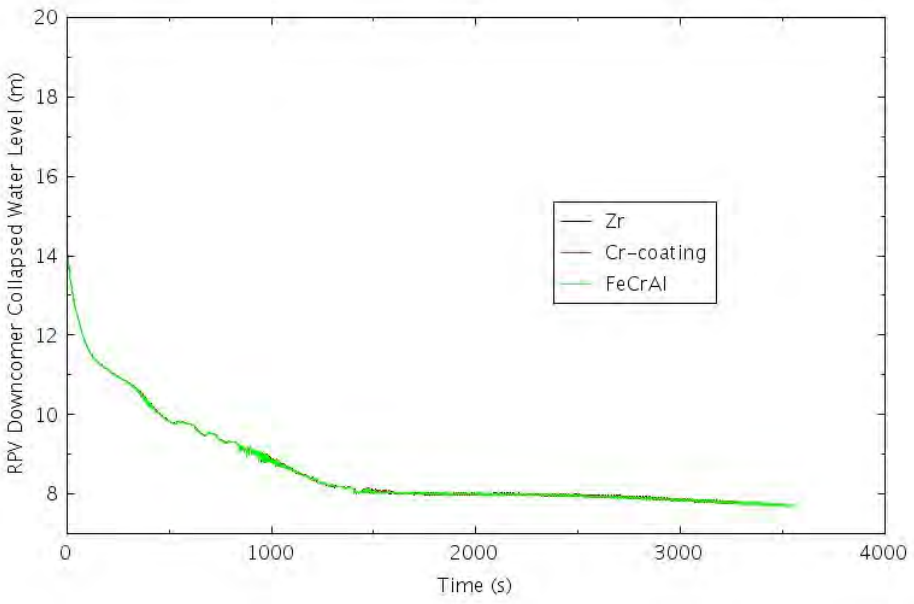

Figure 5-19. RPV Collapsed Water Level for LOMFW-ATWS-1.

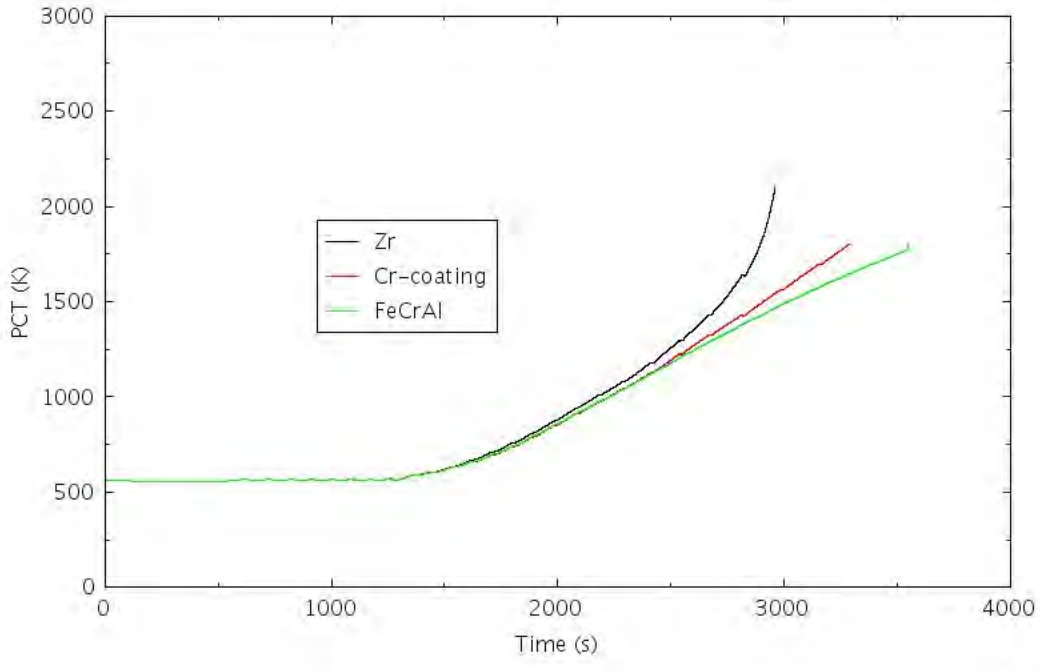

Figure 5-20. PCT as a Function of Time for LOMFW-ATWS-1.

5.2.2.2 LOMFW-ATWS-2

This scenario is similar to LOMFW-ATWS-1. The major difference is the SLCS fails to start to inject boron into the reactor to control the reactivity. In this scenario, it is assumed LOMFW occurs at time zero, and the feedwater flow ceases at about 3 seconds as shown in Figure 5-21. The RPS fails to trip reactor, leading to an ATWS. The LOMFW and recirculation pump trip greatly reduce the coolant flow in the core which leads to increased voiding in the core. Figure 5-22 shows the recirculation pump flow, Figure 5-23 shows the void fraction in the middle of the core for the hot channel, and Figure 5-24 shows the void fraction in the middle of the core for the hot channel for the first 50 seconds. As shown in Figure 5-24, the void fraction in the core increases rapidly following the initiation of the LOMFW flow which introduces negative feedback reactivity as shown in Figure 5-25 for the entire of the transient and Figure 5-26 for the first 200 seconds. The negative feedback reactivity following the initiation of LOMFW promptly deceases reactor power as shown in Figure 5-27 for the duration of the transient and Figure 5-28 for the first 200 seconds of the transient. The RPV dome pressure is shown in Figure 5-29. It can be seen the system pressure initially dropped due to the flow imbalance between LOMFW flow and the loss of inventory through the main steam line. The MSIV stays open, as shown in Figure 5-30, until 240 seconds when the water level drops to the Level 1 setpoint at which the MSIV closes. After the MSIV closes, the system pressure increases, and the SRVs start to cycle to keep the system pressure within a predefined operating range, as shown in Figure 5-31. The RPV collapsed water level is shown in Figure 5-32, and the water level drops precipitously once the feedwater flow stops. Figure 5-33 shows the comparison of PCT for conventional fuel with Zircaloy cladding and ATF with Cr-coated and FeCrAl cladding.

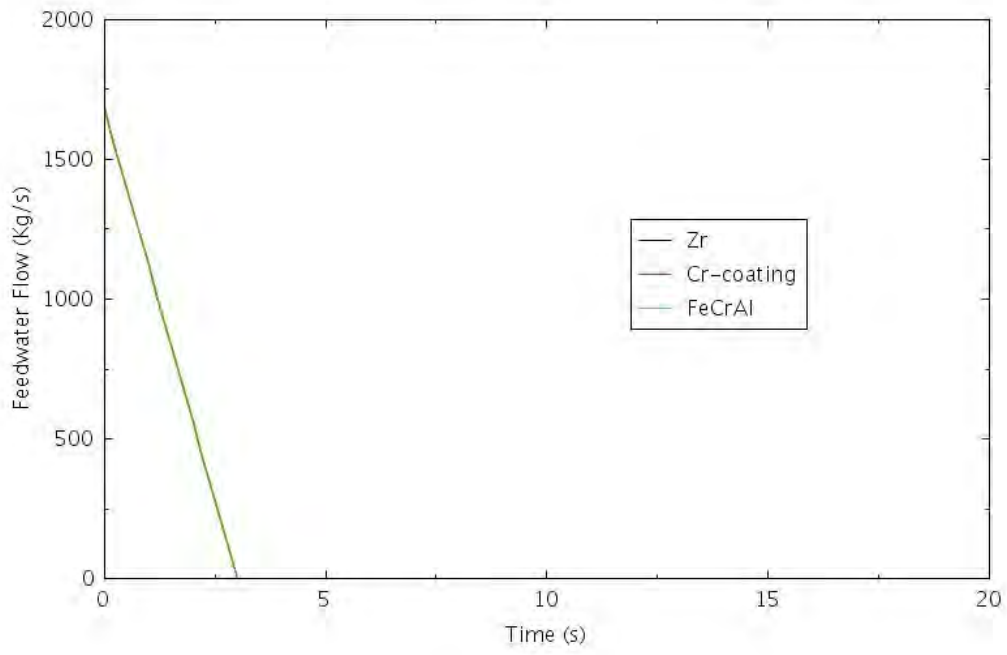

Figure 5-21. Main Feedwater Flow for LOMFW-ATWS-2.

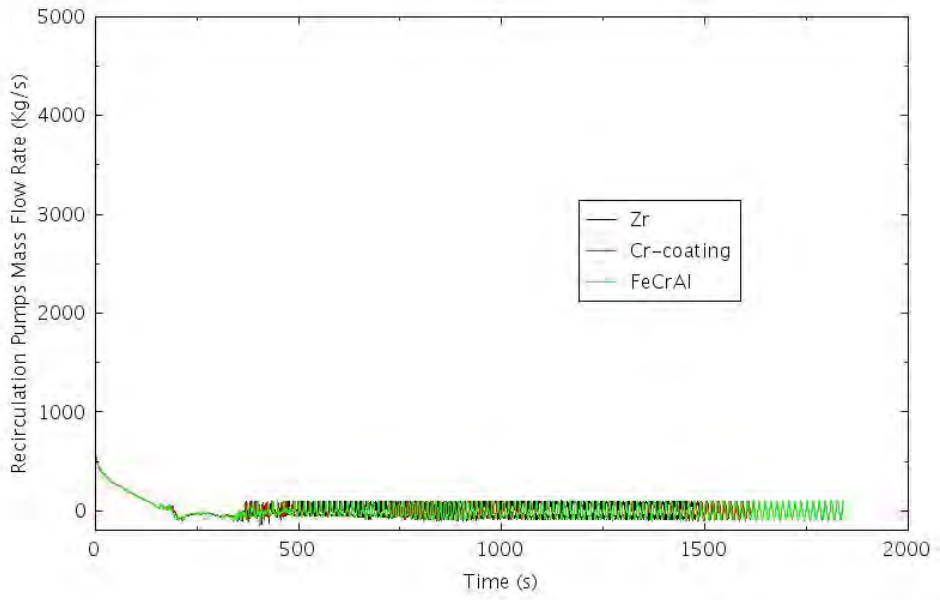

Figure 5-22. Recirculation Pumps Flow for LOMFW-ATWS-2.

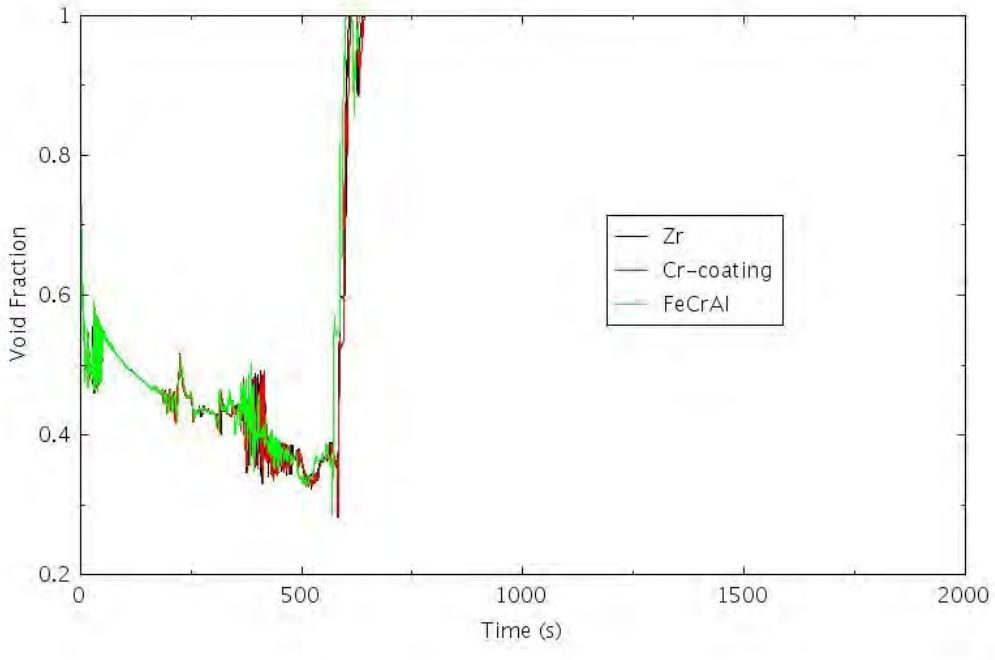

Figure 5-23. Void Fraction in the Middle of the Core in the Hot Channel for LOMFW-ATWS-2.

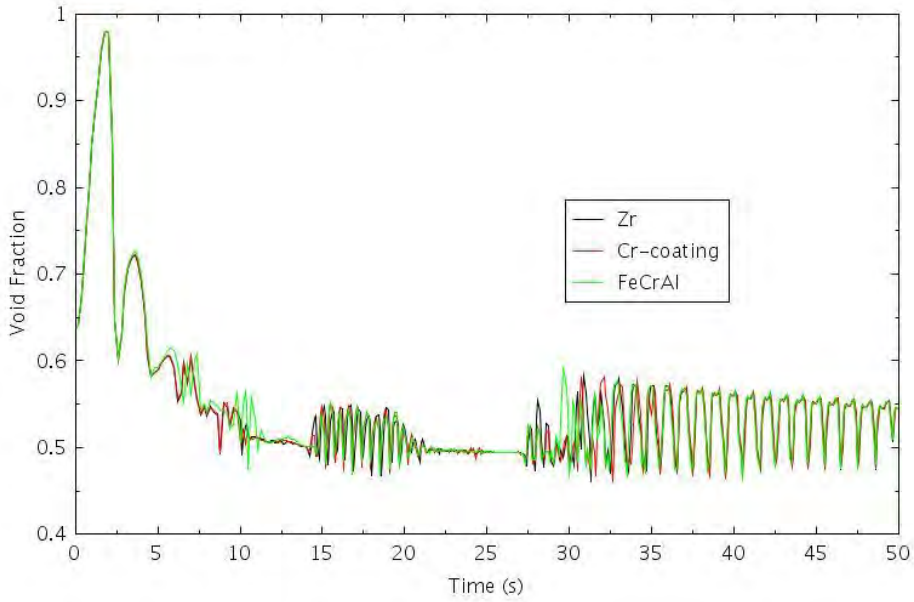

Figure 5-24. Void Fraction in the Middle of the Core in the Hot Channel Within the First 50 Seconds for LOMFW-ATWS-2.

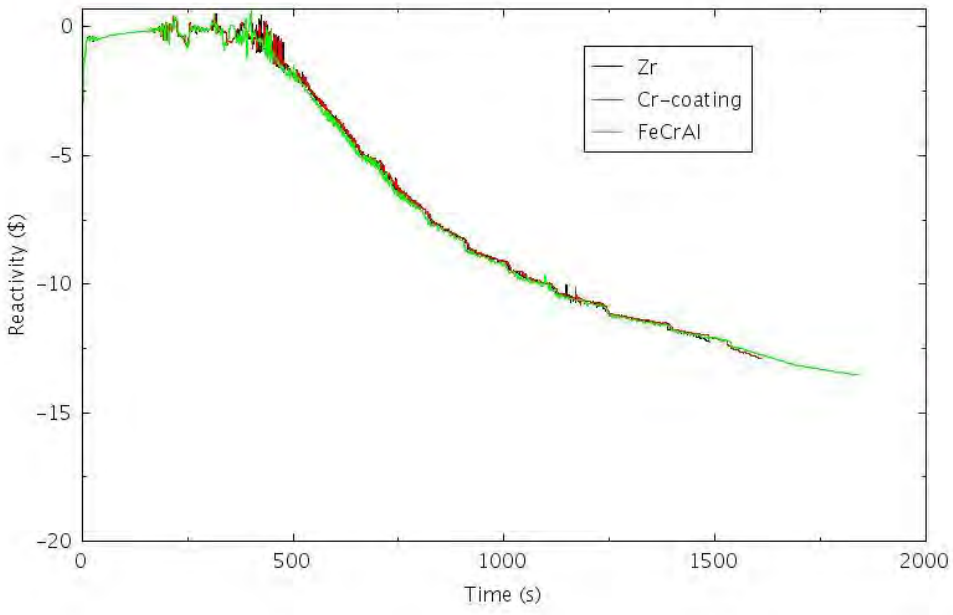

Figure 5-25. Feedback Reactivity for LOMFW-ATWS-2.

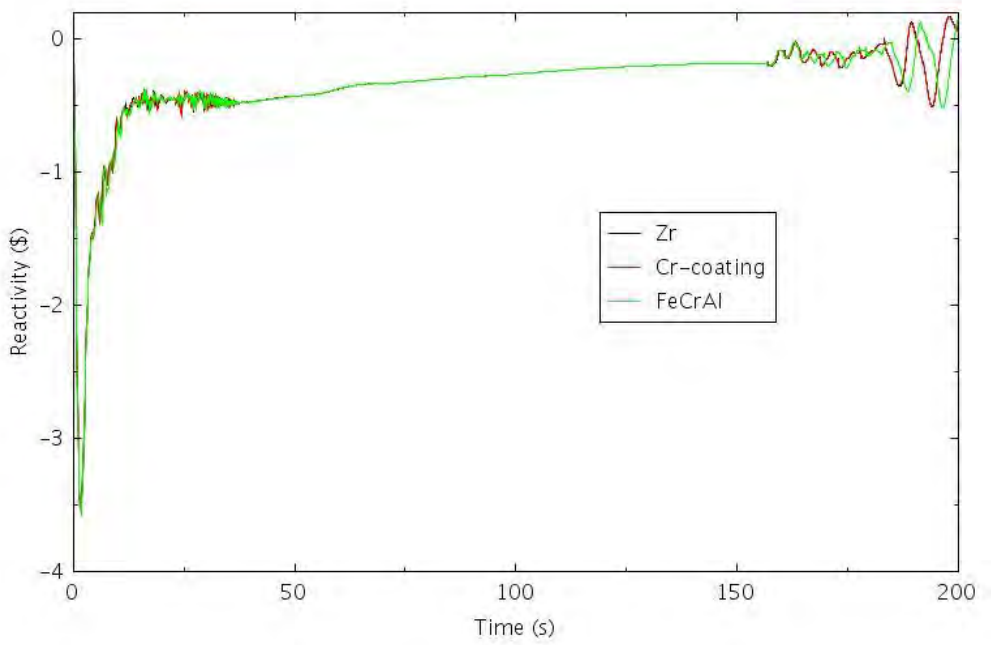

Figure 5-26. Feedback Reactivity During the First 200 Seconds of LOMFW-ATWS-2.

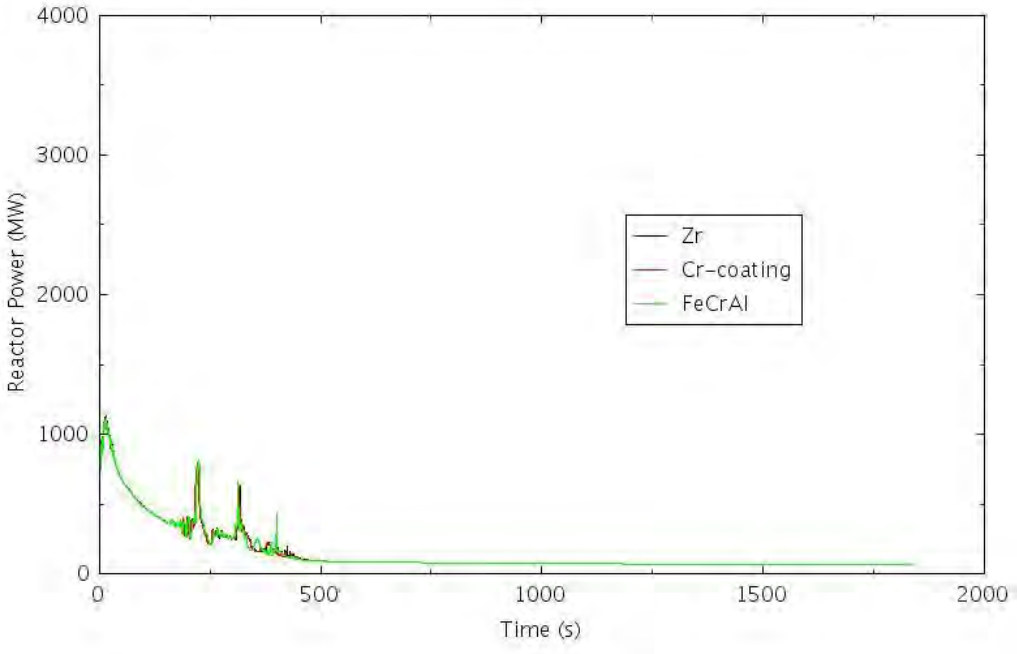

Figure 5-27. Reactor Power for LOMFW-ATWS-2.

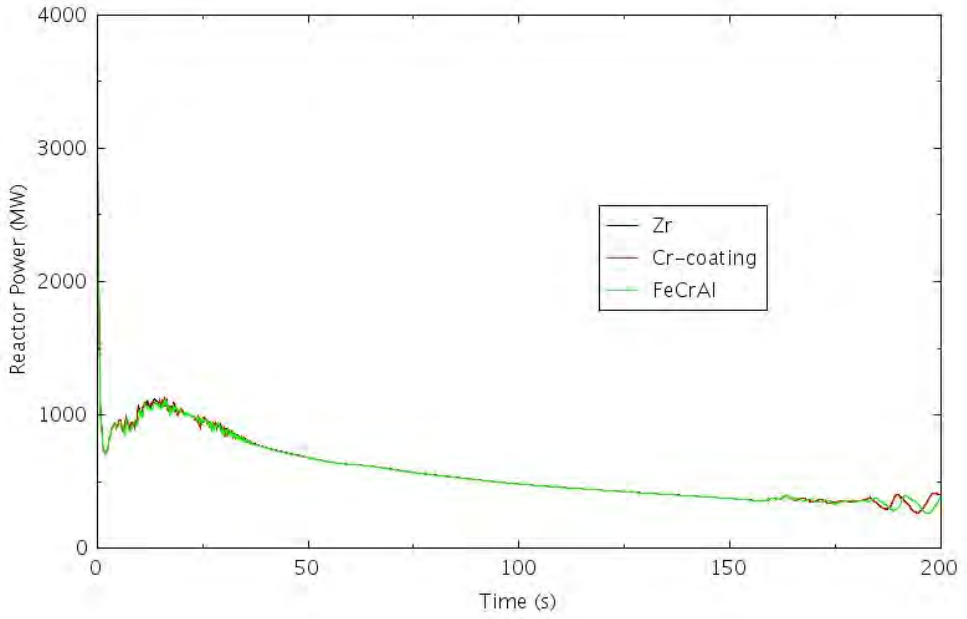

Figure 5-28. Reactor Power within the First 200 Seconds of LOMFW-ATWS-2.

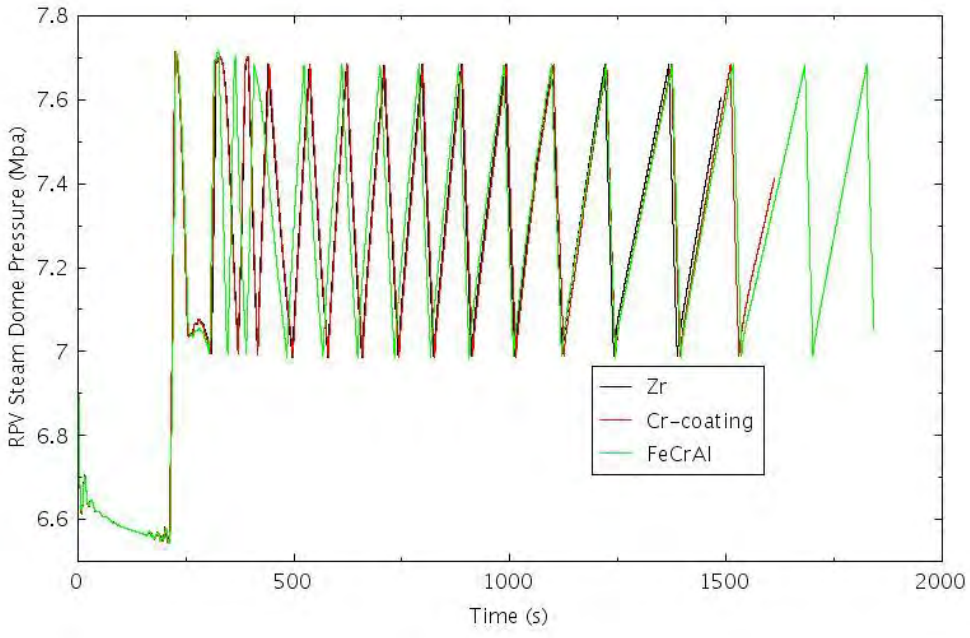

Figure 5-29. RPV Dome Pressure for LOMFW-ATWS-2.

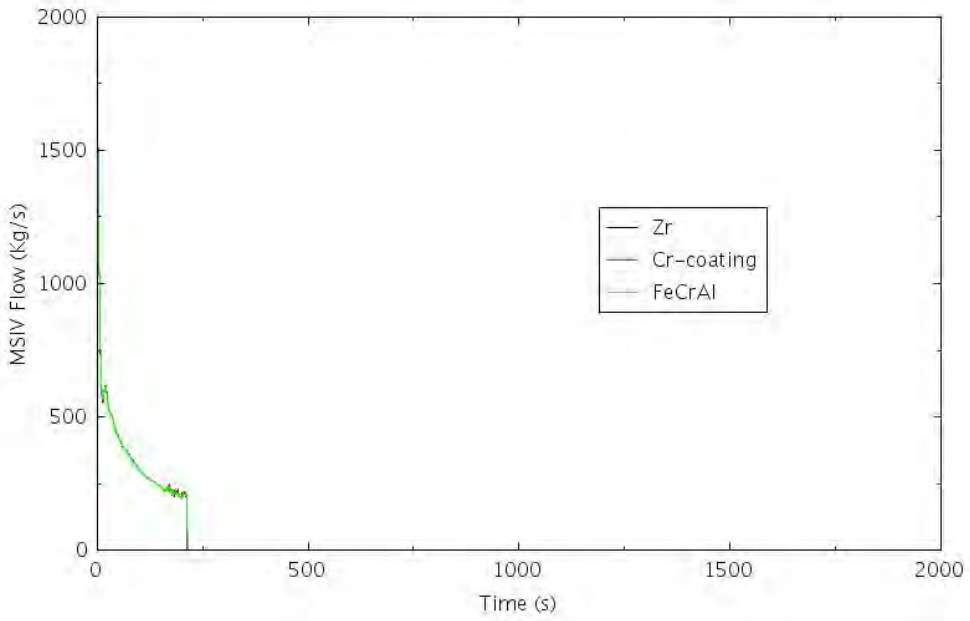

Figure 5-30. MSIV Mass Flow Rate for LOMFW-ATWS-2.

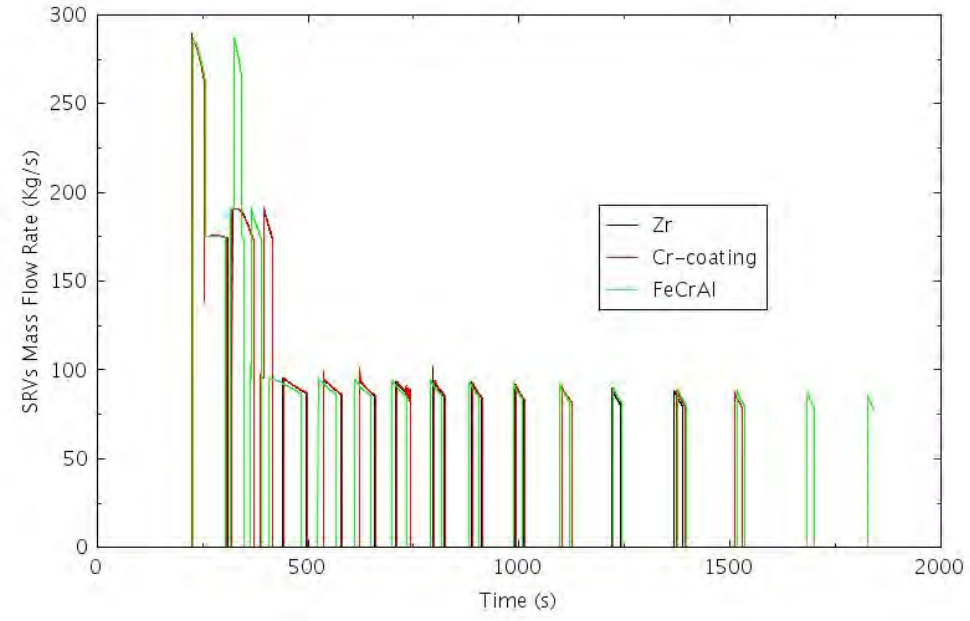

Figure 5-31. SRVs Mass Flow Rate for LOMFW-ATWS-2.

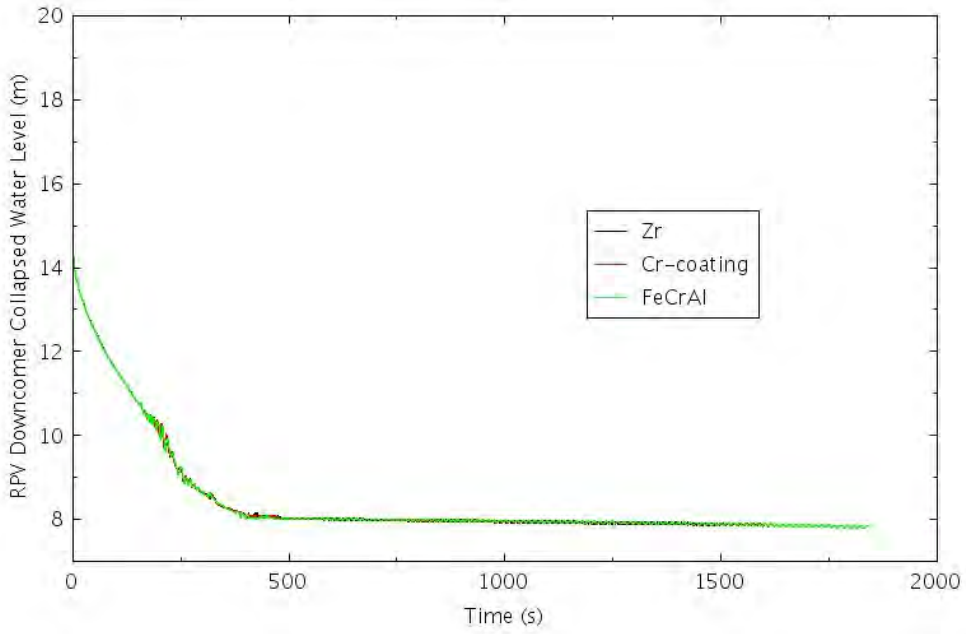

Figure 5-32. RPV Collapsed Water Level for LOMFW-ATWS-2.

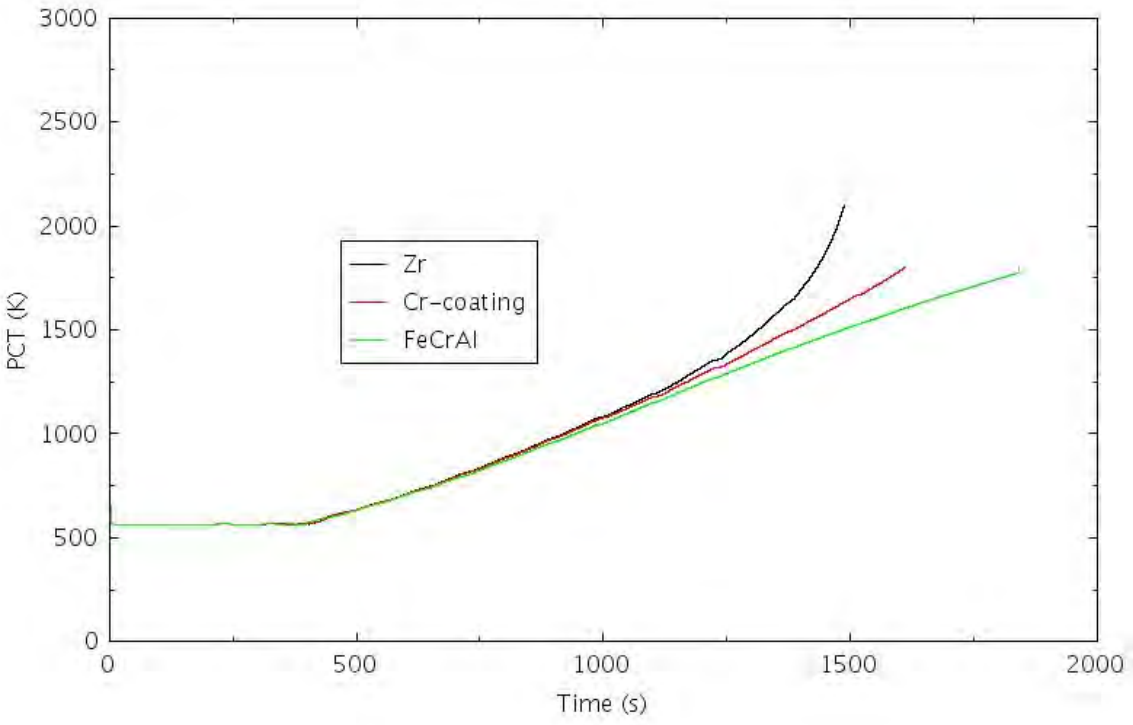

Figure 5-33. PCT for LOMFW-ATWS-2.

5.2.2.3 LOMFW-ATWS-3

In this scenario, it is assumed the LOMFW occurs at time zero, and the feedwater flow ceases at about 3 seconds as shown in Figure 5-34. The RPS fails to trip reactor leading to an ATWS. The LOMFW and recirculation pump trip greatly reduce the coolant flow in the core which leads to increased voiding in the core. Figure 5-35 shows the recirculation pump flow. The reduced flow in the core causes the void fraction in the core to rise initially following the accident, as shown in Figure 5-36, for the void fraction in the middle of the core for the hot channel during the first 20 years of the accident. Figure 5-37 shows the void fraction evolution for the entire transient. The initial rise of void fraction introduces negative feedback reactivity as shown in Figure 5-38 for the first 200 seconds of the transient. Figure 5-39 shows the feedback reactivity for the duration of the transient. With the LOMFW flow and the assumption that the HPI fails to start, the water level decreases, as shown in Figure 5-40. When the RPV water level, as shown in Figure 5-40, reaches the Level 1 setpoint; MSIV fully closes at about 526 seconds. The MSIV flow is shown in Figure 5-41. When the RPV water level reaches the Level 1 setpoint, the RPV is also depressurized. The RPV dome pressure is shown in Figure 5-42. Before the manual depressurization of the RPV, the system pressure stays lower than the setpoint values that would activate the opening of SRVs, and there is no flow through SRVs. Figure 5-43 shows the mass flow rates through the SRVs. Once the RPV is depressurized, the LPCI is assumed to start successfully. Figure 5-44 shows the LPCI water injection rate. Once the LPCI starts to inject coolant into the RPV, the RPV water starts to increase. While the water level is rising, the void fraction in the core is decreasing, as shown in Figure 5-37. The decreasing void fraction introduces less negative feedback to the reactor. When the RPV is overfilled with water, the feedback reactivity becomes positive in turn causing a reactor power spike as shown in Figure 5-45. The instantaneous power spike presents challenges for RELAP5-3D to converge, and a much lower peak PCT criterion of 1275 K is used to stop the simulations for the baseline fuel design as well as ATF design. Figure 5-46 shows the comparison of PCT for conventional fuel with Zircaloy cladding and ATF with Cr-coated and FeCrAl cladding.

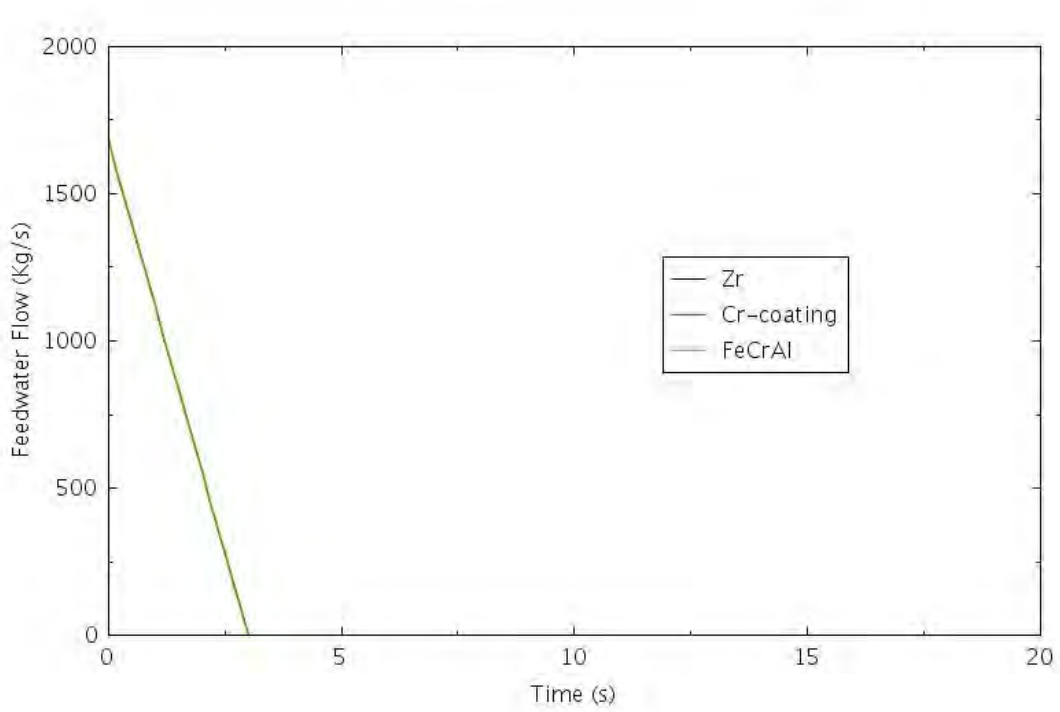

Figure 5-34. Main Feedwater Flow for LOMFW-ATWS-3.

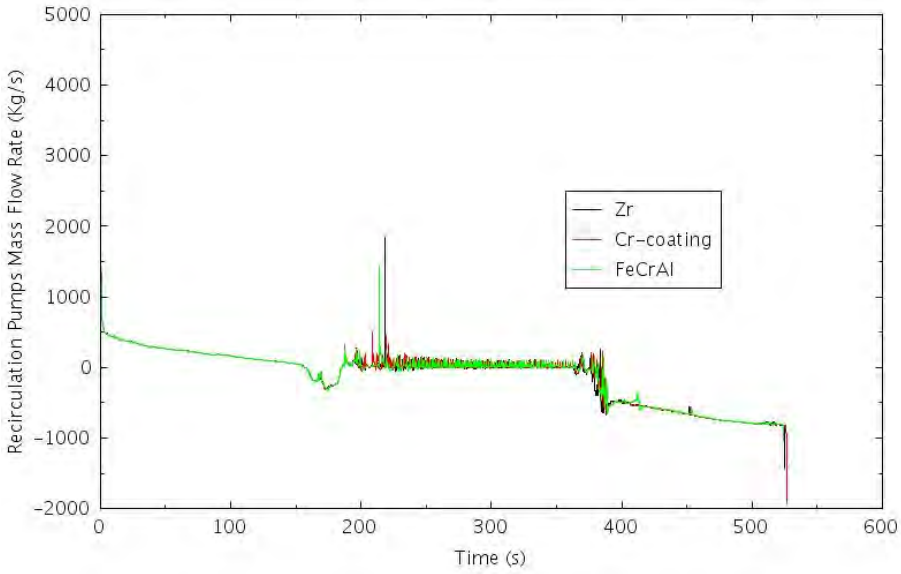

Figure 5-35. Recirculation Pumps Flow for LOMFW-ATWS-3.

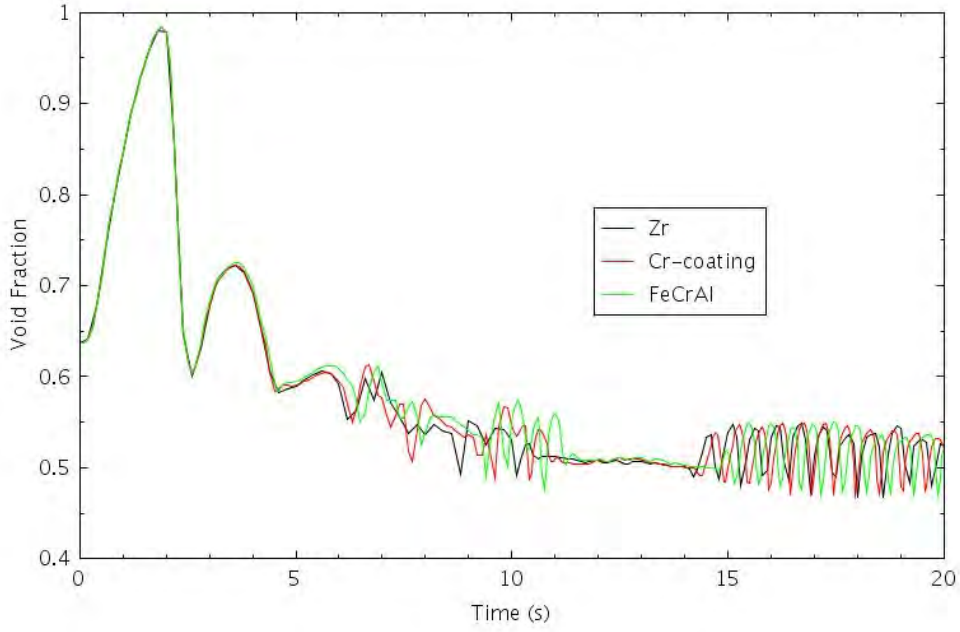

Figure 5-36. Void Fraction in the Middle of the Core for the Hot Channel Within the First 20 Seconds of LOMFW-ATWS-3.

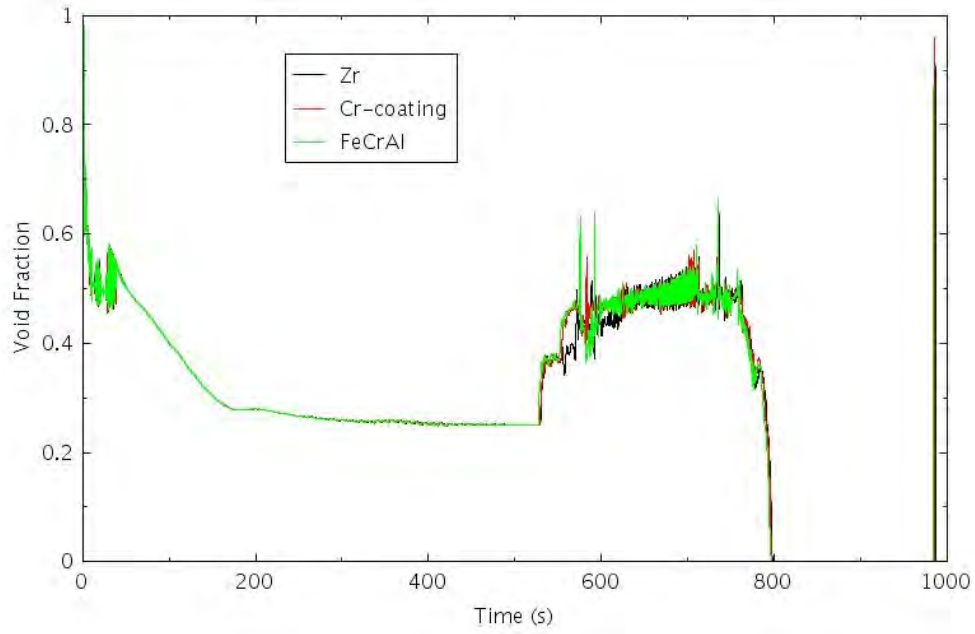

Figure 5-37. Void Fraction in the Middle of the Core for the Hot Channel for LOMFW-ATWS-3.

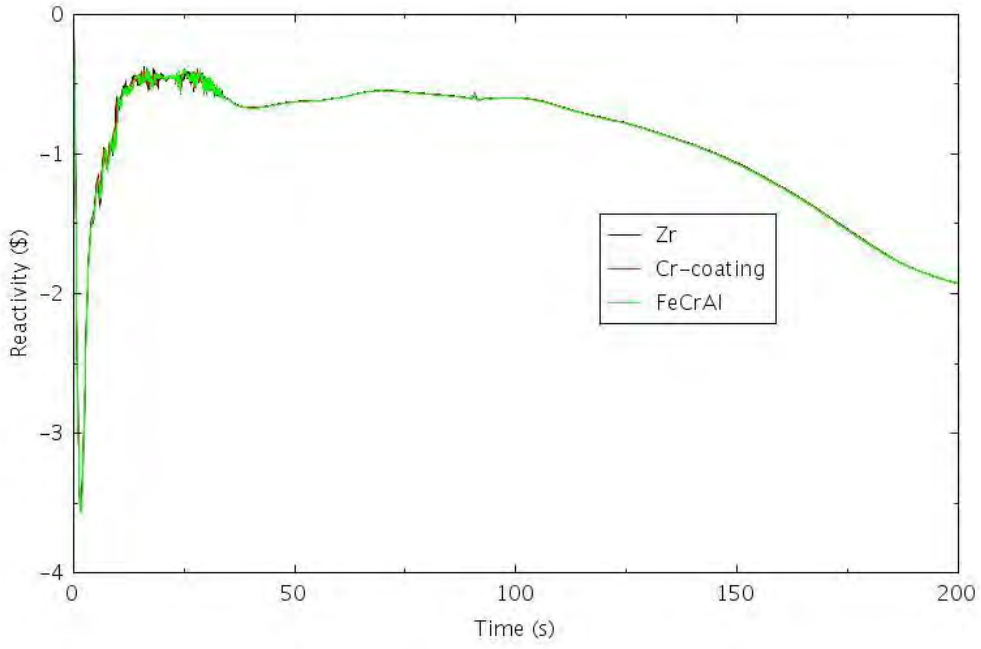

Figure 5-38. Feedback Reactivity Within the First 200 Seconds of LOMFW-ATWS-3.

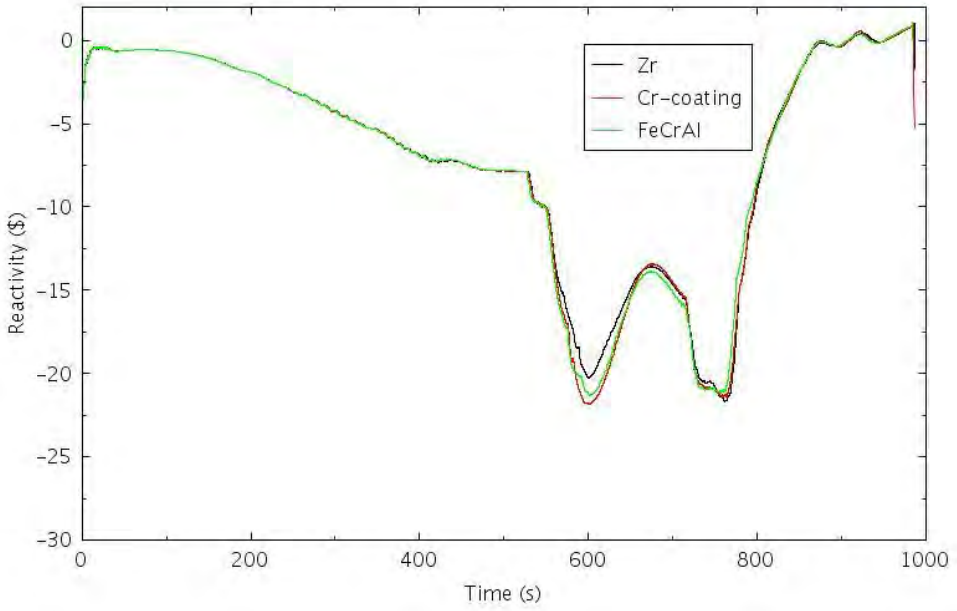

Figure 5-39. Feedback Reactivity for LOMFW-ATWS-3.

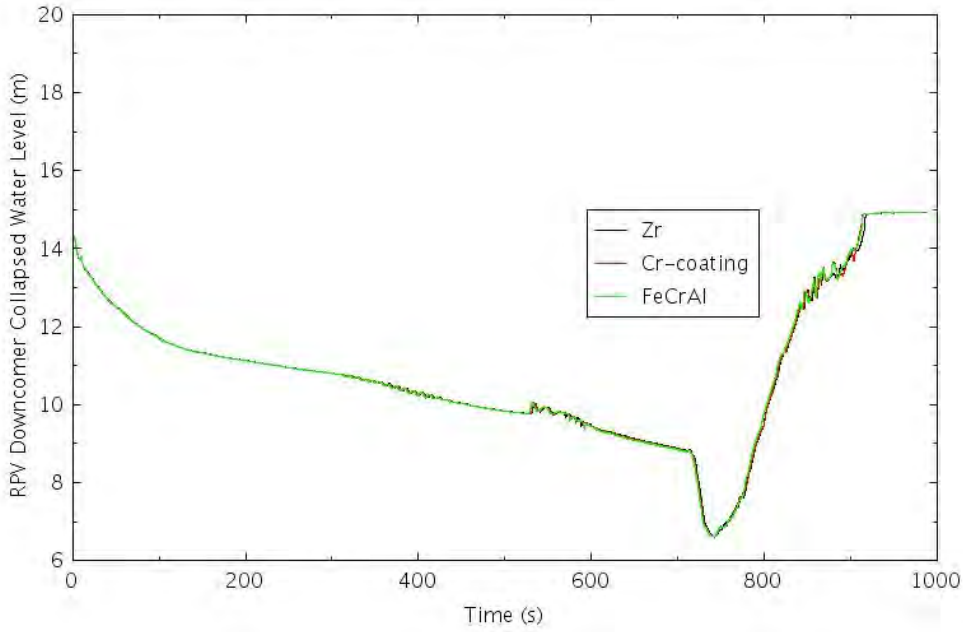

Figure 5-40. RPV Collapsed Water Level for LOMFW-ATWS-3.

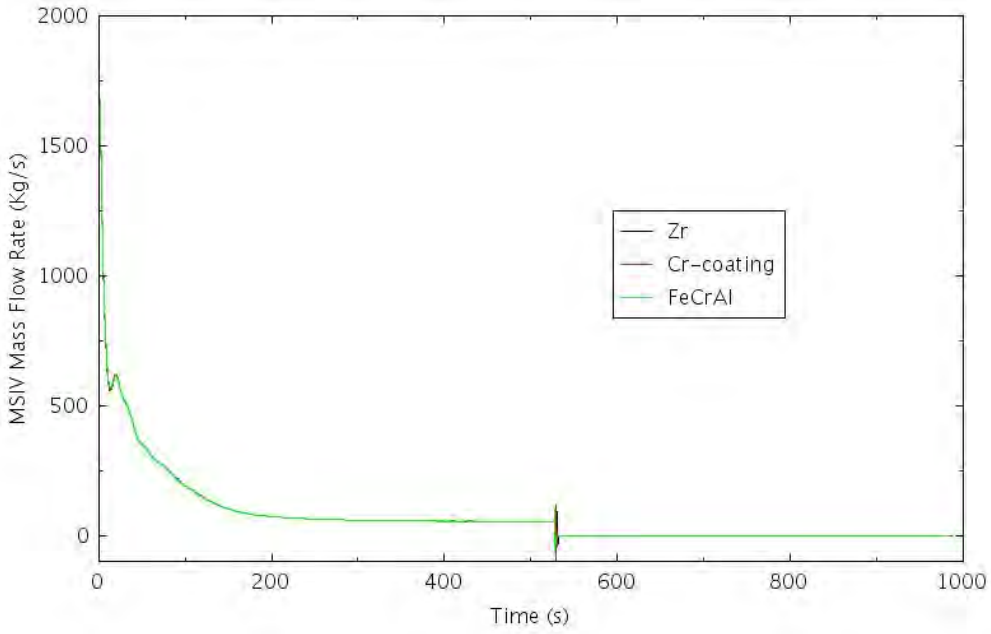

Figure 5-41. MSIV Flow for LOMFW-ATWS-3.

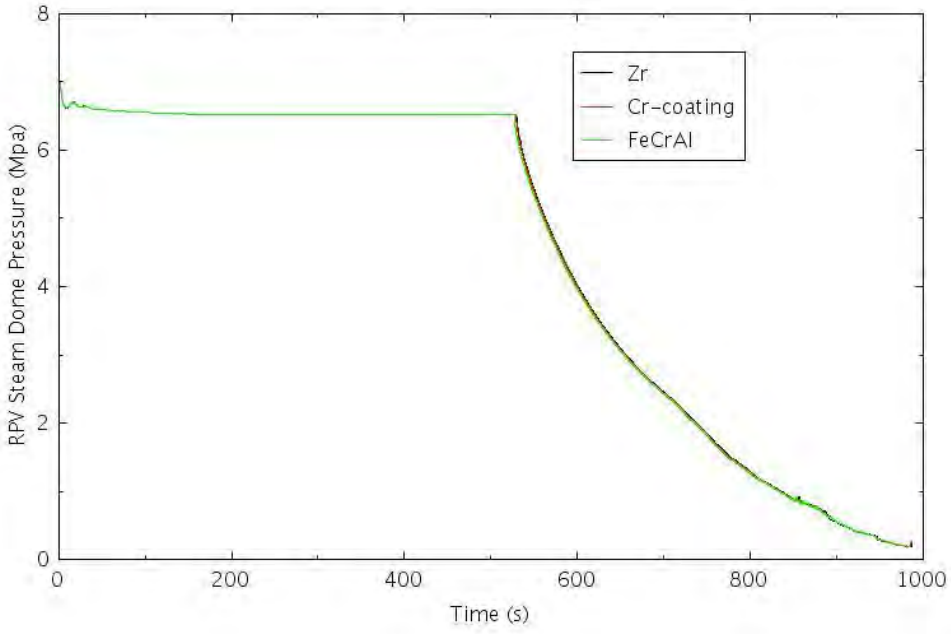

Figure 5-42. RPV Dome Pressure for LOMFW-ATWS-3.

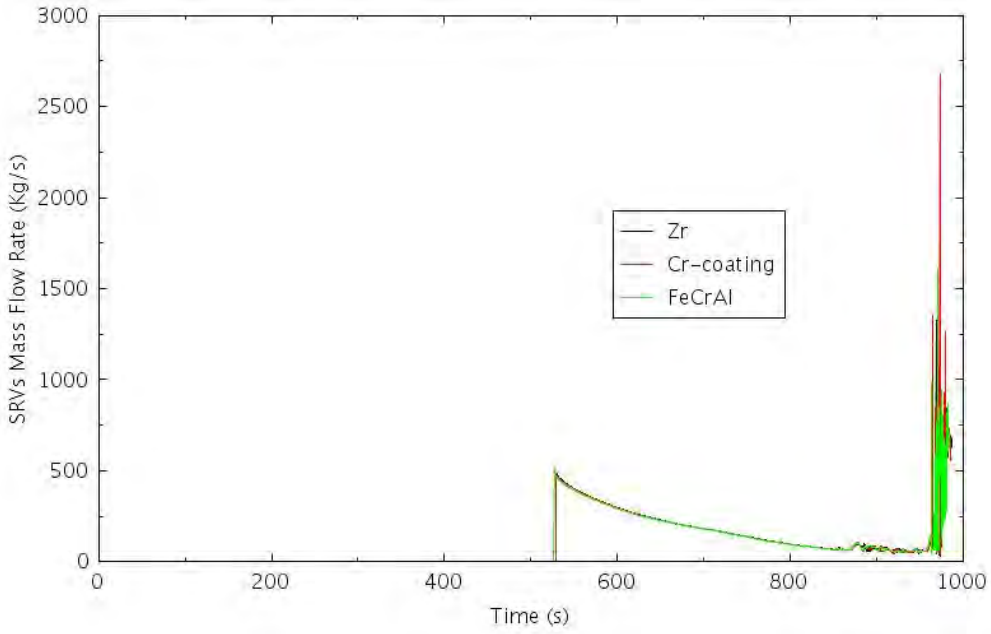

Figure 5-43. Mass Flow Rates through SRVs for LOMFW-ATWS-3.

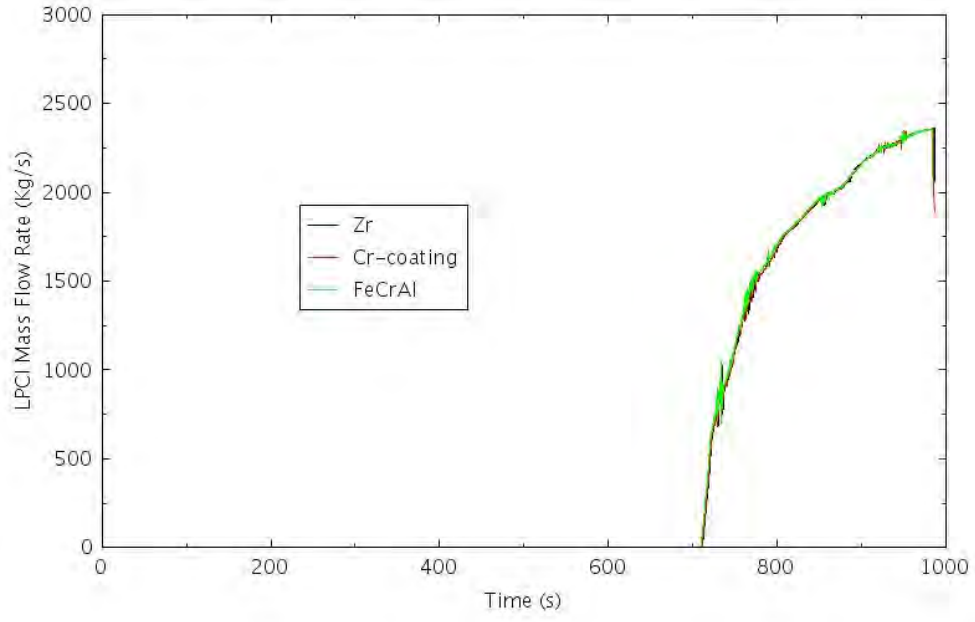

Figure 5-44. LPCI Mass Flow Rate for LOMFW-ATWS-3.

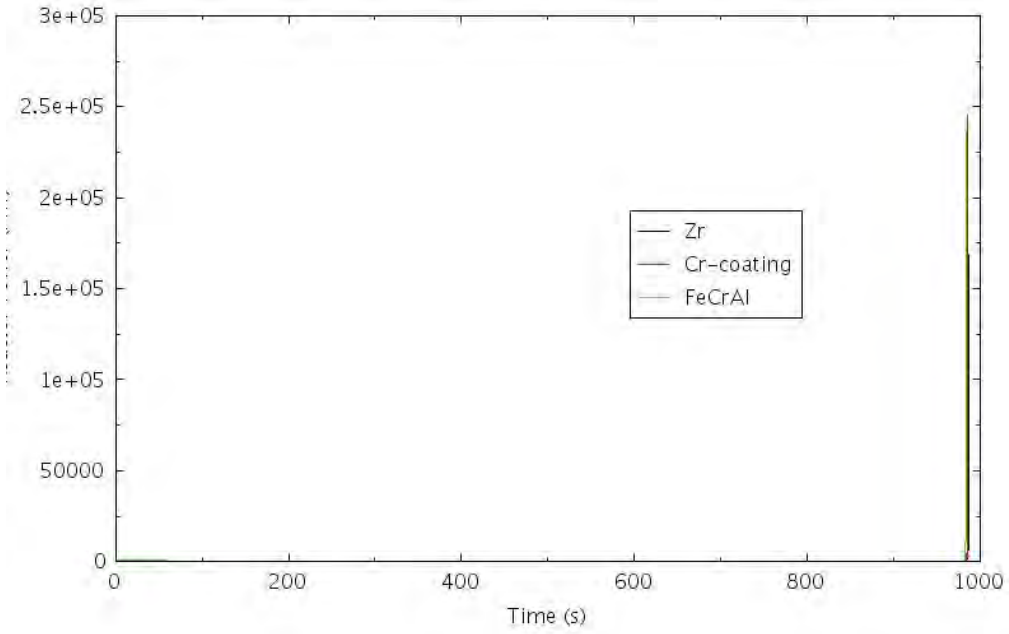

Figure 5-45. Reactor Power for LOMFW-ATWS-3.

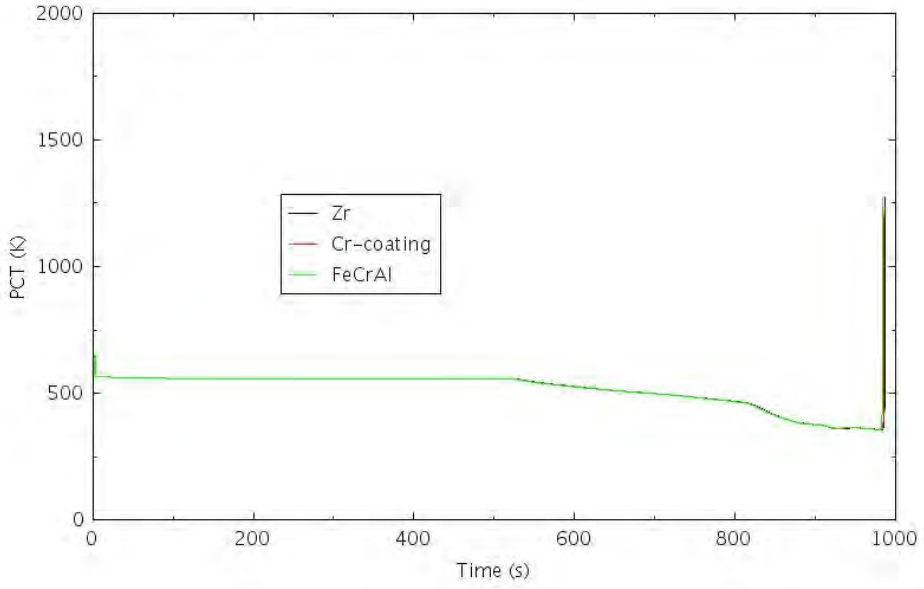

Figure 5-46. PCT for LOMFW-ATWS-3.

5.3 Summary of BWR LOMFW Analyses

5.3.1 Results for LOMFW with Scram

For completeness, this section presents the summary of the coping time gain and the reduction of hydrogen production for LOMFWS-4 scenario as well as the eight scenarios that have been analyzed in general transients.

Table 5-6 compares the times to CD for ATF designs (FeCrAl and Cr-coated claddings) with those for existing Zircaloy-clad designs in different general transient scenarios with reactor scram. Other than LOMFW-4, the results for the other eight scenarios were obtained from the calculations performed from the general transients. The table shows the gain of coping time, or the delay of time to CD, is less than or equal to 30 minutes for most scenarios. For FeCrAl, a gain of coping time ranges from 9 to 35 minutes. For Cr-coated cladding, a gain of coping time ranges from 5 to 22 minutes. With only a marginal increase of the time to core damage with FeCrAl and Cr-coated against the conventional Zry-cladding design based on the RELAP5-3D simulation results, the risk-benefit on behalf of CDF as the risk metric would be very small and it is not quantified.

However, the RELAP5-3D simulation results show the clear benefit in adopting ATF due to much less hydrogen produced at the time of CD. Table 5-7 compares the hydrogen production for ATF designs (FeCrAl and Cr-coated claddings) with that for existing Zircaloy-clad design in different general transient scenarios. The table shows the hydrogen production can be a few times lower for the Cr-coated cladding and up to two orders of magnitude lower for FeCrAl cladding than that with Zircaloy cladding cases.

Table 5-6. Comparison of Time to CD with ATF Designs for LOMFW with Reactor Scram.

Scenario	Scenario Description	Time to CD t_{CD} (hh:mm)					
		Zry	Cr-coated	Δt	Zry	FeCrAl	Δt
LOMFW-1	LOMFW IE, Reactor scram, no HPI, no DEP	1:07	1:12	0:05	1:07	1:17	0:10
LOMFW-2	LOMFW IE, Reactor scram, AC, HPI, DEP, Control Rod Drive Injection, no Containment HR	10:02	10:13	0:11	10:02	10:27	0:25
LOMFW-3	Reactor trip, AC, HPI, no DEP	8:01	8:14	0:13	8:01	8:28	0:27
LOMFW-4	LOMFW IE, Reactor scram, AC, no HPI, DEP, CS, no Containment HR	16:08	16:30	0:22	16:08	16:32	0:24
LOMFW-SORV-1	LOMFW IE, Reactor scram, AC, 1 SRV Open, no HPI, no DEP	0:57	1:02	0:05	0:57	1:06	0:09
LOMFW-SORV-2	LOMFW IE, Reactor scram, 1 SRV Open, DEP, CS, no Containment HR	13:46	14:05	0:19	13:46	14:21	0:35
LOMFW-SORV-3	LOMFW IE, Reactor scram, 1 SRV Open, no DEP, no LPCI	8:14	8:19	0:05	8:14	8:28	0:14
LOMFW-SORV-4	LOMFW IE, Reactor scram, AC, 2 SRVs Open, DEP, CS, no Containment HR	13:42	13:53	0:11	13:42	14:13	0:31
LOMFW-LOOP-1	LOMFW IE, Reactor scram, LOOP, AC, HPI, DEP, LPCI, no Containment HR	18:44	19:02	0:18	18:44	19:14	0:30

Table 5-7. Comparison of H_2 Productions with ATF Designs for LOMFW with Reactor Scram.

Scenario	Scenario Description	Total H_2 (kg)			H_2 %	
		Zry	Cr-coated	FeCrAl	Cr-coated	FeCrAl
LOMFW-1	LOMFW IE, Reactor scram, no HPI, no DEP	21.2	5.6	0.4	26.6	1.9
LOMFW-2	LOMFW IE, Reactor scram, AC, HPI, DEP, Control Rod Drive Injection, no Containment HR	13.6	2.6	0.2	18.8	1.2
LOMFW-3	Reactor trip, AC, HPI, no DEP	31.2	6.0	0.6	19.4	1.9
LOMFW-4	LOMFW IE, Reactor scram, AC, no HPI, DEP, CS, no Containment HR	20.6	5.3	0.4	25.8	1.8
LOMFW-SORV-1	LOMFW IE, Reactor scram, AC, 1 SRV Open, no HPI, no DEP	51.1	5.4	0.5	10.5	1.0
LOMFW-SORV-2	LOMFW IE, Reactor scram, 1 SRV Open, DEP, CS, no Containment HR	20.4	5.2	0.3	25.3	1.7
LOMFW-SORV-3	LOMFW IE, Reactor scram, 1 SRV Open, no DEP, no LPCI	12.2	3.3	0.2	27.3	1.5
LOMFW-SORV-4	LOMFW IE, Reactor scram, AC, 2 SRVs Open, DEP, CS, no Containment HR	18.2	11.2	0.3	61.6	1.8
LOMFW-LOOP-1	LOMFW IE, Reactor scram, LOOP, AC, HPI, DEP, LPCI, no Containment HR	21.2	5.6	0.4	26.6	1.9

5.3.2 Results for LOMFW-Initiated ATWS

Table 5-8 compares the times to CD for ATF designs (FeCrAl and Cr-coated claddings) with those for existing Zircaloy-clad designs in three LOMFW-initiated ATWS scenarios. The table shows the gain of coping time, or the delay of time to CD, is less than 10 minutes for all the scenarios. For FeCrAl, a gain of coping time is about 10 minutes for LOMFW-ATWS-1, 7 minutes for LOMFW-ATWS-2, and no gain for LOMFW-ATWS-3. For Cr-coated cladding, a gain of coping time is about 5 minutes for LOMFW-ATWS-1, 3 minutes for LOMFW-ATWS-2, and no gain for LOMFW-ATWS-3. With only a marginal increase of the time to core damage with FeCrAl and Cr-coated against the conventional Zry-cladding design based on the RELAP5-3D simulation results, the risk-benefit on behalf of CDF as the risk metric would be very small and it is not quantified.

However, the RELAP5-3D simulation results show the clear benefit in adopting ATF due to much less hydrogen produced at the time of CD. Table 5-9 compares the hydrogen production for ATF designs (FeCrAl and Cr-coated claddings) with that for existing Zircaloy-clad designs in the three LOMFW-initiated ATWS scenarios. The table shows the hydrogen production can be a few times lower for the Cr-coated cladding, and up to two orders of magnitude lower for FeCrAl cladding than that with Zircaloy cladding cases.

Table 5-8. Time to CD Comparison for LOMFW-ATWS Scenarios with ATF Designs.

Scenario	Scenario Description	Time to CD t_{CD} (hh:mm)					
		Zry	Cr-coated	Δt	Zry	FeCrAl	Δt
LOMFW-ATWS-1	No trip, AC, SRVs Open, Recirc Pump Tripped, SLCS, No ADS, No DEP, No LPI	0:53	0:58	0:05	0:53	1:03	0:10
LOMFW-ATWS-2	No trip, AC, SRVs Open, Recirc Pump Tripped, No SLCS, No ADS, No DEP, No LPI	0:30	0:33	0:03	0:30	0:37	0:07
LOMFW-ATWS-3	No trip, AC, SRVs Open, Recirc Pump Tripped, SLCS, ADS, DEP, LPI	0:16	0:16	0:00	0:16	0:16	0:00

Table 5-9. Comparing H_2 Productions for LOMFW-ATWS Scenarios with ATF Designs.

Scenario	Scenario Description	Total H_2 (kg)			H_2 %	
		Zry	Cr-coated	FeCrAl	Cr-coated	FeCrAl
LOMFW-ATWS-1	No trip, AC, SRVs Open, Recirc Pump Tripped, SLCS, No ADS, No DEP, No LPI	22.4	3.8	0.3	16.9	1.2
LOMFW-ATWS-2	No trip, AC, SRVs Open, Recirc Pump Tripped, No SLCS, No ADS, No DEP, No LPI	18.5	2.7	0.2	14.7	1.0
LOMFW-ATWS-3[a]	No trip, AC, SRVs Open, Recirc Pump Tripped, SLCS, ADS, DEP, LPI	1.0E-02	2.9E-07	2.3E-08	0.0	0.0

a. Due to convergence issues, simulations stopped when peak PCT reaches 1275 K for LOMFW-ATWS-3. Additionally, the PCT reaches the limit almost instantaneously due to the power spike and the short time duration results in very small hydrogen production.

6. RISK-INFORMED ATF ANALYSIS OF BWR SMALL LOSS-OF-COOLANT ACCIDENT SCENARIOS

The risk-informed analysis of near-term ATF designs for BWR SLOCA scenarios is presented in this section. The BWR SLOCA SAPHIRE model and scenarios are presented in Section 6.1. The RELAP5-3D analyses of ATF designs for the SLOCA scenarios are presented in Section 6.2. The analysis results are summarized in Section 0.

6.1 BWR SLOCA SAPHIRE Model and Scenarios

The generic BWR SLOCA SAPHIRE model starts with the occurrence of SLOCA. The model includes a main event tree SLOCA and a transfer tree ATWS. The structure of the SLOCA event tree is provided in Figure

6-1. The transfer tree ATWS is the same as the one transferred from the TRANS main event tree and thus not provided again in this section.

The ETs were quantified with SAPHIRE 8 using a truncation level of 1E-12 per reactor year. There are 41 CD sequences with a total SLOCA CDF of 5.54E-08 per reactor year. Among the 41 CD sequences, 8 sequences have non-zero (or non-truncated) CDF; 3 sequences have greater-than-0.1% contribution to total LOMFW CDF with a sum of 99.9 % of total SLOCA CDF. The three sequences are shown in Table 6-1 and selected for RELAP5-3D analysis with short descriptions provided in Table 6-2 and detailed mitigating system statuses provided in Table 6-3.

Table 6-1. BWR SLOCA Sequences with Greater-Than-0.1% CDF Contribution.

No.	BWR SLOCA Sequence	CDF	RELAP5 Scenario
1	SLOCA:32	5.44E-08	SLOCA-1
2	SLOCA:09	8.55E-10	SLOCA-2
3	SLOCA:16	1.24E-10	SLOCA-3

Table 6-2. BWR SLOCA Scenarios Developed for RELAP5-3D Analysis.

No.	RELAP5 Scenario	Scenario Description
1	SLOCA-1	SLOCA, RCS inventory control failed (no HPI or DEP)
2	SLOCA-2	SLOCA, containment heat removal failed (using HPI for RCS inventory control)
3	SLOCA-3	SLOCA, containment heat removal failed (using DEP + condensate system for RCS inventory control)

- **SLOCA-1:** An SLOCA IE occurs, and reactor automatically shuts down. HPI fails to maintain RCS inventory. Neither does DEP succeed to allow low-pressure coolant injection. CD occurs.
- **SLOCA-2:** An SLOCA IE occurs, and reactor automatically shuts down. HPI succeeds to meet the need of short-term RCS inventory control.CD still occurs due to failure of decay heat removal.
- **SLOCA-3:** An SLOCA IE occurs, and reactor automatically shuts down. Although HPI fails, RCS inventory is maintained through DEP plus condensate system injection. CD still occurs due to failure of decay heat removal.

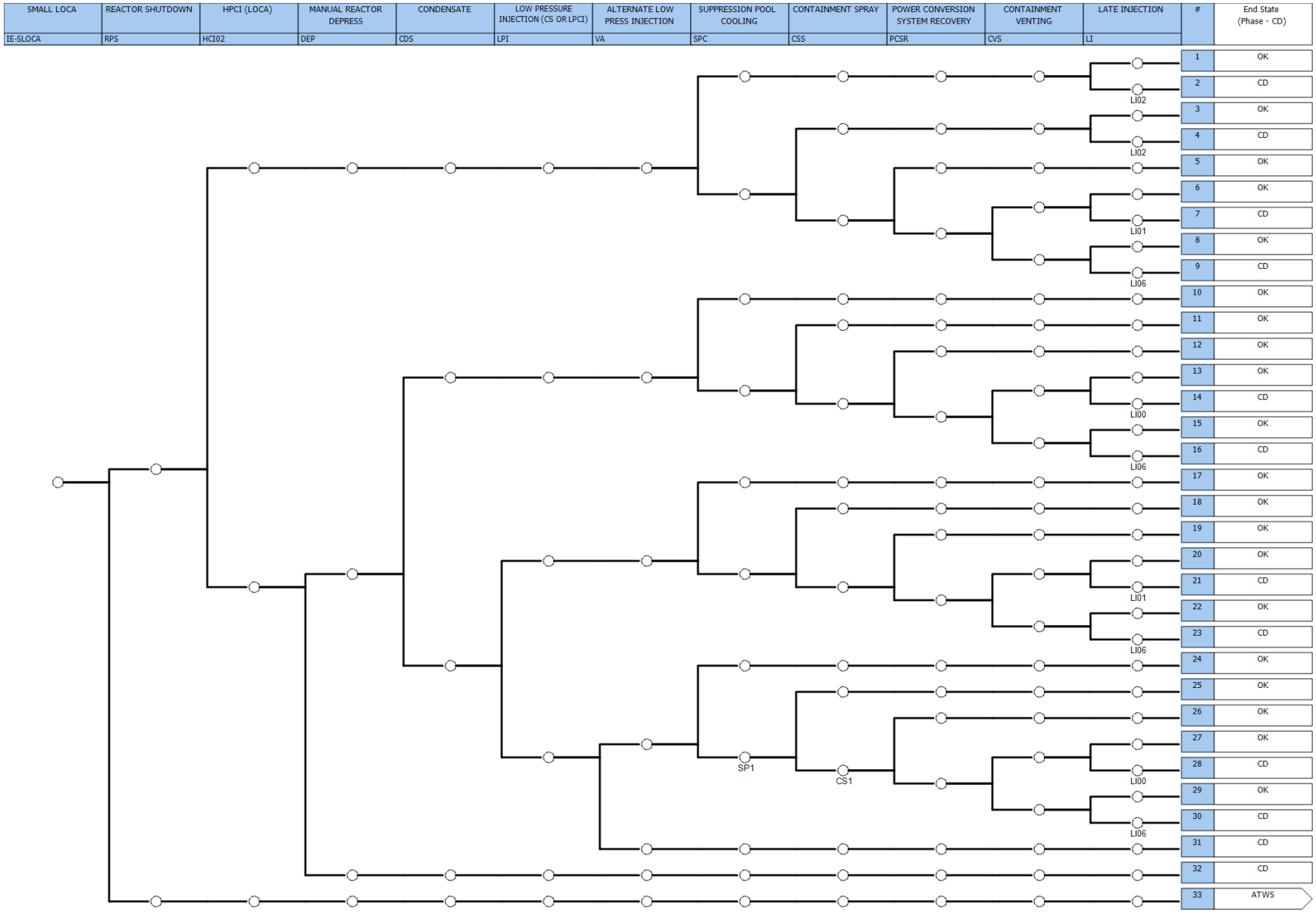

Figure 6-1. Generic BWR SLOCA Event Tree.

Table 6-3. BWR SLOCA Scenarios for RELAP-5 3D Analysis: Mitigating System Statuses.

RELAP5 SLOCA Scenario	SLOCA Main Event Tree								
#	Rx	HPCI Success	DEP Success	Condensate System Success	SPC Success	Containment Spray Success	PCS Recovery	Containment Venting Success	Late Injection Success
SLOCA-1	Trip	No	No						
SLOCA-2	Trip	Yes			No	No	No	No	No
SLOCA-3	Trip	No	Yes	Yes	No	No	No	No	No

6.2 BWR SLOCA RELAP5-3D Analysis

Previous studies on BWR LOCA from open literatures indicate the most limiting LOCA case of a BWR/4 reactor is a break on the recirculation suction line. In this study, it is assumed the break happens on the recirculation suction line between the RPV and the recirculation pump. The break size is assumed to be 1 inch in diameter with the break area of 0.005454 ft^2 which represents about 0.14% of the area of the recirculation suction line. This break size falls within the conventional definition of a small break size of less than 0.1 ft^2. A BWR/4 plant has two recirculation loops. However, the generic RELAP5-3D plant model lumped the two recirculation loops into one. In order to provide more realistic simulation of small LOCA behaviors in a BWR/4, the generic RELAP5-3D plant model has been expanded to include two recirculation loops. It is assumed the break only happens at one of the recirculation loops while the other loop stays intact.

The reactor is successfully scrammed ensuing the initiation of small LOCA. The reactor scram can be triggered by the signals from high-DW pressure, low reactor water level, high vessel pressure, or high flux, etc. For LOCA, the high-DW pressure or low-water level are the most important. The scram signal of the DW high pressure is found to be activated earlier than the other scram signals.

6.2.1 SLOCA-1

In this scenario, the reactor power is shut down after a small LOCA happens. The vapor suppression is successful to ensure the integrity of the containment DW. It is further assumed HPCI fails to provide water injection to the RPV and manual depressurization of RPV fails such that LPCI systems are not able to provide water injection to the RPV. As the result, with absence of makeup water to the RPV after the initiation of small LOCA, the coolant inventory will boil off due to the decay heat and eventually lead to fuel damage.

Figure 6-2 shows the mass flow rate at the break for the duration of the transient. Figure 6-3 shows the RPV downcomer collapsed water level. Figure 6-4 shows the RPV dome pressure. Since the break size is quite small, the reactor system pressure is kept high and within the range of the operating pressure with the cycling of the SRVs. Figure 6-5 shows the mass flow rate through the SRVs. Figure 6-6 shows the comparison of PCTs for the Zircaloy fuel versus ATF with Cr-coated and FeCrAl cladding.

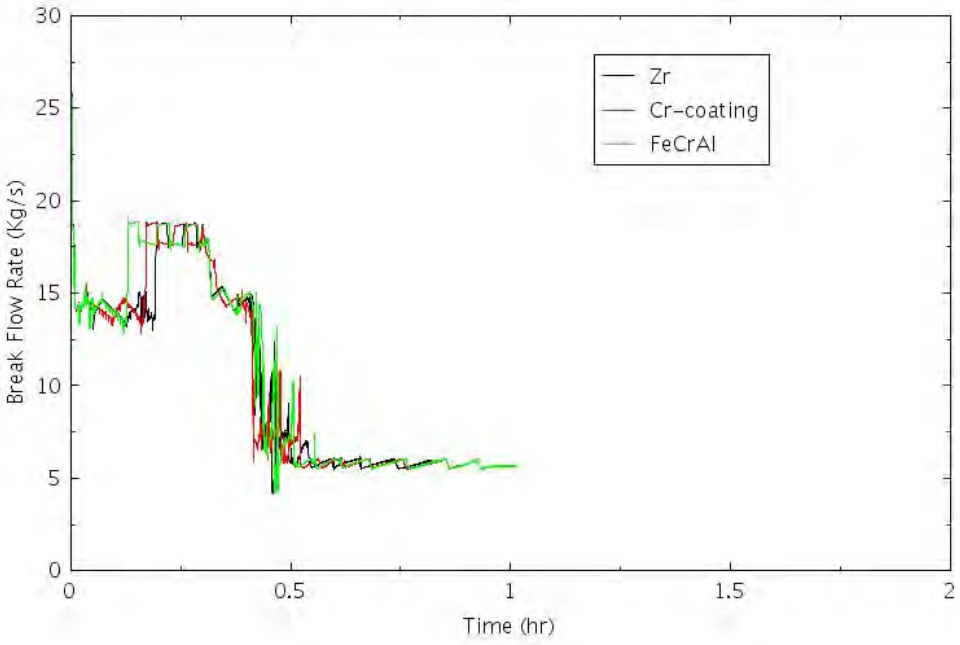

Figure 6-2. Break Flow Rate for SLOCA-1.

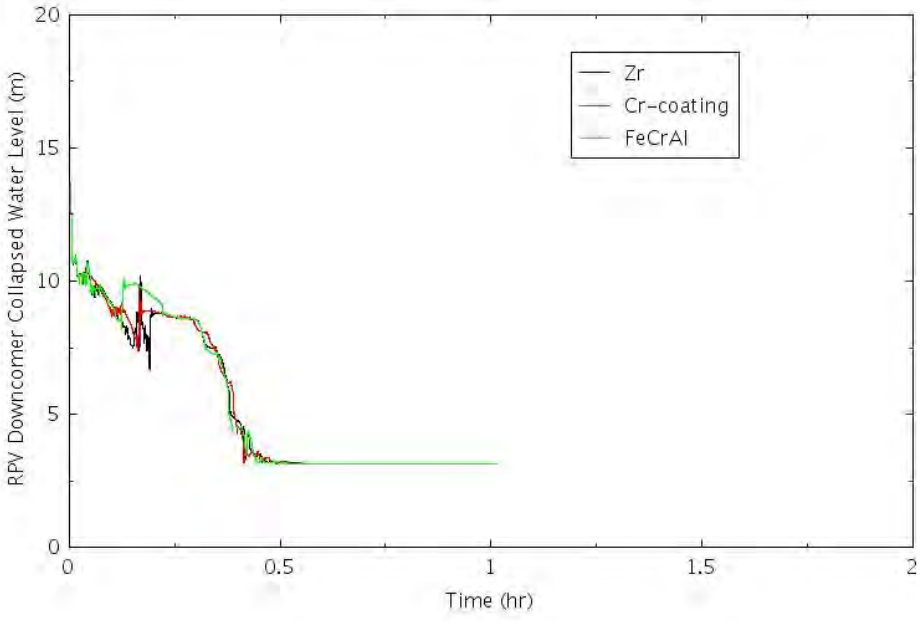

Figure 6-3. RPV Downcomer Collapsed Water Level for SLOCA-1.

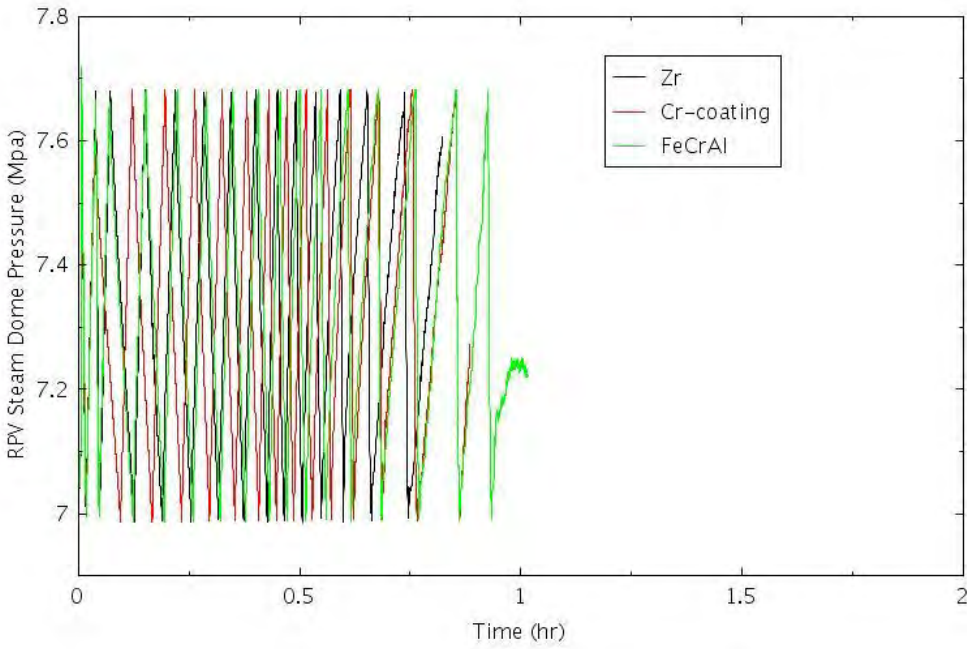

Figure 6-4. RPV Dome Pressure for SLOCA-1.

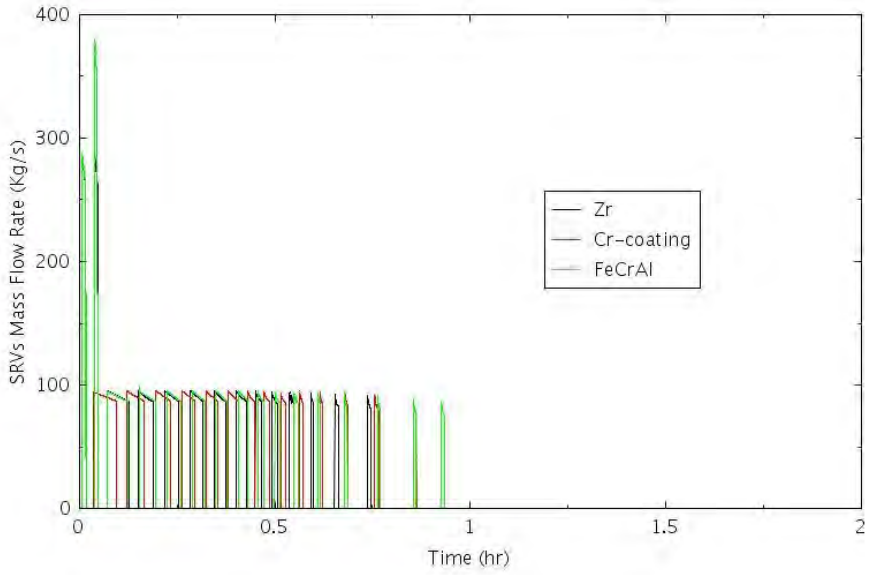

Figure 6-5. SRV Mass Flow Rate for SLOCA-1.

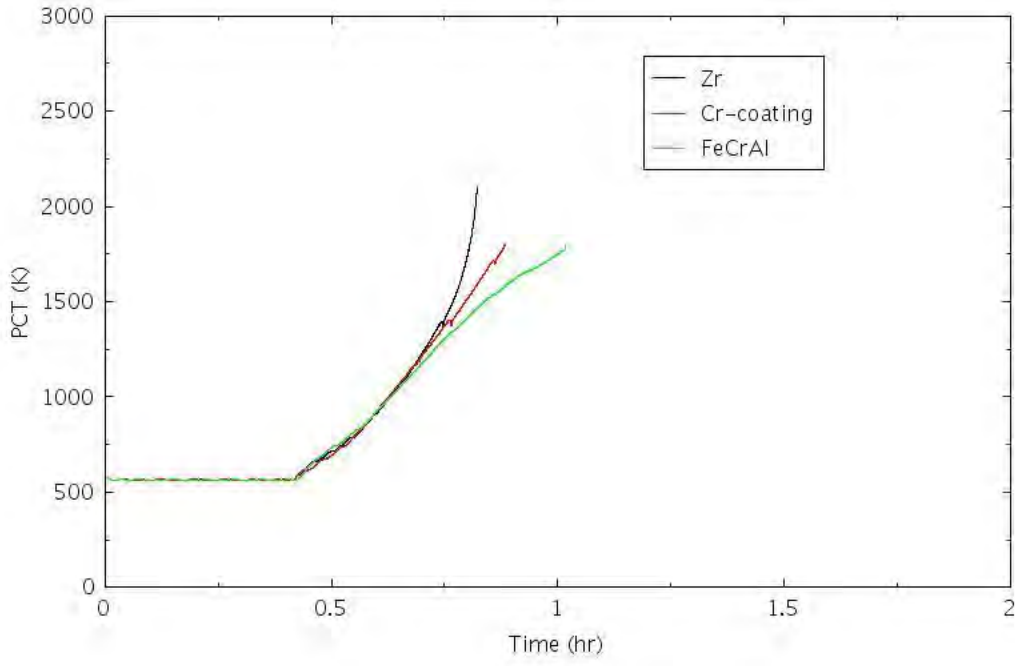

Figure 6-6. PCT Comparison for SLOCA-1.

6.2.2 SLOCA-2

In this scenario, the reactor power is shut down after a small LOCA happens. The vapor suppression is successful to ensure the integrity of the containment DW. The HPI systems are able to provide water injection to the RPV. However, the SP is not cooled due to the failure of the decay heat removal system. It is assumed the HPI systems would stop injecting water into the RPV when the SP temperature reaches 361 K (190°F). It is further assumed the RPV is not depressurized such that low-pressure injection systems are not able to provide water injection to the RPV. As the result, with absence of makeup water to the RPV after the initiation of small LOCA, the coolant inventory will boil off due to the decay heat and eventually lead to fuel damage.

Figure 6-7 shows the mass flow rate at the break for the duration of the transient. Figure 6-8 shows the HPI mass flow rate. The HPI systems stop when the SP temperature reaches 361 K (190°F), as shown in Figure 6-9. After the HPI systems stop injecting water into the RPV, there is no makeup water into the RPV. With the inventory loss through the break as shown in Figure 6-7 as well as the flow through SRVs as shown in Figure 6-10, the coolant in the core boils off. Figure 6-11 shows the RPV downcomer collapsed water level. Figure 6-12 shows the RPV dome pressure. Figure 6-13 shows the comparison of PCTs for the Zircaloy fuel versus ATF with Cr-coated cladding and FeCrAl cladding.

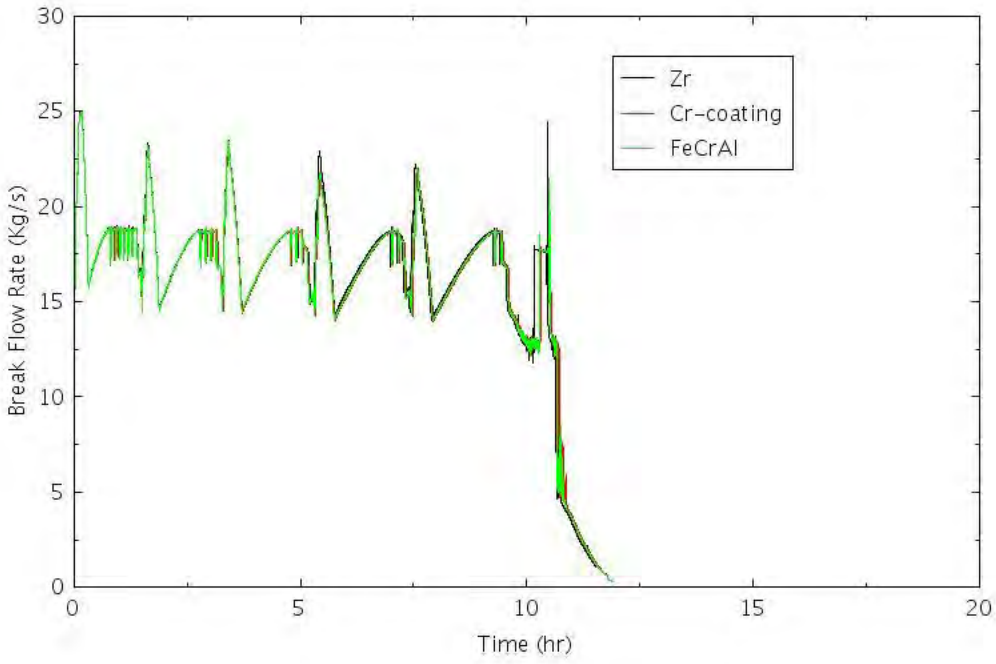

Figure 6-7. Break Area Mass Flow Rate for SLOCA-2.

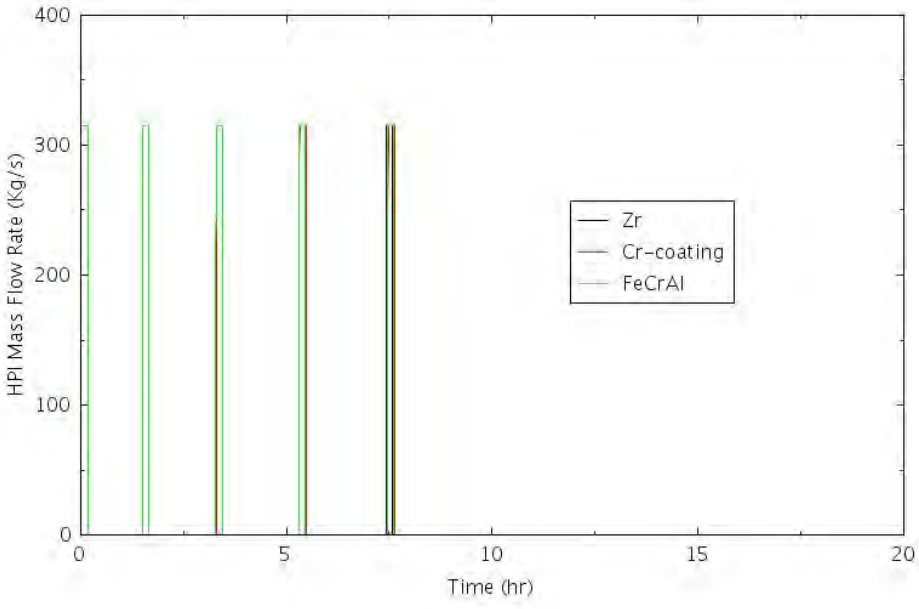

Figure 6-8. HPI Mass Flow Rate for SLOCA-2.

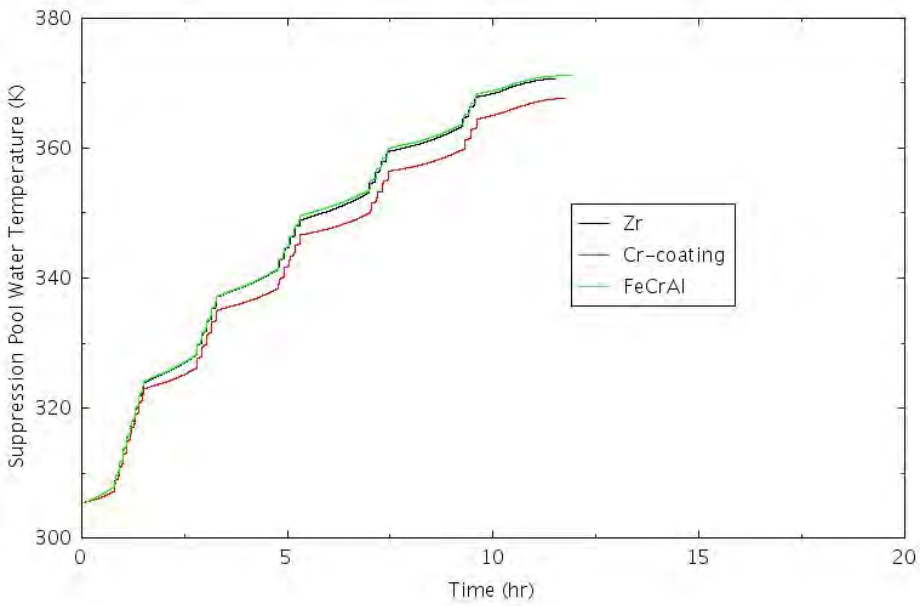

Figure 6-9. SP Water Temperature for SLOCA-2.

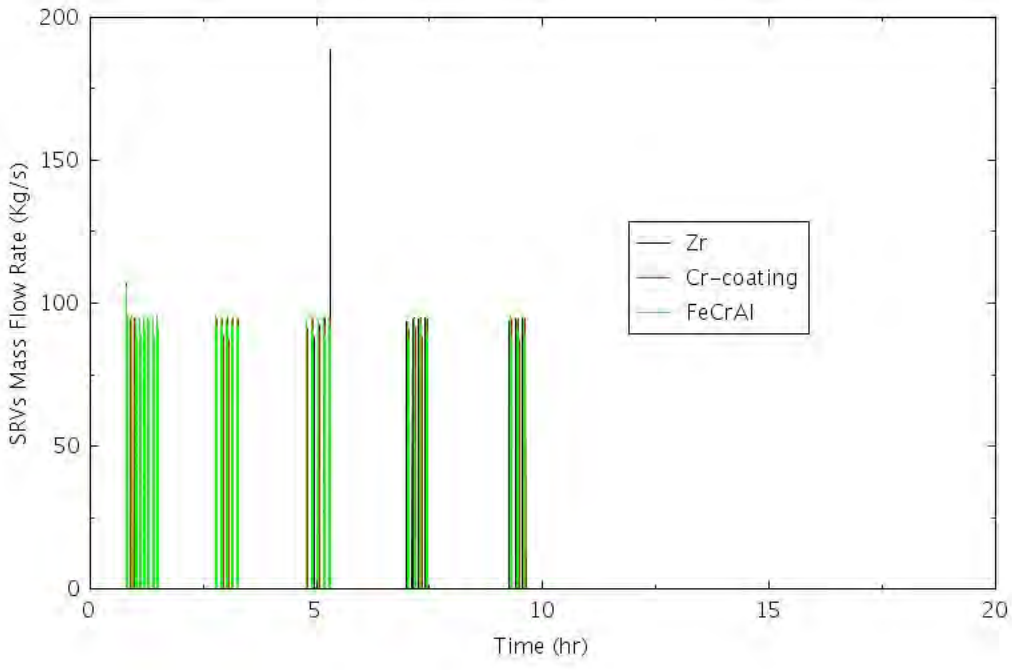

Figure 6-10. SRV Mass Flow Rate for SBLOCA-2.

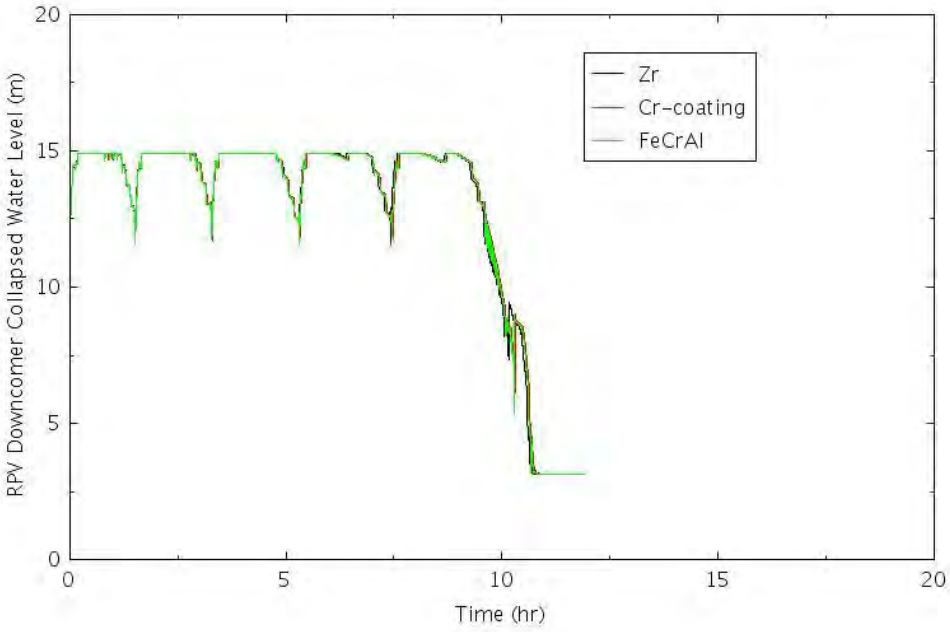

Figure 6-11. RPV Downcomer Collapsed Water Level for SLOCA-2.

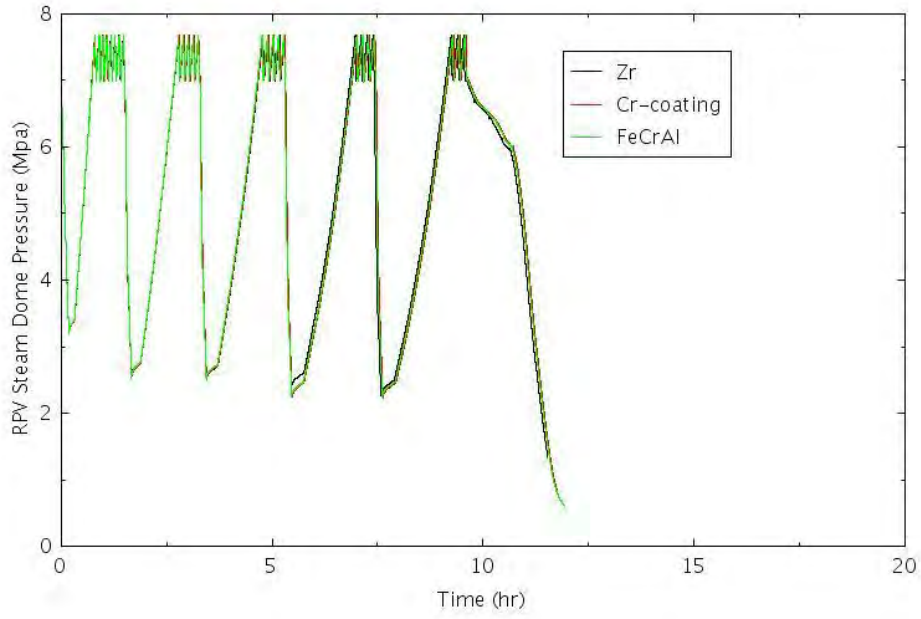

Figure 6-12. RPV Dome Pressure for SLOCA-2.

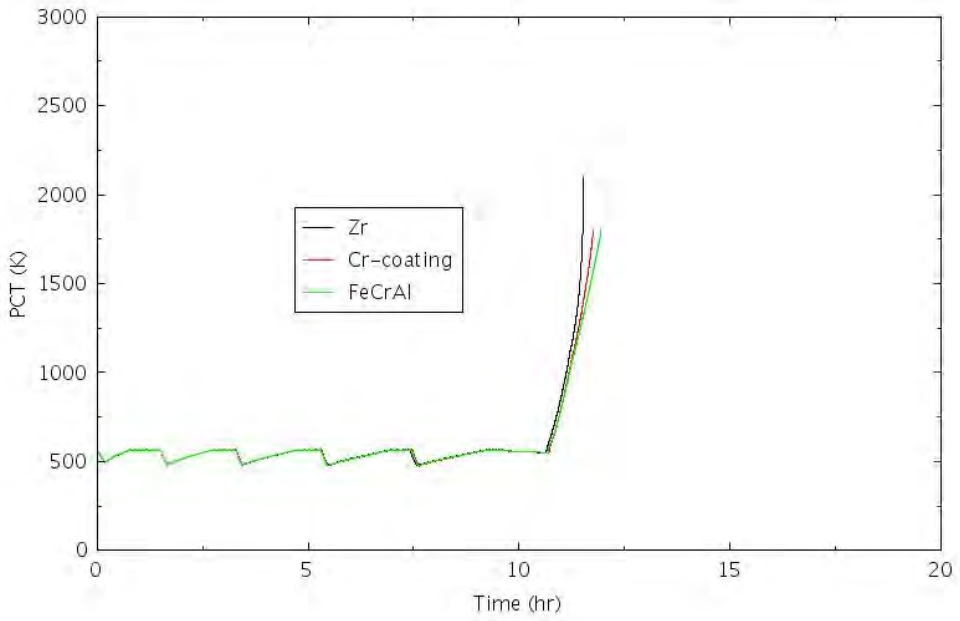

Figure 6-13. PCT Comparison for SLOCA-2.

6.2.3 SLOCA-3

In this scenario, the reactor power is shut down after a small LOCA happens. The vapor suppression is successful to ensure the integrity of the containment DW. It is assumed the HPI systems fail to provide water injection to the RPV. It is further assumed the RPV is depressurized to allow the low-pressure injection systems to actuate. However, the SP is not cooled due to the failure of the decay heat removal system. The RELAP5-3D simulations for this scenario failed to converge. The RELAP5-3D runs will be investigated in the future to find out the root causes. Since the CDF contribution from this scenario is much smaller than that from SLOCA-1 and SLOCA-2, omitting this scenario from the PRA analysis would have a minimal impact on the plant total CDF.

6.3 Summary of BWR SLOCA Analyses

Table 3 compares the times to CD for ATF designs (FeCrAl and Cr-coated claddings) with those for existing Zircaloy-clad design in the two SLOCA scenarios. The table shows the gain of coping time, or the delay of time to CD, is less than 24 minutes for all scenarios. For FeCrAl, a gain of coping time of 12 minutes and 24 minutes for SLOCA-1 and SLOCA-2, respectively. Cr-coated cladding had a gain of coping time of 4 minutes and 13 minutes for SLOCA-1 and SLOCA-2, respectively. With only a marginal increase of the time to core damage with FeCrAl and Cr-coated against the conventional Zry-cladding design based on the RELAP5-3D simulation results, the risk-benefit on behalf of CDF as the risk metric would be very small and it is not quantified.

Similar to the results obtained from the analyses performed for other scenarios, the RELAP5-3D simulation results show the clear benefit in adopting ATF due to much less hydrogen produced at the time of CD. Table 4 compares the hydrogen production for ATF designs (FeCrAl and Cr-coated claddings) with that for existing Zircaloy-clad design in the two SLOCA scenarios. The table shows the hydrogen production can be a few times lower for the Cr-coated cladding and up to two orders of magnitude lower for FeCrAl cladding than that with Zircaloy cladding cases.

Table 6-4. Time to CD Comparison for SLOCA Scenarios with ATF Designs.

Scenario	Scenario Description	Time to CD t_{CD} (hh:mm)					
		Zry	Cr-coated	Δt	Zry	FeCrAl	Δt
SLOCA-1	SLOCA IE, Reactor scram, no HPI, no DEP	0:49	0:53	0:04	0:49	1:01	0:12
SLOCA-2	SLOCA IE, Reactor scram, AC, HPI, no DEP, no LPI, no Containment HR	11:32	11:45	0:13	11:32	11:56	0:24

Table 6-5. Comparison of H_2 Productions for SLOCA Scenarios with ATF Designs.

Scenario	Scenario Description	Total H_2 (kg)			H_2 %	
		Zry	Cr-coated	FeCrAl	Cr-coated	FeCrAl
SLOCA-1	SLOCA IE, Reactor scram, no HPI, no DEP	29.5	6.9	0.6	23.4	2.1
SLOCA-2	SLOCA IE, Reactor scram, AC, HPI, no DEP, no LPI, no Containment HR	43.5	6.0	0.8	13.8	1.8

7. RISK-INFORMED ATF ANALYSIS OF BWR INADVERTENT OPEN RELIEF VALVE SCENARIOS

The risk-informed analysis of the near-term ATF designs for BWR IORV scenarios is presented in this section. The BWR IORV SAPHIRE model and scenarios are presented in Section 7.1. The RELAP5-3D analyses of ATF designs for the IORV scenarios are presented in Section 7.2. The analysis results are summarized in Section 7.3.

7.1 BWR IORV SAPHIRE Model and Scenarios

The generic BWR IORV accident SAPHIRE model starts with the occurrence of IORV. The model includes a main event tree, IORV, and two transfer trees, LOOP and ATWS. The structure of the IORV main event tree is shown in Figure 7-1. The structures of the transfer trees LOOP and ATWS are the same as those transferred from the TRANS main event tree and thus are not provided again in this section.

The ETs were quantified with SAPHIRE 8 using a truncation level of 1E-12 per reactor year. There are 47 CD sequences with a total IORV CDF of 2.06E-08 per reactor year. Among the 47 CD sequences, 16 sequences have non-zero (or non-truncated) CDF; nine sequences have greater-than-0.1% contribution to total IORV CDF with a sum of 99.7 % of total IORV CDF. The nine sequences are shown in Table 7-1.

Considering IORV CDF is very low, three representative sequences are selected for RELAP5-3D analysis, including sequences IORV:45 (the most risk-significant and the most limiting), IORV:25 (no manual depressurization to allow continued inventory control), and IORV:17 (no long-term cooling). Although not risk significant (i.e., contributing greater than 0.1% to total IORV CDF), one sequence (IORV: 44, with low-pressure injection failure) is added for RELAP5-3D analysis based on Jensen Hugh's recommendation. Hence, a total of four IORV scenarios are selected for RELAP5-3D analysis with short descriptions in Table 7-2 and detailed information of mitigating system statuses in Table 7-3.

Table 7-1. BWR IORV Sequences with Greater-Than-0.1% CDF Contribution.

No.	BWR IORV Sequence	CDF	RELAP5 Scenario
1	IORV:45	6.81E-09	IORV-1
2	IORV:11	6.65E-09	n/a
3	IORV:25	4.86E-09	IORV-2
4	IORV:17	1.14E-09	IORV-3
5	IORV:47-05	5.72E-10	n/a
6	IORV:48	1.63E-10	n/a
7	IORV:47-10	1.56E-10	n/a
8	IORV:31	1.43E-10	n/a
9	IORV:47-02-07	7.69E-11	n/a

Table 7-2. BWR IORV Scenarios Developed for RELAP5-3D Analysis.

No.	RELAP5 Scenario	Scenario Description
1	IORV-1	IORV, RCS inventory control failed (no HPI or DEP)
2	IORV-2	IORV, RCS inventory control failed (no DEP)
3	IORV-3	IORV, containment heat removal failed
4	IORV-4[a]	IORV, RCS inventory control failed (no LPI)
a. Scenario IORV-4 corresponds to sequence IORV:44.		

- **IORV-1:** An IORV IE occurs, reactor automatically shuts down, AC power is available, but PCS fails. HPI fails to maintain RCS inventory. Neither does DEP succeed to allow LPI. CD occurs.
- **IORV-2:** An IORV IE occurs, reactor automatically shuts down, AC power is available, but PCS fails. HPI initially succeeds to maintain RCS inventory but finally fails from inadequate lube oil cooling as a result of pump suction from overheated SP. Neither does DEP succeed to allow LPI. CD occurs.
- **IORV-3:** An IORV IE occurs, reactor automatically shuts down, AC power is available, but PCS fails. RCS inventory is successfully maintained, initially through HPI and later through DEP plus LPI. However, CD occurs due to failure of decay heat removal.
- **IORV-4:** An IORV IE occurs, reactor automatically shuts down, AC power is available, but PCS fails. HPI fails to maintain RCS inventory. DEP succeeds but LPI fails. CD occurs.

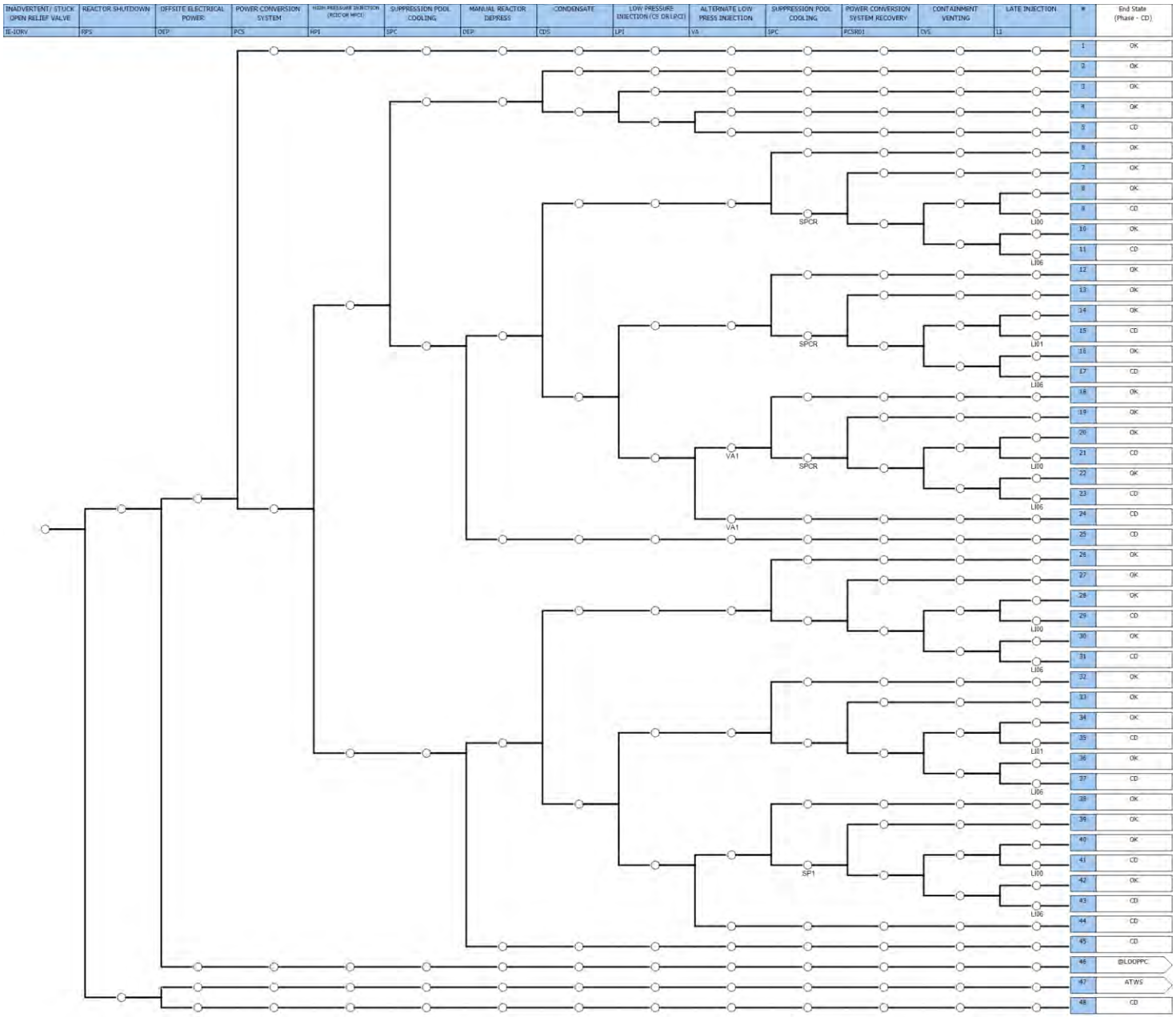

Figure 7-1. Generic BWR IORV Event Tree.

Table 7-3. BWR IORV Scenarios for RELAP-5 3D Analysis: Mitigating System Statuses.

RELAP5 IORV Scenario	IORV Main Event Tree											
#	Rx	AC Power Available	PCS Success	HPI Success	SPC Success	DEP Success	Condensate System Success	LPI Success	SPC Recovery	PCS Recovery	Containment Venting Success	Late Injection Success
IORV-1	Trip	Yes	No	No		No						
IORV-2	Trip	Yes	No	Yes	No	No						
IORV-3	Trip	Yes	No	Yes	No	Yes	No	Yes	No	No	No	No
IORV-4	Trip	Yes	No	No		Yes	No	No				

7.2 BWR IORV RELAP5-3D Analysis

7.2.1 IORV-1

The IORV-1 scenario is the same as TRANS-SORV-1 in the BWR general transient scenarios. Therefore, the results obtained from the RELAP5-3D calculations for TRANS-SORV-1 are used for the IORV-1 scenario.

7.2.2 IORV-2

The IORV-2 scenario is the same as TRANS-SORV-3 in the BWR general transient scenarios, and the results obtained from the RELAP5-3D calculations for TRANS-SORV-3 are used for the IORV-2 scenario.

7.2.3 IORV-3

The IORV-3 scenario is the same as TRANS-SORV-2 in the BWR general transient scenarios, and the results obtained from the RELAP5-3D calculations for TRANS-SORV-2 are used for the IORV-3 scenario.

7.2.4 IORV-4

In this scenario, it is assumed an IORV IE causes the reactor to automatically shut down. AC power is available; however, the HPI systems fail to start. One SRV is stuck once it is opened due to the increase in system pressure after the initiation of the transient. As the result of one stuck-open SRV, the system pressure starts to decrease rapidly. The PCS failed so all steam is guided to the SP where it condenses. It is further assumed the ADS succeeds to actuate to further depressurize the RPV once the RPV downcomer water level reaches the Level 1 setpoint value. However, the LPI system fails to inject water to the RPV. With the absence of makeup water from either the HPI or LPI system, the coolant in the reactor core boils off rapidly and leads to CD in less than 1 hour. Figure 7-2 shows the RPV dome pressure, which indicates the system pressure decreases rapidly with the stuck-open SRV and the actuation of the ADS. Figure 7-3 shows the mass flow rate through the SRVs. Figure 7-4 shows the RPV downcomer water during the transient, and Figure 7-5 shows the PCT comparisons for the Zr cladding and the ATF claddings.

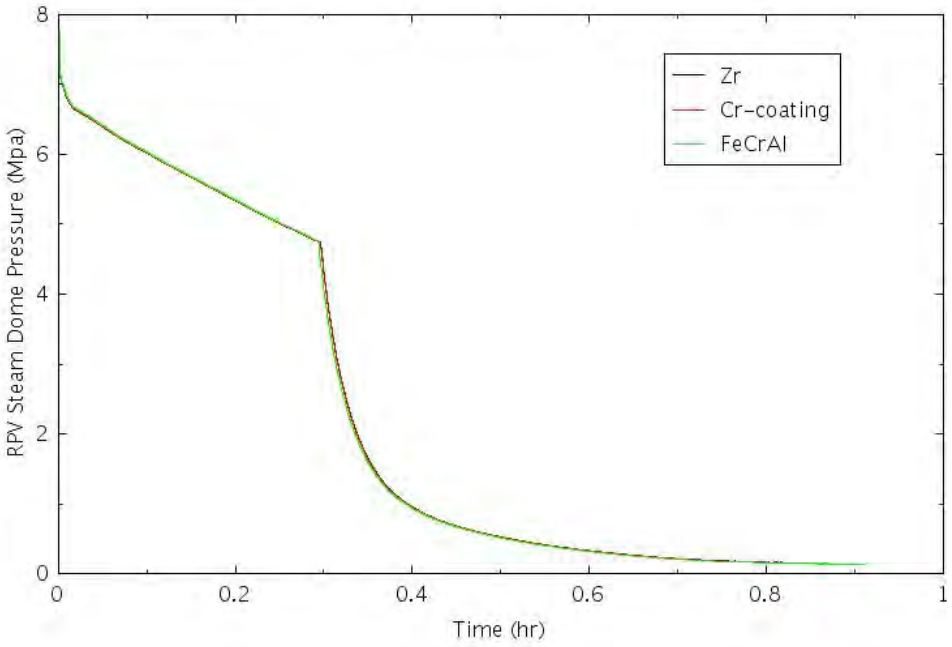

Figure 7-2. RPV Dome Pressure for IORV-4.

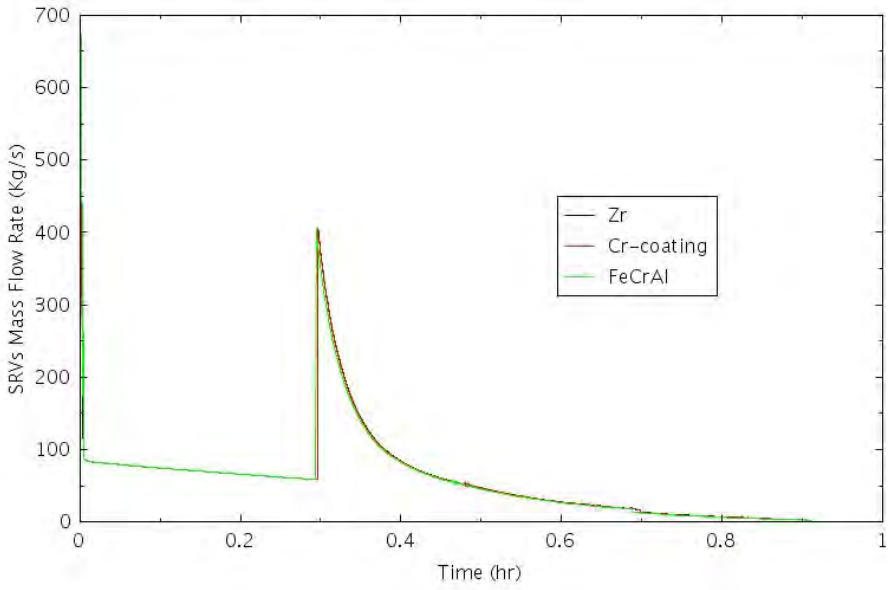

Figure 7-3. Mass Flow Rate through SRVs for IORV-4.

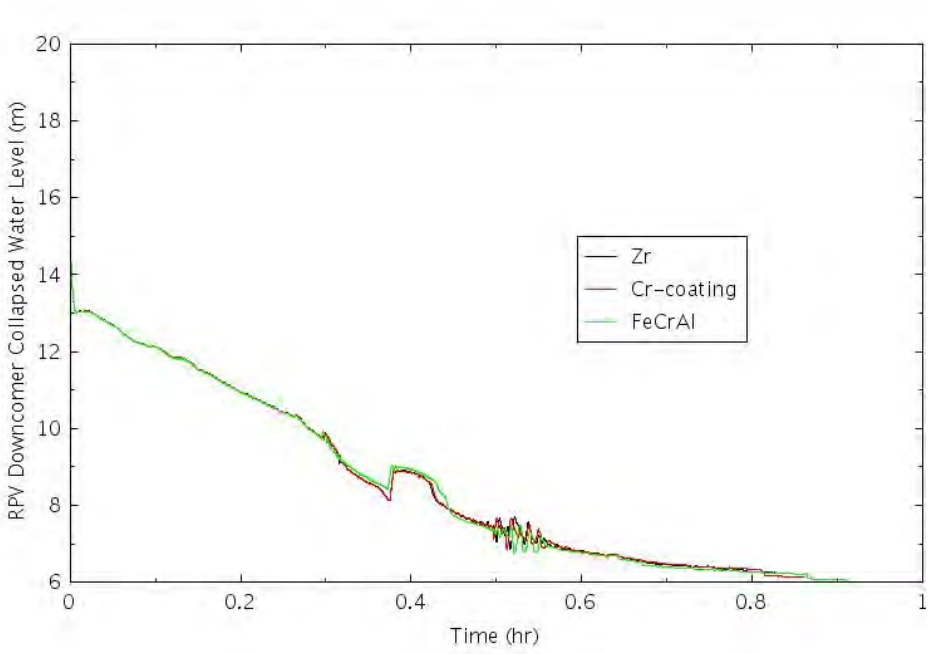

Figure 7-4. RPV Downcomer Collapsed Water Level for IORV-4.

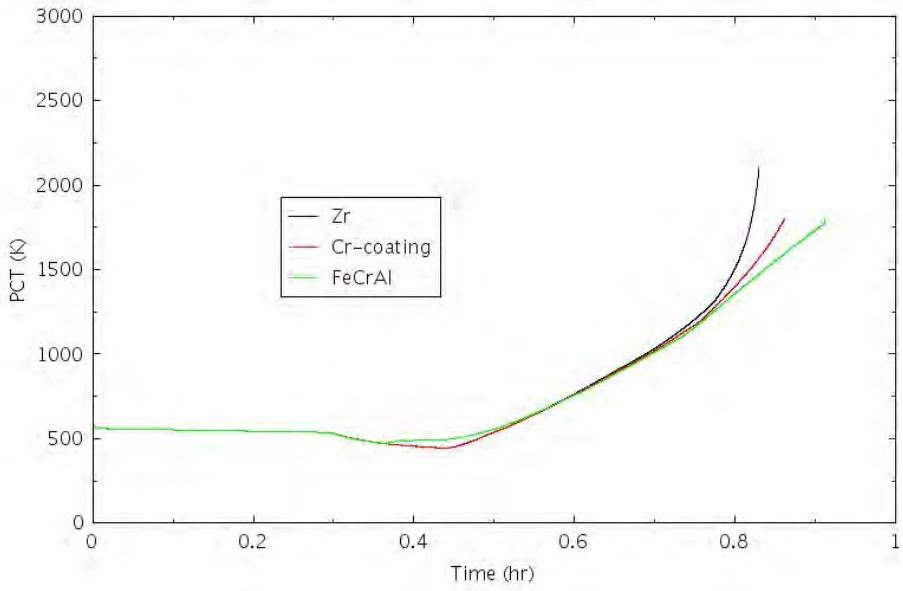

Figure 7-5. PCT Comparisons for IORV-4.

7.3 Summary of BWR IORV Analyses

Table 7-4 compares the times to CD for ATF designs (FeCrAl and Cr-coated claddings) with those for existing Zircaloy-clad design for general transient scenarios with reactor scram. The table shows the gain of coping time, or the delay of time to CD, ranges from 5 to 35 minutes for FeCrAl cladding and 2 to 19 minutes for Cr-coated cladding. With only a marginal increase of the time to core damage with FeCrAl and Cr-coated against the conventional Zircaloy cladding design based on the RELAP5-3D simulation results, the risk-benefit on behalf of CDF as the risk metric would be very small and it is not quantified.

However, the RELAP5-3D simulation results show the clear benefit in adopting ATF due to much less hydrogen produced at the time of CD. Table 7-5 compares the hydrogen production for ATF designs (FeCrAl and Cr-coated claddings) with that for existing Zircaloy-clad design in different IORV scenarios. The table shows the hydrogen production can be a few times lower for the Cr-coated cladding and up to two orders of magnitude lower for FeCrAl cladding than with Zircaloy cladding cases.

Table 7-4. Comparison of Time to CD with ATF Designs for IORV Accident.

Scenario	Scenario Description	Time to CD t_{CD} (hh:mm)					
		Zry	Cr-coated	Δt	Zry	FeCrAl	Δt
IORV-1	IORV, Reactor trip, AC, no HPI, no DEP	0:57	1:02	0:05	0:57	1:06	0:09
IORV-2	IORV, Reactor trip, AC, HPI, no DEP, no LPI	8:14	8:19	0:05	8:14	8:28	0:14
IORV-3	IORV, Reactor trip, AC, HPI, DEP, CS, no Containment HR	13:46	14:05	0:19	13:46	14:21	0:35
IORV-4	IORV, Reactor trip, AC, no HPI, DEP, no LPI	0:50	0:52	0:02	0:50	0:55	0:05

Table 7-5. Comparison of H_2 Productions with ATF Designs for IORV Accident.

Scenario	Scenario Description	Total H_2 (kg)			H_2 %	
		Zry	Cr-coated	FeCrAl	Cr-coated	FeCrAl
IORV-1	IORV, Reactor trip, AC, no HPI, no DEP	51.1	5.4	0.5	10.5	1.0
IORV-2	IORV, Reactor trip, AC, HPI, no DEP, no LPI	12.2	3.3	0.2	27.3	1.5
IORV-3	IORV, Reactor trip, AC, HPI, DEP, CS, no Containment HR	20.4	5.2	0.3	25.3	1.7
IORV-4	IORV, Reactor trip, AC, no HPI, DEP, no LPI	22.8	2.8	0.15	12.3	0.66

8. BENCHMARK STUDY BETWEEN GENERIC PWR SAPHIRE MODEL AND A REFERENCE PLANT PRA MODEL

This section summarizes the findings from comparing the accident sequences from the generic PWR SAPHIRE model and a reference plant PRA model. Both models were reviewed and compared by a third-party consulting company Jensen Hughes. The review areas are focused on top risk-contributing sequences (Section 8.1), event tree structures (Section 8.2), and assumptions (Section 8.3). These sections are written in a review-response format with the reviews provided by Jensen Hughes (denoted as "JH Review") and the responses provided by the INL (denoted as "INL Response.") The review conclusions are provided in Section 8.4.

8.1 Top Risk-Contributing Sequences

JH Review:

For the reference plant PRA model, any event sequence contributing more than 0.5% of CDF was reviewed in detail for this effort. Therefore, about 30 sequences were reviewed which represent over 93% of the reference plant CDF. Review of the sequences that had similar accident progression between the generic PWR model and the reference plant PRA model were found to reach the similar end state of CD. Therefore, it was concluded the basic logic and structure of the two models are similar, and the conclusions drawn regarding key sequences and their relative importance identified in the generic PWR model would adequately represent the reference plant in the evaluation of the performance of various ATF concepts. The following sequences contributed to greater than 5% of the reference plant CDF; however, details of the corresponding similar sequences in the generic PWR model could not be found in publicly available materials hence further discussion was necessary.

INL Response:

We checked corresponding sequences in the generic PWR SAPHIRE model and believe they are similar to those in the reference plant PRA model. Detailed explanations are provided in the responses below.

8.1.1 Top Sequence 1: ML-1 – Sequence 1 of Medium LOCA ET

JH Review:

The reference plant MLOCA ET model does not require auxiliary feedwater (AFW), accumulators, or LPI if HPI is successful. Given success of HPI, all that is required is high-pressure recirculation (HPR) at the reference plant to prevent CD. Additionally, if HPR fails, CD is postulated as the plant Accident Sequence and Success Criteria Notebooks state for MLOCAs, given a failure of HPR, RCS depressurization is not modeled, and therefore, no low-pressure recirculation (LPR) is modeled in this scenario.

Within the generic PWR model, the MLOCA ET has different combinations of AFW, RCS cooldown, and HPR being required given success of HPI. Additionally, in each sequence where there is a failure of HPR, the generic PWR model ETs always require LPR to fail in order to reach the CD end state.

While this is a difference between the MLOCA ET structures for the reference plant sequence (ML-1), it could be considered closely related to the INT-MLOCA-3 sequence of the generic PWR model. Alternatively, the generic PWR model MLOCA ET could be enhanced to include a sequence leading to an OK end state that requires only HPR given HPI success. The generic PWR model sequences with HPR failure could also lead directly to CD as opposed to requiring LPR to fail in addition for CD to be reached. Adding these sequences (with appropriate house event selection logic) would permit the generic PWR SAPHIRE model to reflect the reference plant response.

INL Response:

We agree a discrepancy exists between the reference plant and the generic PWR MLOCA ET structures. Given HPI success, the generic PWR model requires one of two paths to prevent core damage—one is HPR success, and the other is successes of LPR and its prerequisite (i.e., AFW and cooldown); if both paths fail, CD will occur. In the generic PWR MLOCA ET model, three sequences with HPI success end in CD, including INT-MLOCA-3, 5, and 7. In sequence INT-MLOCA-3, both HPR and LPR fail. In sequences INT-MLOCA-5 and 7, HPR fails and LPR is skipped since its prerequisites (AFW or cooldown) fail. There should be a similar sequence in the generic PWR model to the reference plant ML-1 sequence. However, we have not yet conducted any RELAP5-3D analysis for PWR MLOCA sequences.

8.1.2 Top Sequence 2: LOSP-1 – Sequence 2 of LOOP ET

JH Review:

This sequence models the LOOP IE with success of emergency diesel generators (EDGs), pressurizer (PZR)

PZR valves reseating, and RCP seal integrity maintained. Given success of the RCP seals, AFW is still required to avoid CD. Alternatively, if AFW is failed, feed and bleed (F&B) is required to avoid CD. However, in the generic PWR model LOOP event tree, success of the EDGs, PZR valves reseating, and maintaining RCP seal cooling leads to an OK end state. The generic model could consider adding additional sequences to account for those PWR models that have the requirement of AFW or F&B, given RCP seals remain intact.

INL Response:

We believe the reference plant and the generic PWR LOOP ET structures are similar. The generic PWR model questions AFW prior to PZR valve reseating and RCP seal integrity. As such, it does require AFW success to avoid CD. If AFW fails, the model then requires F&B to prevent CD. There should be a similar sequence in the generic PWR model to the reference plant LOSP-2. However, we have not conducted any RELAP5-3D analysis for the non-SBO LOOP sequences in the generic PWR model.

8.1.3 Top Sequence 3: CONSLOCAL-9 – Sequence 9 of Consequential SLOCA ET

JH Review:

It should be noted this discussion of ET differences applies to all variations of the reference plant SLOCA ETs. The reference plant SLOCA ETs model sequences that have a failure of HPI and AFW as leading directly to CD. The generic PWR model includes the failure of AFW and a subsequent failure of F&B as leading to CD.

It is likely generic PWR model sequence INT-SLOCA-18 (failure of AFW and F&B) represents a similar sequence as all the reference plant SLOCA*-9 sequences. However, if not, it should be considered to add a generic PWR sequence with failure of HPI and AFW leading directly to CD. Further research evaluating the specific differences in the actual ET models (vs. review of summary information provided in the plant PRA notebooks and the INL summary reports) would be needed to determine the extent to which the INT-SLOCA-18 sequence is similar to the reference plant SLOCA sequences.

INL Response:

We believe the INT-SLOCA-18 sequence is similar to the reference plant SLOCA*-9 sequences. The INT-SLOCA-18 sequence is a CD scenario led by failures of AFW and F&B, and HPI failure is included as part of the F&B fault tree. We have conducted RELAP5-3D analysis for the INT-SLOCA-18 sequence, which is the SBLOCA-3.0 scenario in Section 2 of INL/EXT-19-56215 (Ma, et al., 2019b).

8.1.4 Top Sequence 4: SBO Scenario RCP Seal Leakages

JH Review:

The reference plant SBO event tree asks the status of the RCP seal prior to evaluation of turbine-driven AFW pump; whereas, the generic PWR model SBO event tree asks for AFW and reseating of the power-operated relief valves (PORVs) prior to asking RCP seal status. While this should not lead to a major difference in comparable SBO sequences, it could allow for the reference plant AFW and PZR valve modeling to be specific to the size of the RCP leaks.

Additionally, the reference plant model has multiple SBO with RCP seal leakage ETs where each handles different RCP seal leakage rates (21 gpm, 76 gpm, 182 gpm, and 480 gpm). For each event tree, failure of AFW in combination with no AC power recovery leads directly to CD. The generic PWR model ETs model the failure of AFW, no AC power recovery sequences as one sequence (INT-LOOPGR:16-45), and not as refined sequences based on the RCP seal leakage rates as occurs in the reference plant PRA model.

Based on review of the AFW and AC power recovery nodes used in each of the reference plant SBO ETs, it doesn't seem like this nodal logic is specific to the RCP leakage rates. Therefore, the sequence modeling in the reference plant ETs for these failures of AFW and AC power recovery sequences is determined to be similar to the logic represented in the generic PWR model and should provide comparable results.

INL Response:

Agreed.

8.2 Event Tree Structures

JH Review:

In some cases, the generic PWR ETs included additional branches, nodes, or sequences in comparison to the reference plant ETs. A discussion on these differences is provided in this section for those differences that were considered to potentially be significant or determined to potentially lead to a difference in results between the models.

8.2.1 Event Tree 1: SBO Event Tree

JH Review:

The generic PWR model SBO event tree models numerous sequences which model RCP seal leakages that are not applicable to the reference plant PRA model. It is assumed this is modeled in the generic PWR model to cover the various RCP seal leakage rates that can be experienced in the industry. However, as more plants implement "shutdown" RCP seals, it is likely many of the branches that reflect intermediate leakage rates can be pruned from the tree for the generic PWR model. (Currently, many operating plants have already installed "shutdown" RCP seals with remainder planning to adopt them in the near future).

This difference in sequence structure is not expected to lead to a significant difference in modeling or results. Although this model structure could be considered to include the ability to turn sequences "on" or "off" depending on which type of PWR would be represented by the generic PWR model (e.g., the reference plant would turn "on" the sequences with 21 gpm, 76 gpm, 182 gpm, and 480 gpm leakages but turn "off" the sequences with other leakages), the approach complicates the model significantly. Pruning the generic PWR model to reflect the adoption of shutdown RCP seals as indicated above would provide the most straightforward and consistent comparison between the plant-specific PRA models and the generic PWR model.

INL Response:

Agreed.

8.2.2 Event Tree 2: Loss of RCP Seal Cooling Following Transients Event Tree

JH Review:

The reference plant RCPSLCLGT event tree models RCPSLCLGT specific sequences or transfers to the CONSLOCAL (consequential SLOCA) event tree. The generic PWR model loss of seal cooling (LOSC) event tree transfers to either the SLOCA or MLOCA ETs. This is noted as a difference between the event tree sequence structures although it is not expected to result in a significant difference in the overall results of these models.

INL Response:

Agreed.

8.3 Assumptions

JH Review:

When performing the comparison review, a few assumptions were made which are explained in this section.

8.3.1 Assumption 1: Reactor Vessel Rupture

JH Review:

The reference plant PRA model postulates the reactor vessel rupture IE would lead directly to CD because of the break size and, by definition, would exceed the capacity of ECCS. Therefore, no event tree is developed. While this assumption could not be confirmed with the INL references (Ma, et al., 2018; Ma, et al., 2019a; Ma, et al., 2019b), it is assumed that similar evaluations and assumptions were made for the generic PWR model.

Additionally, due to the very low likelihood of a RPV rupture event, any differences related to this sequence would not be expected to produce significantly different results or conclusions.

INL Response:

The generic PWR model has a similar modeling logic, and the reactor vessel rupture IE would lead directly to CD.

8.3.2 Assumption 2: Reference Plant ETs Simplified by Generic PWR Model

JH Review:

The reference plant model had numerous ETs that were not specifically identified as unique ETs in the generic PWR model. As a result, it was assumed the generic PWR model covered these ETs with a different (or generic, similar, etc.) event tree as the accident progression is likely similar. Table 8-1 provides these ETs from the reference plant model and identifies the event trees that were assumed to be used by the generic PWR model to replicate similar accident progression. Further research evaluating the specific differences in the actual ET models (vs. review of summary information provided in the INL summary reports) would be needed to determine the extent to which these sequences are represented in the generic PWR model.

INL Response:

Detailed responses are provided in the "INL Response" column in Table 8-1.

Table 8-1. Event Tree Comparison.

Reference Plant PRA Model		Correspondence in Generic PWR Model (JH Assumption)	Correspondence in Generic PWR Model (INL Response)
Event Tree	Description	Event Tree	Event Tree
LO4160V	Loss of 4KV Bus	TRANS	LOACA
TTRIP	Turbine Trip	TRANS	TRANS
RTRIP	Reactor Trip	TRANS	TRANS
LO125VDC	Loss of DC Bus	TRANS	LODCA/B
OTRAN	Other Transients	TRANS	TRANS
LOC	Loss of Condenser	TRANS	LOCHS
CONSLOCAL	Consequential SLOCA (RCP Seal LOCA > 21 gpm/pump)	SLOCA	LOSC (see Note 2)
CONSLOCAT	Consequential SLOCA due to failure of PZR PORVs or safety valves to reseat after transients	SLOCA	TRANS (see Note 3)
SSB	Secondary Side Break	See Note 1	SLBOC (steam line break outside containment) (see Note 4)
ATWT	Anticipated Transient Without Trip	See Note 1	ATWS
LONSCW	Loss of Nuclear Service Cooling Water	See Note 1	LONSW

1. While it is assumed these ETs are included in the generic PWR model, similar ETs could not be reviewed as they were not provided in the INL references (Ma, et al., 2018; Ma, et al., 2019a; Ma, et al., 2019b).
2. The generic PWR model has an event tree for LOSC. The LOSC sequences with >21 gpm are further transferred to SLOCA (if <480 gpm) or MLOCA (if =480 gpm).
3. In the generic PWR TRANS event tree, such scenarios are not transferred to SLOCA but lead to OK or CD depending on the statuses of other mitigation systems (i.e., HPI, secondary cooling, RHR, and HPR).
4. Other secondary side break scenarios are not modeled due to low-risk significance.

8.4 Conclusions

JH Review:

As a result of this review, some minor differences have been identified when comparing the accident sequences from the reference plant ETs to the generic PWR ETs. Some potential adjustments to the generic PWR model have been suggested based on these identified differences. However, as the generic PWR SAPHIRE model stands, it should adequately portray ATF risk insights to the PRA model such that the reference plant could use these insights to support their license amendment request submittal for the use of ATF.

INL Response:

Agreed.

9. AN APPROACH TO FLEX DYNAMIC HUMAN RELIABILITY ANALYSIS

FLEX-related human actions have different characteristics than tasks using main control room (MCR) panels and local fixed equipment. These actions generally require a relatively long time to perform, have a high degree of timeline uncertainty, make use of mobile or flexible equipment, and are sensitive to environmental factors such as debris from natural disasters. Accordingly, there have been limitations to analyze these actions using existing static HRA methods. For this reason, INL researchers have developed an approach to FLEX dynamic HRA using EMRALD software (Prescott, Smith, & Vang, 2018) within the ERP project under the RISA Pathway of the U.S. DOE LWRS Program. The EMRALD tool was developed to support the increasing need for dynamic PRA models capable of responding to evolving plant conditions during simulations. This extension to FLEX dynamic HRA using the software is favorable to the analysis of the FLEX human actions because it allows for modeling the specific moment at which an action is performed, the time to perform the action, and the failure probability of that action—all modeled simultaneously, not as separate analytic activities. In addition, the modeling approach enables estimation not only of the time required to perform an action but also the evaluation of overtime failure by comparing the time required against the time window for that human action.

This section introduces an ongoing effort on how to realistically analyze FLEX-related human actions in beyond design basis external event (BDBEE) scenarios and estimate their human error probabilities (HEPs) for their application in PRA models. This section consists of four subsections regarding the approach to dynamic FLEX HRA: (1) previous efforts for FLEX dynamic HRA, (2) hybrid EMRALD HRA method, (3) application of the method to an extended loss-of-AC-power (ELAP) scenario, and (4) discussion. Section 9.1 introduces the two previous efforts: procedure-based EMRALD modeling and PRA/HRA-based EMRALD modeling approaches. Section 9.2 introduces the hybrid EMRALD HRA method, which is a combined approach of the two EMRALD modeling approaches. In fact, each modeling approach has its own characteristics, pros, and cons in terms of the HRA modeling. The hybrid method was designed to complement the challenges that each approach faces, suggest a more structured and systemic way to analyze human actions in HRA, and provide HEPs to existing PRA models. In Section 9.3, application of the hybrid method to an ELAP scenario and develop an EMRALD model is introduced. Lastly, the major result obtained from the EMRALD model is discussed in Section 9.4.

9.1 Previous Efforts for FLEX Dynamic HRA

In previous research (Ma, et al., 2020; Park, J., et al., 2021; Ulrich, T.A., et al., 2020), we developed two different approaches to FLEX dynamic HRA using the EMRALD software. Table 9-1 summarizes characteristics of the two different EMRALD modeling approaches to FLEX dynamic HRA. The procedure-based EMRALD modeling approach suggests a way to specifically model procedure steps that describe what operators or plant personnel should do in a given situation, while the PRA/HRA-based EMRALD modeling approach makes the most of concepts and techniques that are used in existing PRA and HRA. These approaches

have been validated with an example scenario. The details are described in the authors' previous papers (Park, J., et al., 2021; Ulrich, T.A., et al., 2020).

The two approaches encountered a couple of limitations. The procedure-based EMRALD modeling does not communicate with PRA parts such as equipment failure. In actual situations, required operator actions may vary, depending on whether certain equipment works or not. If components in PRA FT are not considered in the approach, the method may be highly limited for evaluating various scenarios that lead to failure. Furthermore, the method was tested using only a small subset of procedures. A method for treating numerous procedure steps that could be used in a scenario is not explicitly suggested. In addition, this modeling approach does not consider performance shaping factors (PSFs), meaning factors that influence human performance and are used to highlight error contributors and adjust basic HEPs. For PRA/HRA-based EMRALD modeling, previous research identified two main issues, namely how to assume timeline uncertainly for each basic event and how to specifically model certain major HRA concepts (e.g., recovery opportunities).

Table 9-1. Characteristics of Two Different EMRALD Modeling Approaches to FLEX Dynamic HRA (Ma, et al., 2020)

	Procedure-based EMRALD Modeling	PRA/HRA-based EMRALD Modeling
Description	Specifically models procedure contexts	Models basic events and human failure events (HFEs) already considered in PRA and HRA
Characteristics	Useful in accounting for context uncertainties that complicate the determination of HEPs	Within PRA/HRA modeling, it could be used to validate timeline uncertainties not covered in existing PRA/HRA

9.2 Hybrid EMRALD HRA Method

To complement the challenges that each approach faces, a more structured and systemic way to analyze human actions in HRA was introduced, which provides HEPs to existing PRA models. RISA research team has developed a hybrid method by combining the two EMRALD modeling approaches introduced in the previous section. In existing HRA, human actions are modeled as basic events equivalent to system, component, or equipment failure that are modeled in PRA, whereas this method suggests human actions (or procedures)-centered modeling approach to more realistically evaluate human actions based on the simulations.

Figure 9-1 shows a conceptual design of the hybrid method, which models both procedure contexts representing human actions as well as equipment failure. In the figure, the heading events (i.e., Heading #0, #1 and #2) mean IEs, existing PRA headings modeled in ETs, or any event contributing to delay of a scenario. The procedure paths refer to combinations of procedure contexts between the heading events or between a heading event and an end state (i.e., OK or CD). The procedure paths lead to different scenarios, mitigation strategies, and plant states depending on the heading events. For example, if availability of diesel generators (DGs) is a heading event after an IE, the success of the heading represents a LOOP scenario, while the failure of the heading event represents a station black out scenario. Operators will use different sets of procedures respective to each scenario. If a mitigation strategy is successful, the end state will be "OK." Otherwise, the end state will be "CD."

Figure 9-2 shows a summary of the hybrid EMRALD HRA method. It consists of four steps: (1) procedure-based task analysis, (2) task-unit analysis for procedures used in a scenario, (3) development of a procedure-based EMRALD model, and (4) model analysis and integration into PRA model.

First step refers to the process of collecting and analyzing task-related information necessary for performing HRA (Park, J., A.M. Arigi, and J. Kim, 2019). In this step, we collect input data required for modeling procedures and implementing the method such as PRA models, relevant information for HFEs such as PSF data

and relevant procedures, and then we develop an event sequence diagram (ESD) like Figure 9-1 and identify its actual timeline.

In the second step, procedure paths in the ESD are decomposed in the task-unit level. Basically, a procedure path consists of a couple of procedures, which include many procedure steps. A procedure step is also composed of a couple of task-units. The task-unit refers to the procedure task type that has defined in the Human Reliability data EXtraction (HuREX) (Jung, W., et al., 2020) framework and the GOMS-HRA method (Boring and Rasmussen, 2016).Then, time and HEP information are assigned per each task-unit. For the time information, it is assumed by GOMS-HRA, which suggests statistical time distribution with mean value, standard deviation, 5^{th} percentile, and 95^{th} percentile depending on task-units. The time data has been collected through experimental work using actual operators and Human Systems Simulation Laboratory (Joe, J.C. and R.L. Boring,, 2017; Boring, R., et al., 2016), which is INL's full-scope simulator designed to conduct critical safety focused human factors R&D. For the HEP information, it is credited only to task-units critical to a failure of HFE. Depending on the approach to HEP calculation in existing HRA, a HEP is calculated from the relationship between a basic HEP and PSF multiplier values (Park, J., A.M. Arigi, and J. Kim, 2019). In this study, the basic HEPs for task-units are assumed from the HuREX database, while PSFs are adopted from the Standardized Plant Analysis Risk-HRA (SPAR-H) (Gertman et al., 2005) method.

In the third step, a procedure-based EMRALD model is developed. The model includes all the information obtained from the previous steps and is used for evaluating HEPs and time information for HFEs. The task-units relevant to critical human actions are only used for the HEP evaluation, while the time evaluation is performed for all task-units modeled in a scenario.

The last step evaluates HFE failure paths, HEPs, and overtime failure for HFEs. The HFE failure paths based on cut-sets generated from simulation log describe the reason why a scenario is failed. These can be used for correcting modeling errors in the EMRALD model. The determined HEPs in this model are available to support HFEs considered in static PRA models. The overtime HFEs evaluate if operator actions are finished within their time windows. If an action is not completed within allowed time window, it is considered as a guaranteed failure (i.e., HEP = 1.0).

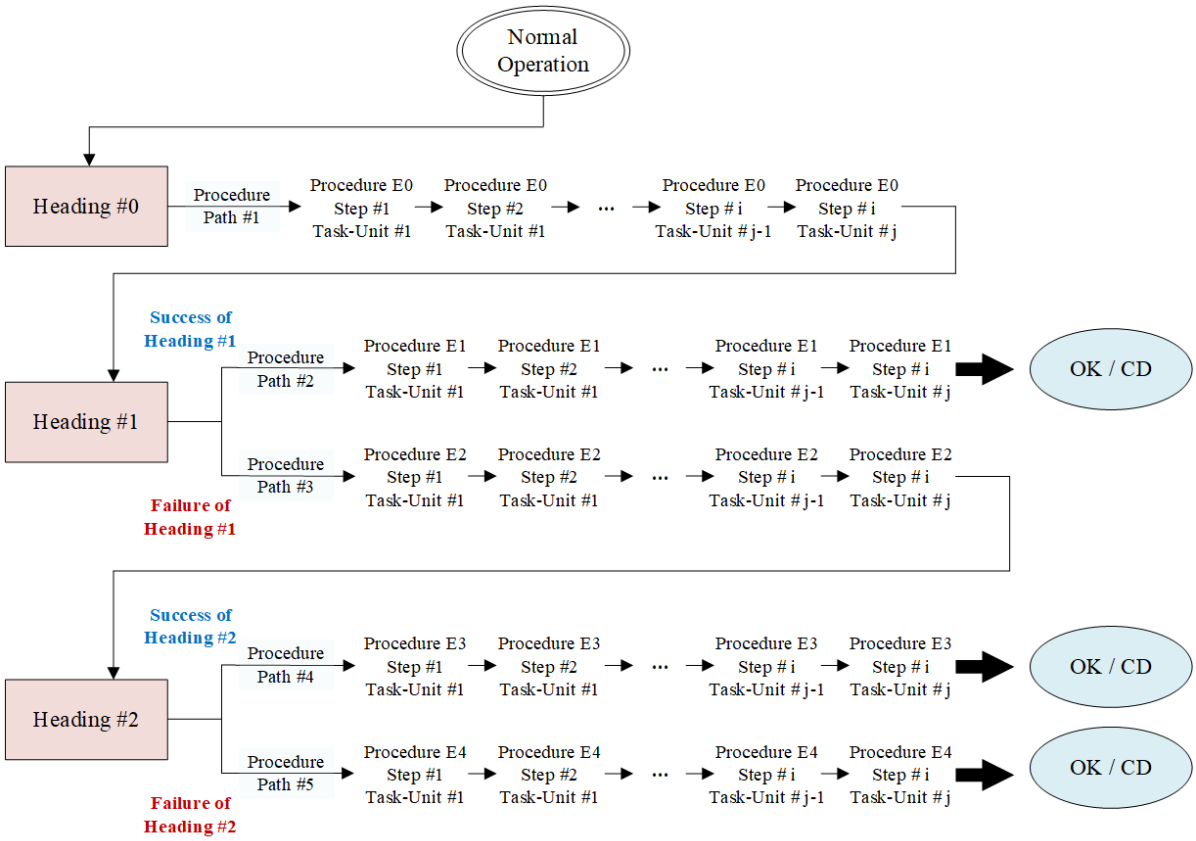

Figure 9-1. Conceptual Design of the Hybrid Method.

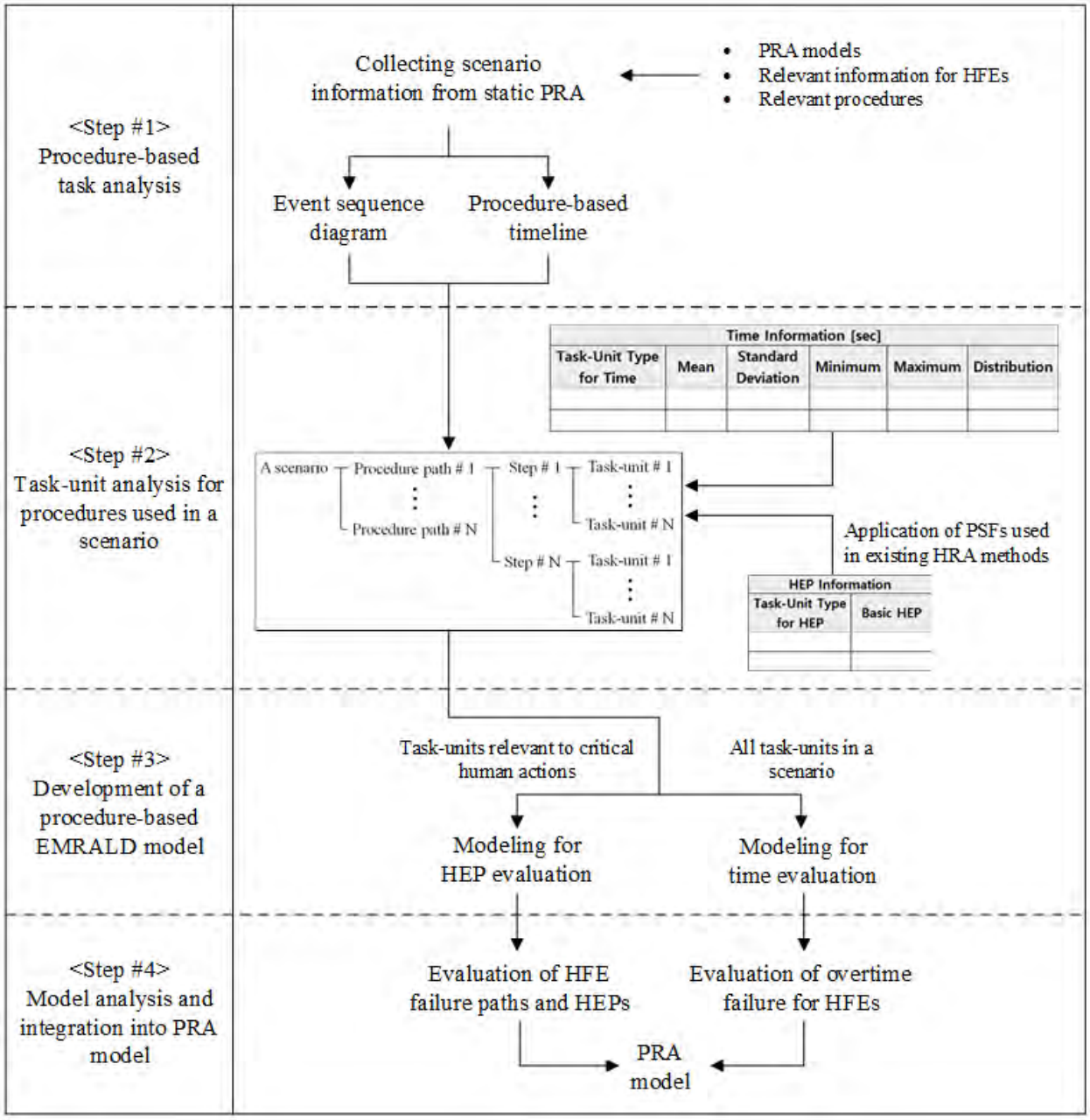

Figure 9-2. Summary of the Hybrid Method.

9.3 Application of the Method to An ELAP Scenario

The research presented here applied the hybrid method to an ELAP scenario. The ELAP scenario refers to a station blackout scenario during which offsite power, EDGs, and alternate AC (ACC) DGs are not available (Gunther, W., et al., 2015). In the scenario, FLEX DGs are used for providing AC power required to support the reactor cooldown. In this research, we specifically developed an ELAP scenario where FLEX DGs are deployed and connected to the plant. The scenario was developed based on observation in some stress test experience (Park, J., A.M. Arigi, and J. Kim, 2019). In the scenario, it is assumed that once the IE occurs, MCR panel indicators suddenly become unavailable due to blackout in the MCR. It is assumed operators experience a high degree of disorientation and stress and are not equipped with flashlights. And the battery power connection is assumed to delay for 15 minutes. In other words, the battery power associated with MCR indicator and emergency light functionality is assumed to be automatically restored after 15 minutes. Also, operators are

assumed to be able to obtain flashlights outside of the MCR. Once some of the indicators are restored and some flashlights become available, MCR operators perform procedures. They first diagnose the IE. By following procedures, they evaluate if AC power sources are difficult to restore and as the result declare an ELAP scenario. Then, there are two operator actions performed almost simultaneously. First, MCR operators perform DC load shedding with local operators. The local operators should finish all mission activities locally, but they actually miss a couple of manipulations. They notice the fault after they come back and communicate with MCR operators, then return to finalize the manipulations. Second, the MCR operators communicate with the designated personnel to deploy FLEX DGs. After the call with the MCR operators, the FLEX personnel move to the mobile equipment garage and then deploy all the relevant equipment to the designated place to connect them with the plant. During the deployment, there is some debris along the way. It is assumed it takes 2 hours and 20 minutes to finalize the debris removal. After that, the FLEX personnel keep deploying the equipment and connecting FLEX DGs to the plant. The scenario is concluded if both operator actions are successful within the time window, and these actions are successfully reported to the MCR operators.

As the first step of the hybrid method, we performed the procedure-based task analysis based on the scenario described above. Figure 9-3 and Figure 9-4 show the ESD and the procedure-based timeline for the ELAP scenario. These are simplified for illustrating this ELAP scenario.

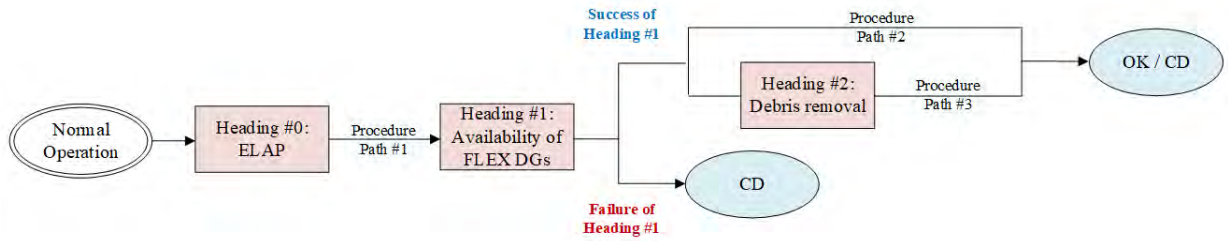

Figure 9-3. ESD for an ELAP Scenario.

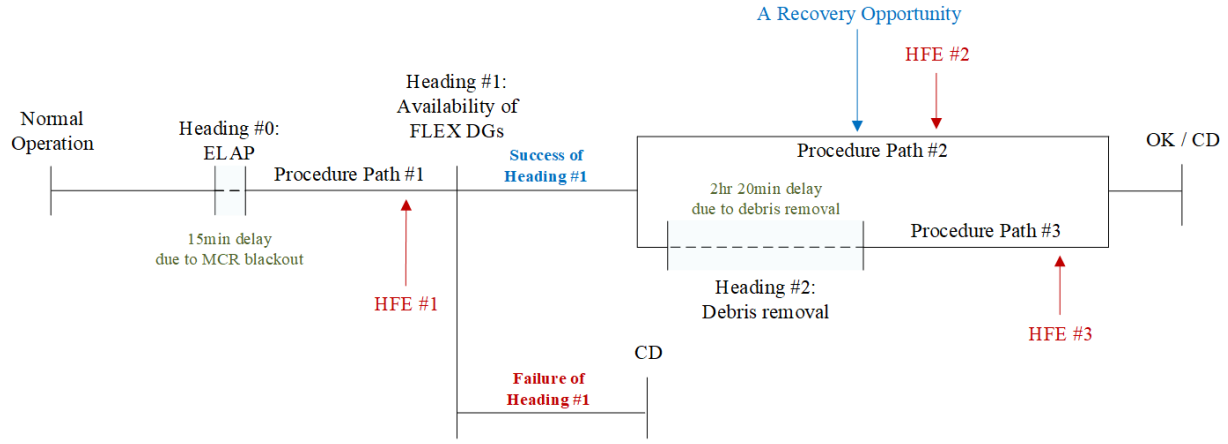

Figure 9-4. Procedure-based timeline for an ELAP Scenario.

First, there are three headings (i.e., Heading #0, #1, and #2). The first heading event is the IE causing 15 minutes delay due to the MCR blackout. The second one divides branches into cases where FLEX DGs are available or not. If FLEX DGs are not available, it is assumed it leads to the CD state. The failure of this heading is determined by a static fault tree logic developed in the author's previous report (Ma, Z. et al., 2019a). The logic is also modeled within the EMRALD software. The last heading causes 2 hours and 20 minutes delay for removing debris.

Second, three procedure paths (i.e., Procedure Path #1, #2, and #3) are considered in this scenario. The first path consists of post-trip action procedures from the IE occurrence to the procedure step for checking availability of FLEX DGs. It may include emergency operating procedures (EOPs) like "EOP-E-0" in Westinghouse type NPPs and the standard post-trip action and the diagnosis action procedures in combustion engineering type NPPs. The early stage of FLEX support guidelines (FSGs) is also involved in the path. For the second and the third procedure paths, these are mostly composed of specified FSGs guiding DG load shedding and FLEX DG deployment and installation.

Third, three HFEs that have been considered as critical events in static FLEX HRA analyses (U.S. Nuclear Regulatory Commission, 2020) are involved in procedure paths. Table 9-2 summarizes HFE information from static HRA. It includes the SPAR-H PSF evaluation and time window for each HFE. These are assumed based on the relevant literature (Park, J., A.M. Arigi, and J. Kim, 2019; U.S. Nuclear Regulatory Commission, 2020).

Table 9-2. A Summary of HFE Information from Static HRA.

		HFE #1	HFE #2	HFE #3
Description		Operator fails to declare ELAP.	Operator fails to perform FLEX DC load shed.	Operator fails to deploy and connect FLEX DGs.
SPAR-H PSFs	Available time	Extra time	Extra time	Extra time
	Stress/stressor	Extreme	High	High
	Complexity	Moderately complex	Nominal	Nominal
	Experience /training	Nominal	Low	Low
	Procedures	Nominal	Nominal	Nominal
	Ergonomics/HSI	Nominal	Nominal	Nominal
	Fitness for duty	Nominal	Nominal	Nominal
	Work process	Nominal	Nominal	Nominal
Time window		1hour	1.5 hour	6hour

Based on the information introduced above, this study performed the task-unit analysis, which is the second step of the hybrid method. Figure 9-5 and Figure 9-6 show an example of the task-unit analysis. In the figures, there are fixed task-units (i.e., "E0_S3_TU1," "E0_S3_TU2," "E0_S3_TU3," "E0_S3_TU4," "ECA_S1_TU1," and "ECA_S1_TU2") included in the Procedure Path #1. The description, actor, work device, time information and HEP information for each task-unit are also summarized in the figures. As mentioned in the previous section, time and HEP information were investigated on the basis of the HuREX database (Jung, W., et al., 2020) and the GOMS-HRA method (Boring and Rasmussen, 2016), respectively. The task-units starting as "EO" are the procedure contents that belong to post-trip action procedures of EOPs, while those starting as "ECA" are involved in the EOP specialized to the loss of all AC power sources. In the analysis, only one task-unit (i.e., "EO_S3_TU2") is selected as the task-unit critical to the failure of HFE #1.

Procedure Path	Relevent HFE	Diagram Name in EMRALD	Action	Actor	Work Device	Time Information [sec]					
						Task-Unit Type for Time	Mean	Standard Deviation	Minimum	Maximum	Distribution
#1	-	E0_S3_TU1	Verify vital AC buses have electrical power	MCR Operator	MCR Board	T-M-Check	2.14	0.76	2.44	29.9	Lognormal
#1	HFE#1	E0_S3_TU2	Verify at least a vital AC bus has electrical power	MCR Operator	MCR Board	T-M-Check	2.14	0.76	2.44	29.9	Lognormal
#1	-	E0_S3_TU3	Connect at least a vital AC bus. If at least a vital AC power is not available, go to ECA-0.0 (Loss of All AC Power).	MCR Operator	MCR Board	T-M-Action	2.23	1.18	1.32	65.3	Lognormal
		E0_S3_TU4				T-M-Action	2.23	1.18	1.32	65.3	Lognormal
#1	-	ECA_S1_TU1	Check if RCS is isolated	MCR Operator	MCR Board	T-M-Check	2.14	0.76	2.44	29.9	Lognormal
#1	-	ECA_S1_TU2	PRZR PORVs - Closed	MCR Operator	MCR Board	T-M-Check	2.14	0.76	2.44	29.9	Lognormal

Figure 9-5. An Example of the Task-Unit Analysis: Time Information.

Procedure Path	Relevent HFE	Diagram Name in EMRALD	Action	Actor	Work Device	HEP Information			
						Task-Unit Type for HEP	Basic HEP	PSF muliplier	Final HEP
#1	-	E0_S3_TU1	Verify vital AC buses have electrical power	MCR Operator	MCR Board	-	-	-	-
#1	HFE#1	E0_S3_TU2	Verify at least a vital AC bus has electrical power	MCR Operator	MCR Board	H-M-Indicator	2.30E-03	1.0	2.30E-03
#1	-	E0_S3_TU3	Connect at least a vital AC bus. If at least a vital AC power is not available, go to ECA-0.0 (Loss of All AC Power).	MCR Operator	MCR Board	-	-	-	-
		E0_S3_TU4				-	-	-	-
#1	-	ECA_S1_TU1	Check if RCS is isolated	MCR Operator	MCR Board	-	-	-	-
#1	-	ECA_S1_TU2	PRZR PORVs - Closed	MCR Operator	MCR Board	-	-	-	-

Figure 9-6. An Example of the Task-Unit Analysis: HEP Information.

As the third step of the hybrid method, we developed the procedure-based EMRALD model. It consists of three parts: (1) main model, (2) heading model, and (3) procedure model. First, the main model shows an overview of the scenario with heading events. It is developed based on the ESD. Figure 9-7 shows the main model for the ELAP scenario. Second, the heading model includes logic to determine the success or failure of a heading event. If a heading does not divide branches like Heading #0 and #2 in Figure 9-3, it does not need to be modeled. The heading model is developed based on static fault tree logics. Figure 9-8 indicates the heading model for Heading #1. In the figure, the five basic events are modeled in the heading model as below. Each basic event contributes to the failure of Heading #1, and its failure probability is assumed from (Ma, Z. et al., 2019a):

- DGs_Fail_CCF_Run: CCF of FLEX DGs to Run
- DGs_Fail_CCF_Start: CCF of FLEX DGs to Start
- DGs_Fail_Run: FLEX DGs Fail to Run
- DGs_Fail_Start: FLEX DGs Fail to Start
- DGs_Fail_TM: FLEX DGs Fail Due to Test and Maintenance.

Lastly, the procedure model reflects all the information obtained from the task-unit analysis. Figure 9-9 indicates the procedure model for Procedure Path #2. In the figure, the dotted red boxes are the task-units critical to the failure of HFE #2, while the solid red boxes that are the diagrams for HFE #2 and its overtime failure visually combine the task-units. The dotted blue boxes and the solid blue box indicate the task-units relevant to recovery failure and the diagram visually combining the task-units, respectively.

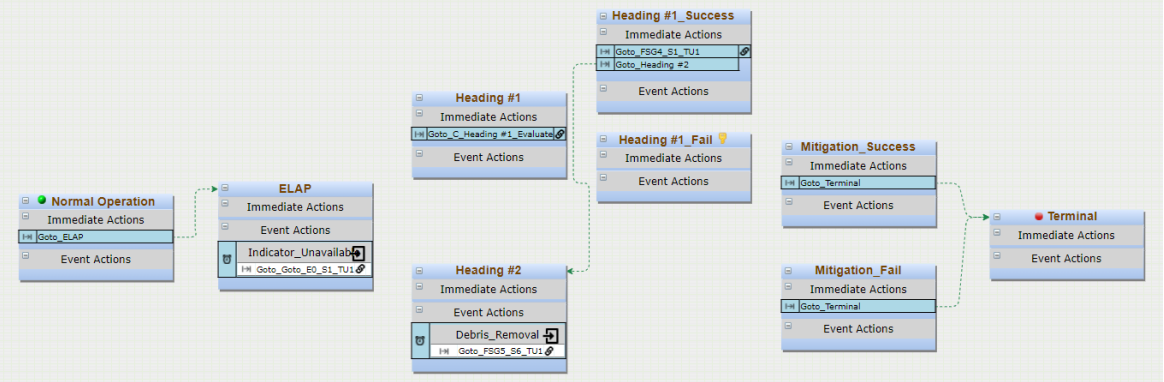

Figure 9-7. Main Model for the ELAP Scenario.

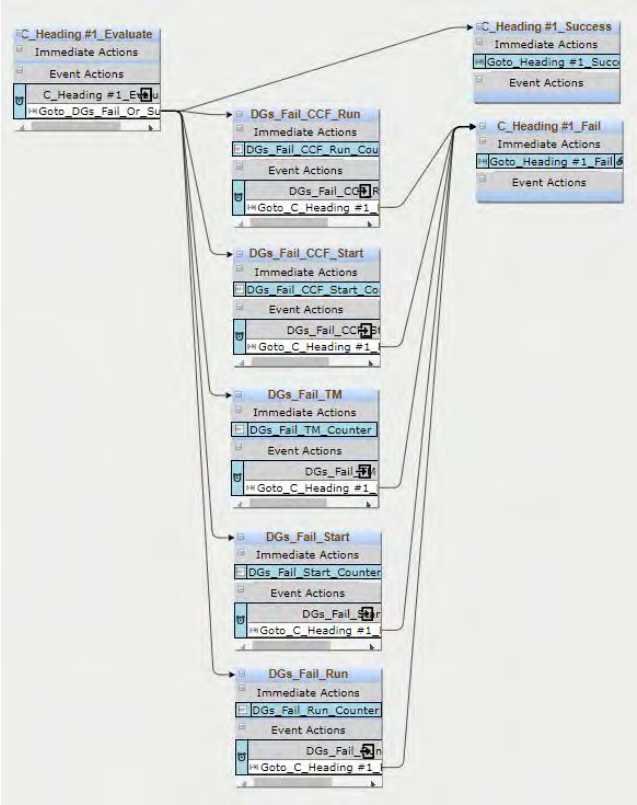

Figure 9-8. Heading Model for Heading #1.

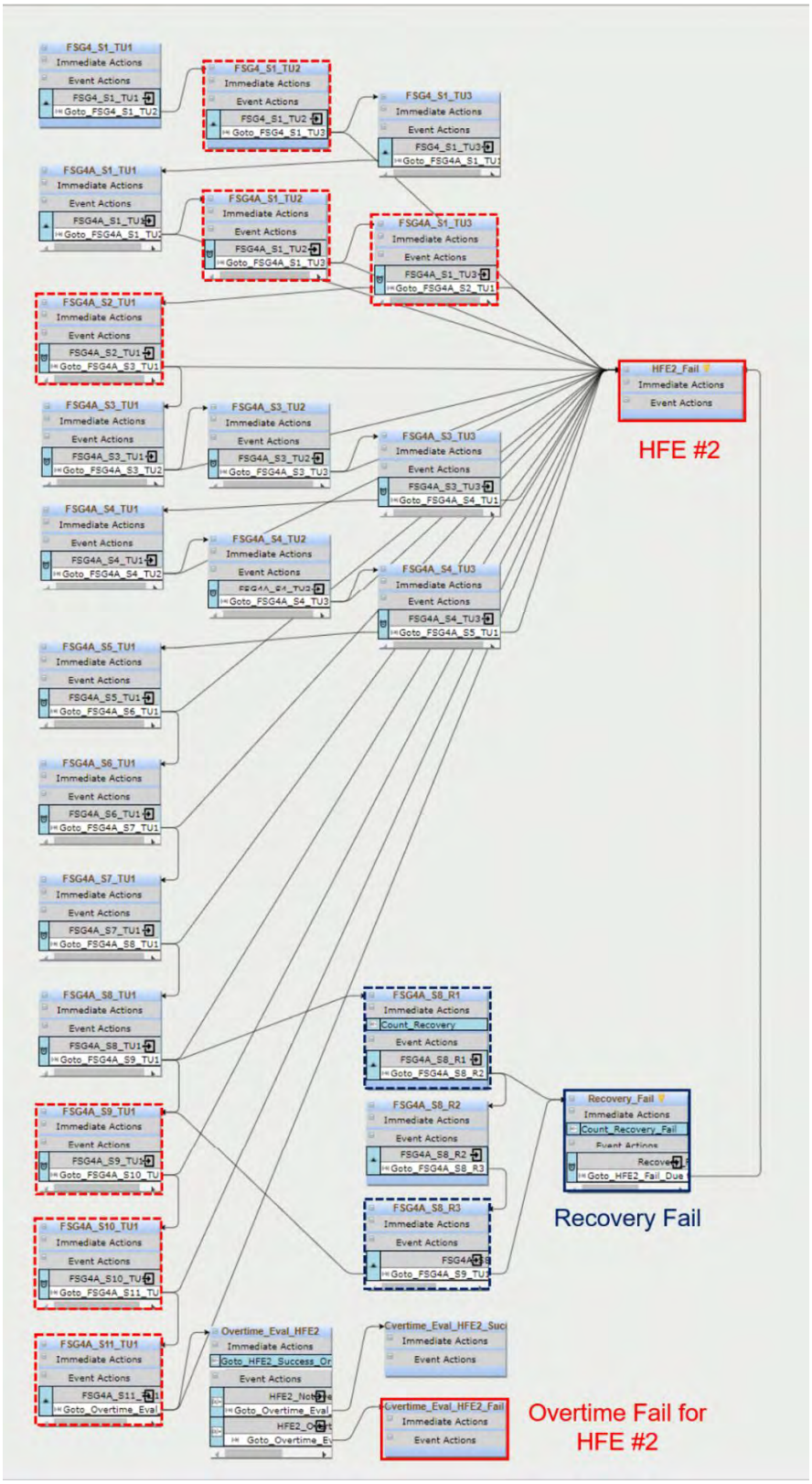

Figure 9-9. Procedure Model for Procedure Path #2.

In the last step of the hybrid method, we analyze the EMRALD model and integrate the major result into static PRA models. In this step, we also evaluate if HFE failure paths and HEPs are reasonable and if all the HFEs are done within time windows. Figure 9-10 represents the result of the EMRALD model simulation with 100,000 trials. The number of failures for HFEs, recovery human actions and component failures are shown in the figure. For the HFE failures, there are two types counted: (1) HFE failure caused by the failure of the task-units and (2) HFE failure due to overtime. The former one has the same definition with the existing static PRA and HRA in terms of the HEP definition, while the latter one is counted if the total time required for an HFE takes longer than its time window.

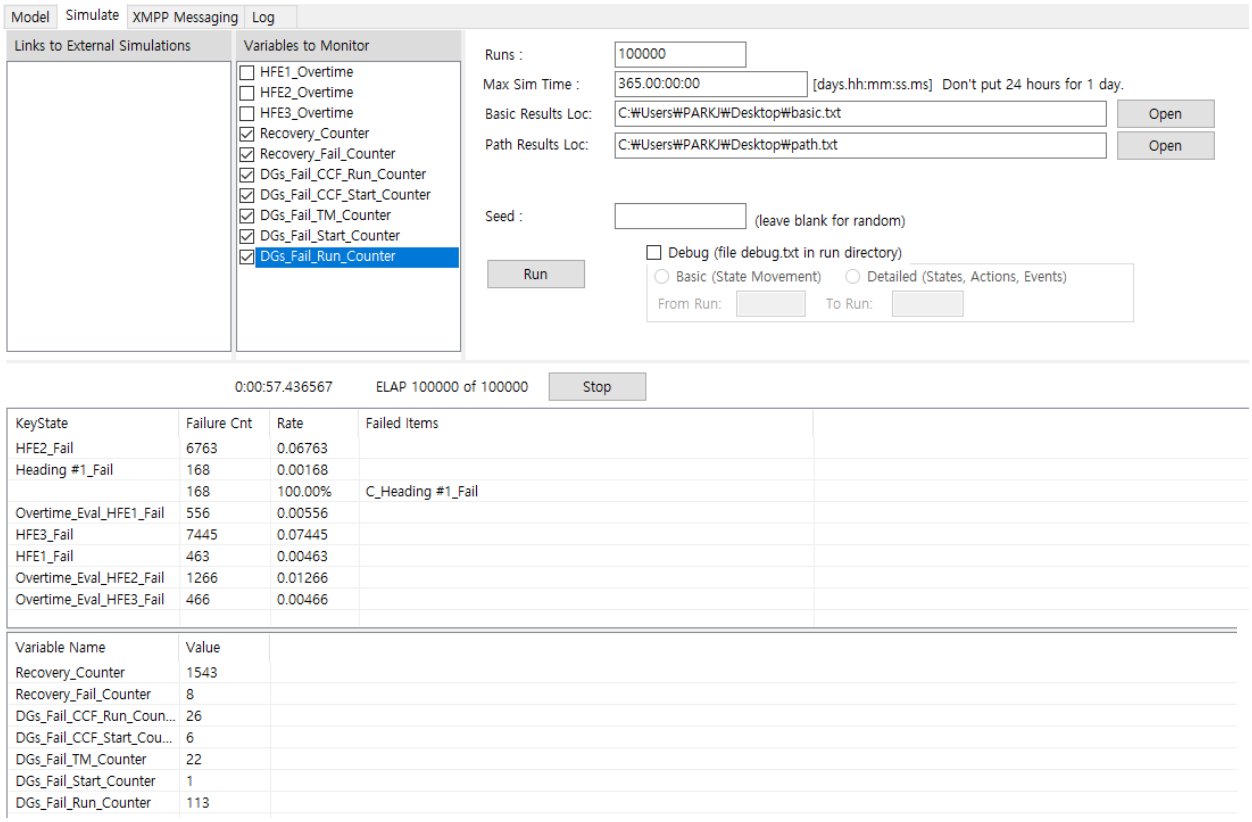

Figure 9-10. Result of the EMRALD Model Simulation with 100,000 Trials.

As shown in Table 9-3, this research compared the HEPs from the EMRALD model and a static HRA method, (i.e., Integrated Decision-tree Human Event Analysis System for Event and Condition Assessment [IDHEAS-ECA]) (Xing, J., Y. Chang, and J. DeJesus, 2020). The IDHEAS-ECA is the latest HRA method endorsed by U.S. Nuclear Regulatory Commission (U.S. NRC). A technical report (U.S. Nuclear Regulatory Commission, 2020) issued by U.S. NRC has analyzed FLEX-related actions using the IDHEAS-ECA method. In this study, we investigated differences between the HEPs from the EMRALD model and the IDHEAS-RCA method. As shown in the table, the HEP for HFE #1 from the EMRALD model is included in the HEP range from the IDHEAS-ECA method. On the other hand, the HEPs for HFE #2 and #3 from the EMRALD model indicate higher values than those calculated by the IDHEAS-ECA method. For the recovery failure and overtime fails of HFE #1, #2 and #3, these are not compared because these are only estimated from the EMRALD model.

Table 9-3. A Comparison of HEPs from the EMRALD Model and the IDHEAS-ECA Method (U.S. Nuclear Regulatory Commission, 2020).

	HEPs from EMRALD Model	HEPs from IDHEAS-ECA
HFE #1 (ELAP Declaration)	4.6e-3	1.1e-3 ~ 1.1e-1
HFE #2 (DC Load Shed)	6.8e-2	2.0e-3 ~ 6.0e-3
HFE #3 (Deploy and Connect FLEX DGs)	7.4e-2	1.3e-3 ~ 1.2e-2
HFE #1_Overtime Failure	5.6e-3	N/A
HFE #2_Overtime Failure	1.3e-2	N/A
HFE #3_Overtime Failure	4.7e-3	N/A
Recovery Failure	5.2e-3	N/A

9.4 Discussion

This research has attempted to develop an enhanced approach to FLEX dynamic HRA using the EMRALD software. It has been upgraded by addressing a couple limitations of the previous methods such as the procedure-based EMRALD modeling and the PRA/HRA-based EMRALD modeling approaches. This study also assumed an ELAP scenario including detailed assumptions based on observation in some stress test experience (Park, J., A.M. Arigi, and J. Kim, 2019) and applied the hybrid method to the scenario. As a result, this study observed that the HEPs from the EMRALD model are similar or a little bit higher in comparison with those from the IDHEAS-ECA method. Such difference in the HEP values is a result from the difference in the probabilities of making errors numbers using different approaches. The procedure-based approach has a higher error-making probability since it involves the modeling of a large volume of procedure contexts. In addition, the new type of human error that is considered implicitly in existing HRA methods, i.e., overtime failure, is modeled using the EMRALD for each HFE. This study also estimated failure probabilities of recovery actions by application of a unique methodology not available in any other HRA methods.

This approach suggested in this research may have benefits for providing stronger background and more concrete evaluation criteria to estimate a HEP. In existing HRA, how to define analytical subjects and divide a HFE into the level that the analysis is available has been a challenge that varies HRA results depending on the analysts (Park, J., A.M. Arigi, and J. Kim, 2019). A couple of HRA methods, such as Technique for Human Error Rate Prediction (THERP) (Swain, A.D. and H.E. Guttmann, 1983) and K-HRA (Jung, W., D. Kang, and J. Kim, 2005), decompose a HFE into subtasks to estimate an HEP, while some HRA methods like SPAR-H do not break an HFE into subtasks. On the other hand, the approach using the EMRALD software uses procedures which may be the more objective rather than the subtask concept in the existing HRA and assigns values from the HuREX database and the GOMS-HRA method that provide the latest version of HRA data in the most reasonable manner.

This study counts overtime failures that have not been explicitly considered in existing HRA which may be useful to support the human factors engineering program. Originally, in the human factors engineering program in NUREG-0711 (O'Hara, Higgins, Fleger, & Pieringer, 2012), there is an HRA process to identify operator actions are feasible to accomplish within allotted time windows. The time required refers to the duration of time that is required for operators to perform a task, while time available is the time period within which the operators must perform a task in order to avoid undesired consequences (e.g., an action to refill a tank should be initiated before tank is empty). If the time required for an HFE is longer than the time available, it is evaluated as a guaranteed failure (HEP = 1.0) and assumed the plant state would be irreversible. To date, the available time window has been calculated by thermal hydraulic and other physics-based analyses that produce accurate values from simulations. On the other hand, the time required for FLEX deployment relies on structured interviews with instructors, operators, or other knowledgeable experts rather than using actual data or simulation approach. Basically, the estimation of the time required is complicated because many factors may affect it. Therefore, reliance only on experience for reasonable time estimates may be challengeable considering all the variables in NPPs. In this aspect, the EMRALD-based HRA method may be useful to estimate the time required

and support the HRA part in the human factors engineering program by evaluating overtime HEPs or whether an overtime failure is counted or not.

This study may be useful to specifically evaluate human action recoveries. To date, the existing HRA has considered a recovery as a successive action. For example, when estimating a final HEP, a recovery probability is a multiplier for an HEP. However, the recovery action does not always happen. Recovery is predicated on a cue that makes the person recognize his or her fault. Furthermore, there will be different mechanisms to the mitigation after the error is recovered, but these are not sufficiently explained in the existing HRA. In this aspect, the EMRALD-based simulation approach may be a breakthrough. The ELAP scenario introduced in the previous section includes the local operators' fault that very specifically accounts for a recovery opportunity feasible in NPPs. This will be further researched to provide a way to reasonably reflect recovery opportunities when estimating HEPs in HRA.

10. RISK AND ECONOMY IMPACT ANALYSES OF NEW BATTERY TECHNOLOGY WITH INCREASED CAPACITY

This section presents risk and economy impact analyses of deploying new battery technology with increased capacity at a generic BWR plant. It should be noted the battery study is an illustrative generic example, and its results do not represent benefits in any real-world plant. Section 10.1 develops a set of alternatives to extending battery capacity. Section 10.2 quantifies the potential benefits in reducing plant risk. Section 10.3 qualitatively discusses and ranks the potential costs. Section 10.4 compares all the alternatives based on their impacts on plant risk and cost. Section 10.5 outlines conclusions and future work plan.

10.1 Developing Alternatives for Extending Battery Capacity

Nuclear industry has been actively seeking for solutions of expanding battery capacity by exploring new battery technologies with improved energy density (e.g., lithium-ion batteries) and developing new battery-powered systems supplying power more rapidly and more precisely (Nuclear Energy Institute, 2020). This section conducts an independent evaluation and develops alternatives for extending battery capacity at a generic BWR plant. Most safety-critical functions at NPPs are supported by AC and DC electric power. Plant AC power is usually supplied from offsite; if LOOP occurs, AC power is provided by onsite standby power sources, typically EDGs. If LOOP occurs with concurrent standby AC power-source failures, there will be no AC power available and the plant will enter an SBO situation. When AC power restoration is in progress, onsite batteries may continue to supply DC power with a limited capacity (e.g., 4 to 8 hours) and maintain safety-critical functions.

On one hand, extending battery capacity could provide additional DC power supply. In the generic BWR plant used for this case study, DC power supply is very critical for mitigating SBO. Many SBO mitigating systems (e.g., HPI system and low-pressure injection system) are dependent on DC power. Although many mitigating systems are designed to be capable of performing their safety functions when AC power supply is lost, they may need DC power for control and instrumentation purposes. In addition, the time to battery depletion sets time windows for offsite and onsite AC power recovery. On the other hand, extending battery capacity might supply additional AC power converted from the battery-generated DC power.

Nine alternatives of extending battery capacity are developed and presented in Table 10-1. It should be noted that the list is not intended to be exhaustive since it is a conceptual and illustrative example. The list is subject to change after engaging industry partners to evaluate the feasibility of listed alternatives and potentially propose additional alternatives. The battery depletion time in the generic BWR plant is currently assumed to be 4 hours; on this basis, alternatives are developed to extend battery life to 8 hours, 12 hours, and 24 hours. Even with the same objective (e.g., extending battery life from 4 hours to 8 hours), a variety of alternatives can be formulated given different options in the battery portfolio (i.e., existing vs. new batteries), connection types (i.e., in series vs. in parallel), and so forth.

Table 10-1. Alternatives of Extending Battery Capacity at a Generic BWR Plant.

Table 10-1. (continued).

No.	Alternative	Purpose
1	Extending battery life to 8 hours (extending life of existing batteries by load shedding)	Providing additional DC power
2	Extending battery life to 8 hours (keeping existing batteries and introducing additional new batteries)	Providing additional DC power
3	Extending battery life to 8 hours (replacing existing batteries with new batteries with extended life)	Providing additional DC power
4	Extending battery life to 12 hours (extending life of existing batteries by load shedding)	Providing additional DC power
5	Extending battery life to 12 hours (keeping existing batteries and introducing additional new batteries)	Providing additional DC power
6	Extending battery life to 12 hours (replacing existing batteries with new batteries with extended life)	Providing additional DC power
7	Extending battery life to 24 hours (keeping existing batteries and introducing additional new batteries)	Providing additional DC power
8	Extending battery life to 24 hours (replacing existing batteries with new batteries with extended life)	Providing additional DC power
9	Introducing new batteries as backup for onsite EDGs	Providing additional AC power

10.2 Quantifying Impacts on Plant Risk

This section quantifies the impact on plant risk due to implementation of each alternative. The risk metric adopted in this paper is CDF estimated using PRA. Although a variety of IEs could lead to CD, this paper focuses on SBO scenarios where DC power supply play a critical role.

This study features a generic PRA model developed using SAPHIRE 8 for a generic BWR plant for LOOP scenario analysis. The generic BWR LOOP PRA model starts with the occurrence of a LOOP event. A LOOP event can be assigned to one of four categories, including grid-related (GR), plant-centered (PC), switchyard-centered (SC), and weather-related (WR). Four LOOP ETs are developed corresponding to four LOOP categories. All four LOOP ETs share the same tree structure but differ in IE frequencies and AC power non-recovery probabilities. The four LOOP ETs are quantified with SAPHIRE 8. Table 10-2 presents the quantification results, which are used as the baseline risk estimates to compare and examine the risk impacts of battery capacity extension alternatives.

Table 10-2. LOOP ETs Quantification Results (Baseline Risk).

LOOP Category	No. of LOOP CD Sequences	No. of SBO CD Sequences	No. of Non-SBO CD Sequences	CDF (per reactor year)
LOOPGR	159	104	55	5.0E-07
LOOPPC	159	104	55	7.4E-08
LOOPSC	159	104	55	5.8E-07
LOOPWR	159	104	55	5.6E-07
Total	636	104	55	1.7E-06

10.2.1 Risk Impacts of Alternatives Providing Additional DC Power

In the generic BWR LOOP PRA model, the impacts of batteries are reflected through two paths. One path is directly incorporating battery failure modes into the FT representing hardware failures. As shown in Figure 10-1, an example is a fault tree for “diesel generator 1A support power faults.” Two battery-related basic events are directly incorporated into the fault tree, including (1) DCP-BAT-LP-1A, (independent) failure of Train 1

125V DC battery, and (2) DCP-BAT-CF-125V, common-cause failure of two 125V DC batteries. However, the risk impact of a battery from such direct incorporation is negligible—the scenarios containing battery failures account for 2% of total LOOP CDF. It could be expected the risk impact of battery capacity extension can be trivial as well. Hence, this path of direct incorporation will not be examined in further analysis.

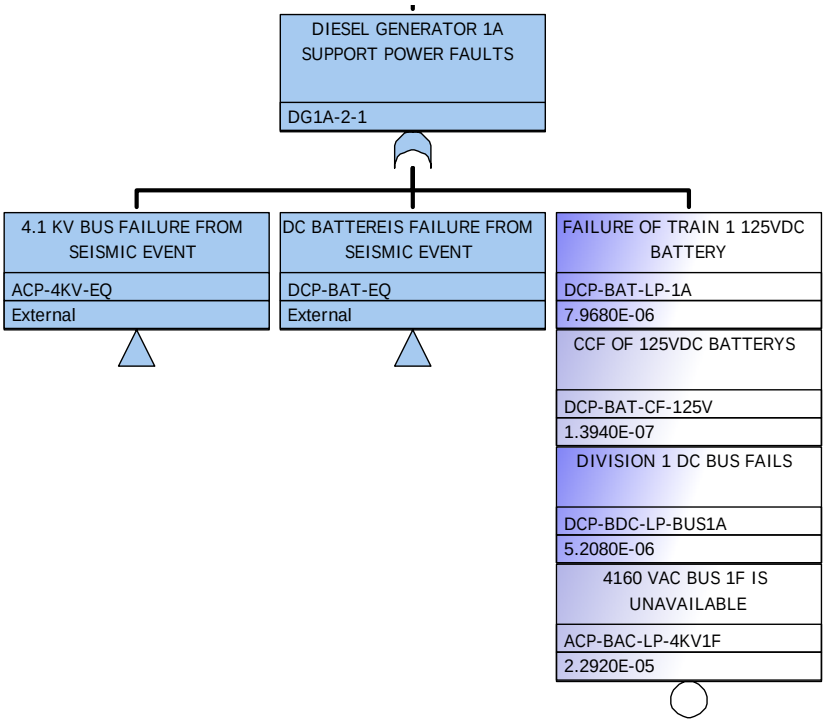

Figure 10-1. Example of Direct Incorporation of Battery Failures into PRA Model.

The other path is evaluating the risk impact of battery in the LOOP PRA model as related to AC power recovery. Based on the U.S. NPP operating experience (OpE) data, the probability of non-recovery offsite power and onsite EDGs were found to be the best fit with a lognormal distribution and a Weibull distribution, respectively (Johnson and Schroeder, 2016). The corresponding probabilities can be estimated using the following equations (Johnson and Schroeder, 2016).

$$P_{OPR(t)} = \Phi[\frac{ln(t)-\mu}{\sigma}] \quad (10\text{-}1)$$

$$P_{DGR(t)} = e^{-(\frac{t}{\beta})^{\alpha}} \quad (10\text{-}2)$$

where:

t	=	AC power (from offsite source or onsite EDGs) recovery time is measured in hours
$P_{OPR(t)}$	=	Probability of an operator failing to recover offsite power within t hours
$P_{DGR(t)}$	=	Probability of an operator failing to recover EDG within t hours
μ, σ	=	Lognormal distribution parameters
α, β	=	Weibull distribution parameters

The lognormal and Weibull distribution parameter values used in this study were determined based on (Johnson and Schroeder, 2016), which was the latest available version when the generic BWR SAPHIRE model was developed. It should be noted usually these values are being updated annually. As of April 2021, the most recent versions are provided in (Johnson and Ma, 2019) and (Ma, 2019). Based on the above equations, it is

possible to estimate the non-recovery probabilities for offsite power and onsite EDGs given extended battery life shown in Table 10-3. The LOOP CDF values given extended battery life are then quantified with SAPHIRE 8 and presented in Table 10-4. If the battery life can be extended from 4 hours to 8 hours, 12 hours, and 24 hours, the LOOP CDF is estimated to reduce by 6%, 11%, and 20%, respectively.

Table 10-3. AC Power Recovery HEPs.

t	P_(OPR(t))	P_(DGR(t))
4 hours (baseline)	3.1E-01 (GR); 1.1E-01 (PC); 2.1E-01 (SC); 5.5E-01 (WR)	7.3E-01
8 hours	1.4E-01 (GR); 4.7E-02 (PC); 1.0E-01 (SC); 4.1E-01 (WR)	6.0E-01
12 hours	7.4E-02 (GR); 2.6E-02 (PC); 6.2E-02 (SC); 3.4E-01 (WR)	5.1E-01
24 hours	2.1E-02 (GR); 8.1E-03 (PC); 2.3E-02 (SC); 2.1E-01 (WR)	3.3E-01

Table 10-4. LOOP CDF Results (Per Reactor Year) Given Extended Battery Life.

LOOP Category	4 hours (baseline)	8 hours	12 hours	24 hours
LOOPGR	5.0E-07	4.7E-07	4.6E-07	4.3E-07
LOOPPC	7.4E-08	7.2E-08	7.1E-08	6.9E-08
LOOPSC	5.8E-07	5.6E-07	5.4E-07	5.1E-07
LOOPWR	5.6E-07	5.0E-07	4.6E-07	3.7E-07
Total	1.7E-06	1.6E-06	1.5E-06	1.4E-06
Delta	0.0E+00	-1.1E-07	-1.8E-07	-3.3E-07
Delta%	0%	-6%	-11%	-20%

The results shown in Table 10-4 assume the battery (including switchyard batteries when needed) life is successfully extended. However, the alternatives of extending battery capacity are conditioned on battery reliability and different sets of human actions which need to be performed after LOOP occurs and are not always successful. When calculating the risk impacts of each battery capacity extension alternative, the results in Table 10-4 need to be adjusted by considering the success probabilities of extension alternatives. If assuming the reliability of new batteries is on the same or better level than the existing batteries, the battery failure probability is usually much lower than error probabilities of human actions and thus are not further examined. The human actions determining alternative success probability are presented in Table 10-5.

- For Alternatives 1 and 4, operators need to perform load shedding to extend battery life. A recent U.S. NRC study (Cooper and Franklin, 2020) on performing load shedding at a BWR was used as the basis to estimate the load-shedding HEPs for this paper. Although the NRC study was conducted for scenarios using FLEX strategy, it has an analogy to this study in both the BWR focus and the LOOP-mitigation context. The NRC study estimated the HEP of performing FLEX DC load shedding for a BWR ranges from 2E-03 to 6E-03. This study adopts the minimum and average of this range as the HEPs for Human Action #1.1 and #4.1, respectively, considering that extending to a longer life requires shedding more loads, involves more manipulations, and increases the probability of human error.
- For Alternatives 2, 5, and 7, existing batteries and new batteries were used in series to provide prolonged DC power supply. Before existing batteries deplete, operators need to start new batteries to continue power supply. This study assumes the level of complexity does not vary with the capacities of new batteries and adopts a generic value of 1.1E-02 as the same HEP for Human Actions #2.1, #5.1, and #7.1. Such value is obtained by adding up a diagnosis HEP of 1E-02 and an action HEP of 1E-03, which are the base rates used in the Standardized Plant Analysis Risk-Human Reliability Analysis (SPAR-H) method (Gertman et al., 2005).
- For Alternatives 3, 6, and 8, existing batteries were replaced by new batteries with extended capacity. Such replacements should be completed during normal plant operations and maintenance, and no additional human actions need to be performed after LOOP. The corresponding HEPs are thus assumed as zero.

Table 10-5. Post-LOOP Human Actions Affecting Alternatives of Providing Additional DC Power.

No.	Alternative	Influencing Human Action	HEP
1	Extending battery life to 8 hours (extending life of existing batteries by load shedding)	(#1.1) Operators perform load shedding	2E-03
2	Extending battery life to 8 hours (keeping existing batteries and introducing new batteries)	(#2.1) Operators start new batteries before existing batteries deplete	1.1E-02
3	Extending battery life to 8 hours (replacing existing batteries with new batteries with extended life)	None	0
4	Extending battery life to 12 hours (extending life of existing batteries by load shedding)	(#4.1) Operator perform load shedding	4E-03
5	Extending battery life to 12 hours (keeping existing batteries and introducing new batteries)	(#5.1) Operators start new batteries before existing batteries deplete	1.1E-02
6	Extending battery life to 12 hours (replacing existing batteries with new batteries with extended life)	None	0
7	Extending battery life to 24 hours (keeping existing batteries and introducing new batteries)	(#8.1) Operators start new batteries before existing batteries deplete	1.1E-02
8	Extending battery life to 24 hours (replacing existing batteries with new batteries with extended life)	None	0

By incorporating the effects of extended AC power recovery time windows and potential human errors when extending the time windows in the PRA model, the projected risk-reduction impacts of Alternatives #1–8 were calculated and shown in Table 10-6. It can be observed the effects on LOOP CDF reduction of multiplying (1-HEP) are negligible since the HEPs are quite low. But this does not suggest waiving the process of estimating and incorporating HEPs. The study in this paper is a generic, illustrative example, and the plant-specific, real-world analyses may yield significantly different HEP estimates.

Table 10-6. LOOP CDF Reduction Impacts of Alternatives for Providing Additional DC Power.

No.	Alternative	LOOP CDF Reduction (%)
1-3	Extending battery life to 8 hours	6%
4-6	Extending battery life to 12 hours	11%
7	Extending battery life to 24 hours (keeping existing batteries and introducing new batteries)	19%
8	Extending battery life to 24 hours (replacing existing batteries with new batteries with extended life)	20%

10.2.2 Risk Impact of Alternative Providing Additional AC Power

In the generic BWR LOOP scenarios, AC power can be supplied by one of three onsite EDGs (two regular and one supplementary). To evaluate the risk impact of Alternative #9, a system consisting of battery and inverter (converting DC power to AC power) is incorporated into the FT as the fourth onsite AC supply source. Hardware failure modes of this alternative include battery failure and inverter failure, but their failure probabilities are usually much lower than error probabilities of human actions. This alternative involves one human action of aligning the battery and inverter. The HEP of this action is estimated as 1.1E-02 in a similar way of estimating HEPs for Human Actions #2.1, #5.1 and #7.1. The projected risk-reduction impact of Alternative #9 is quantified with SAPHIRE 8 and presented in Table 10-7.

Table 10-7. LOOP CDF Reduction Impact of Alternative Providing Additional AC Power.

No.	Alternative	LOOP CDF Reduction (%)
9	Introducing new batteries as backup for onsite EDGs	41%

10.3 Evaluating Impacts on Plant Economics

This section qualitatively discusses the projected costs of implementing the alternatives of extending battery capacity at the generic BWR plant. The projected costs are additional costs compared to the current base case of utilizing batteries with 4-hour life. As shown in Table 10-8, all the alternatives are projected to incur the cost of updating procedures and conducting associated trainings to accommodate the mitigation strategy changes. Alternatives #2, 5, 7, and 9 are projected to incur additional maintenance costs since existing batteries are kept, and new batteries are introduced. With the exception of Alternatives #1 and 4, all alternatives are projected to incur costs of purchasing and installing new batteries and/or inverters, and the costs are projected to vary with battery capacity. Assuming the batteries ordered for Alternative #9 have a larger capacity than the batteries ordered for Alternative #8 and further assuming the costs of purchasing batteries are much higher than maintenance costs, the projected costs of all the alternatives can be ranked as: C9 > C8 > C7 > C6 > C5 > C3 > C2 > C1 = C4. The projected costs of the alternatives can also be preliminarily categorized as three levels, including High Cost (Alternative #9), Medium Cost (Alternatives #2, 3, 5, 6, 7, and 8), and Low Cost (Alternatives 1 and 4).

Table 10-8. LOOP CDF Reduction Impact of Alternative Providing Additional AC Power.

No.	Alternative	Projected Costs
1	Extending battery life to 8 hours (extending life of existing batteries by load shedding)	Cost of updating procedures and training
2	Extending battery life to 8 hours (keeping existing batteries and introducing new batteries)	Cost of purchasing and installing new batteries with 4-hour life; cost of updating procedures and training; maintenance cost for new batteries
3	Extending battery life to 8 hours (replacing existing batteries with new batteries with extended life)	Cost of purchasing and installing new batteries with 8-hour life; cost of updating procedures and training
4	Extending battery life to 12 hours (extending life of existing batteries by load shedding)	Cost of updating procedures and conducting training
5	Extending battery life to 12 hours (keeping existing batteries and introducing new batteries)	Cost of purchasing and installing new batteries with 8-hour life; cost of updating procedures and training; maintenance cost for new batteries
6	Extending battery life to 12 hours (replacing existing batteries with new batteries with extended life)	Cost of purchasing and installing new batteries with 12-hour life; cost of updating procedures and training
7	Extending battery life to 24 hours (keeping existing batteries and introducing new batteries)	Cost of purchasing and installing new batteries with 20-hour life; cost of updating procedures and training; maintenance cost for new batteries
8	Extending battery life to 24 hours (replacing existing batteries with new batteries with extended life)	Cost of purchasing and installing new batteries with 24-hour life; cost of updating procedures and training
9	Introducing new batteries as backup for onsite EDGs	Cost of purchasing and installing inverters and new batteries with capacities comparable to EDGs; cost of updating procedures and training; maintenance cost for new batteries

10.4 Conducting Alternative Comparison

This section compares the alternatives of extending battery capacity from the perspectives of plant risk and plant economics. The risk impacts (quantified in Section 10.2) and the cost impacts (qualitatively ranked in Section 10.3) of all the alternatives are displayed in Figure 10-2. Risk impact is quantitatively measured using percentage of LOOP CDF reduction in y-axis. Cost impact is not quantified but qualitatively ranked in x-axis (1 as lowest cost and 9 as highest cost).

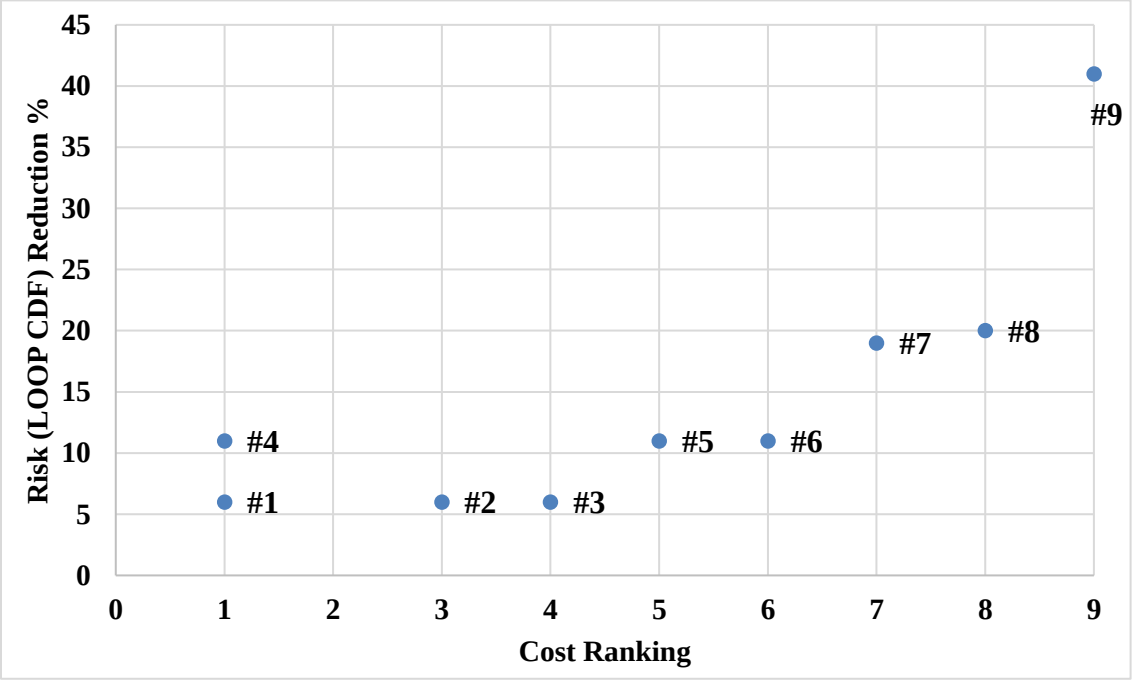

Figure 10-2. Impacts on Plant Risk and Cost of Implementing Alternatives of Extending Battery Capacity at a Generic BWR Plant.

It can be observed Alternative #9 is estimated to have the largest risk reduction but with the largest projected cost. Alternatives #1 and 4 are projected to have the same lowest cost but Alternative #4 is estimated to have a larger risk reduction. Based on this figure, the impacts on plant risk and economics appear to be competing against each other. It is worthwhile to mention this competing relationship is obtained from the limited analysis scope in this paper which only considers the accident-mitigation benefits of batteries. If the benefits of supporting normal operation and maintenance can be evaluated in future research, the relationship between plant risk and cost impacts may be different.

10.5 Conclusion and Future Work Plan

This study conducts a preliminary evaluation of the potential costs and benefits of deploying increased-capacity batteries at a generic BWR plant. Nine alternatives for extending battery capacity are developed, including eight alternatives for providing additional DC power and one alternative for providing additional AC power. Potential benefits of reducing plant risk are quantified through incorporating the alternatives into LOOP scenarios of the generic BWR SAPHIRE model. Potential costs of implementing the alternatives are qualitatively discussed and ranked. The alternatives are compared based on their impacts on plant risk and economics. The current list of alternatives will be presented to industry partners to evaluate the feasibility of listed alternatives and potentially propose additional alternatives. For future work, a multi-criterion benefit evaluation (MCBE) methodology, which is developed under the ERP project (Ma, et al., 2020; Zhang et al., 2021), will be utilized for a more comprehensive evaluation.

11. MITIGATING SYSTEM PERFORMANCE INDEX OPTIMIZATION PROCESS

11.1 Background

MSPI is one of the risk-informed, plant-specific performance indicators of the U.S. NRC Reactor Oversight Process (ROP). It is used by the regulator and nuclear industry to monitor and assess the performance of plant mitigating systems. The MSPI was developed by the NRC's Office of Nuclear Regulatory Research (RES) to replace the previously adopted safety system unavailability (SSU) performance index (PI), because the NRC and industry identified several drawbacks associated with the use of SSU PI in the ROP. For example, the use of fault exposure hours and short-term unavailability to estimate unreliability, the use of generic performance thresholds without consideration of the risk significance of the system, potential for double-counting support system failures, inconsistency between SSU PI and the NRC's Maintenance Rule, as well as the indicators issued by World Association of Nuclear Operators and Institute of Nuclear Power Operations (INPO), etc. (U.S. Nuclear Regulatory Commission, 2005).

To address those identified issues related to the use of SSU PI, the Risk-Based Performance Indicator (RBPI) development program was initiated by NRC to explore further improvements to the ROP PIs (U.S. Nuclear Regulatory Commission, 2002). In the first phase of this program, the plant-specific standardized plant analysis risk models were proposed to be used for quantifying the risk significance resulted from the changes in unavailability and unreliability, the enhancement showed the feasibility to solve most of the issues mentioned above. However, the RBPIs also showed some disadvantages, for instance, by implementing separate unavailability and unreliability indicators; the amount of the indicators would increase, which may result in concerns about the effect on the action matrix, as well as the numerical inaccuracy (U.S. Nuclear Regulatory Commission, 2005).

Based on the achieved improvement as well as accounting for the new issues raised by the proliferation of indicators in the RBPI development program, the new approach, known as the MSPI, was developed by the NRC's Office of RES to quantify the risk significance of changes in unreliability and unavailability separately and combines them into a single system-level indicator using a simplified formula based on importance measures, which eliminate the need of manipulations of the entire risk model. To assess the new MSPI approach, the RES staff and industry initiated a 12-month MSPI pilot program in 2002 with 20 plants participating. This program included 6 months of data collection and 6 months of data analysis (U.S. Nuclear Regulatory Commission, 2005). The result of this pilot program proved the MSPI feasibility to a certain degree.

In FY 2021, Tennessee Valley Authority (TVA) and the INL ERP team collaborated and conducted an investigation of optimizing MSPI through advanced AI and ML techniques to improve NPP safety and efficiency. TVA has the willingness to improve its safety and economy through its fleet and could contribute to the effort by providing the plant-specific operational data. On the other hand, the INL ERP research has the mission to enhance existing reactors' safety features and to substantially reduce operating costs of nuclear plants through risk-informed approaches. The purpose of this collaboration is to develop a process to optimize MSPI with the data-based reasoning to address the off-normal equipment conditions, to utilize the ranking of the root causes and potential resolutions to find the best option of economically reducing MSPI value, and to facilitate and simplify the risk-informed and reliability-related decision-making for continuous improvement. The MSPI optimization process could provide practical insights and options to make the safety, risk-informed and reliability-based decision for performance and cost efficient. This process can be extended to other industry or plant specific performance index (PI).

In the remaining of this section, Section 11.2 describes how MSPI is calculated; Section 11.3 presents the MSPI optimization approaches as well as the tasks associated with the optimization process; Section 11.4 introduces an integrated MSPI calculation and optimization process which combines the existing MSPI program and the new proposed MSPI optimization, as well as the development of an MSPI calculation using the Python programming language to automate the MSPI calculation and generate MSPI report; Section 11.5 provides a summary of the section.

11.2 MSPI Calculation

11.2.1 MSPI Basic Calculation

According to NEI 99-02 (Nuclear Energy Institute, 2013), "Regulatory Assessment Performance Indicator Guideline," the purpose of the MSPI is to monitor the performance of selected systems based on their ability to perform risk-significant functions. The MSPI is calculated individually for each of the mitigating systems that are chosen to be monitored in the MSPI program for PWR and BWR (see **Error! Reference source not found.**). In general, these mitigating systems are selected due to their capability of mitigating the effects of initiating events to prevent CD. In the current practice, each reactor unit has MSPIs for five safety-important systems. The MSPI is used to determine the cumulative significance of the system/component failures and unavailability over the monitored time period.

Table 11-1. MSPI Mitigating Systems for PWR and BWR.

Index[a]	PWR Systems	BWR Systems
MS06 (emergency AC [EAC])	EAC Power System	EAC Power System
MS07 (HPI)	HPI System	HPI System
MS08 (heat removal))	AFW System	RCIC System (or isolation condenser)
MS09 (residual heat removal)	RHR System	RHR System
MS10 (support cooling)	Cooling Water Support System[b]	Cooling Water Support System[b]

[a] The index numbering does not start with 01, because the MSPIs discussed in this section are part of the NRC regulatory assessment performance indicators (Nuclear Energy Institute, 2013).

[b] Cooling water support system includes service water, component cooling water, or the equivalent system).

The MSPI is the numerical sum of changes in a simplified CDF evaluation due to the differences in unavailability (UA) and unreliability (UR) relative to industry baseline values for the previous 12 quarters. The MSPI is calculated for each monitored mitigating system and is the sum of the Unavailability Index (UAI) and the Unreliability Index (URI) due to UA and UR of the system, respectively.

$$MSPI = UAI + URI \qquad (11\text{-}1)$$

The above MSPI basic calculation is then supplemented by the risk cap (see Section 11.2.2) and system component performance limits (see Section 11.2.3).

The UAI is evaluated for all trains within each mitigating system, while URI is evaluated for all monitored components within each mitigating system. The UAI and URI are calculated as follows:

$$UAI = CDF_P \left(\Sigma \frac{FV_P}{UA_P} \right) (UA_C - UA_B) \qquad (11\text{-}2)$$

$$URI = CDF_P \left(\Sigma \frac{FV_P}{UR_P} \right) (UR_C - UR_B) \qquad (11\text{-}3)$$

where:

CDF_P = Plant-specific CD frequency (from plant PRA)

FV_P = Fussell-Vesely importance measure of the train or component (from plant PRA)

UA_P = Plant-specific train unavailability (from plant PRA)

UA_C = Current train unavailability (data from most recent 12 quarters)

UA_B = Baseline train unavailability (from Appendix F of NEI 99-02)

UR_P = Plant-specific component UR (from plant PRA)

UR_C = Current component UR (Bayesian update using data from most recent 12 quarters)

UR_B = Baseline component UR (from Appendix F of NEI 99-02)

An example set of the industry baseline values for train UA and component UR are shown in Table 11-2 and Table 11-3. These baseline values are updated for the industry periodically.

Table 11-2. Industry Baseline Data for Train UA (Eide & Zeek, 2004).

System	Train Type	Baseline UA
EAC power system	EDG	1.30E-02
HPI	Motor-operated valve (MOV)	5.80E-03
HPCI	Turbine-driven pump (TDP)	1.00E-02
AFW	Motor-driven pump (MDP)	4.80E-03
	TDP	4.90E-03
	Diesel-driven pump	8.40E-03
RCIC	TDP	1.20E-02
RHR (BWR)	MDP	6.20E-03
RHR(PWR)	MDP	6.00E-03
Service water system	MDP	2.00E-02
Component cooling system	MDP	8.20E-03

Table 11-3. Baseline Data for Component UR (Nuclear Energy Institute, 2013).

Component	Failure Mode	Baseline UR
Circuit breaker	Fail to open (or close)	8.00E-04
Hydraulic-operated valve	Fail to open (or close)	1.00E-03
MOV	Fail to open (or close)	7.00E-04
Solenoid-operated valve	Fail to open (or close)	1.00E-03
Air-operated valve	Fail to open (or close)	1.00E-03
MDP, standby	Fail to start	1.90E-03
	Fail to run	5.00E-05
MDP, running/alternating	Fail to start	1.00E-03
	Fail to run	5.00E-06
TDP, AFW	Fail to start	9.00E-03
	Fail to run	2.00E-04
TDP, HPCI or RCIC	Fail to start	1.30E-02
	Fail to run	2.00E-04
Diesel-driven pump, AFWS	Fail to start	1.20E-02
	Fail to run	2.00E-04
EDG	Fail to start	5.00E-03
	Fail to load/run	3.00E-03
	Fail to run	8.00E-04

As shown in Table 11-4, a performance color is assigned to the MSPI results for each mitigating system according to its numerical value.

Table 11-4. MSPI Limits and Color Scale.

Condition	Performance Color
MSPI $\leq 10^{-6}$	GREEN
$10^{-6} <$ MSPI $\leq 10^{-5}$	WHITE
$10^{-5} <$ MSPI $\leq 10^{-4}$	YELLOW
MSPI $\leq 10^{-4}$	RED

11.2.2 MSPI Frontstop (Risk Cap)

According to the MSPI pilot program report NUREG-1816 (U.S. Nuclear Regulatory Commission, 2005), several significant issues were identified regarding the MSPI methodology described in NEI 99-02, and some major recommendations were provided based on the issues to improve the MSPI methodology. Among the six major recommendations, two of them are associated with the sensitive issues of MSPI: frontstop and backstop. The concept of "frontstop" was proposed to address the "invalid" or "false positive" indicator issue, while the concept of "backstop" was proposed to address the "insensitive" indicator issue.

Within the MSPI pilot program, the NRC staff recognized there is a significant probability the performance of a mitigating system will cross over the GREEN/WHITE threshold and turn into WHITE due to just one failure above baseline during the 12-quarter monitoring period. These sensitive indicators were so-called "invalid" or "false positive" indicators. Therefore, the "frontstop" then was proposed to treat this sensitive issue, this concept was discussed in detail in Appendix D of the NUREG-1816.

In general, the introduced "frontstop" solution applies a risk cap (5.0E-07) for the most risk significant failure to ensure one failure beyond the expected number of failures would not result in WHITE (MSPI > 10^{-6}). However, the "frontstop" is only applied if the original MSPI value is below GREEN/WHITE threshold (10^{-6}).

11.2.3 MSPI Backstop (Performance Limit)

In contrast to the sensitive indicator issue, the insensitive indicator issue was addressed using the proposed "backstop" concept. The insensitive indicator refers to the components for which a significant amount of failures would be required to result in the MSPI greater than the GREEN/WHITE threshold (10^{-6}). To address the insensitive issue, a performance-based limit was developed such that a system would be placed in the WHITE band when there is a high confidence that system performance has degraded even though the MSPI value is below the GREEN/WHITE threshold (10^{-6}). The "backstop" concept was discussed in detail in Appendix E of NUREG-1816 and Appendix F of NEI 99-02.

Generally speaking, if the actual number of failures (F_a) for a specific component type within a mitigating system of the plant that exceeds a performance-based limit (backstop value) during the 12-quarter monitoring period, then the performance of this mitigating system would be placed at WHITE band regardless of the calculated MSPI value.

The expected number of component failures is calculated using a linear correlation as follows:

$$F_e = N_d * p + \lambda * T_r \quad (11\text{-}4)$$

where:

F_e = Expected number of failures

N_d = Number of demands

p = Probability of component failure on demand (from Table 11-3)

λ = Component failure rate (from Table 11-3)

T_r = Runtime of the component

The performance limit (maximum number of component failures) is determined as follows:

$$F_m = 4.65 * F_e + 4.2 \quad (11\text{-}5)$$

where:

F_m = Maximum number of component failures

Based on the backstop definition, if $F_a > F_m$ for a given component type within the monitoring period, the performance of the MSPI would be placed in the WHITE performance band. Taking into account the backstop concept, the updated performance thresholds of the MSPI and the corresponding color scale are shown in Table 11-5.

Table 11-5. Updated MSPI Limits and Color Scale.

Condition	Performance color
MSPI $\leq 10^{-6}$ and $F_a \leq F_m$	GREEN
MSPI $\leq 10^{-6}$ and $F_a > F_m$	WHITE
$10^{-6} <$ MSPI $\leq 10^{-5}$	
$10^{-5} <$ MSPI $\leq 10^{-4}$	YELLOW
MSPI $> 10^{-4}$	RED

11.3 MSPI Optimization

The investigation of MSPI optimization includes applying the data-based reasoning to address the off-normal equipment conditions, to utilize the ranking of the root causes and potential resolutions to find the best option of economically reducing MSPI value, and to facilitate and simplify the risk-informed and reliability-related decision-making for continuous improvement. The product of this effort is to design and develop the MSPI optimization process to improve the safety, reliability, and economy of NPPs. The optimization process can provide practical insights and options to make the safety, risk-informed and reliability-based decision for performance and cost efficient. This is a bi-direction process from data to the equipment reliability, to the plant-specific PI and industry-wise PI (which can be developed); and vice versa.

11.3.1 MSPI Optimization Approaches

There are two types of MSPI optimization approach (Figure 11-1). One is PI/MSPI oriented approach in which MSPI optimization process can be developed based on data, PRA model, and plant operation inputs, with the following stages:

- Data collection and characterization stage—to collect the parameters of plant designs and baselines, as well as the immediate plant operation data

- Calculation stage—to generate the optimization equations and enumerate all the acceptable PI case
- Visualization stage—to present the data in graphs for the decision-making.

The other one in data-oriented approach in which the MSPI optimization process starts from a target PI and dive into the database to identify the contributing events and find the root causes from the data analysis of the numeric and text data and summarize the information for resolutions.

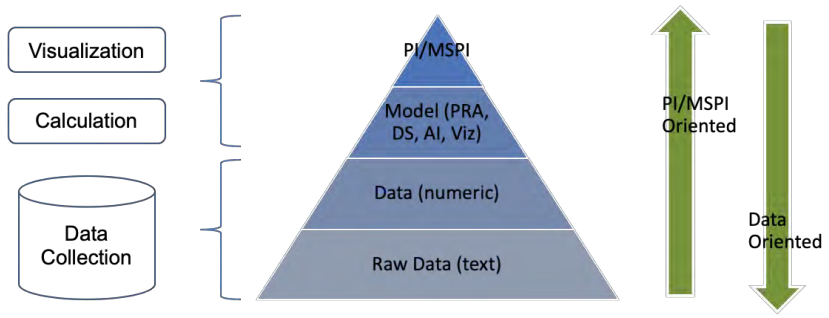

Figure 11-1. MSPI Optimization Approaches.

Development of MSPI optimization methodology is an interdisciplinary effort. It is a fusion of technical fields of PRA modeling, data science (DS) techniques (e.g. big data, statistic and probability, data mining techniques), AI and ML techniques including natural language processing (NPL), decision trees, and visualization (Viz).

11.3.2 MSPI Optimization Tasks

To reduce risk, improve reliability, and build a model for risk-informed decision-making, there are three major tasks in developing the MSPI optimization process:

1. Develop MSPI system objective functions
2. Extend MSPI system objective functions and fusion with AI technique
3. Develop MSPI plant objective function by aggregating system objective functions into one plant level MSPI optimization function.

11.3.2.1 Developing MSPI System Objective Functions

This task will derive and implement system objective functions in the existing MSPI program. With all the information in the MSPI margin objective equation, the analyst can pre-define the maximum allowed combinations of UA time and UR failures for each system and closely monitor the low-margin MSPI systems, thus the MSPI margin and risk can be tightly controlled and keep remaining green, especially when there are less margin (e.g., no more than three UR failures).

11.3.2.2 Extension of MSPI System Objective Function and Fusion with AI Technique

One set of core parameters of the objective functions is the risk importance. The risk information about the plant design, its operation and maintenance is directly or indirectly encoded into risk importance parameters. Higher risk importance means higher risk. From the high-risk importance, one can identify the risk significant contributors and reduce its risk impact accordingly. The other set of key parameters embedded in the objective functions are UA and UR performance and baselines, where the performance expectations are directly or indirectly encoded into the performance baselines. The tasks planned for this step include the following:

(1) Develop a method to find the root cause of the risk-significant contributors to the risk importance such as IE frequency, equipment failure probability or rate (run time and demand), or operator action, etc. Using the PRA software like SAPHIRE, the risk-significant contributors can immediately become available after the PRA model is quantified. However, it can be a tedious, labor-intensive, and time-consuming process to look into the root cause of the risk-significant contributors and find the related

potential events in the industry OpE database. Such process is a top to bottom data/facts oriented process and can be automated and empowered using the AI techniques. Use AI techniques like NPL could be helpful to search and group the root causes and/or effects and extract and summarize supporting information such as time, correlation, frequency, and potential solutions from OpE database. Based on risk or cost significance, use AI techniques like ML and pattern recognition can help to rank the causes and correction actions.

(2) Develop a method to balance maintenance cost/frequency and reliability improvements for risk significant equipment. The goal is to reduce maintenance frequency while maintaining or improving risk metrics.

11.3.2.3 Developing MSPI Plant Objective Function

The above optimization/objective equations are the MSPI margin management at a system-level. It can be extended to plant level by aggregating five MSPI system objective functions into one MSPI plant objective function, so the plant can focus its resource and efforts on the risk-important structures, systems, and components (based on PRA and risk application 50.69) efficiently.

11.4 Integrated MSPI Calculation and Optimization Process

This section presents the integrated MSPI calculation and optimization process that combines the current MSPI program based on the NEI 99-02 guideline and the MSPI optimization process described in Section 11.3. The integrated process consists of four main stages as shown in Figure 11-2: (1) input preparation stage, (2) MSPI calculation stage, (3) result analysis stage, and (4) optimization stage.

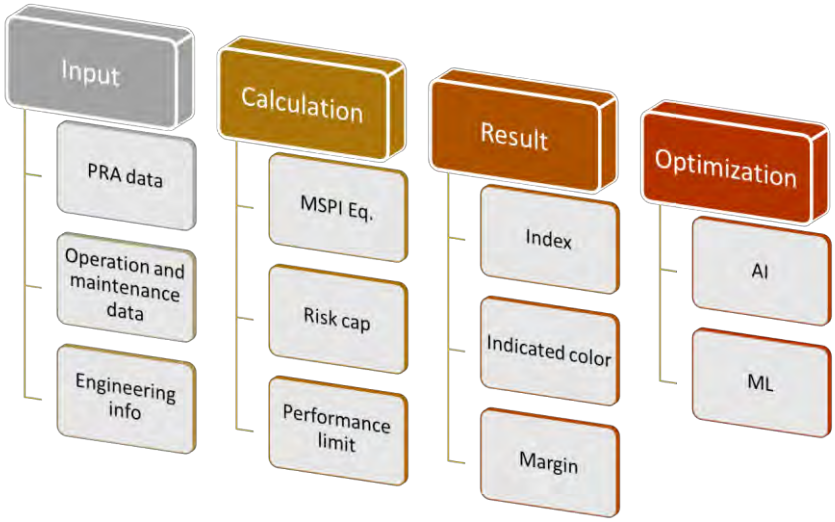

Figure 11-2. MSPI Optimization Stages.

11.4.1 Stage 1: Input Preparation

In the first stage, the input data used to evaluate the MSPI includes PRA data, plant engineering information, and plant operation and maintenance data. More detailed information is shown in Table 11-6.

Table 11-6. Input Data for MSPI Evaluation.

PRA data	• CDF • Fussell-Vesely Importance
Engineering info	• Identification of monitored systems trains - Determine the system boundaries

	- Identify the trains within the system boundary • Identification monitored components for each system - Use of system boundaries - Use of SC
Plant operation and maintenance data	• UAI - Current train unavailability (planned and unplanned) data for the previous 12-quarter monitoring period - Baseline data – Plant planned unavailability baselines: NEI 99-02 states that these values are based upon actual plant-specific values from 2002 to 2004. – Generic unplanned unavailability baselines (see Table 11-7 for the values provided by NEI 99-02 based on ROP industry data from 1999 through 2001)
	• URI - Current component unreliability: Bayesian corrected plant-specific values for all failure modes (Failure modes defined for each component type are shown in Table 11-3) - Baseline data: values of unreliability for all failure modes (see Table 11-3 for the example data set)
	• Maintenance info

Table 11-7. Historical Unplanned Unavailability Train Values (Nuclear Energy Institute, 2013).

System	Unplanned Unavailability/Train
EAC	1.7E-03
PWR HPI	6.1E-04
PWR AFW (turbine-driven)	9.1E-04
PWR AFW (motor-driven)	6.9E-04
PWR AFW (diesel-driven)	7.6E-04
PWR RHR (except Combustion Engineering design)	4.2E-04
PWR RHR (Combustion Engineering design)	1.1E-03
BWR HPCI	3.3E-03
BWR high-pressure core spray	5.4E-04
BWR feedwater coolant injection	Use plant-specific Maintenance Rule data for 2002-2004
BWR RCIC	2.9E-03
BWR IC	1.4E-03
BWR RHR	1.2E-03
Support cooling	Use plant-specific Maintenance Rule data for 2002-2004

11.4.2 Stage 2: MSPI Calculation

To develop the MSPI optimization process, the calculation of MSPI is required to be performed first. Normally the MSPI calculation in the industry is performed by the INPO's Consolidated Data Entry web-based tool. However, this tool is only available to its members. There are also other MSPI calculation tools that were developed by various companies and are available for purchase. In this section, following the MSPI evaluation as well as the frontstop (risk cap) and backstop (performance limit) described in Section 11.2, an MSPI calculation tool has been developed using the Python programming language, by incorporating the plant operation data, PRA data, and industry baseline values to automate the calculation process of MSPI and generation of the report.

The MSPI calculation tool starts from raw industry data as well as plant-specific data for IEs, equipment reliability and unavailability, etc. In addition, the system-level and plant-level PRA modeling (plant design, operation, maintenance, operator actions, etc.), PRA quantification and risk insights, PI/MSPI program (plant online time, system train unavailable time and equipment unreliability failures, engineering data, expected baselines) are taken into account.

The MSPI calculation flow chart is depicted in Figure 11-3. In general, the calculation is performed in five major steps:

- Determine the MSPI system
- Identify the trains and components of the selected MSPI system
- Data collection and input file preparation: including the system information, operational data, and PRA data
- MSPI calculation with frontstop (risk cap) and backstop (performance limit) incorporated
- Result generation.

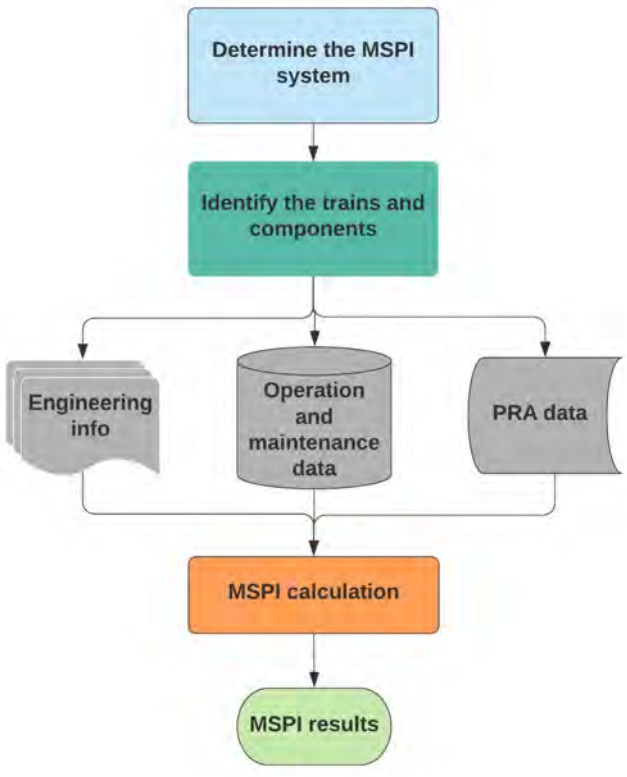

Figure 11-3. MSPI Calculation Flowchart.

11.4.3 Stage 3: Result Analysis

To examine the applicability and validation of the algorithm, the MSPI calculation tool was tested with the data from a collaborating NPP. The EAC system of this plant was selected. The input data including the train unavailability and component unreliability for Unit 1 and Unit 2 are shown from Table 11-8 to Table 11-11, respectively. The calculated MSPI value generated by the MSPI tool for Unit 1 and Unit 2 agrees well with the one from the plant which demonstrates the feasibility of the calculation tool.

After the MSPI value was generated using the MSPI calculation tool in the previous stage, further analysis will be conducted in this stage, consisting of assigning the associated performance color to the MSPI results according to Table 11-5 in Section 11.2, and safety margin evaluation done by comparing the calculated value with the objective value.

Table 11-8. Unit 1 EAC Train Unavailability Data.

	Risk Importance	Plant	Time (h)	Baseline	Time (h)
TRN1A	1.13E-10	Planned UA	212.75	Planned Baseline	250.4
TRN1A		Unplanned UA	8.62	Unplanned Baseline	39.05
TRN1B	1.13E-10	Planned UA	402.72	Planned Baseline	214.11
TRN1B		Unplanned UA	12.47	Unplanned Baseline	39.05
TRN2A	1.13E-10	Planned UA	240.32	Planned Baseline	234.32
TRN2A		Unplanned UA	81.78	Unplanned Baseline	39.05
TRN2B	1.13E-10	Planned UA	465.66	Planned Baseline	228.58
TRN2B		Unplanned UA	140.46	Unplanned Baseline	39.05

Table 11-9. Unit 1 EAC Component Unreliability Data.

Component	Risk Importance	Failure numbers
DG Fail to Start (FTS) Failure(s)	2.16E-08	2
DG Fail to Load (FTL) Failure(s)	1.832E-08	1
DG Fail to Run (FTR) Failure(s)	1.47E-07	1

Table 11-10. Unit 2 EAC Train Unavailability Data.

	Risk Importance	Plant	Time (h)	Baseline	Time (h)
TRN1A	1.32E-10	Planned UA	213.97	Planned Baseline	228.47
TRN1A		Unplanned UA	8.62	Unplanned Baseline	35.63
TRN1B	1.32E-10	Planned UA	403.45	Planned Baseline	195.35
TRN1B		Unplanned UA	70.14	Unplanned Baseline	35.63
TRN2A	1.32E-10	Planned UA	115.51	Planned Baseline	213.8
TRN2A		Unplanned UA	81.78	Unplanned Baseline	35.63
TRN2B	1.32E-10	Planned UA	265.46	Planned Baseline	208.56
TRN2B		Unplanned UA	140.46	Unplanned Baseline	35.63

Table 11-11. Unit 2 EAC Component Unreliability Data.

Component	Risk Importance	Failure Numbers
DG Fail to Start (FTS) Failure(s)	2.16E-08	2
DG Fail to Load (FTL) Failure(s)	1.84E-08	1
DG Fail to Run (FTR) Failure(s)	1.48E-07	1

11.4.4 Stage 4: MSPI Optimization

Due to the resource limitation, the MSPI optimization process and tasks are not conducted in FY 2021. Future research efforts will be dedicated to accomplish the MSPI optimization tasks described in Section 11.3.

11.5 Summary of MSPI Optimization Process

This section documents the collaborate activity conducted by TVA and INL to investigate the optimization of MSPI through advanced AI and ML techniques to improve NPP safety and efficiency. The background information on MSPI as well as how MSPI is calculated in current MSPI program are described. Two types of MSPI optimization approaches are introduced. The PI/MSPI oriented approach starts from data, PRA model, and plant operation inputs to generate MSPI optimization equations (or object functions) and present results to decision-maker. The data-oriented approach starts from a target PI and dive into the database to identify the contributing events and find the root causes from the data analysis of the numeric and text data and summarize the information for resolutions. The three major tasks for MSPI optimization include developing MSPI system objective functions, extending MSPI system objective functions and fused with AI technique, and developing MSPI plant objective function by aggregating system objective functions into one plant level MSPI optimization function. An integrated MSPI calculation and optimization process is then proposed to combine the current MSPI program developed based on the NEI 99-02 guideline and the MSPI optimization process.

As the first step of the integrated MSPI calculation and optimization process, an MSPI tool was developed with the incorporation of the plant operation data, plant PRA data, and industry baseline values to automate the calculation process of MSPI and the generation of MSPI report. The tool was verified with the example data sets from an NPP. The case study demonstrates the feasibility of the proposed calculation tool.

12. CONCLUSIONS AND FUTURE WORK

This report presents the ERP R&D efforts in FY 2021, which are focused on three industry initiatives, including ATF, FLEX, and advanced battery technology with extended capacity. One focus area of the ATF efforts is to extend the FY 2020 analyses on a generic BWR. The same analysis process and analysis tools as in the FY 2020 work were used with two near-term ATF cladding (i.e., FeCrAl cladding and Cr-coated cladding) designs under four types of postulated scenarios, including general transient, LOMFW, SLOCA, and IORV. Another focus area of the ATF efforts is to conduct a benchmark study between a generic PWR SAPHIRE model, which was used in the FYs 2018 and 2019 ATF analyses under the ERP project, and a plant-specific PRA model of a reference NPP. An agreement was reached between the ERP team and the nuclear power industry to conduct a benchmark study between the generic PRA model and a representative plant-specific PRA model. A third-party consulting company, Jensen Hughes, was subcontracted to conduct the benchmark study. The FLEX efforts are focused on continued development of a dynamic approach for FLEX HRA with EMRALD. The efforts on the advanced battery technology include a risk impact analysis and an economic impact analysis of deploying batteries with extended capacity at a generic BWR plant. Besides the industry-initiative-focused analyses, the work of optimizing MSPI is also planned under the ERP project, and some preliminary work is done in the FY 2021.

For future work, we recommend the following activities for the ERP R&D:

- Coordinate and collaborate with industry leading institutions to apply RISA methods and toolkit to evaluate non-ELAP scenarios (e.g., loss of heat sink) where FLEX and other portable equipment are used for mitigation
- Collaborate with industry leading institutions to perform safety analyses focusing on risk-informed methodology with emphasis on fuel fragmentation, relocation, and dispersal for ATF with increased enrichment and extended burnup
- Crediting terry turbine for extended operation using the results from the completed terry turbine expended operating band testing and experimental work
- Refine the MCBE methodology, improve the existing MCBE case studies (i.e., FLEX and new battery technologies), and explore applying MCBE to evaluate additional plant safety enhancements.

13. REFERENCES

Boring and Rasmussen. (2016). GOMS-HRA: A method for treating subtasks in dynamic human reliability analysis. *Risk, Reliability and Safety: Innovating Theory and Practice, Proceedings of the 2016 European Safety and Reliability Conference*, (pp. 956-963).

Boring, R., et al. (2016). *Integration of Human Reliability Analysis Models into the Simulation-Based Framework for the Risk-Informed Safety Margin Characterization Toolkit.* Idaho National Laboratory.

Cathcart, J. V., & et al. (1977). *Reaction Rate Studies, IV, Zirconium Metal-Water Oxidation Kinetics.*

Cooper and Franklin. (2020). FLEX HRA using IDHEAS-ECA. *Advisory Committee on Reactor Safeguards Probabilistic Risk Assessment Subcommittee Meeting.* U.S. Nuclear Regulatory Commission.

Dallman, R. J., Gottula, R. C., Holcomb, E. E., Jouse, W. C., Wagoner, S. R., & Wheatley, P. D. (1987). *Severe Accident Sequence Analysis Program—Anticipated Transient Without Scram Simulations for Browns Ferry Nuclear Plant Unit 1, NUREG/CR-4165, EGG-2379.* EG and G Idaho, Inc.

Eide, S., & Zeek, D. (2004). Mitigating Systems Performance Index. *Probabilistic Safety Assessment and Management (pp. 1158–1162).* Springer, London.

EPRI. (2012, April 16). *Modular Accident Analysis Program: A Software Toll for Analyzing Nuclear Plant Accident Scenarios.* Electric Power Research Institute. Retrieved April 16, 2018, from https://www.epri.com/#/pages/product/000000000001025795

Field, K. G., Snead, M. A., Yamamoto, Y., & Terrani, K. A. (2017). *Handbook on the Material Properties of FeCrAl Alloys for Nuclear Power Production Applications.* Oak Ridge National Laboratory, Nuclear Technology R&D.

Gauntt, R. O., Cash, J., Cole, R. K., Erickson, C. M., Humphries, L., Rodriguez, S. B., & Young, M. F. (2005). *MELCOR Computer Code Manuals.* Nuclear Regulatory Commission.

Gertman et al. (2005). *The SPAR-H human reliability analysis method (NUREG/CR-6883).* U.S. Nuclear Regulatory Commission.

Global Nuclear Fuel. (2006). *GE14 for ESBWR Fuel Rod Thermal-Mechanical Design Report, Licensing Topical Report (NEDO-33242).* Global Nuclear Fuel.

GSE. (n.d.). *BWR Simulator Training Manuals.*

Gunther, W., et al. (2015). *Testing to Evaluate Extended Battery Operation in Nuclear Power Plants.* U.S. Nuclear Regulatory Commission.

Holzwarth, U., & Stamm, H. (2002). Mechanical and thermomechanical properties of commercially pure chromium and chromium alloys. *Journal of Nuclear Materials, 300*, 161-177.

Idaho National Laboratory. (2018). *Light Water Reactor Sustainability Program Integrated Program Plan.* Idaho National Laboratory.

Joe, J.C. and R.L. Boring,. (2017). Using the human systems simulation laboratory at Idaho national laboratory for safety focused research. *Advances in Human Factors in Energy: Oil, Gas, Nuclear and Electric Power Industries*, p. 193-201.

Johnson and Ma. (2019). *Analysis of Loss-of-Offsite-Power Events: 1987–2018, INL/EXT-19-54699.* Idaho National Laboratory.

Johnson and Schroeder. (2016). *Analysis of Loss-of-Offsite-Power Events 1997–2015, INL/EXT-16-39575.* Idaho National Laboratory.

Jung, W., D. Kang, and J. Kim. (2005). *A standard HRA method for PSA in nuclear power plant; K-HRA method. KAERI/TR-2961.*

Jung, W., et al. (2020). HuREX–A framework of HRA data collection from simulators in nuclear power plants. *Reliability Engineering & System Safety*, 194: p. 106235.

Ma. (2019). *Enhanced Component Performance Study: Emergency Diesel Generators 1998–2018, INL/EXT-19-54609.* Idaho National Laboratory.

Ma, et al. (2018). *Plant-Level Scenario-Based Risk Analysis for Enhanced Resilient PWR – SBO and LBLOCA.* Idaho National Laboratory.

Ma, et al. (2020). *Risk-Informed ATF and FLEX Analysis for an Enhanced Resilient BWR Under Design-Basis and Beyond-Design-Basis Accidents.* Idaho National Laboratory.

Ma, Z. et al. (2019a). *Risk-Informed Analysis for an Enhanced Resilient PWR with ATF, FLEX, and Passive Cooling (INL/EXT-19-53556).* Idaho National Laboratory. Retrieved from https://lwrs.inl.gov/RiskInformed%20Safety%20Margin%20Characterization/Risk-Informed_Analysis_for_ERP_w_ATF_FLEX.pdf

Ma, Z., et al. (2019b). *Evaluation of the Benefits of ATF, FLEX, and Passive Cooling System for an Enhanced Resilient PWR Model (INL/EXT/-19-56215).* Idaho National Laboratory. Retrieved from https://lwrs.inl.gov/RiskInformed%20Safety%20Margin%20Characterization/Evaluation_of_Benefits_of_ATF_FLEX_and_Passive_Cooling_System.pdf

Matev, A. (2006). Analysis of Operator Response to Station Blackout. *International RELAP5-3D User Group Meeting* . West Yellowstone: Idaho National Laboratory.

Nuclear Energy Institute. (2013). *Regulatory Assessment Performance Indicator Guideline (NEI 99-02, Revision 7).*

Nuclear Energy Institute. (2020). *Delivering the Nuclear Promise 2020 Top Innovative Practice: Exelon – BlackStarTechTM.*

Nuclear Engineering International. (2007, September). Fuel Design Data. *Nuclear Engineering International, 52*(638), p. 32.

OHara, J., J. Higgins, and S. Fleger. (2012). *Human factors engineering program review model (NUREG-0711) revision 3: update methodology and key revisions.* BROOKHAVEN NATIONAL LABORATORY.

Park, J., A.M. Arigi, and J. Kim. (2019). A comparison of the quantification aspects of human reliability analysis methods in nuclear power plants. *Annals of Nuclear Energy*, 133: p. 297-312.

Park, J., A.M. Arigi, and J. Kim. (2019). Treatment of human and organizational factors for multi-unit HRA: Application of SPAR-H method. *Annals of Nuclear Energy*, 132: p. 656-678.

Park, J., et al. (2021). Modeling FLEX Human Actions using the EMRALD Dynamic Risk Assessment Tool. *2021 International Topical Meeting on Probabilistic Safety Assessment and Analysis (PSA 2021).* Columbus, OH, USA.

Prescott, S., Smith, C., & Vang, L. (2018). EMRALD, Dynamic PRA for the Traditional Modeler. *In Proceedings of the 14th International Probabilistic Safety Assessment and Management Conference.* Los Angeles, CA.

Prosek, A., & Cizelj, L. (2013, April). Long-Term Station Blackout Accident Analyses of a PWR with RELAP5/MOD3.3. *Science and Technology of Nuclear Installations, 2013*.

RELAP5-3D Code Development Team. (2018). *RELAP5-3D Code Manual Volume I.* Idaho National Laboratory. Idaho Falls: Idaho National Laboratory.

Robb, K. R., Howell, M., & Ott, L. J. (2017). *Parametric and Experimentally Informed BWR Severe Accident Analysis Using FeCrAl.* Oak Ridge National Laboratory, Nuclear Technology R & D.

Schultz, R. R. (2015). *RELAP5-3D(c) Code Manual Volume V: User`s Guidelines.* Idaho National Laboratory. Idaho Falls: Idaho National Laboratory.

Smith, C. L., & Wood, S. T. (2011). *Systems Analysis Programs for Hands-on Integrated Reliability Evaluations (SAPHIRE).* Idaho National Laboratory. Idaho Falls: US NRC.

Swain, A.D. and H.E. Guttmann. (1983). *Handbook of human-reliability analysis with emphasis on nuclear power plant applications.* Sandia National Labs.

U.S. Nuclear Regulatory Commission. (2002). *Risk-Based Performance Indicators: Results of Phase 1 Development (NUREG-1753).*

U.S. Nuclear Regulatory Commission. (2005). *Independent Verification of the Mitigating Systems Performance Index (MSPI) Results for the Pilot Plants (NUREG-1816).*

U.S. Nuclear Regulatory Commission. (2011). *General Electric Systems Technology Manual Chapter 2.2 Fuel and Control Rods System (ML11258A302).* U.S. Nuclear Regulatory Commission. Retrieved August 2020, from https://www.nrc.gov/docs/ML1125/ML11258A302.pdf

U.S. Nuclear Regulatory Commission. (2012). *Reactor Concepts Manual -- Boiling Water Reactor Systems (ML120970422).* U.S. Nuclear Regulatory Commission.

U.S. Nuclear Regulatory Commission. (2012). *TRACE V5.0 Theory Manual: Field Equations, Solution Methods, and Physical Models*. (N. R. Commission, Producer) Retrieved April 16, 2018, from https://www.nrc.gov/docs/ML0710/ML071000097.pdf

U.S. Nuclear Regulatory Commission. (2017). Acceptance criteria for emergency core cooling systems for light-water nuclear power reactors, Title 10, Part 50.46, of the Code of Federal Regulations.

U.S. Nuclear Regulatory Commission. (2020). *DRAFT - Flexible Coping Strategies (FLEX) HRA Using IDHEAS-ECA.*

U.S. Nuclear Regulatory Commission. (2020). *NRC Inspection Manual Chapter 0609 - Significance Determination Process.*

U.S. Nuclear Regulatory Commission. (2020). *U.S. Nuclear Regulatory Commission Accident Sequence Precursor Program Summary Description (Revision 1).*

Ulrich, T.A., et al. (2020). Dynamic Modeling of Field Operators in Human Reliability Analysis: An EMRALD and GOMS-HRA Dynamic Model of FLEX Operator Actions. *International Conference on Applied Human Factors and Ergonomics.* Springer.

Wang, J., Dailey, M., & Corradini, M. (2019). Performance evaluation of accident tolerant fuels (ATF) and reactor core isolation cooling (RCIC) for boiling water reactor. *In Proceedings of American Nuclear Society Winter Meeting.* Washington, D.C.

Wu, X., & Shirvan, K. (2019). System code evaluation of near-term accident tolerant claddings during boiling water reactor short-term and long-term station blackout accidents. *Nuclear Engineering and Design*.

Xing, J., Y. Chang, and J. DeJesus. (2020). *Integrated Human Event Analysis System for Event and Condition Assessment (IDHEAS-ECA).* U.S. Nuclear Regulatory Commission.

Zhang et al. (2021). Multicriterion Benefit Evaluation Methodology for Safety Enhancements in Nuclear Power Plants and Application for FLEX Strategies. *Nuclear Engineering and Design*, Volume 376.